Praha, 2023

Charles University Faculty of Science
Karlova Univerzita, Přírodovědecká fakulta

Ph.D. study program: Parasitology
Doktorský studijní program: Parazitologie

Effect of various stress factors on mitochondrial processes of pathogenic protists

Vliv různých stresových faktorů na mitochondriální procesy patogenních protistů

Ph.D. thesis / Disertační práce

Mgr. Kateřina Ženíšková

Supervisor: RNDr. Róbert Šuťák Ph.D.

Declaration of the author

I declare that this thesis was elaborated on my own. The data presented in this Ph.D. thesis results from my research work and the collaboration of the co-authors. Also, the literary sources used in this work were cited appropriately and neither this work nor the data presented within this work were used to reach any other academic degree.

Mgr. Kateřina Ženíšková

Declaration of the thesis supervisor

The data presented in this work are the results of the research activity of Mgr. Kateřina Ženíšková and collaboration of colleagues, the coauthors of enclosed publications. I declare that her involvement was substantial, and she contributed significantly to obtaining the results.

RNDr. Róbert Šuťák Ph.D.

Acknowledgments

I would like to thank my supervisor Róbert Šuťák, who fought for me and provided me with a great opportunity and background that allowed me to work on these projects. I would like to thank him for his patience and mentorship throughout my studies. I also thank all the members of ROBOlab, especially Dominik Arbon, Ronald Malych, and Maria Grechnikova, who helped me both in the lab and in my personal life. I would also like to thank Honza Mach, who taught me most of the methods in the lab that I know now and who never said no when I came to him for advice.

Furthermore, I would like to thank Ivan Hrdý and Zdeněk Verner for sharing their knowledge in the field of biochemistry, and for countless consultations and advice during my studies. I would also like to thank the entire parasitology/protistology group at Biocev for creating a beautiful and inspiring working environment.

In the end, I would like to thank my family and my Tomášek, who stood by me even in times of crisis, for their support and words of comfort and encouragement in times of greatest need.

Abstract

Mitochondria perform various important functions in cells. They are the main site of energy metabolism, biosynthetic and regulatory processes, and the center of iron metabolism. Additionally, mitochondria are also the central organelle responsible for the production of potentially dangerous reactive oxygen species and possess a self-destructive arsenal capable of inducing whole-cell apoptosis. This single organelle thus controls the fate of the entire cell. Given these facts, this organelle has become the focus of interest for many scientists and pharmaceutical companies developing drugs targeting mitochondria. During evolution, unicellular parasites have evolved several mechanisms to survive, defend themselves and reproduce in the hostile environment of their host. One of these mechanisms is the ability to adapt its mitochondrial metabolism to maintain the viability of the whole cell.

This work focuses on mitochondria from two different perspectives:

First, concerning the phenomenon of nutritional immunity, we studied the effect of iron and copper deprivation on the mitochondria of the "brain-eating" amoeba *Naegleria fowleri.* Proteomic analysis of cells pre-incubated with specific chelators, together with the determination of several enzyme activities and measurements of oxygen consumption, revealed that *N. fowleri* mitochondria adapt to these limiting factors by upregulating alternative components of the branched electron transport chain (ETC) to compensate for lower activity of other components in ETC. Moreover, in the case of iron deprivation, we demonstrated an interesting trend of downregulation of iron-dependent cytosolic enzymes in an attempt to spare iron to maintain a vital pathway of energy metabolism, the ETC.

Second, we elucidated the mode of action of the mitochondrially targeted anti-cancer drug MitoTam on the bloodstream form of *Trypanosoma brucei*. The mode of action in cancer cells is often associated with the activity of complex I, which is rather dispensable in the bloodstream form of *T. brucei*. Functional analysis showed a rapid effect of MitoTam on mitochondrial processes, manifested by reduction of cellular respiration, lowering of ATP levels, rapid dissipation of mitochondrial membrane potential, and also disruption of mitochondrial integrity leading to cell death. Altogether, we have identified another potential candidate drug to combat sleeping sickness and confirmed that drug repurposing is a powerful tool for finding new therapeutic options for neglected diseases.

Abstrakt

Mitochondrie plní v buňkách různé důležité funkce. Jsou hlavním místem energetického metabolismu, biosyntetických a regulačních procesů a také centrem metabolismu železa. Kromě toho jsou mitochondrie také ústřední organelou odpovědnou za produkci potenciálně nebezpečných reaktivních forem kyslíku a disponují sebedestruktivním arzenálem schopným vyvolat apoptózu celé buňky. Tato jediná organela tak řídí osud celé buňky. Vzhledem k těmto skutečnostem se tato organela stala středem zájmu mnoha vědců a farmaceutických společností vyvíjejících léčiva cílená na mitochondrie. Jednobuněční parazité si během evoluce vyvinuli několik mechanismů, jak přežít, bránit se a rozmnožovat se v nepřátelském prostředí svého hostitele. Jedním z těchto mechanismů je schopnost přizpůsobit svůj mitochondriální metabolismus k udržení životaschopnosti celé buňky.

Tato práce se zaměřuje na mitochondrie ze dvou různých hledisek:

Za prvé, s ohledem na fenomén nutriční imunity, jsme studovali vliv deprivace železa a mědi na mitochondrie "mozkožravé" améby *Naegleria fowleri*. Proteomická analýza buněk předem preinkubovaných se specifickými chelátory, spolu se stanovením aktivit enzymů a měřením spotřeby kyslíku ukázala, že mitochondrie *N. fowleri* se těmto limitujícím faktorům přizpůsobují upregulací alternativních složek rozvětveného elektronového transportního řetězce (ETC), aby kompenzovaly nižší aktivitu jiných složek v ETC. V případě deprivace železa jsme navíc prokázali zajímavý trend downregulace cytosolických enzymů závislých na železe ve snaze ušetřit železo pro zachování životně důležité dráhy energetického metabolismu, ETC.

Za druhé, jsme objasnili způsob účinku mitochondriálně cíleného protinádorového léčiva MitoTam na krevní formu *Trypanosoma brucei*. Způsob účinku v nádorových buňkách je často spojován s aktivitou komplexu I, který je v krevním stádiu *T. brucei* spíše postradatelný. Funkční analýza ukázala rychlý účinek MitoTamu na mitochondriální procesy, což se projevilo redukcí buněčného dýchání, snížením hladiny ATP, rychlým rozpadem mitochondriálního membránového potenciálu a také narušením mitochondriální integrity vedoucí k buněčné smrti. Celkově se nám povedlo identifikovat další potenciální kandidátní léčivo pro boj se spavou nemocí a potvrdili jsme tezi, že tzv. „drug repurposing“ je mocným nástrojem pro hledání nových terapeutických možností pro opomíjené nemoci.

Table of content

1 Introduction

1.1 Mitochondrion: the powerhouse of the cell

One of the main features that distinguish eukaryotic cells from prokaryotic cells is compartmentalization. The possessing membrane-separated compartments within cells enables important processes to occur that would not be possible otherwise. One example is the presence of low pH in lysosomes, which is crucial for biomolecules degradation, but simultaneously is incompatible with the other metabolic processes. Moreover, compartmentalization ensures the efficiency of the whole system by concentrating the necessary components in one place.

The mitochondrion is one of the most important compartments in the cell in terms of energy metabolism in most eukaryotic organisms. It is a complex organelle that originally arose from the alpha-proteobacteria (Margulis, 1996; Roger et al., 2017; Sagan, 1967), surrounded by two membranes that divide the organelle into four distinct compartments - the outer membrane (OMM), the intermembrane space (IMS), the inner membrane (IMM), and the matrix (MM). The OMM separates the mitochondrion from the cytoplasm and is porous so that a small and uncharged molecule can easily pass through the membrane via voltage-dependent porins, pore-forming membrane proteins such as VDAC (Shoshan-Barmatz et al., 2010). Special translocases are involved in the transport of larger molecules. Moreover, the OMM mediates communication with other cellular compartments and allows the recognition and subsequent import of mitochondrial proteins encoded in the cell nucleus. Due to the presence of pores, there is no membrane potential across the outer membrane. On the other hand, the IMM of the mitochondrion is impermeable to most molecules. Transport into the mitochondrial lumen, otherwise known as the mitochondrial matrix, is mediated by specific membrane proteins, which are selected only for specific ions and molecules. As a result of this selectivity, the mitochondrial membrane potential of about 180 mV is generated across the inner membrane (Mitchell and Moyle, 1969; Nicholls, 1974).

1.1.1 Electron transport chain

The IMM is strongly folded and can be divided into the inner boundary membrane and formations called cristae, which are essentially membrane invaginations into the mitochondrial matrix. The formation of cristae greatly increases the surface area of the entire inner mitochondrial membrane, which houses the oxidative phosphorylation system (OXPHOS), a key player in the bioenergetics of the cell (see Figure 1).

The source of energy for use at the cellular level is adenosine triphosphate (ATP) which provides readily releasable energy in macroergic bonds between the second and the third phosphate groups. The synthesis of this cellular "energy currency" is maintained by the substrate phosphorylation in glycolysis localized in cytosol or the tricarboxylic acid cycle (TCA cycle) in the mitochondrial matrix or anaerobically for instance by the process of lactic or alcohol fermentation in the cytosol. However, it is the OXPHOS at the inner mitochondrial membrane that supplies the majority of ATP to the cell and produces a total of 32 to 34 ATP molecules per glucose molecule (Cooper, 2000).

In definition, the OXPHOS is an electron transport chain (ETC) known also as a respiration chain driven by substrate oxidation coupled to the generation of membrane potential and activity of F_oF_1 ATP synthase. The ETC consists of membrane complexes I-IV and electron carriers free-moving: ubiquinone and cytochrome c. Complexes I-IV are localized together in the mitochondrial cristae and ATP synthase is localized in the cristae bend (Figure 1). The complexes have different redox potentials, and the electrons are transferred from electron carriers with a lower redox potential to carriers with a higher redox potential. When electrons are transferred across the complexes, the electron itself loses energy, which is used to translocate the protons across the membrane, creating a proton motive force.

Under normal conditions, complex IV of the ETC transfers the electron to the terminal electron acceptor, oxygen, to form H_2O. However, during electron transport through complexes I, III and IV, and III, electron leakage occurs, and a single electron transfer to oxygen results in the formation of the reactive superoxide ($O_2^{\bullet-}$) member of reactive oxygen species (ROS) (Zhao et al., 2019). This molecule is highly reactive thus it rapidly dismutases into hydrogen peroxide by superoxide dismutase (SOD) as a protection mechanism. Although low and moderate levels of ROS are necessary, for example, for signaling processes and immune responses, an imbalance between ROS production and

detoxification exposes the cell to oxidative stress that can cause DNA damage, lipid peroxidation, membrane damage, protein dysfunction, and ultimately cell death (Dröge, 2002; Pizzino et al., 2017; Poprac et al., 2017; Willcox et al., 2004; Young and Woodside, 2001). The main source of ROS in the cell is electron leakage in ETC and the second is NADPH oxidase (Zhao et al., 2019).

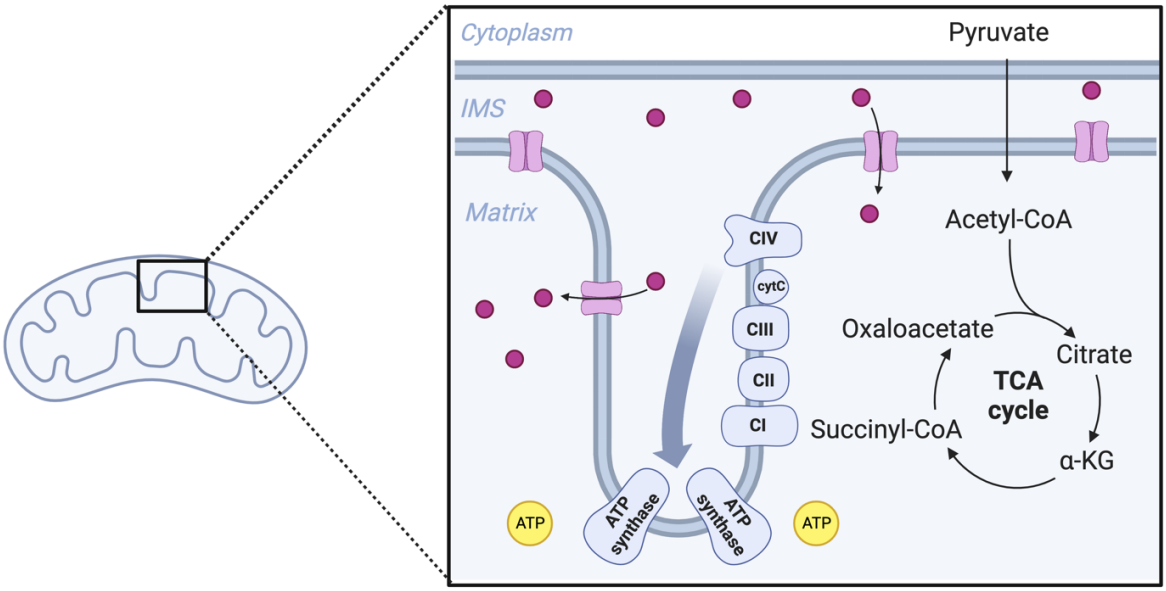

Figure 1 Detail of mitochondrial cristae with highlighted ETC. The TCA cycle is localized in the mitochondrial matrix, while ETC I-IV complexes are localized in the cristae formed by the inner mitochondrial membrane with ATP synthase localized in the cristae bend. The thick gray arrow indicates the electron flow. In pink shades, the Ca^{2+} cations with mitochondrial calcium uniporters (MCUs) are depicted. CI-CIV: complexes I-IV, cytC: cytochrome c. The figure is adapted from (Gottschalk et al., 2022). Created with BioRender.com

1.1.1.1 Complex I and the alternative NADH dehydrogenase

An entry point for most of the electrons into the ETC is through the NADH: ubiquinone oxidoreductase (complex I), which catalyzes the transfer of two electrons from NADH, produced in the TCA cycle or mediated by malate aspartate shuttle, to coenzyme Q10 also called ubiquinone (Brandt, 2006; Hirst, 2013; Ohnishi et al., 2010). Complex I is the largest and most complicated protein complex of ETC, with a relatively high molecular mass of about 1 MDa (mammalian homolog). Together with cytochrome c reductase (complex III) and cytochrome c oxidase (complex IV), it is one of the three energy-transferring enzymes that, in addition to transferring electrons, also translocate four protons across the inner mitochondrial membrane per one molecule of NADH to create the proton motive force that drives ATP synthase (Walker, 1992; Wikström, 1984). Mammalian

complex I consist of 45 subunits (Carroll et al., 2006) and 8 canonical Fe-S clusters, and one non-covalently bound flavin mononucleotide (FMN) localized within the peripheral arm of the complex that serves as a redox cofactors (Ohnishi, 1998; Rasmussen et al., 2001). One of the most used inhibitors of complex I is rotenone, the lipophilic and naturally occurring compound derived from *Derris* and *Lonchocarpus* plants. The mode of action of rotenone is the inhibition of electron transfer from Fe-S clusters to ubiquinone, leading to a decrease in ATP production (Gutman et al., 1970).

In addition to the rotenone-sensitive NADH dehydrogenase activity attributed to complex I, other enzymes performing a similar function have been identified in bacteria (Björklöf et al., 2000), *Archaea* (Gomes et al., 2001), protozoa (Lin et al., 2011; Verner et al., 2013), fungi (de Vries and Grivell, 1988; Weiss et al., 1970) and plants (Møller and Palmer, 1982). The type II NADH: quinone oxidoreductase, also known as alternative NADH dehydrogenase (NDH2), is a rotenone-insensitive peripheral membrane protein that catalyzes the two-electron transfer from NADH (NADPH) to ubiquinol. NDH2 is much smaller and simpler than complex I with only one subunit and a molecular weight in the range of 40-70 kDa (Kerscher et al., 2008; Melo et al., 2004) and may interact with the external or the internal surface of the IMM. Another difference is that it does not pump protons into the intermembrane space and therefore does not participate in the generation of the proton motive force that drives ATP synthase. There is a great diversity among these enzymes, according to the conserved motifs in their primary and secondary structures, NDH2 enzymes can be divided into three groups: Group A mainly includes homologs found in bacteria, archaea, and eukaryotes, which have two adenine dinucleotide-binding motifs to bind the NADPH and flavins; Group B consists exclusively of fungi (Melo et al., 1999) and plants homologs (Rasmusson et al., 1999) possessing EF-hand fold and two binding sites for ADP; Group C - contains only the homologous enzymes from the hyperthermophilic archaea with the presence of a single dinucleotide binding motif and covalently bound flavin (Melo et al., 2004). The NDH2 can be present in addition to canonical complex I or it can be the only enzyme responsible for the oxidation of NADH in the ETC such as in the case of *Saccharomyces cerevisiae* (Luttik et al., 1998) or *Plasmodium falciparum* (Uyemura et al., 2004). The fact that this enzyme is not occurring in humans and is also vital for some life-threatening human pathogens (Duarte et al., 2021) has attracted the attention of scientists and makes inhibitors of this enzyme attractive drug candidates.

1.1.1.2 Complex II

Complex II, also known as succinate dehydrogenase, is the direct link between ETC and the TCA cycle. In contrast to other respiration complexes, all proteins of this complex are nuclear encoded. This complex catalyzes the oxidative conversion of succinate to fumarate while simultaneously transferring electrons to ubiquinone, which is reduced to ubiquinol. Complex II transfers the electrons in parallel to complex I, but in contrast, no protons are pumped from the MM. This complex is a relatively small heterotetramer (mammalian homolog = 123 kDa). Subunits A and B are hydrophilic and are attached to the hydrophobic subunits C and D. Succinate dehydrogenase contains a variety of cofactors and prosthetic groups such as FAD, heme B, and a chain of Fe-S centers.

1.1.1.3 Complex III

Complex III, also known as mitochondrial cytochrome c reductase, catalyzes the oxidation of ubiquinol and the associated reduction of cytochrome c. The mammalian homolog contains four prosthetic groups: two hemes b and heme c as part of cytochrome b and cytochrome c1, respectively, and an unusual "Rieske-type" Fe-S center where iron atoms are bound by two cysteine and two histidine residues. The process of electron transfer from ubiquinol to cytochrome c is referred to as the Q-cycle (Slater, 1983). In this cycle, the first electron from ubiquinol is transferred through the Rieske center to cytochrome c1 and then to cytochrome c, which is transiently bound to complex III on the intermembrane side of the membrane. Cytochrome c is then released by one-electron reduction and migrates to complex IV. The path of the second electron leads to cytochrome b and then partially reduces the ubiquinone attached to another binding site on complex III to a radical called semiquinone. When another molecule of ubiquinol interacts with complex III, one electron again goes to the oxidized cytochrome c, while the other fully reduces the semiquinone and, with two protons from the matrix side, forms ubiquinol.

1.1.1.4 Complex IV and alternative oxidase

Complex IV, also known as cytochrome c oxidase, is the last member of the canonical ETC. Electrons from the complexes described above are transferred from cytochrome c via complex IV to oxygen, which is the terminal electron acceptor in aerobic cellular respiration. Complex IV contains two copper centers CuA and CuB, two cytochromes, and heme a and heme a3. This complex also contributed to the proton gradient by pumping four protons into the intermembrane space. One of the most used inhibitors of complex IV is cyanide, which binds to ferric ions in heme-containing proteins, leading to inhibition of oxygen reduction and thus depletion of ATP production, ultimately leading to cell death (Huzar et al., 2013; Stannard and Horecker, 1948; Zoltani, 2015).

In many fungi, prokaryotes, and plants, in addition to the canonical cytochrome c oxidase, there is also an additional terminal oxidase insensitive to cyanide, called alternative oxidase (AOX). AOX is a small (~36 kDa) monotopic protein localized to the matrix side of the inner mitochondrial membrane that belongs to a subfamily of di-iron proteins including, for example, fatty acid desaturases, rubrerythrin, and monooxygenases (Moore et al., 2013). AOX bypasses the activity of complex III and IV and catalyzes a similar reaction as complex IV, i.e. direct electron transfer to the final electron acceptor, oxygen, except that in this case, the reduced form of ubiquinone serves as the electron donor. Moreover, the AOX is not sensitive to cyanide, the inhibitor of complex IV. Similarly, to NDH2, this alternative component of ETC also does not transfer protons across the membrane, therefore, like NDH2, it is not involved in ATP production.

Originally, alternative oxidase was thought to be restricted to plant mitochondria, where AOX expression is induced in response to various stress factors such as high ROS production, ETC inhibition, and pathogen invasion (Manbir et al., 2022; Simons et al., 1999; Vishwakarma et al., 2015). However, recent advanced DNA analyses and genome sequencing have found that this alternative ETC component is widespread and found in the genomes of bacteria, fungi, protozoa, and even in the genomes of some members of the Animalia kingdom (McDonald, 2009; McDonald et al., 2009a; McDonald and Vanlerberghe, 2006; Rogov et al., 2014; Rogov and Zvyagilskaya, 2015), with the exception of vertebrates, which have lost AOX during evolution (McDonald et al., 2009a). Functional AOX has also been identified in various human pathogens, for instance, *Trypanosoma brucei*, the causative agent of the vector-borne disease human African trypanosomiasis (Clarkson et al., 1989). Interestingly, AOX is the only oxygen-consuming

ETC enzyme expressed in the bloodstream form of this pathogen, and its role is to maintain redox balance by allowing reoxidation of NADH via mitochondrial glycerol-3-phosphate dehydrogenase to maintain glycolysis, the main pathway for ATP production in this form (Opperdoes et al., 1977).

1.1.1.5 F_oF_1 ATPase (complex V)

The last complex in the OXPHOS pathway is the F_o F_1 ATP synthase, commonly known as a complex V, which catalyzes the synthesis of ATP from adenosine diphosphate (ADP) and inorganic phosphate (Pi), which is an energetically unfavorable reaction (Capaldi et al., 1994; Nijtmans et al., 1995). ATP synthase couples the conversion of ADP and Pi to ATP with the electrochemical potential generated by the difference in proton concertation across the IMM (Capaldi et al., 1994). ATP synthase is a relatively large complex that functions as a rotary motor system. It consists of two parts, the hydrophilic F_1 part which contains the catalytic sites, and the hydrophobic F_o part, which contains a transmembrane channel for proton flux (Boyer, 1997; Pedersen and Amzel, 1993). When the F_o part is protonated, it rotates, causing conformational changes in the F_1 part, which catalyzes the formation of ATP from ADP and Pi. For every four H^+ ions pumped from the IMS to the matrix, one molecule of ATP is formed. ATP synthase can also work in reverse, hydrolyzing ATP and pumping protons across the membrane, which is relatively uncommon under physiological conditions and only occurs under certain conditions such as anoxia or hypoxia (Chinopoulos and Adam-Vizi, 2010; St-Pierre et al., 2000). However, in the bloodstream form of *T. brucei*, the reverse function of ATP synthase ensures the generation of mitochondrial membrane potential (Brown et al., 2006).

One of the best-known F_oF_1 ATP synthase inhibitors is oligomycin A. It is an antibiotic oligopeptide found in *Streptomyces* that binds to a 25 kDa polypeptide in the F_o part of the rotary motor system, preventing the pumping of protons into the mitochondrial matrix (Lee and O'Brien, 2010; Shchepina et al., 2002). An example of a branched ETC is shown in Figure 2**.**

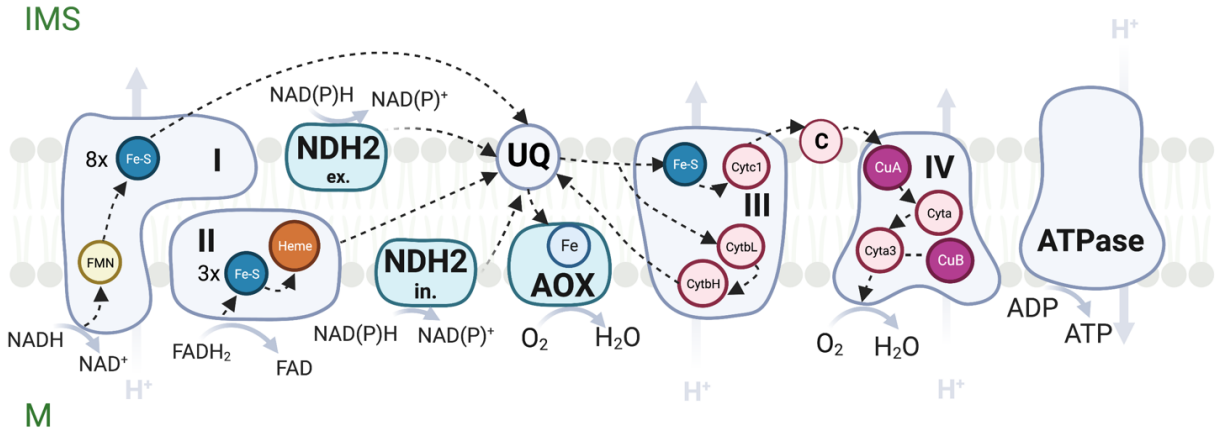

Figure 2 An example of the branched mitochondrial electron transport chain. Scheme of the arrangement of the plant ETC with cofactors and prosthetic groups, according to (Vanlerberghe, 2013).NADH is oxidized by complex I and this process is coupled to proton translocation from the mitochondrial matrix to the intermembrane space. NADPH is oxidized through the series of alternative NADH dehydrogenase, localized on the external resp. the internal part of the inner mitochondrial membrane, this reaction is not coupled to proton transport. The reduction of O_2 to H_2O is maintained by complex IV and this reaction is also coupled to proton translocation, while the same reaction maintained by alternative oxidase is not. IMS: intermembrane space; M. matrix; I, II, III, IV: complexes I-IV; NDH2 ex.: external oriented alternative NADH dehydrogenase; NDH2 in.: internal oriented alternative NADH dehydrogenase; AOX: alternative oxidase; ATPase: F_oF_1 ATP synthase; FMN: flavin mononucleotide; UQ: ubiquinol pool. Created with BioRender.com

1.1.1 Other functions of mitochondria in the energy metabolism of the cell

In addition to cellular respiration, other important energy metabolism processes such as fatty acid oxidation and the tricarboxylic acid (TCA) cycle take place in the mitochondrial matrix. These pathways produce reducing equivalents such as NADH and $FADH_2$, which serve as electron donors for ATP production and the generation of mitochondrial membrane potential ($m\Delta\psi$) in the ETC.

ß-oxidation is a multistep process that cleaves long fatty acids into acetyl-CoA, the main fuel for the TCA cycle. A similar process also takes place in peroxisomes, where very long-chain fatty acids are processed to produce long-chain fatty acid fragments that need to be further broken down in the mitochondria by the process of ß -oxidation. Per round of oxidation, the ß-oxidation yields 17 ATP equivalents in the form of one acetyl CoA molecule, one $FADH_2$, and one NADH (Talley and Mohiuddin, 2022).

The TCA cycle, also known as the Krebs cycle or citrate cycle, is closely related to the ETC. Another entry point of acetyl-CoA into the TCA cycle is the oxidative decarboxylation of pyruvate originating from glycolysis localized in the cytosol. The

initiation step of the Krebs cycle is the conversion of acetyl-CoA to citrate in a reaction with oxaloacetate catalyzed by citrate synthase. This is followed by seven enzymatic reactions that result in the conversion of citrate back to oxaloacetate, which continues the cycle, and two molecules of carbon dioxide. The liberated free energy per each acetyl-CoA that enters the cycle is stored in one molecule of $FADH_2$, one molecule of GTP, and three molecules of NADH and is used directly in the ETC. The whole pathway and its connection to ETC are depicted in Figure 3. Another source of Acetyl CoA is, for instance, the catabolism of amino acids such as threonine, alanine, glycine, tryptophan, etc.

Mitochondria are also important for calcium homeostasis in the cell. The endoplasmic reticulum is the main reservoir of calcium (Koch, 1990), but calcium is also transiently stored in mitochondria (Deluca and Engstrom, 1961). Calcium is a very flexible second messenger that is essential for signal transduction and cell proliferation and is also a key regulator of many processes in the cell, particularly in the mitochondria (Chappell and Crofts, 1965; Clapham, 1995; Rizzuto et al., 2000). For example, mitochondrial calcium uptake or release is a sensor mechanism for the regulation of OXPHOS, and key regulators of the Krebs cycle, such as pyruvate dehydrogenase, isocitrate dehydrogenase, and 2-oxoglutarate, are activated by certain levels of calcium in the mitochondrial matrix (Ivannikov and Macleod, 2013; McCormack et al., 1990; Traaseth et al., 2004). On the other hand, both increases and decreases in mitochondrial Ca^{2+} levels are involved in mitochondrial dysfunction, which increases ROS levels, and can lead to cell death (Orrenius et al., 2015; Zhivotovsky and Orrenius, 2011).

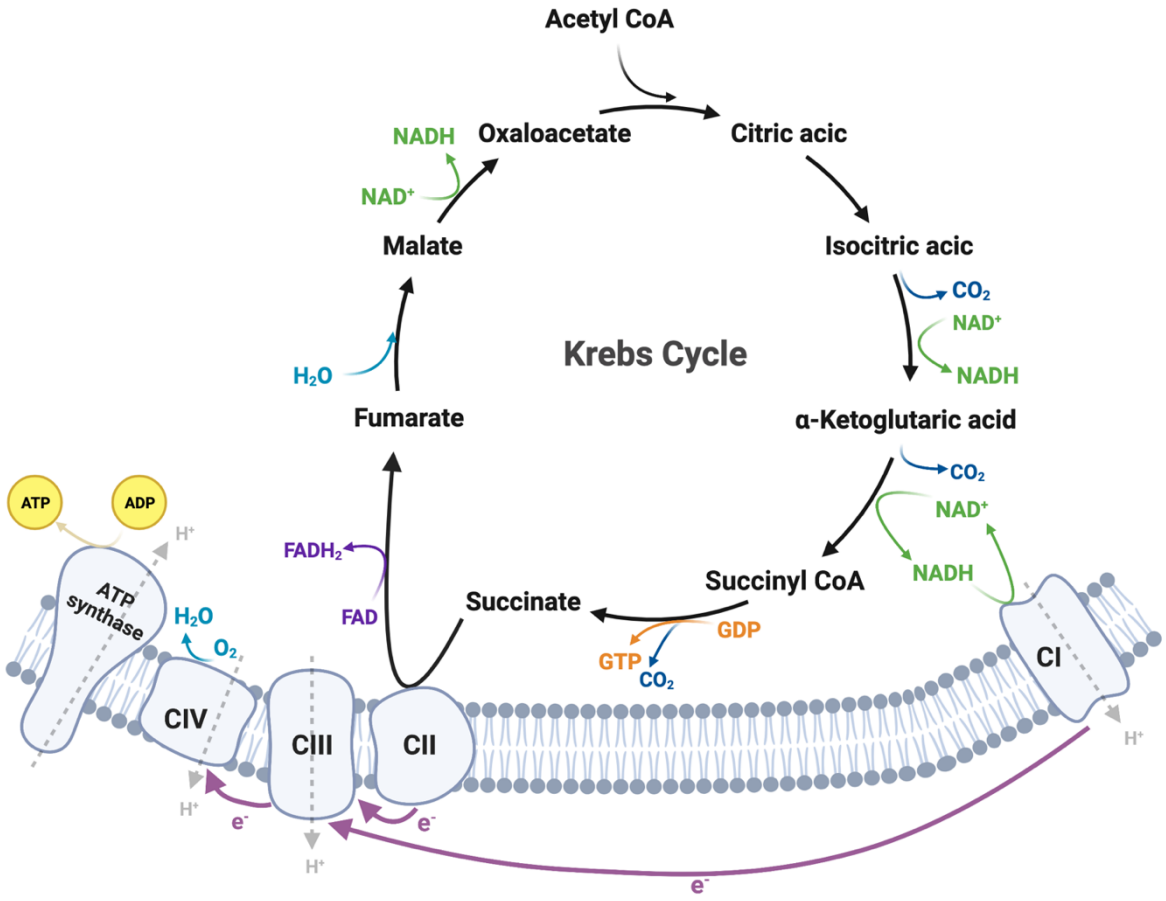

Figure 3 Krebs cycle linked to the electron transport chain. Scheme of the Krebs cycle localized in the mitochondrial matrix producing the reducing equivalents NADH, GTP, and $FADH_2$ which are required in ETC for ATP synthesis and generation of mitochondrial membrane potential. The process is known as oxidative phosphorylation. CI: complex I; CII: complex; CIII: complex III; CIV: complex IV; ATP synthase: F_oF_1 ATP synthase. The figure was adapted according to (Martínez-Reyes and Chandel, 2020). Created with BioRender.com

1.2 Mitochondria-targeted drugs as a therapeutic strategy

Mitochondria and mitochondria-targeted drugs are in the crosshairs of many scientists and pharmaceutical companies because, in addition to supplying most of the ATP to the cell, mitochondria are also in control of lethal processes such as the initiation of cell necrosis and apoptosis, the ROS production, or Ca^{2+} homeostasis, which can trigger pathologies that can eventually lead to cell death (Baines, 2010; Duchen, 2004; Giorgi et al., 2012; Kroemer and Reed, 2000; Lemasters et al., 1998; Szewczyk and Wojtczak, 2002). Moreover, mitochondrial dysfunction caused by mutations in genes encoding mitochondrial proteins contributes to the development of a wide range of disorders, such as metabolic, cardiovascular, and neurogenerative diseases (Ballinger, 2005; Cadonic et al., 2016; Rosca and Hoppel, 2013; Vásquez-Trincado et al., 2016).

Drugs targeting mitochondria are particularly important in the treatment of cancer. Indeed, a key feature of cancer cells is the metabolic reprogramming of mitochondrial processes to meet the higher energy demands caused by continuous growth and proliferation (Kroemer, 2006; Wisnovsky et al., 2016). Inhibition of the induction of apoptosis, a process leading to programmed cell death, is a hallmark of cancer cells; mutations in mDNA that lead to inhibition of OXPHOS are also common in several cancer types such as melanoma and renal cancer (Gaude and Frezza, 2016; Shackelford et al., 2013; Warburg, 1956). This may result in increased ROS production, which contributes to neoplastic transformation when apoptosis is inhibited (Liou and Storz, 2010; Schumacker, 2006). However, since the 1950's this hypothesis has been challenged, because there was mounting evidence, that in several types of cancer, the OXPHOS is upregulated and contributes greatly to satisfy the high energy demands required for cancer proliferation (Fantin et al., 2006; Wenner et al., 1952). Another hallmark of cancer cells is enhanced glucose uptake and upregulation of glycolytic enzymes such as pyruvate kinase and hexokinase, which allow fermentation of glucose to lactate even when oxygen, the final electron acceptor of the aerobic ETC, is present. This common mechanism of cancer cells is known as the Warburg effect described by the Nobel laureate Otto Heinrich Warburg (Cori and Cori, 1925; Warburg et al., 1927).

The Warburg phenomenon might put mitochondria in a position where they would seem to be dispensable organelles for cancer development, but it is mitochondria that

supply cancer cells with the necessary ATP and building blocks such as amino acids, heme, pyrimidines, and play a key role in cancer viability (de Berardinis and Chandel, 2016). Indeed, it has been shown that tumor cells lacking mitochondria DNA exhibit lower tumorigenesis potential and slower overall tumor growth (Cavalli LR, 1997; Magda et al., 2008; Morais et al., 1994). Another aspect of mitochondria in cancer cells is the increased protonmotive force which is reflected by an elevated $m\Delta\psi$. This unique feature can be exploited to develop targeted therapeutic strategies (Davis et al., 1985; Madar et al., 1999; Rideout et al., 1989; Rugolo and Lenaz, 1987).

An important mitochondrial feature that can be used for targeting strategy is the fact that the mitochondrion possesses a negative charge inside. Because of the $m\Delta\psi$, the lipophilic cations are accumulated in the mitochondrial matrix against a concentration gradient (Smith et al., 2012, 2011). The accumulation of singly charged cations is governed by the Nernst equation, which states that for every 61.5 mV, there is a tenfold accumulation at 37 °C, hence the concentration of these charged biomolecules in the mitochondrion then can be even a thousand times higher than in the extracellular environment (Ross et al., 2008a; Zielonka et al., 2017).

The triphenylphosphonium cation (TPP^+) is a small, well-known molecule consisting of a positively charged phosphorus atom with three hydrophobic phenyl groups that give the entire molecule an extended hydrophobic surface, which, combined with the presence of a positive charge, provides a great ability to readily cross the phospholipid bilayer (James et al., 2005; Ross et al., 2005). TPP^+-containing molecules were first used to study OXPHOS coupling and determination of $m\Delta\psi$ (Hoek, Nicholls, and Williamson 1980; Lichtshtein, Kaback, and Blume 1979), and later the properties of this anchor were extensively exploited to generate many active biomolecules used in various chemotherapeutics (Wang et al., 2020; Zielonka et al., 2017). TPP^+-based compounds have been also heavily studied *in vivo* (Rodriguez-Cuenca et al., 2010a; Smith et al., 2003) and it was shown that in just 5 min after the intravenous administration, the compound could be completely absorbed by mitochondria in the tissue (Ross et al., 2008b). In terms of the safety of TPP^+-based compounds, TPP^+ itself has been shown to be safe, remaining unmodified and excreted in urine and bile. Cytotoxicity comes primarily from the "cargo" of the molecule that is associated with TPP^+, but TPP-based compounds are generally considered to be less toxic compounds to mammalian cells causing no significant organ

damage (Porteous et al., 2010; Smith et al., 2003) and can be used in long-term chemotherapeutic regimens, as has been demonstrated in several rodent models (Mcmanus et al., 2011; Rodriguez-Cuenca et al., 2010b), and more importantly, have even been orally administered to humans for one year in phase II evaluation without any safety concerns (Gane et al., 2010; Snow et al., 2010).

1.3 The importance of iron and copper in mitochondrial processes

Biometals such as iron and copper are vital trace elements that play an indispensable role in many biological processes, and their deficiency and excess pose a certain threat and can lead to many pathological conditions. Due to their physicochemical properties, these "two-faced" bio-metals are involved in the catalysis of numerous enzymatic reactions, electron transport, or the stabilization of protein structure (Andreini et al., 2008; Maret, 2010). Proteins that are associated with these metals are known as metalloproteins and are crucial in many cellular processes such as proliferation, respiration, transcriptions, signal transduction, and glycolysis. The maintenance of physiological levels of these metals inside the cell is a strictly regulated process; regulation of homeostasis takes place at the level of uptake, storage, intracellular trafficking, and detoxification of the appropriate metal.

1.3.1 Iron

One of the four most abundant transition metals on earth and the most prevalent biometal in the cell is iron (Frey and Reed, 2012). The prevalence of this metal in nature is probably due to the high abundance of the water-soluble reduced form of iron in waters during the prebiotic period, just before the increase in atmospheric oxygen levels due to photosynthesis led to the precipitation of iron into the insoluble form (Crichton and Pierre, 2001). Due to this fact, almost all living organisms have an iron-dependent metabolism. Only two organisms are considered to have iron-free metabolism; the causative agent of Lyme disease, *Borrelia burgdorferi*, which can replace iron in its metalloproteins with neighboring elements in the periodic table, such as manganese or zinc (Nguyen et al., 2007; Posey and Gherardini, 2000; Troxell et al., 2012) and possibly the *Lactobacillus plantarum* (Archibald, 1983).

The electron configuration of iron allows cycling between the two oxidation states Fe^{2+} and Fe^{3+} which makes it an ideal acceptor or donor of electrons, thus iron cofactors such as Fe-S clusters, iron-oxo center, or heme are involved in many redox reactions within broad electrochemical potential (E^0 -500 mV to +500 mV) (Williams, 2012). However, this redox capability of iron is also potentially dangerous in terms of oxidative stress. The free unbound iron can participate in a Fenton reaction, the process where Fe^{2+} reacts with hydrogen peroxide (H_2O_2) to generate highly reactive hydroxyl radical ($OH^{\bullet}$) and hydroxyl ion (OH^-).

1.3.1.1 The role of iron in mitochondria

One of the oldest cofactors are Fe-S clusters, which are essential for the function of more than 100 proteins involved in many cellular processes including DNA replication, translation, and respiration (Johnson et al., 2005). Although their chemical structure is relatively simple, the biogenesis of Fe-S clusters is quite complex. Different mechanisms of Fe-S cluster assembly have been identified in Archaea, Bacteria, and Eukaryotes. The sulfur-forming pathway (SUF) (Takahashi and Tokumoto, 2002), the nitrogen-fixation pathway (NIF) (Jacobson et al. 1989), and the cysteine sulfinate desulfinate system (CSD) (Loiseau et al., 2005) have been associated with bacteria and archaea, whereas in eukaryotic systems the mitochondrial iron-sulfur cluster assembly (ISC) pathway along with the cytosolic iron-sulfur cluster assembly (CIA) pathway predominates (Lill et al., 2015; Paul and Lill, 2015; Stehling et al., 2013). Here, we focus more on the ISC pathway to highlight the importance of iron in mitochondria.

A typical ISC pathway can be divided into four steps. First, the [2Fe-2S] clusters are newly assembled (*de novo*), followed by the trafficking of [2Fe2S] and its export to the cytosol or insertion into an apoprotein localized in mitochondria, the third step is the conversion of the [2Fe-2S] clusters into cubic [4Fe-4S], and the last step involves the trafficking and its insertion into mitochondrial apoproteins such as complex I and II and lipoate synthase (Braymer and Lill, 2017; Maio and Rouault, 2020). The biogenesis of Fe-S clusters is present in all eukaryotes harboring mitochondria and it is retained even when mitochondria are reduced in anaerobic or microaerobic organisms, such as *Giardia intestinalis* (Motyčková et al., 2022; Tovar et al., 2003), *Cryptosporidium parvum* (Miller et al., 2018) and intracellular obligate parasite *Microsporidium* (Freibert et al., 2017; Goldberg et al., 2008), underscoring the necessity of this pathway. In these organisms with reduced mitochondria, steps involving the formation and transport of [4Fe-4S] forms are missing due to the absence of mitochondrial proteins requiring these specific forms of the Fe-S cluster.

The most common forms of these prosthetic groups found in biological systems are [2Fe-2S], [3Fe-4S], and [4Fe-4S], but simple forms such as [1Fe-0S], found in the rubredoxins of sulfur-metabolizing archaea (Luo et al., 2010), or the more complex form [8Fe-7S], found in nitrogen-fixing bacterial nitrogenase (Burén et al., 2020), have also been identified. In mitochondria, Fe-S cofactors are found, for example, in aconitase, an enzyme of the Krebs cycle responsible for the second step of citrate conversion (Beinert et al.,

1996), or predominantly in the ETC. A total of 12 Fe-S clusters have been found in ETC complexes, and complex I contains the majority of these; two in the [2Fe-2S] form and the remaining six in the [4Fe-4S] form. Interestingly, the alternative NDH2, which replaces or bypasses the function of complex I in several plant or fungal organisms, lacks Fe-S clusters (Friedrich et al., 1995; Yagi, 1991). The other three Fe-S clusters of ETC are localized in complex II in different forms: [2Fe-2S], [4Fe-4S], and [3Fe-4S]. The last and rather unusual type, commonly known as a "Rieske type" [2Fe-2S] cluster is found in the Q cycle of complex III, where one of two iron atoms is coordinated by two histidines and two cysteine residues (Iwata et al., 1996).

Another indispensable iron-containing prosthetic group for many proteins is heme. Heme is formed by four tetrapyrrole rings linked via methenyl bridges named protoporphyrin IX with ferrous iron in the center. The biosynthesis of this complex cofactor is localized partly in mitochondria and partly in the cytosol. In most eukaryotes, this pathway consists of eight steps, with the first step localized in the mitochondrial matrix where glycine, and succinyl-CoA, are converted to 5-aminolevulinate (ALA) by 5-aminolevulinate synthase (ALAS) (Hunter and Ferreira, 2011). An alternative and more complex pathway, which is found in bacteria or plastid-containing eukaryotes, consists of two intermediate steps before ALA formation involving glutamyl-tRNA synthetase, glutamyl-tRNA reductase and glutamate-1-semialdehyde 2,1 aminomutase with the L-glutamate amino acid as a substrate (Brzezowski et al., 2015; Panek and O'Brian, 2002). ALA is then transported into the cytosol, where four more conversion steps occur to produce the final cytosolic product coproporphyrinogen III. Then this pathway returns to the mitochondria, where three more conversion steps follow, including a final step involving a Fe-S cluster-dependent ferrochelatase that is responsible for iron incorporation into the ring. Unlike the Fe-S pathway, heme biosynthesis is not conserved in all mitochondria-containing organisms, and in some cases, this pathway may be lost, for example in pathogenic protists such as *T. brucei* or *Leishmania mexicana*, which acquire heme or its late precursors from their hosts and are able to incorporate them into their proteins (Cenci et al., 2016; Kořený et al., 2013).

The most well-known function of heme is the transport of oxygen in hemoglobin, but the heme is part of many proteins with a wide range of functions including electron transfer, control of gene expression, signal transduction, and oxygen storage (Poulos, 2014). Specifically, in mitochondria, heme is abundantly represented in the ETC, where it

serves as a prosthetic group for various cytochromes, such as in complex II, cytochrome bc1 in complex III, cytochrome c itself, and cytochrome c oxidase.

In brief, mitochondria serve as the main center of iron utilization in cells. In the matrix of this organelle, the biogenesis of essential iron-containing cofactors involved in key bioenergetic pathways takes place. Disruption of iron homeostasis can lead to mitochondrial dysfunction, which can ultimately lead to cell death.

1.3.2 Copper

Similarly, to iron, copper is a vital micronutrient important for many cellular processes of almost all organisms. Due to its ability to readily convert from oxidized Cu^{2+} to reduced Cu^{1+}, copper serves as a cofactor in essential proteins. As with iron, copper excess poses a certain threat to organisms, so it is necessary to ensure strict regulation of either its uptake into the cell, its intracellular distribution to different cellular compartments, or its effective detoxification. Copper toxicity is usually associated with its involvement in the generation of ROS, in particular through a reaction known as the Fenton and Haber-Weiss reaction, which generates the hydroxyl radical, the most dangerous representative of ROS (Gaetke and Chow, 2003). However, recent studies suggest that the main target of copper toxicity is the interference with Fe-S cluster biogenesis (Chillappagari et al., 2010; Macomber and Imlay, 2009; Tan et al., 2014). Copper-induced inhibition of the entire [4Fe-4S] cluster assembly pathway has been described in bacteria (Brancaccio et al., 2017). In this case, copper binds competitively to the IscA protein involved in Fe-S cluster assembly, thereby preventing iron binding (Tan et al., 2014). A similar mechanism has been described in the human pathogen *Cryptococcus neoformans* and *Saccharomyces cerevisiae* (Garcia-Santamarina et al. 2017).

1.3.2.1 The role of copper in mitochondria

The main copper-dependent proteins in mitochondria are complex IV, found in the inner mitochondrial membrane, and superoxide dismutase, localized in the intermembrane space. There are a total of three copper ions in complex IV, which are located in two copper centers, with the catalytic site CuA containing two copper ions and the CuB site containing one. Together with two heme groups, they form the catalytic core required for cytochrome oxidation and oxygen reduction. Due to this fact, the proper function and biogenesis of ETCs depend on copper. It has been found that copper deficiency can disrupt the biogenesis of complex IV, causing a decrease in the level of produced ATP, changes in the morphology

of the ETC complex, and a decrease in the efficiency of oxygen reduction (Bustos et al. 2013; Jensen et al. 2019; B. E. Kim et al. 2010; Ruiz et al. 2014).

Superoxide dismutase catalyzes the dismutation of superoxide to hydrogen peroxide, which is then independently detoxified by catalase and glutathione peroxidase. SOD enzymes have various metal cofactors, such as manganese found in eukaryotes, nickel, and iron described in protists and bacteria, or zinc and copper. Cu, Zn SOD is predominantly localized in the cytosol, but 5-10% is found in the mitochondria along with the Mn SOD enzyme, where it plays a key role in controlling ROS levels in the mitochondrial intermembrane space (Fukai and Ushio-Fukai, 2011; Zelko et al., 2002). Interestingly, a recent study on the human fungal pathogen *Candida albicans* shows that copper starvation suppresses Cu, Zn SOD and induces an alternative cytosolic Mn SOD to spare copper availability for mitochondrial processes such as complex IV activity, which remains unchanged at low copper levels. In addition, alternative oxidase activity is induced by this limiting factor to keep mitochondrial ROS at low levels in the absence of mitochondrially localized Cu, Zn SOD (Broxton and Culotta, 2016).

1.3.2.2 Copper acquisition and its homeostasis

Copper uptake into the intracellular space is mediated in many eukaryotes by high-affinity membrane transport proteins called Copper TRansporters (CTRs), whose function and structure are conserved from yeast to humans (Maryon et al., 2007; Nose et al., 2006). To date, little information is available on copper uptake proteins in parasitic protozoa, except for the description of a copper-binding membrane protein with a motif typical of copper transporters in *Plasmodium falciparum* (Choveaux et al., 2012). Two homologous genes for CTR1 and CTR3 have been identified in *S. cerevisiae* (Dancis et al., 1994; Knight et al., 1996). Both these integral membrane proteins are localized on the cell surface and have three predicted transmembrane domains. Homologs of these proteins have been identified in the organisms studied in our laboratory, non-pathogenic *Naegleria gruberi* and pathogenic *Naegleria fowleri* (Ženíšková et al., 2022).

In biological systems, copper is efficiently sequestered after its transport into the cytoplasmic compartment by binding to molecules such as glutathione, metallothioneins, or specific metallochaperones that mediate copper transport to different compartments where it is available to copper-binding proteins. Metallochaperones are mostly small soluble proteins with the ability to reversibly bind various metals, such as copper, and mediate their transport to target proteins (Palumaa, 2013). In *S. cerevisiae*, several proteins

with chaperone function have been described that transport copper to specific copper-binding proteins with different localizations, such as the CCO protein, which transports copper to the major copper-containing protein cytochrome c oxidase localized in the mitochondrion. Another chaperone is CCS, which transports copper to superoxide dismutase (Cu, Zn SOD). Finally, the ATX1 chaperone is described to transport copper to the copper transport protein CCC2, a highly conserved P-type ATPase localized in the Golgi apparatus. The latter pumps copper via secretory vesicles to the cell surface where it is available to copper-binding proteins such as the iron transport multicopper oxidase (FET3) (Kim et al., 2008). Due to the potential toxicity of copper in the intracellular space, free copper is virtually absent in the cell. The main copper detoxification mechanisms include binding to metallothioneins, small cysteine-rich proteins with a high affinity for metals, or to glutathione, a tripeptide with the ability to effectively buffer copper or copper exporting ATPase. An efficient copper detoxification system has been shown to be crucial for the virulence of pathogenic fungi (Ding et al., 2013; Smith et al., 2017). In *Cryptococcus neoformans*, the two metallothionein-encoding genes ctm1 and cmt2 showed highly elevated expression in response to copper excess (Ding et al., 2011).

1.4 Nutritional immunity: the battle for nutrient metals at the host-pathogen interface

A process known as "nutritional immunity" is part of the innate immune response, where the host deliberately limits the metals from the pathogen. This phenomenon has been described mainly concerning iron, which is particularly important in various microbial infections (Cassat and Skaar, 2012; Haley and Skaar, 2012; Nobles and Maresso, 2011; Ong et al., 2006). Indeed, the mammalian host redistributes its iron stores when confronted with infection and inflammation in an attempt to deprive the challenged intracellular or extracellular pathogens of iron.

This was first noticed in the 1940s by Caroline and Schade, who identified an iron-binding protein in egg white and described its antimicrobial function in sequestering iron from pathogens, referring to it as ovotransferrin (Schade and Caroline, 1946, 1944). In mammals, iron is mainly complexed in heme in hemoglobin, the iron-containing metalloprotein for oxygen transport in red blood cells and myoglobin in muscles, respectively, or free non-heme iron is mostly bound to transferrin, which delivers iron to cells via a specific receptor in the endosome, where iron is released from transferrin due to the acidic pH. Alternatively, iron is stored in ferritin, a globular intracellular protein with a binding capacity of up to 4500 iron atoms. Another iron-transporting protein closely related to transferrin, lactoferrin, is expressed during infection but does not release iron even at much more acidic pHs, e.g. 3.5, to ensure iron sequestration during infection when the pH is generally reduced in infected tissues. In conclusion, all these proteins described above ensure that almost all iron in mammals is bound so its availability to a pathogen is limited (Murdoch and Skaar, 2022).

Nutritional immunity is very challenging for pathogenic fungi such as *Candida albicans*, an important opportunistic human pathogen. This pathogen starts its route in a human host in the gastrointestinal tract of a human host, where there is a relatively high concentration of iron due to unabsorbed iron from the diet (McCance and Widdowson, 1938; Miret et al., 2003), but then when it disseminates to the bloodstream, where the immune system reacts and intentionally sequesters the iron (Martin et al., 1987).

However, pathogens have evolved several mechanisms to “steal” iron despite its sequestration (Palmer and Skaar, 2016). One of the possible strategies is to use the siderophores, low molecular weight molecules with the ability to chelate iron in its oxidized form with higher affinity than lactoferrin or transferrin (Schalk, 2008). The siderophore-Fe complex is recognized, for example, by the ATP-binding cassette of the ABC transporter family, which facilitates the transport into the cell. When the siderophore-Fe complex is inside the cell, iron is released by the reduction or degradation of the siderophore. This mechanism is mainly common in bacterial or fungal pathogens. Another strategy is the acquisition of heme by specific heme receptors or hemophores, proteins that complex extracellular heme and that are functionally similar to siderophores (Cescau et al., 2007; Fabian et al., 2009). The release of iron from the tetrapyrrole ring inside the cell occurs due to the activity of heme oxygenase (Kim et al., 2006; Sutak et al., 2008). Another described strategy is the utilization of iron-containing proteins such as transferrin or ferritin; this mechanism usually also requires specific receptors. At first, the whole protein is firstly transported to the lysosome where it is digested and the released iron is then transported to the cytosol (Kariuki et al., 2019). This strategy is common, for example, in important pathogens such as *Entamoeba histolytica* or *Trypanosoma brucei* (López-Soto et al., 2009; Sehgal et al., 2012; Verma et al., 2015). The last mechanism discussed here is the reductive iron uptake from the ferric complexes, which was first described in *Saccharomyces cerevisiae*. The first step of this mechanism involves ferric reductases at the plasma membrane, which can reduce a wide variety of Fe^{3+} sources (Askwith et al., 1994; Lesuisse and Labbe, 1994). The next step in yeast is accomplished by the Fet3-Ftr1 complex, which contains a multicopper ferroxidase and a permease. This complex facilitates the reoxidation of iron Fe^{2+} (Fet3) and the subsequent transport of iron into the cell (Ftr1) (Askwith et al., 1994; Philpott, 2006; Stearman et al., 1996).

1.5 ***Naegleria spp.***

Naegleria is a unicellular organism belonging to the supergroup Excavate inhabiting freshwater environments such as lakes, ponds, and hot springs, as well as soil and mud. Members of the genus *Naegleria* were isolated from around the world indicating their abundant distribution (de Jonckheere, 2002; Fulton, 1993). This organism occurs in three different morphological stages: a) feeding and dividing amoeboid stage (trophozoite), a feeding and dividing form; b) transient flagellate; c) inactive resistant cyst (Fritz-Laylin et al., 2011, 2010; Fulton, 1993). The genus *Naegleria* consists of 47 described species, but the best known and studied are non-pathogenic *Naegleria gruberi*, considered a model organism for studying the "most famous" thermophilic pathogen named *Naegleria fowleri*, which is the only *Naegleria* which can infect the human host (de Jonckheere, 2011).

This organism is normally dependent on bacteria as a source of nutrients, like its other relatives, but when contaminated water enters the human nasal cavity, the trophozoite of *N. fowleri* is able to attach to the nasal mucosa, and from there migrate along the olfactory nerves and across the olfactory bone separating the nasal cavity from the cranial cavity (Grace et al., 2015; Siddiqui et al., 2016). Once the trophozoites penetrate the cranial cavity, they cause extensive inflammatory damage to the nervous system, leading to cerebral edema and, in more than 95% of cases, death of the patient (Jarolim et al., 2000; Visvesvara et al., 2007). The disease caused by *N. fowleri* is known as primary amoebic meningoencephalitis. The first non-specific symptoms appear approximately 5 days after infection. These usually include headache, fever, and malaise, followed by neck stiffness, loss of stability, and hallucinations leading to coma and death approximately 5 days after the first symptoms appear (Baig, 2015). A wide range of antifungals and antibiotics are used to treat PAM, with amphotericin B and miltefosine currently being the most commonly used and partially effective drugs. Unfortunately, the ability of these agents to cross the blood-brain barrier into the central nervous system is low (Monogue et al., 2020; Nau et al., 2010; Roy et al., 2015; Vogelsinger et al., 2006).

1.5.1 Naegleria metabolism

Naegleria possesses a unique metabolism. Even though the amoeba is thought to be fully aerobic, traits common to anaerobic organisms have been identified in its genome leading to a possible ability to alternate between aerobic and anaerobic metabolism (Fritz-Laylin et al., 2010; Opperdoes et al., 2011). One of these marks is Fe-Fe hydrogenase and the other three enzymes important for its assembly. All four proteins were predicted with the presence of N-terminal mitochondrial targeting signals, however, data presented by Tsaousis et al. 2014 provide evidence of fully functional Fe-Fe hydrogenase localized in the cytosol. Fe-Fe hydrogenases are typically localized in hydrogenosomes, mitochondria-like organelles found in anaerobic organisms such as flagellates, fungi, and ciliates. However, other protists such as *Entamoeba histolytica*, *Giardia intestinalis,* and *Trichomonas vaginalis*, also possess hydrogenase localized in the cytosol (Lloyd et al., 2002; Nixon et al., 2003; Smutná et al., 2022). *Naegleria* has a full set of mitochondrial and nuclear genes that encode the complete Krebs cycle and the respiration chain, with a few differences compared to other eukaryotes, such as the possession of a glucokinase instead of a hexokinase and the presence of a PPi-dependent phosphofructokinase in addition to the classical pyruvate kinase. *Naegleria* also possesses parts of the branched ETC, such as AOX and NDH2 (Fritz-Laylin et al., 2011, 2010), which explains the fact that respiration (oxygen consumption) is not fully inhibited by the addition of KCN (Cantoni et al., 2022; Weik and John, 1979). Given the enzyme repertoire and its natural water habitat of *Naegleria*, one would expect glucose to be the main source of energy for this amoeba, as is the case for common aerobes, but a recent study shows a surprising preference for fatty acids as the main substrate over glucose (Bexkens et al., 2018).
The schematic of *N. gruberi* metabolism is depicted in Figure 4.

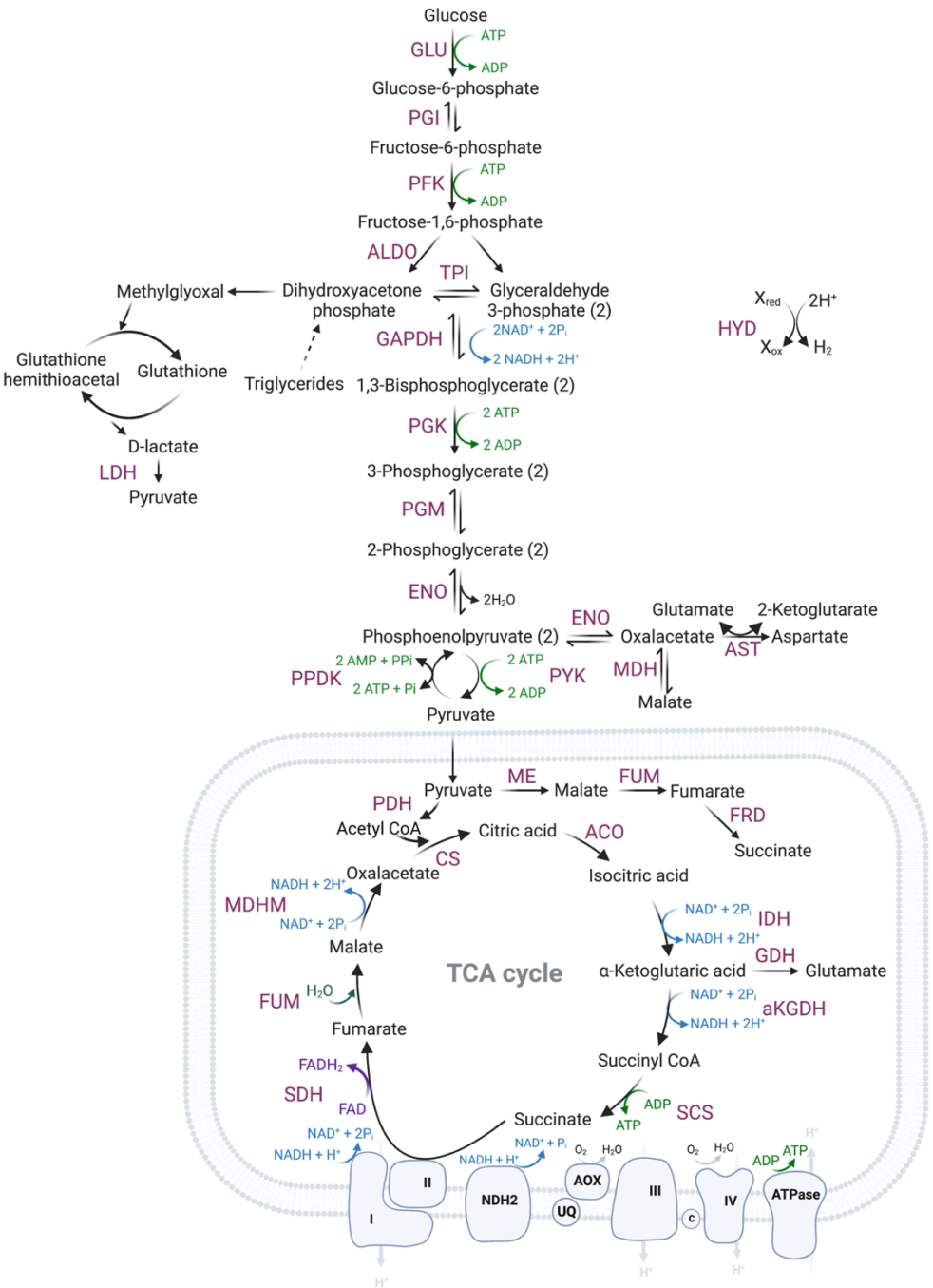

Figure 4 ***Naegleria gruberi*** **metabolism.** Simplified metabolic map based on (Opperdoes, de Jonckheere, and Tielens 2011). Enzymes: GLU, glucokinase; PGI, phosphoglucose isomerase; PFK, PPi-dependent phosphofructokinase; ALDO, fructose-bisphosphate aldolase; TPI, triosephosphate isomerase; GAPDH, glyceraldehyde-3-phosphate dehydrogenase; PGK, phosphoglycerate kinase; PGM, phosphoglycerate mutase; ENO, enolase; PYK, pyruvate kinase; LDH, D-lactate dehydrogenase; PPCK, phosphoenolpyruvate carboxykinase; AST, aspartate aminotransferase; MDH, malate dehydrogenase (cytosolic); PDH, pyruvate dehydrogenase; CS, citrate synthase; ACO, aconitase; IDH, isocitrate dehydrogenase; aKGDH, 2-oxoglutarate dehydrogenase; SCS, succinyl-CoA synthetase; SDH, succinate dehydrogenase; FUM, fumarate hydratase; MDHM, malate dehydrogenase (mitochondrial); PDC, pyruvate decarboxylase; ADH, alcohol dehydrogenase; ME, malic enzyme; GDH, glutamate dehydrogenase; Hyd, [Fe]-hydrogenase; TCA, tricarboxylic acid.

1.6 Trypanosoma brucei

Another model organism discussed in this work is *Trypanosoma brucei*. *T. brucei* is an extracellular parasite with a digenic life cycle involving a tsetse fly vector (*Glossina*) and a mammalian host. *Trypanosoma brucei* is a species complex that includes animal infective subspecies, such as *T. b. brucei*, *T. b. evansi,* and *T. b. equiperdum*, and human infective subspecies, such as *T. b. rhodesiense* and *T. b. gambiense*, causing an insect-borne parasitic infection called human African trypanosomiasis (HAT). The subspecies *T. b. brucei* does not pose a significant risk to humans due to the presence of a trypanolytic factor in human serum (Laveran et al., 1912; Pays et al., 2006; Rifkin, 1991, 1978), however, together with *T. vivax* and *T. congolense* it causes an economically devastating disease in cattle called nagana. Due to the biological requirements of the *Glossina* vectors, nagana, and HAT are mainly found in an area called the 'tse tse zone' located in tropical Africa. While *T. b. rhodesiense* inhabits mainly eastern and southern Africa, *T. b. gambiense* is restricted to west and central Africa. These subspecies do not generally overlap with one exception, namely Uganda, where both subspecies occur together (Picozzi et al., 2005).

1.6.1 Life cycle

The infection of the vector begins when the *Glossina* bites the infected mammalian host and the blood meal containing the bloodstream form (short, stumpy) of *T. brucei* ends in the midgut of the insect. Due to certain stimuli in the midgut, such as increased pH, drop in temperature, etc., the short stumpy form differentiates into early procyclic forms (PF) (Roditi et al., 2016; Shaw et al., 2022) and, after a week, into late PF that start to migrate into the proventriculus (Imhof et al., 2014). In the proventriculus, the late PF transforms into long-dividing epimastigotes, after which asymmetric division occurs and short non-dividing epimastigotes are produced that continue the journey to the salivary glands. The second asymmetric division occurs there and results in the production of non-dividing quiescent metacyclic trypanosomes (Dyer et al., 2013; Rotureau and van den Abbeele, 2013). In these forms, the trypanosomes wait in the saliva to be injected by the tsetse fly into a mammalian host during blood feeding. Once metacyclic infective forms of trypanosomes enter the bloodstream of the host, they rapidly differentiate into long slender bloodstream forms (BF). These forms later differentiate into cell cycle arrested short stumpy forms. This differentiation is population-density dependent, and it is an irreversible

process (MacGregor et al., 2012). The disease is complicated by a unique antigenic variation allowing it to evade the immune system, exploited by long slender BFs. The genome of trypanosomes contains up to 1000 distinct genes for variable surface glycoprotein (VSG) that forms the protective layer on the parasite. While the host immune system starts to produce antibodies against one variant of the VSG, trypanosomes switch VSG expression to another form and create a new layer of VSG (Mugnier et al., 2016).

1.6.2 Trypanosome mitochondria and their metabolic reprogramming

Trypanosomes belong to the group Kinetoplastida, which is characterized by the presence of a dense structure made of DNA localized in a kinetoplast, a specialized part of the cell single mitochondrion of the cell named kinetoplast (C. Brack et al., 1972; Ch. Brack et al., 1972; Riou and Delain, 1969; Riou and Paoletti, 1967). This DNA is referred to as kinetoplast DNA and consists of a network of two types of catenated circular DNA: a few dozen maxi circles and thousands of mini circles. Maxicircles share function with classical mtDNA and encode genes for OXPHOS and ribosomal proteins. Minicircles on the other hand encode tools for RNA editing of some of the maxicircle-encoded mRNA transcripts in mitochondria (Hajduk and Ochsenreiter, 2010; Vickerman, 1965, 1962). The single mitochondrion of this parasite changes both in shape and size during its life cycle (Priest and Hajduk, 1994; Vickerman, 1965). PF possesses strongly enlarged mitochondria forming a complex network with discoid cristae housing the ETC complexes that supply the cell with ATP. On the other hand, the shape of the BF mitochondria looks like a tube that runs from the posterior to the anterior of the cell with an acristate morphology like the promitochondrion of anaerobically grown yeast (Cope and Ali, 2016; Matthews, 2005).

Due to the complex life cycle with different hosts, including different nutrient and oxygen availability, the energy metabolism of trypanosomes also varies greatly (Figueiredo et al., 2017). In the bloodstream of the mammalian host, a high level of glucose is present, whereas in the insect environment, the glucose level is low, but the level of amino acids such as proline is high. Due to this fact, the BF generates ATP predominantly by glycolysis from glucose as the main energy source and instead of being metabolized into lactate or ethanol, most of the pyruvate is excreted and only 1% is converted into the succinate (Creek et al., 2015; Mazet et al., 2013). On the other hand, PF generates ATP by OXPHOS from proline as the main energy source. In addition to the classical electron-transporting I-V complexes, PF trypanosomes also contain the non-energy conserving components of ETC,

the trypanosomal alternative oxidase (TAO), and the NDH2. TAO plays a key role in energy metabolism in BF, where it completely replaces complex IV; TAO protein expression is therefore up to 100-fold higher than in PF (Chaudhuri et al., 2006). TAO is tightly connected to glycolysis processes via the mitochondrial FAD-dependent glycerol-3-phosphate dehydrogenase, which transfers the electrons from glycerol-3-phosphate to ubiquinol, and via TAO, the electrons are transferred to the final electron acceptor, molecular oxygen (Opperdoes et al., 1977). In PF, TAO coexists with the complex IV but contributes only 20 % to cellular respiration (Gnipová et al., 2012).

Another unique feature of BF trypanosomes is the reverse activity of F_oF_1 ATP synthase. Because the ETC complexes that normally translocate protons and contribute to the generation of the proton gradient are not present in this form, the $m\Delta\psi$ necessary for protein translocation and substrate transport is generated by ATP hydrolysis (Schnaufer et al., 2005). In contrast, PF F_oF_1 ATP synthase works in the conventional direction and contributes substantially to the supply of ATP to the cell; moreover, its activity is required for powering motility and development of trypanosomes in the vector (Dewar et al., 2022). Overall, complex V is a key player in the energy metabolism of both forms, although its physiological role is distinctly different.

In addition to the mitochondrial processes, metabolism in glycosome, the peroxisome-related organelle unique for kinetoplastids and diplonemids, varies also during the life cycle. In PF the glycosome contains the first six glycolytic enzymes and in BF even more, seven (Gualdrón-López et al. 2012). Other functions of glycosome are similar to peroxisomal functions, such as purine salvage, beta-oxidation of fatty acids, and ether lipid synthesis. The schematic representation of the carbon source metabolism of BF of *T. brucei* is shown in Figure 5.

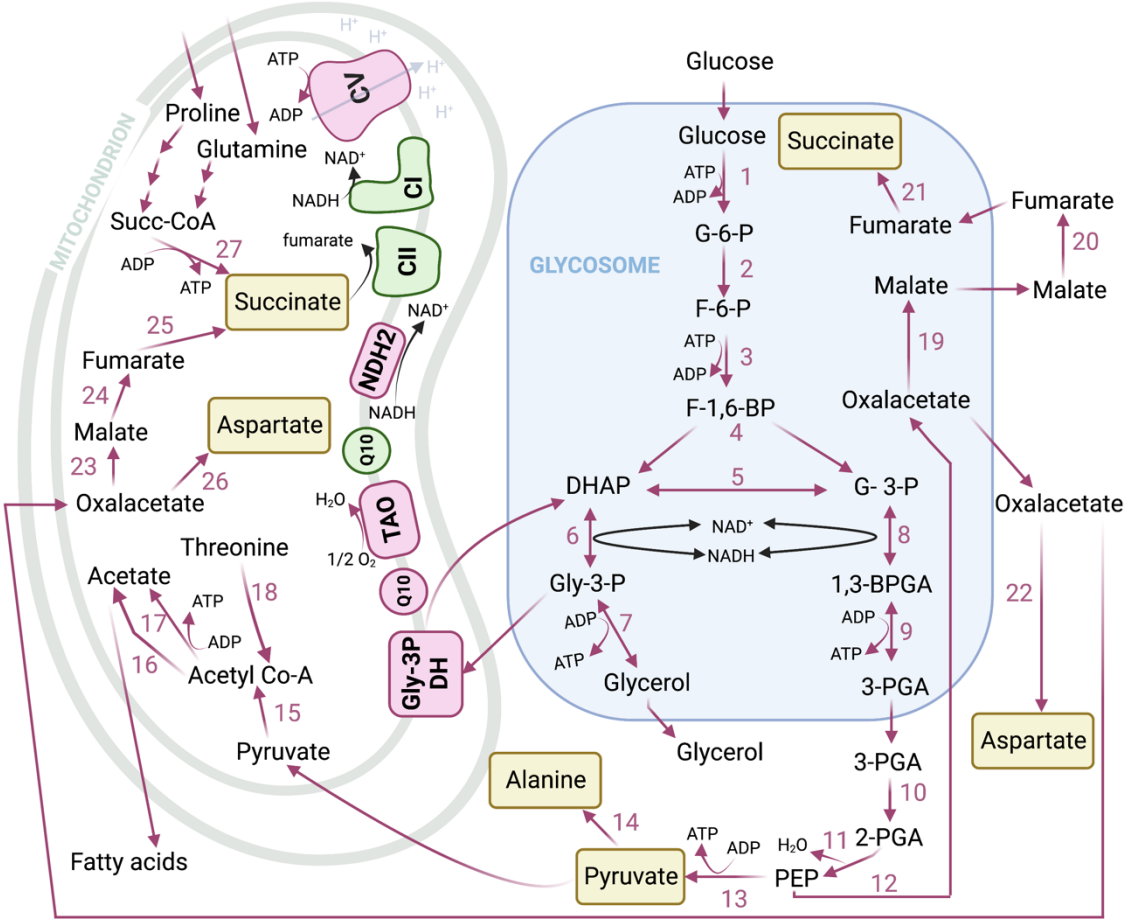

Figure 5 The schematic representation of carbon source metabolism in the bloodstream form of *Trypanosoma brucei*. Simplified scheme of metabolic pathways in glycosome and mitochondria of the BF of *T. brucei* inspired by (Michels et al., 2006; Zíková, 2022; Zíková et al., 2017). Essential components of ETC in BF are depicted in pink, and non-active ones in green color. G-6-P: glucose-6-phosphate, F-6-P: fructose-6-phosphate, F-1,6-BP fructose-1,6-bisphosphate, DHAP: 28ihydroxyacetone phosphate, Gly-3-P: glycerol-3-phosphate, G-3-P: glyceraldehyde-3-phosphate, 1,3BPGA: 1,3-bisphosphoglycerate; 3-PGA, 3-phosphoglycerate, 2-PGA, 2-phosphoglycerate, PEP: phosphoenolpyruvate, Gly-3P DH: FAD-dependent glycerol-3-phosphatedehydrogenase, Q10: ubiquinol pool, TAO: alternative oxidase, NDH2: alternative dehydrogenase, CI-CV: complexes I-V. Enzymes: 1 hexokinase; 2, glucose-6-phosphate isomerase; 3, phosphofructokinase; 4, aldolase; 5, triphosphate isomerase; 6, glycerol-3-phosphate dehydrogenase; 7, glycerol kinase; 8, glyceraldehyde-3-phosphate dehydrogenase; 9, glycosomal phosphoglycerate kinase; 10, phosphoglycerate mutase; 11, enolase; 12, phosphoenolpyruvate carboxykinase; 13, pyruvate kinase; 14, alanine transaminase;15, pyruvate dehydrogenase; 16, acetyl-CoA thioesterase; 17, acetate: succinate CoA-transferase; 18, 2-amino-3-ketobutyrate coenzyme A ligase, threonine dehydrogenase; 19, malate dehydrogenase; 20, fumarase; 21, fumarate reductase; 22, aspartate transaminase; 23, malate dehydrogenase; 24, fumarase; 25, fumarate dehydrogenase; 26, aspartate transaminase, 27, succinyl-CoA synthetase. Created with BioRender.com

2 The main aims of the thesis

1. To characterize the effect of low availability of iron on the mitochondria of *Naegleria fowleri*
2. To elucidate the effect of copper deprivation on the mitochondria of *Naegleria gruberi* and close relative brain-eating amoeba *Naegleria fowleri*
3. To study the effect of mitochondrially targeted Tamoxifen (MitoTam) on the mitochondria of the bloodstream form of *Trypanosoma brucei*

3 The list of publications and the author's contribution

Arbon, D.*, Ženíšková, K., Mach, J., Grechnikova, M., Malych, R., Talacko, P., & Sutak, R. (2020). Adaptive iron utilization compensates for the lack of an inducible uptake system in *Naegleria fowleri* and represents a potential target for therapeutic intervention. PLoS neglected tropical diseases, 14(6), e0007759. https://doi.org/10.1371/journal.pntd.0007759

Iron uptake using ^{55}Fe radioisotope, transferrin uptake, measuring the ferric reductase activity, cell respiration, activity of cytosolic hydrogenase, complex I

Ženíšková, K.*, Grechnikova, M., & Sutak, R. (2022). Copper Metabolism in *Naegleria gruberi* and Its Deadly Relative *Naegleria fowleri*. Frontiers in cell and developmental biology, 10, 853463. https://doi.org/10.3389/fcell.2022.853463

Growth curves, samples preparation for proteomic analysis, proteomic data analysis, ICP-MS sample preparation, RT-qPCR sample preparation, preparation of recombinant DJ-1 protein for antibody, antibody purification, western blot analysis, immunofluorescence microscopy, oxygen consumption measurements, determination of complex I and NDH2 activity, fluorescence microscopy

Arbon, D.*, Ženíšková K.*, Šubrtová, K., Mach, J., Štursa, J., Machado, M., Zahedifard, F., Leštinová, T., Hierro-Yap, C., Neuzil, J., Volf, P., Ganter, M., Zoltner, M., Zíková, A., Werner, L., & Sutak, R. (2022). Repurposing of MitoTam: Novel Anti-Cancer Drug Candidate Exhibits Potent Activity against Major Protozoan and Fungal Pathogens. Antimicrobial agents and chemotherapy, 66(8), e0072722. https://doi.org/10.118/aac.00727-22

Mitochondrial membrane potential measurements using TMRE in live cells and also by a fluorescent probe Safranine O, high-resolution respirometry, western blot analysis, measurements of the ATP/ADP ratio, in situ measurements of ATP levels, ROS determination

**Indicates the first author*

4 Conclusion and perspectives

Mitochondria are often called the powerhouse of the cell because they are the main site of key energy metabolism processes in aerobic eukaryotic organisms. Any disruption of mitochondrial processes or mitochondrial integrity by various stress factors can trigger programmed cell death. Given this fact, mitochondria can decide the fate of the entire cell. Not surprisingly, mitochondria are one of the most studied organelles, and the development of mitochondria-targeted drugs is a major goal for scientists and pharmaceutical companies. My Ph.D. thesis is focused on the effect of various stress factors on the mitochondria of pathogenic protists such as the amoeboflagellate *Naegleria fowleri*, and the BF form of *Trypanosoma brucei brucei*.

4.1 Metabolic adaptation of *Naegleria fowleri* mitochondria to low iron and copper availability

First, we studied the ability of the pathogenic amoeba *Naegleria fowleri* to adapt to the low availability of vital metals iron and copper in the context of a phenomenon called "nutritional immunity" discussed in the introduction part of this thesis.

Our first project focused on the effect of low iron availability on *N. fowleri*. We initially tested several potential mechanisms of iron uptake, then investigated the effect of iron starvation on the acquisition of this metal. Furthermore, the ability of hemin to restore the growth of iron-depleted cells was investigated. Our results showed that *N. fowleri* prefers the reduced form of iron to its oxidized form and the uptake of ferric iron is inhibited by ferrous iron chelator, suggesting the necessity of a reduction step, as has been shown in *Saccharomyces cerevisiae* (van Ho, Ward, and Kaplan 2002; Kosman 2003; Philpott 2006b). Surprisingly, ferric reductase activity and overall iron acquisition in *N. fowleri* are not upregulated to help the amoeba cope with iron deficiency, in contrast to *S. cerevisiae*, which is able to induce its ferric reductase, a key player in reductive iron uptake, several-fold times under iron-deficient conditions (Dancis et al. 1992). Pathogens have different strategies to obtain iron from their host, such as the ability not to “be picky" about the source of iron. For example, the obligate bovine parasite *Tritrichomonas foetus*, which also has a non-inducible iron uptake system, has been shown to be able to process various iron sources such as transferrin, lactoferrin, or siderophores (Sutak et al. 2004; Tachezy et al.

1998). In contrast, our results show that *N. fowleri* does not utilize transferrin as an iron source, and hemin is only partially able to restore growth in severely iron-deprived cultures, suggesting that it is not a preferred iron source.

As tools for genetic manipulation of *N. fowleri* are still lacking, comparative proteomic analysis was used to study the effect of the low availability of both metals on the metabolism of this organism. In the iron-focused project, we observed an interesting trend of downregulation of non-essential iron-containing proteins localized in the cytosol, but at the same time, proteins involved in mitochondrial Fe-S cluster assembly processes were upregulated, probably to maintain ETC. To confirm this hypothesis, the activities of cytosolic hydrogenase and different components of ETC were measured. As previously shown, *N. gruberi* hydrogenase is active and surprisingly localized in the cytosol (Tsaousis et al., 2014). Our measurements show a strong reduction of hydrogenase activity under low iron conditions in its pathogenic relative, suggesting that it does not play a major role in its metabolism. On the other hand, complex I, which is the major electron input to the ETC, was upregulated. In addition, we showed that AOX activity is also significantly affected by low iron availability, balancing the reduced activity of the more iron-demanding complex IV under iron deficiency. Thus, our results support the hypothesis that although *N. fowleri* cannot reflect changes in iron availability at the level of uptake like *Saccharomyces cerevisiae*, there is a metabolic adaptation in favor of mitochondrial processes in which iron is concentrated in mitochondria to maintain key processes such as the ISC or ETC pathway. A similar trend was also observed in our previous work on the non-pathogenic relative *Naegleria gruberi* (Mach et al., 2018).

Another project was focused on copper metabolism in *Naegleria.* This project was built on the knowledge gained during my Master's studies when I studied the effect of low copper conditions on the metabolism of the non-pathogenic amoeba *N. gruberi*. During my Ph.D. project, I studied the effect of copper deficiency on *N. fowleri* and compared the metabolic adaptation of this opportunistic pathogen with my findings from my MSc studies. The comparative proteomic analysis revealed changes at the protein level in cells preincubated with copper excess and two copper chelating agents: the extracellular copper chelator batrocuproinedisulfonic acid (BCS) and the lipophilic, i.e. intracellular, chelator neocuproine. Interestingly, the effect of the two chelating agents differs for these close relatives. While BCS caused significant changes mainly in mitochondrial proteins of *N. gruberi*, such as AOX and DJ-1, *N. fowleri* responded mainly to copper deprivation caused

by the intracellular chelator neocuproine. In contrast to *N. gruberi*, alternative oxidase does not contribute to whole-cell oxygen consumption in *N. fowleri* to such an extent and is not affected by copper deprivation. However, the expression of another component of the branched respiratory chain of this pathogen reflects this limiting condition. Proteomic analysis revealed massive upregulation of rotenone-insensitive NDH2 in the neocuproine-induced low-copper state. This result was confirmed by enzymatic activity measurements as well as using specific antibody produced against this protein after the separation of mitochondrial fractions on native PAGE.
Another aim of this project was to identify the main transporters responsible for supplying *Naegleria* cells with copper. Several CTR protein homologs have been bioinformatically identified in both organisms, but only one of them in each organism functionally complements the yeast mutant strain defective in copper transport and shows a typical localization in the yeast cell membrane after heterologous expression with GFP.

Overall, our results indicate that the ability of *N. fowleri* to adapt to iron and copper limited conditions occurs at the level of alternation of mitochondrial processes. Due to the increased activity of alternative components of branched ETC, this organism compensates for the activity of other metal-dependent ETC members that are compromised by these limiting factors.

4.2 Elucidation of the effect of MitoTam on *Trypanosoma brucei* mitochondria

MitoTam is a mitochondrially targeted tamoxifen, which is a drug used in hormone therapy to treat breast cancer. Conjugation of the drug with the TTP^+ leads to an efficient mitochondrial accumulation driven by the Nernst equation, making MitoTam even more effective than tamoxifen in the fight against breast cancer. MitoTam has been shown to cause inhibition of complex I, resulting in increased ROS and rapid dissipation of $m\Delta\psi$, leading to disruption of mitochondrial supercomplexes which ultimately triggers cell death in cancer cells (Rohlenova et al., 2017). Recently, MitoTam successfully passed a phase 1/1b clinical trial with a positive outcome (MitoTam-01 trial; EudraCT 2017-004441-25).

In our laboratory, we have conducted extensive *in vitro* testing of the MitoTam activity against various eukaryotic pathogens, which revealed strong efficacy against, among others, the BF of the parasite *T. brucei.* The BF of *T. brucei* is a well-studied model organism possessing a single mitochondrion with unique metabolism, including, for instance, a reverse activity of complex V or dispensable activity of complex I (Surve et al., 2012). Our goal was to elucidate the high potency of MitoTam on this organism in light of the claimed mode of action of MitoTam in cancer cells, strongly associated with the activity of complex I. To determine the direct effect on mitochondria, several attributes of mitochondrial processes were analyzed. *T. brucei* cells were pre-incubated for 16 hours or 24 hours at two concentrations of MitoTam corresponding to 2x EC_{50} and 4x EC_{50}, respectively. In agreement with the finding in cancer cells, cellular ROS levels increased in pre-incubated *T. brucei* cells in contrast to mitochondrial ROS levels measured by MitoSox, which decreased, indicating a different mode of action in this parasite. High-resolution measurements of glycerol-3-phosphate-stimulated respiration showed highly inhibited activity of TAO, the only oxygen-consuming component of BF of *T. brucei*. In addition, similar to cancer cells, MitoTam-treated cells also showed a rapid decrease in $m\Delta\psi$. The mitochondrial membrane potential in BF *T. brucei* is generated exclusively by the reverse activity of complex V and is therefore dependent on sufficient ATP levels, which are also significantly reduced after treatment. To clarify whether low ATP levels alone were responsible for this rapid decrease in potential, in situ measurements were performed using the Safranin O probe on ATP-supplemented digitonin-treated cells. However, the $m\Delta\psi$ was extremely low even in the presence of additional ATP. Moreover, the rapid and dose-dependent dissipation of the potential was caused by the addition of MitoTam to untreated cells. These findings suggested a possible inhibitory effect of MitoTam on complex V, similar to the known inhibitor of the F_o part, oligomycin, or simply a physicochemical disruption of the membrane integrity by the drug. The second hypothesis was confirmed by determining membrane integrity on isolated mitochondria using the enzyme activity of the mitochondrial marker enzyme threonine dehydrogenase.

Taken together, our analysis of *T. brucei* mitochondrial function showed a rapid effect of MitoTam on several key processes, which may likely be due to the physicochemical disruption of membrane integrity by the drug. To sum up, our results demonstrate the powerful and promising effect of this drug and highlight that repurposing is a potent tool for discovering new therapeutic strategies to combat various diseases.

5 References

Andreini, C., Bertini, I., Cavallaro, G., Holliday, G.L., Thornton, J.M., 2008. Metal ions in biological catalysis: from enzyme databases to general principles. J Biol Inorg Chem 13, 1205–1218. https://doi.org/10.1007/S00775-008-0404-5

Archibald, F., 1983. *Lactobacillus plantarum*, an organism not requiring iron. FEMS Microbiol Lett 19, 29–32. https://doi.org/10.1111/J.1574-6968.1983.TB00504.X

Askwith, C., Eide, D., Ho, A. van, Bernard, P.S., Li, L., Davis-Kaplan, S., Sipe, D.M., Kaplan, J., 1994. The FET3 gene of *S. cerevisiae* encodes a multicopper oxidase required for ferrous iron uptake. Cell 76, 403–410. https://doi.org/10.1016/0092-8674(94)90346-8

Baig, A.M., 2015. Pathogenesis of amoebic encephalitis: Are the amoebae being credited to an 'inside job' done by the host immune response? Acta Trop 148, 72–76. https://doi.org/10.1016/J.ACTATROPICA.2015.04.022

Baines, C.P., 2010. Role of the Mitochondrion in Programmed Necrosis. Front Physiol 1. https://doi.org/10.3389/FPHYS.2010.00156

Ballinger, S.W., 2005. Mitochondrial dysfunction in cardiovascular disease. Free Radic Biol Med 38, 1278–1295. https://doi.org/10.1016/J.FREERADBIOMED.2005.02.014

Beinert, H., Kennedy, M.C., Stout, C.D., 1996. Aconitase as iron-sulfur protein, enzyme, and iron-regulatory protein. Chem Rev 96, 2335–2373. https://doi.org/10.1021/CR950040Z/ASSET/CR950040Z.FP.PNG_V03

Bexkens, M.L., Zimorski, V., Sarink, M.J., Wienk, H., Brouwers, J.F., de Jonckheere, J.F., Martin, W.F., Opperdoes, F.R., van Hellemond, J.J., Tielens, A.G.M., 2018. Lipids Are the Preferred Substrate of the Protist *Naegleria gruberi*, Relative of a Human Brain Pathogen. Cell Rep 25, 537–543. https://doi.org/10.1016/J.CELREP.2018.09.055

Björklöf, K., Zickermann, V., Finel, M., 2000. Purification of the 45 kDa, membrane bound NADH dehydrogenase of *Escherichia coli* (NDH-2) and analysis of its interaction with ubiquinone analogues. FEBS Lett 467, 105–110. https://doi.org/10.1016/S0014-5793(00)01130-3

Boyer, P.D., 1997. The ATP synthase - a Splendid Molecular Machine. Annu. Rev. Biochem 66, 717–766. https://doi.org/10.1146/annurev.biochem.66.1.717

Brack, C., Delain, E., Riou, G., 1972. Replicating, Covalently Closed, Circular DNA from Kinetoplasts of *Trypanosoma cruzi*. Proceedings of the National Academy of Sciences 69, 1642–1646. https://doi.org/10.1073/PNAS.69.6.1642

Brack, Ch., Delain, E., Riou, G., Festy, B., 1972. Molecular organization of the kinetoplast DNA of *Trypanosoma cruzi* treated with berenil, a DNA interacting drug. J Ultrastruct Res 39, 568–579. https://doi.org/10.1016/S0022-5320(72)90122-0

Brancaccio, D., Gallo, A., Piccioli, M., Novellino, E., Ciofi-Baffoni, S., Banci, L., 2017. [4Fe-4S] cluster assembly in mitochondria and its impairment by copper. J Am Chem Soc 139, 719–730. https://doi.org/10.1021/JACS.6B09567/SUPPL_FILE/JA6B09567_SI_001.PDF

Brandt, U., 2006. Energy Converting NADH: Quinone Oxidoreductase (Complex I). Annu Rev Biochem 75, 69–92. https://doi.org/10.1146/ANNUREV.BIOCHEM.75.103004.142539

Braymer, J.J., Lill, R., 2017. Iron–sulfur cluster biogenesis and trafficking in mitochondria. J Bio Chem 292, 12754–12763. https://doi.org/10.1074/JBC.R117.787101

Brown, S. v., Hosking, P., Li, J., Williams, N., 2006. ATP Synthase Is Responsible for Maintaining Mitochondrial Membrane Potential in Bloodstream Form *Trypanosoma brucei*. Eukaryot Cell 5, 45-53. https://doi.org/10.1128/EC.5.1.45-53.2006

Broxton, C.N., Culotta, V.C., 2016. An Adaptation to Low Copper in *Candida albicans* Involving SOD Enzymes and the Alternative Oxidase. PLoS One 11, e0168400. https://doi.org/10.1371/journal.pone.0168400

Brzezowski, P., Richter, A.S., Grimm, B., 2015. Regulation and function of tetrapyrrole biosynthesis in plants and algae. Biochimica et Biophysica Acta (BBA) - Bioenergetics 1847, 968–985. https://doi.org/10.1016/J.BBABIO.2015.05.007

Burén, S., Jiménez-Vicente, E., Echavarri-Erasun, C., Rubio, L.M., 2020. Biosynthesis of Nitrogenase Cofactors. Chem Rev 120, 4921–4968. https://doi.org/10.1021/ACS.CHEMREV.9B00489/ASSET/IMAGES/LARGE/CR9B00489_0027.JPEG

Bustos, R.I., Jensen, E.L., Ruiz, L.M., Rivera, S., Ruiz, S., Simon, F., Riedel, C., Ferrick, D., Elorza, A.A., 2013. Copper deficiency alters cell bioenergetics and induces mitochondrial fusion through up-regulation of MFN2 and OPA1 in erythropoietic cells. Biochem Biophys Res Commun 437, 426–432. https://doi.org/10.1016/J.BBRC.2013.06.095

Cadonic, C., Sabbir, M.G., Albensi, B.C., 2016. Mechanisms of Mitochondrial Dysfunction in Alzheimer's Disease. Mol Neurobiol 53, 6078–6090. https://doi.org/10.1007/S12035-015-9515-5

Cantoni, D., Osborne, A., Taib, N., Thompson, G., Martín-Escolano, R., Kazana, E., Edrich, E., Brown, I.R., Gribaldo, S., Gourlay, C.W., Tsaousis, A.D., 2022. Localization and functional characterization of the alternative oxidase in *Naegleria*. J Eukaryot Microbiol 69, e12908. https://doi.org/10.1111/JEU.12908

Capaldi, R.A., Aggeler, R., Turina, P., Wilkens, S., 1994. Coupling between catalytic sites and the proton channel in F1F0-type ATPases. Trends Biochem Sci 19, 284–289. https://doi.org/10.1016/0968-0004(94)90006-X

Carroll, J., Fearnley, I.M., Skehel, J.M., Shannon, R.J., Hirst, J., Walker, J.E., 2006. Bovine Complex I Is a Complex of 45 Different Subunits. J Bio Chem 281, 32724–32727. https://doi.org/10.1074/JBC.M607135200

Cassat, J.E., Skaar, E.P., 2012. Metal ion acquisition in *Staphylococcus aureus*: overcoming nutritional immunity. Semin Immunopathol 34, 215–235. https://doi.org/10.1007/S00281-011-0294-4

Cavalli LR, V.-G.M.L.BC., 1997. Diminished tumorigenic phenotype after depletion of mitochondrial DNA. Cell Growth Differ 8,11, 1189–98.

Cenci, U., Moog, D., Curtis, B.A., Tanifuji, G., Eme, L., Lukeš, J., Archibald, J.M., 2016. Heme pathway evolution in kinetoplastid protists. BMC Evol Biol 16, 1–18. https://doi.org/10.1186/S12862-016-0664-6

Cescau, S., Cwerman, H., Létoffé, S., Delepelaire, P., Wandersman, C., Biville, F., 2007. Heme acquisition by hemophores. Biometals 20, 603–613. https://doi.org/10.1007/S10534-006-9050-Y

Chappell, J.B., Crofts, A.R., 1965. Calcium ion accumulation and volume changes of isolated liver mitochondria. Calcium ion-induced swelling. Biochem J 95, 378–386. https://doi.org/10.1042/bj0950378

Chaudhuri, M., Ott, R.D., Hill, G.C., 2006. Trypanosome alternative oxidase: from molecule to function. Trends Parasitol 22, 484–491. https://doi.org/10.1016/j.pt.2006.08.007

Chillappagari, S., Seubert, A., Trip, H., Kuipers, O.P., Marahiel, M.A., Miethke, M., 2010. Copper Stress Affects Iron Homeostasis by Destabilizing Iron-Sulfur Cluster Formation in *Bacillus subtilis*. J Bacteriol 192, 2512–2524. https://doi.org/10.1128/JB.00058-10

Chinopoulos, C., Adam-Vizi, V., 2010. Mitochondria as ATP consumers in cellular pathology. Biochim Biophys Acta Mol Basis Dis 1802, 221–227. https://doi.org/10.1016/J.BBADIS.2009.08.008

Choveaux, D.L., Przyborski, J.M., Goldring, J.P.D., 2012. A *Plasmodium falciparum* copper-binding membrane protein with copper transport motifs. Malar J 11. https://doi.org/10.1186/1475-2875-11-397

Clapham, D.E., 1995. Calcium signaling. Cell 80, 259–268. https://doi.org/10.1016/0092-8674(95)90408-5

Clarkson, A., Bienen, E., Pollakis, G., Grady, R., 1989. Respiration of bloodstream forms of the parasite *Trypanosoma brucei brucei* is dependent on a plant-like alternative oxidase. J Bio Chem 17770–17776.

Cooper, G.M., 2000. The Mechanism of Oxidative Phosphorylation, in: The Cell: A Molecular Approach. 2nd Edition. Sinauer Associates.

Cope, J.R., Ali, I.K., 2016. Primary Amebic Meningoencephalitis: What Have We Learned in the Last Five Years? Curr Infect Dis Rep 18, 31. https://doi.org/10.1007/S11908-016-0539-4

Cori, C.F., Cori, G.T., 1925. The carbohydrate metabolism of tumors: II. changes in the sugar, lactic acid, and CO_2- combining power of blood passing through a tumor. J Biol Chem 65, 397–405. https://doi.org/10.1016/S0021-9258(18)84849-9

Creek, D.J., Mazet, M., Achcar, F., Anderson, J., Kim, D.H., Kamour, R., Morand, P., Millerioux, Y., Biran, M., Kerkhoven, E.J., Chokkathukalam, A., Weidt, S.K., Burgess, K.E.V., Breitling, R., Watson, D.G., Bringaud, F., Barrett, M.P., 2015. Probing the metabolic network in bloodstream-form *Trypanosoma brucei* using untargeted metabolomics with stable isotope labelled glucose. PLoS Pathog 11, 1–25. https://doi.org/10.1371/JOURNAL.PPAT.1004689

Crichton, R.R., Pierre, J.L., 2001. Old Iron, Young Copper: from Mars to Venus. Biometals 2001 14:2 14, 99–112. https://doi.org/10.1023/A:1016710810701

Dancis, A., Yuan, D.S., Haile, D., Askwith, C., Eide, D., Moehle, C., Kaplan, J., Klausner, R.D., 1994. Molecular characterization of a copper transport protein in *S. cerevisiae*: an unexpected role for copper in iron transport. Cell 76, 393–402. https://doi.org/10.1016/0092-8674(94)90345-X

Davis, S., Weiss, M.J., Wong, J.R., Lampidis, T.J., Chen, L.B., 1985. Mitochondrial and plasma membrane potentials cause unusual accumulation and retention of rhodamine 123 by human breast

adenocarcinoma-derived MCF-7 cells. J Biol Chem 260, 13844–13850. https://doi.org/10.1016/s0021-9258(17)38802-6

de Berardinis, R.J., Chandel, N.S., 2016. Fundamentals of cancer metabolism. Sci Adv 2. https://doi.org/10.1126/SCIADV.1600200

de Jonckheere, J.F., 2011. Origin and evolution of the worldwide distributed pathogenic amoeboflagellate *Naegleria fowleri*. Infect Genet and Evol. https://doi.org/10.1016/j.meegid.2011.07.023

de Jonckheere, J.F., 2002. A Century of Research on the Amoeboflagellate Genus Naegleria. Acta Protozool 41, 309–342.

de Vries, S., Grivell, L.A., 1988. Purification and characterization of a rotenone-insensitive NADH:Q6 oxidoreductase from mitochondria of *Saccharomyces cerevisiae*. Eur J Biochem 176, 377–384. https://doi.org/10.1111/J.1432-1033.1988.TB14292.X

Deluca, H.F., Engstrom, G.W., 1961. Calcium uptake by rat kidney mitochondria. Proc Natl Acad Sci U S A 47, 1744–1750. https://doi.org/10.1073/PNAS.47.11.1744

Dewar, C.E., Casas-Sanchez, A., Dieme, C., Crouzols, A., Haines, L.R., Acosta-Serrano, Á., Rotureau, B., Schnaufer, A., 2022. Oxidative Phosphorylation Is Required for Powering Motility and Development of the Sleeping Sickness Parasite *Trypanosoma brucei* in the Tsetse Fly Vector. mBio 13. https://doi.org/10.1128/MBIO.02357-21

Ding, C., Festa, R.A., Chen, Y.L., Espart, A., Palacios, Ò., Espín, J., Capdevila, M., Atrian, S., Heitman, J., Thiele, D.J., 2013. *Cryptococcus neoformans* copper detoxification machinery is critical for fungal virulence. Cell Host Microbe 13, 265–276. https://doi.org/10.1016/j.chom.2013.02.002

Ding, C., Yin, J., Tovar, E.M.M., Fitzpatrick, D.A., Higgins, D.G., Thiele, D.J., 2011. The copper regulon of the human fungal pathogen *Cryptococcus neoformans* H99. Mol Microbiol 81, 1560–76. https://doi.org/10.1111/j.1365-2958.2011.07794.x

Dröge, W., 2002. Free radicals in the physiological control of cell function. Physiol Rev 82, 47–95. https://doi.org/10.1152/PHYSREV.00018.2001

Duarte, M., Ferreira, C., Khandpur, G.K., Flohr, T., Zimmermann, J., Castro, H., Herrmann, J.M., Morgan, B., Tomás, A.M., 2021. Leishmania type II dehydrogenase is essential for parasite viability irrespective of the presence of an active complex I. Proc Natl Acad Sci U S A 118. https://doi.org/10.1073/PNAS.2103803118/-/DCSUPPLEMENTAL

Duchen, M.R., 2004. Mitochondria in health and disease: Perspectives on a new mitochondrial biology. Mol Aspects Med 25, 365–451. https://doi.org/10.1016/j.mam.2004.03.001

Dyer, N.A., Rose, C., Ejeh, N.O., Acosta-Serrano, A., 2013. Flying tryps: survival and maturation of trypanosomes in tsetse flies. Trends Parasitol 29, 188–196. https://doi.org/10.1016/J.PT.2013.02.003

Fabian, M., Solomaha, E., Olson, J.S., Maresso, A.W., 2009. Heme Transfer to the Bacterial Cell Envelope Occurs via a Secreted Hemophore in the Gram-positive Pathogen *Bacillus anthracis*. J Biol Chem 284, 32138-48. https://doi.org/10.1074/JBC.M109.040915

Fantin, V.R., St-Pierre, J., Leder, P., 2006. Attenuation of LDH-A expression uncovers a link between glycolysis, mitochondrial physiology, and tumor maintenance. Cancer Cell 9, 425–434. https://doi.org/10.1016/J.CCR.2006.04.023

Figueiredo, L.M., Smith, T.K., Bringaud, F., Nolan, D.P., 2017. Metabolic reprogramming during the *Trypanosoma brucei* life cycle. F1000Res 6. https://doi.org/10.12688/F1000RESEARCH.10342.2

Freibert, S.A., Goldberg, A. v., Hacker, C., Molik, S., Dean, P., Williams, T.A., Nakjang, S., Long, S., Sendra, K., Bill, E., Heinz, E., Hirt, R.P., Lucocq, J.M., Embley, T.M., Lill, R., 2017. Evolutionary conservation and in vitro reconstitution of microsporidian iron–sulfur cluster biosynthesis. Nat Commun 2017 8:1 8, 1–12. https://doi.org/10.1038/ncomms13932

Frey, P.A., Reed, G.H., 2012. The ubiquity of iron. ACS Chem. Biol. 7, 1477–1481. https://doi.org/10.1021/cb300323q

Friedrich, T., Steinmüller, K., Weiss, H., 1995. The proton-pumping respiratory complex I of bacteria and mitochondria and its homologue in chloroplasts. FEBS Lett 367, 107–111. https://doi.org/10.1016/0014-5793(95)00548-N

Fritz-Laylin, L.K., Ginger, M.L., Walsh, C., Dawson, S.C., Fulton, C., 2011. The Naegleria genome: A free-living microbial eukaryote lends unique insights into core eukaryotic cell biology. Res Microbiol 162, 607–618. https://doi.org/10.1016/j.resmic.2011.03.003

Fritz-Laylin, L.K., Prochnik, S.E., Ginger, M.L., Dacks, J.B., Carpenter, M.L., Field, M.C., Kuo, A., Paredez, A., Chapman, J., Pham, J., Shu, S., Neupane, R., Cipriano, M., Mancuso, J., Tu, H., Salamov, A., Lindquist, E., Shapiro, H., Lucas, S., Grigoriev, I. v., Cande, W.Z., Fulton, C., Rokhsar, D.S., Dawson, S.C., 2010. The Genome of *Naegleria gruberi* Illuminates Early Eukaryotic Versatility. Cell 140, 631–642. https://doi.org/10.1016/j.cell.2010.01.032

Fukai, T., Ushio-Fukai, M., 2011. Superoxide dismutases: role in redox signaling, vascular function, and diseases. Antioxid Redox Signal 15, 1583–1606. https://doi.org/10.1089/ARS.2011.3999

Fulton, C., 1993. Naegleria: A Research Partner For Cell and Developmental Biology. J Eukaryot Microbiol 40, 520–532. https://doi.org/10.1111/j.1550-7408.1993.tb04945.x

Gaetke, L.M., Chow, C.K., 2003. Copper toxicity, oxidative stress, and antioxidant nutrients. Toxicology 189. 147-163.https://doi.org/10.1016/S0300-483X(03)00159-8

Gane, E.J., Weilert, F., Orr, D.W., Keogh, G.F., Gibson, M., Lockhart, M.M., Frampton, C.M., Taylor, K.M., Smith, R.A.J., Murphy, M.P., 2010. The mitochondria-targeted anti-oxidant mitoquinone decreases liver damage in a phase II study of hepatitis C patients. Liver Int 30, 1019–1026. https://doi.org/10.1111/J.1478-3231.2010.02250.X

Garcia-Santamarina, S., Uzarska, M.A., Festa, R.A., Lill, R., Thiele, D.J., 2017. *Cryptococcus neoformans* Iron-Sulfur Protein Biogenesis Machinery Is a Novel Layer of Protection against Cu Stress. mBio 8, e01742-17. https://doi.org/10.1128/mBio.01742-17

Gaude, E., Frezza, C., 2016. Tissue-specific and convergent metabolic transformation of cancer correlates with metastatic potential and patient survival. Nat Commun 2016 7:1 7, 1–9. https://doi.org/10.1038/ncomms13041

Giorgi, C., Agnoletto, C., Bononi, A., Bonora, M., de Marchi, E., Marchi, S., Missiroli, S., Patergnani, S., Poletti, F., Rimessi, A., Suski, J.M., Wieckowski, M.R., Pinton, P., 2012. Mitochondrial

calcium homeostasis as potential target for mitochondrial medicine. Mitochondrion 12, 77–85. https://doi.org/10.1016/J.MITO.2011.07.004

Gnipová, A., Panicucci, B., Paris, Z., Verner, Z., Horváth, A., Lukeš, J., Zíková, A., 2012. Disparate phenotypic effects from the knockdown of various *Trypanosoma brucei* cytochrome c oxidase subunits. Mol Biochem Parasitol 184, 90–98. https://doi.org/10.1016/J.MOLBIOPARA.2012.04.013

Goldberg, A. v., Molik, S., Tsaousis, A.D., Neumann, K., Kuhnke, G., Delbac, F., Vivares, C.P., Hirt, R.P., Lill, R., Embley, T.M., 2008. Localization and functionality of microsporidian iron–sulphur cluster assembly proteins. Nature 2008 452:7187 452, 624–628. https://doi.org/10.1038/nature06606

Gomes, C.M., Bandeiras, T.M., Teixeira, M., 2001. A new type-II NADH dehydrogenase from the archaeon Acidianus ambivalens: characterization and in vitro reconstitution of the respiratory chain. J Bioenerg Biomembr 33, 1–8. https://doi.org/10.1023/A:1005630221892

Gottschalk, B., Madreiter-Sokolowski, C.T., Graier, W.F., 2022. Cristae junction as a fundamental switchboard for mitochondrial ion signaling and bioenergetics. Cell Calcium 101, 102517. https://doi.org/10.1016/J.CECA.2021.102517

Grace, E., Asbill, S., Virga, K., 2015. *Naegleria fowleri*: Pathogenesis, Diagnosis, and Treatment Options. Antimicrob Agents Chemother 59, 6677-6681. https://doi.org/10.1128/AAC.01293-15

Gualdrón-López, M., Brennand, A., Hannaert, V., Quiñones, W., Cáceres, A.J., Bringaud, F., Concepción, J.L., Michels, P.A.M., 2012. When, how and why glycolysis became compartmentalised in the Kinetoplastea. A new look at an ancient organelle. Int J Parasitol 42, 1–20. https://doi.org/10.1016/J.IJPARA.2011.10.007

Gutman, M., Singer, T.P., Beinert, H., Casida, J.E., 1970. Reaction sites of rotenone, piericidin A, and amytal in relation to the nonheme iron components of NADH dehydrogenase. Proc Natl Acad Sci U S A 65, 763–770. https://doi.org/10.1073/pnas.65.3.763

Hajduk, S., Ochsenreiter, T., 2010. RNA editing in kinetoplastids. http://dx.doi.org/10.4161/rna.7.2.11393 7, 229–236. https://doi.org/10.4161/RNA.7.2.11393

Haley, K.P., Skaar, E.P., 2012. A battle for iron: host sequestration and *Staphylococcus aureus* acquisition. Microbes Infect 14, 217–227. https://doi.org/10.1016/J.MICINF.2011.11.001

Hirst, J., 2013. Mitochondrial Complex I. Annual reviews 82, 551–575. https://doi.org/10.1146/ANNUREV-BIOCHEM-070511-103700

Hoek, J.B., Nicholls, D.G., Williamson, J.R., 1980. Determination of the Mitochondrial Protonmotive Force in Isolated Hepatocytes. J Biol Chem 255, 1458–1464. https://doi.org/10.1016/S0021-9258(19)86052-0

Hunter, G.A., Ferreira, G.C., 2011. Molecular enzymology of 5-Aminolevulinate synthase, the gatekeeper of heme biosynthesis. Biochimica et Biophysica Acta (BBA) - Proteins and Proteomics 1814, 1467–1473. https://doi.org/10.1016/J.BBAPAP.2010.12.015

Huzar, T.F., George, T., Cross, J.M., 2013. Carbon monoxide and cyanide toxicity: etiology, pathophysiology and treatment in inhalation injury. Expert Rev Respir Med 7, 159–170. https://doi.org/10.1586/ERS.13.9

Imhof, S., Knüsel, S., Gunasekera, K., Vu, X.L., Roditi, I., 2014. Social motility of African trypanosomes is a property of a distinct life-cycle stage that occurs early in tsetse fly transmission. PLoS Pathog 10. https://doi.org/10.1371/JOURNAL.PPAT.1004493

Ivannikov, M. v., Macleod, G.T., 2013. Mitochondrial Free Ca^{2+} Levels and Their Effects on Energy Metabolism in *Drosophila* Motor Nerve Terminals. Biophys J 104, 2353. https://doi.org/10.1016/J.BPJ.2013.03.064

Iwata, S., Saynovits, M., Link, T.A., Michel, H., 1996. Structure of a water soluble fragment of the 'Rieske' iron–sulfur protein of the bovine heart mitochondrial cytochrome bc1 complex determined by MAD phasing at 1.5 å resolution. Structure 4, 567–579. https://doi.org/10.1016/S0969-2126(96)00062-7

Jacobson, M.R., Cash, V.L., Weiss, M.C., Laird, N.F., Newton, W.E., Dean, D.R., 1989. Biochemical and genetic analysis of the nifUSVWZM cluster from *Azotobacter vinelandii*. Molecular and General Genetics MGG 1989 219:1 219, 49–57. https://doi.org/10.1007/BF00261156

James, A.M., Cochemé, H.M., Smith, R.A.J., Murphy, M.P., 2005. Interactions of mitochondria-targeted and untargeted ubiquinones with the mitochondrial respiratory chain and reactive oxygen species. Implications for the use of exogenous ubiquinones as therapies and experimental tools. J Biol Chem 280, 21295–21312. https://doi.org/10.1074/JBC.M501527200

Jarolim, K.L., McCosh, J.K., Howard, M.J., John, D.T., 2000. A light microscopy study of the migration of *Naegleria fowleri* from the nasal submucosa to the central nervous system during the early stage of primary amebic meningoencephalitis in mice. J Parasitol 86, 50–55. https://doi.org/10.1645/0022-3395(2000)086[0050:almsot]2.0.co;2

Jensen, E.L., Gonzalez-Ibanez, A.M., Mendoza, P., Ruiz, L.M., Riedel, C.A., Simon, F., Schuringa, J.J., Elorza, A.A., 2019. Copper deficiency-induced anemia is caused by a mitochondrial metabolic reprograming in erythropoietic cells. Metallomics 11, 282–290. https://doi.org/10.1039/c8mt00224j

Johnson, D.C., Dean, D.R., Smith, A.D., Johnson, M.K., 2005. Structure, function, and formation of biological iron-sulfur clusters. Annu Rev Biochem 74, 247–281. https://doi.org/10.1146/ANNUREV.BIOCHEM.74.082803.133518

Kariuki, C.K., Stijlemans, B., Magez, S., 2019. The Trypanosomal Transferrin Receptor of *Trypanosoma brucei*—A Review. Tropical Medicine and Infectious Disease 2019, Vol. 4, Page 126 4, 126. https://doi.org/10.3390/TROPICALMED4040126

Kerscher, S., Dröse, S., Zickermann, V., Brandt, U., 2008. The three families of respiratory NADH dehydrogenases. Results Probl Cell Differ 45, 185–222. https://doi.org/10.1007/400_2007_028

Kim, B.E., Nevitt, T., Thiele, D.J., 2008. Mechanisms for copper acquisition, distribution and regulation. Nature Chemical Biology 2008 4:3 4, 176–185. https://doi.org/10.1038/nchembio.72

Kim, B.E., Turski, M.L., Nose, Y., Casad, M., Rockman, H.A., Thiele, D.J., 2010. Cardiac copper deficiency activates a systemic signaling mechanism that communicates with the copper acquisition and storage organs. Cell Metab 11, 353–363. https://doi.org/10.1016/j.cmet.2010.04.003

Kim, D., Yukl, E.T., Moënne-Loccoz, P., Ortiz De Montellano, P.R., 2006. Fungal heme oxygenases: Functional expression and characterization of Hmx1 from *Saccharomyces cerevisiae* and CaHmx1 from *Candida albicans*. Biochemistry 45, 14772–14780. https://doi.org/10.1021/BI061429R

Knight, S.A.B., Labbé, S., Kwon, L.F., Kosman, D.J., Thiele, D.J., 1996. A widespread transposable element masks expression of a yeast copper transport gene. Genes Dev 10, 1917–1929. https://doi.org/10.1101/GAD.10.15.1917

Koch, G.L.E., 1990. The endoplasmic reticulum and calcium storage. Bioessays 12, 527–531. https://doi.org/10.1002/BIES.950121105

Kořený, L., Oborník, M., Lukeš, J., 2013. Make It, Take It, or Leave It: Heme Metabolism of Parasites. PLoS Pathog 9, e1003088. https://doi.org/10.1371/JOURNAL.PPAT.1003088

Kroemer, G., 2006. Mitochondria in cancer. Oncogene 25, 4630–4632. https://doi.org/10.1038/SJ.ONC.1209589

Kroemer, G., Reed, J.C., 2000. Mitochondrial control of cell death. Nat Med 6, 513–519. https://doi.org/10.1038/74994

Laveran, Alphonse, Laveran, Alphonse, Mesnil, F., 1912. Trypanosomes et trypanosomiases / par A. Laveran et F. Mesnil, [s.n.], Paris : Masson et Cie. https://doi.org/10.5962/bhl.title.939

Lee, O., O'Brien, P.J., 2010. Modifications of Mitochondrial Function by Toxicants. Comprehensive Toxicology: Second Edition 1–14, 411–445. https://doi.org/10.1016/B978-0-08-046884-6.00119-6

Lemasters, J.J., Nieminen, A.L., Qian, T., Trost, L.C., Elmore, S.P., Nishimura, Y., Crowe, R.A., Cascio, W.E., Bradham, C.A., Brenner, D.A., Herman, B., 1998. The mitochondrial permeability transition in cell death: a common mechanism in necrosis, apoptosis and autophagy. Biochim Biophys Acta 1366, 177–196. https://doi.org/10.1016/S0005-2728(98)00112-1

Lesuisse, E., Labbe, P., 1994. Reductive Iron Assimilation in *Saccharomyces cerevisiae*, in: Metal Ions in Fungi. CRC Press, pp. 149–178. https://doi.org/10.1201/9781003067221-5

Lichtshtein, D., Kaback, H.R., Blume, A.J., 1979. Use of a lipophilic cation for determination of membrane potential in neuroblastoma-glioma hybrid cell suspensions. Proc Natl Acad Sci U S A 76, 650. https://doi.org/10.1073/PNAS.76.2.650

Lill, R., Dutkiewicz, R., Freibert, S.A., Heidenreich, T., Mascarenhas, J., Netz, D.J., Paul, V.D., Pierik, A.J., Richter, N., Stümpfig, M., Srinivasan, V., Stehling, O., Mühlenhoff, U., 2015. The role of mitochondria and the CIA machinery in the maturation of cytosolic and nuclear iron–sulfur proteins. Eur J Cell Biol 94, 280–291. https://doi.org/10.1016/J.EJCB.2015.05.002

Lin, S.S., Gross, U., Bohne, W., 2011. Two internal type II NADH dehydrogenases of *Toxoplasma gondii* are both required for optimal tachyzoite growth. Mol Microbiol 82, 209–221. https://doi.org/10.1111/J.1365-2958.2011.07807.X

Liou, G.Y., Storz, P., 2010. Reactive oxygen species in cancer. Free Radic Res 44, 479–496. https://doi.org/10.3109/10715761003667554

Lloyd, D., Ralphs, J.R., Harris, J.C., 2002. *Giardia intestinalis*, a eukaryote without hydrogenosomes, produces hydrogen. Microbiology (N Y) 148, 727–733. https://doi.org/10.1099/00221287-148-3-727

Loiseau, L., Ollagnier-De Choudens, S., Lascoux, D., Forest, E., Fontecave, M., Barras, F., 2005. Analysis of the heteromeric CsdA-CsdE cysteine desulfurase, assisting Fe-S cluster biogenesis in *Escherichia col*i. J Biol Chem 280, 26760–26769. https://doi.org/10.1074/jbc.M504067200

López-Soto, F., González-Robles, A., Salazar-Villatoro, L., León-Sicairos, N., Piña-Vázquez, C., Salazar, E.P., de la Garza, M., 2009. *Entamoeba histolytica* uses ferritin as an iron source and internalises this protein by means of clathrin-coated vesicles. Int J Parasitol 39, 417–426. https://doi.org/10.1016/J.IJPARA.2008.08.010

Luo, Y., Ergenekan, C.E., Fischer, J.T., Tan, M.L., Ichiye, T., 2010. The Molecular Determinants of the Increased Reduction Potential of the Rubredoxin Domain of Rubrerythrin Relative to Rubredoxin. Biophys J 98, 560–568. https://doi.org/10.1016/J.BPJ.2009.11.006

Luttik, M., Overkamp, K., Kötter, P., de Vries, S., van Dijken, J., JT, P., 1998. The *Saccharomyces cerevisiae* NDE1 and NDE2 genes encode separate mitochondrial NADH dehydrogenases catalyzing the oxidation of cytosolic NADH. J Biol Chem 273, 24529–24534. https://doi.org/10.1074/JBC.273.38.24529

MacGregor, P., Szöo'R, B., Savill, N.J., Matthews, K.R., 2012. Trypanosomal immune evasion, chronicity and transmission: an elegant balancing act. Nat Rev Microbiol 10, 431–438. https://doi.org/10.1038/NRMICRO2779

Mach, J., Bíla, J., Ženíšková, K., Arbon, D., Malych, R., Glavanakovová, M., Nývltová, E., Sutak, R., 2018. Iron economy in *Naegleria gruberi* reflects its metabolic flexibility. Int J Parasitol. https://doi.org/10.1016/j.ijpara.2018.03.005

Macomber, L., Imlay, J.A., 2009. The iron-sulfur clusters of dehydratases are primary intracellular targets of copper toxicity. Proc Natl Acad Sci U S A 106, 8344. https://doi.org/10.1073/PNAS.0812808106

Madar, I., Anderson, J.H., Szabo, Z., Scheffel, U., Kao, P.F., Ravert, H.T., Dannals, R.F., 1999. Enhanced Uptake of [11C]TPMP in Canine Brain Tumor: A PET Study. J Nuc Med 40, 1180–1185.

Magda, D., Lecane, P., Prescott, J., Thiemann, P., Ma, X., Dranchak, P.K., Toleno, D.M., Ramaswamy, K., Siegmund, K.D., Hacia, J.G., 2008. mtDNA depletion confers specific gene expression profiles in human cells grown in culture and in xenograft. BMC Genomics 9, 521. https://doi.org/10.1186/1471-2164-9-521

Maio, N., Rouault, T.A., 2020. Outlining the Complex Pathway of Mammalian Fe-S Cluster Biogenesis. Trends Biochem Sci 45, 411–426. https://doi.org/10.1016/J.TIBS.2020.02.001

Manbir, Singh, P., Kumari, A., Gupta, K.J., 2022. Alternative oxidase plays a role in minimizing ROS and RNS produced under salinity stress in *Arabidopsis thaliana*. Physiol Plant 174. https://doi.org/10.1111/PPL.13649

Maret, W., 2010. Metalloproteomics, metalloproteomes, and the annotation of metalloproteins. Metallomics 2, 117–125. https://doi.org/10.1039/B915804A

Margulis, L., 1996. Archaeal-eubacterial mergers in the origin of Eukarya: phylogenetic classification of life. Proc Natl Acad Sci U S A 93, 1071. https://doi.org/10.1073/PNAS.93.3.1071

Martin, R.B., Savory, J., Brown, S., Bertholf, R.L., Wills, M.R., 1987. Transferrin binding of Al3+ and Fe3+. Clin Chem 33, 405–407. https://doi.org/10.1093/CLINCHEM/33.3.405

Martínez-Reyes, I., Chandel, N.S., 2020. Mitochondrial TCA cycle metabolites control physiology and disease. Nat Commun 11. https://doi.org/10.1038/S41467-019-13668-3

Maryon, E.B., Molloy, S.A., Zimnicka, A.M., Kaplan, J.H., 2007. Copper entry into human cells: Progress and unanswered questions, in: BioMetals. pp. 355–364. https://doi.org/10.1007/s10534-006-9066-3

Matthews, K.R., 2005. The developmental cell biology of Trypanosoma brucei. J Cell Sci 118, 283. https://doi.org/10.1242/JCS.01649

Mazet, M., Morand, P., Biran, M., Bouyssou, G., Courtois, P., Daulouède, S., Millerioux, Y., Franconi, J.M., Vincendeau, P., Moreau, P., Bringaud, F., 2013. Revisiting the Central Metabolism of the Bloodstream Forms of *Trypanosoma brucei*: Production of Acetate in the Mitochondrion Is Essential for Parasite Viability. PLoS Negl Trop Dis 7. https://doi.org/10.1371/JOURNAL.PNTD.0002587

McCance, R.A., Widdowson, E.M., 1938. The absorption and excretion of iron following oral and intravenous administration. J Physiol 94, 148–154. https://doi.org/10.1113/JPHYSIOL.1938.SP003669

McCormack, J.G., Halestrap, A.P., Denton, R.M., 1990. Role of calcium ions in regulation of mammalian intramitochondrial metabolism. Physiol Rev 70, 391–425. https://doi.org/10.1152/PHYSREV.1990.70.2.391

McDonald, A.E., 2009. Alternative oxidase: what information can protein sequence comparisons give us? Physiol Plant 137, 328–341. https://doi.org/10.1111/J.1399-3054.2009.01242.X

McDonald, A.E., Vanlerberghe, G.C., 2006. Origins, evolutionary history, and taxonomic distribution of alternative oxidase and plastoquinol terminal oxidase. Comp Biochem Physiol Part D Genomics Proteomics 1, 357–364. https://doi.org/10.1016/J.CBD.2006.08.001

McDonald, A.E., Vanlerberghe, G.C., Staples, J.F., 2009a. Alternative oxidase in animals: unique characteristics and taxonomic distribution. Journal of Experimental Biology 212, 2627–2634. https://doi.org/10.1242/JEB.032151

Mcmanus, M.J., Murphy, M.P., Franklin, J.L., 2011. The Mitochondria-Targeted Antioxidant MitoQ Prevents Loss of Spatial Memory Retention and Early Neuropathology in a Transgenic Mouse Model of Alzheimer's Disease. The Journal of Neuroscience 31, 15703. https://doi.org/10.1523/JNEUROSCI.0552-11.2011

Melo, A.M.P., Bandeiras, T.M., Teixeira, M., 2004aa. New Insights into Type II NAD(P)H:Quinone Oxidoreductases. Microbiology and Molecular Biology Reviews 68, 603-616. https://doi.org/10.1128/MMBR.68.4.603-616.2004

Melo, A.M.P., Duarte, M., Videira, A., 1999. Primary structure and characterisation of a 64 kDa NADH dehydrogenase from the inner membrane of *Neurospora crassa* mitochondria. Biochim Biophys Acta 1412, 282–287. https://doi.org/10.1016/S0005-2728(99)00072-9

Michels, P.A.M., Bringaud, F., Herman, M., Hannaert, V., 2006. Metabolic functions of glycosomes in trypanosomatids. Biochim Biophys Acta 1763, 1463–1477. https://doi.org/10.1016/J.BBAMCR.2006.08.019

Miller, C.N., Jossé, L., Tsaousis, A.D., 2018. Localization of Fe-S Biosynthesis Machinery in *Cryptosporidium parvum* Mitosome. J Eukaryot Microbiol 65, 913–922. https://doi.org/10.1111/JEU.12663

Miret, S., Simpson, R.J., McKie, A.T., 2003. Physiology and molecular biology of dietary iron absorption. Annu Rev Nutr 23, 283–301. https://doi.org/10.1146/ANNUREV.NUTR.23.011702.073139

Mitchell, P., Moyle, J., 1969. Estimation of Membrane Potential and pH Difference across the Cristae Membrane of Rat Liver Mitochondria. Eur J Biochem 7, 471–484. https://doi.org/10.1111/J.1432-1033.1969.TB19633.X

Møller, I.M., Palmer, J.M., 1982. Direct evidence for the presence of a rotenone-resistant NADH dehydrogenase on the inner surface of the inner membrane of plant mitochondria. Physiol Plant 54, 267–274. https://doi.org/10.1111/J.1399-3054.1982.TB00258.X

Monogue, M.L., Watson, D., Alexander, J.S., Cavuoti, D., Doyle, L.M., Wang, M.Z., Prokesch, B.C., 2020. Minimal Cerebrospinal Fluid Concentration of Miltefosine despite Therapeutic Plasma Levels during the Treatment of Amebic Encephalitis. Antimicrob Agents Chemother 64. https://doi.org/10.1128/AAC.01127-19

Moore, A.L., Shiba, T., Young, L., Harada, S., Kita, K., Ito, K., 2013. Unraveling the heater: new insights into the structure of the alternative oxidase. Annu Rev Plant Biol 64, 637–663. https://doi.org/10.1146/ANNUREV-ARPLANT-042811-105432

Morais, R., Zinkewich-Péotti, K., Parent, M., Wang, H., Babai, F., Zollinger, M., 1994. Tumor-forming ability in athymic nude mice of human cell lines devoid of mitochondrial DNA. Cancer Res 54, 3889–3896.

Motyčková, A., Voleman, L., Najdrová, V., Marková, L., Benda, M., Dohnálek, V., Janowicz, N., Malych, R., Šuťák, R., Ettema, T.J.G., Svärd, S., Stairs, C.W., Doležal, P., 2022. The late ISC pathway interactome reveals mitosomal-cytoplasmic crosstalk in *Giardia intestinalis*. bioRxiv 2022.08.01.502261. https://doi.org/10.1101/2022.08.01.502261

Mugnier, M.R., Stebbins, C.E., Papavasiliou, F.N., 2016. Masters of Disguise: Antigenic Variation and the VSG Coat in *Trypanosoma brucei*. PLoS Pathog 12, e1005784. https://doi.org/10.1371/JOURNAL.PPAT.1005784

Murdoch, C.C., Skaar, E.P., 2022. Nutritional immunity: the battle for nutrient metals at the host–pathogen interface. Nature Reviews Microbiology 2022 1–14. https://doi.org/10.1038/s41579-022-00745-6

Nau, R., Sörgel, F., Eiffert, H., 2010. Penetration of drugs through the blood-cerebrospinal fluid/blood-brain barrier for treatment of central nervous system infections. Clin Microbiol Rev. https://doi.org/10.1128/CMR.00007-10

Nguyen, K.T., Wu, J.C., Boylan, J.A., Gherardini, F.C., Pei, D., 2007. Zinc Is the Metal Cofactor of *Borrelia burgdorferi* Peptide Deformylase. Arch Biochem Biophys 468, 217. https://doi.org/10.1016/J.ABB.2007.09.023

Nicholls, D.G., 1974. The influence of respiration and ATP hydrolysis on the proton-electrochemical gradient across the inner membrane of rat-liver mitochondria as determined by ion distribution. Eur J Biochem 50, 305–315. https://doi.org/10.1111/J.1432-1033.1974.TB03899.X

Nijtmans, L.G.J., Klement, P., Houštěk, J., van den Bogert, C., 1995. Assembly of mitochondrial ATP synthase in cultured human cells: implications for mitochondrial diseases. Biochimica et Biophysica Acta (BBA) - Molecular Basis of Disease 1272, 190–198. https://doi.org/10.1016/0925-4439(95)00087-9

Nixon, J.E.J., Field, J., McArthur, A.G., Sogin, M.L., Yarlett, N., Loftus, B.J., Samuelson, J., 2003. Iron-dependent hydrogenases of *Entamoeba histolytica* and *Giardia lamblia*: Activity of the recombinant entamoebic enzyme and evidence for lateral gene transfer. Biological Bulletin 204, 1–9. https://doi.org/10.2307/1543490

Nobles, C.L., Maresso, A.W., 2011. The theft of host heme by Gram-positive pathogenic bacteria. Metallomics 3, 788–796. https://doi.org/10.1039/C1MT00047K

Nose, Y., Rees, E.M., Thiele, D.J., 2006. Structure of the Ctr1 copper trans'PORE'ter reveals novel architecture. Trends Biochem Sci 31, 604–607. https://doi.org/10.1016/j.tibs.2006.09.003

Ohnishi, T., 1998. Iron–sulfur clusters/semiquinones in Complex I. Biochimica et Biophysica Acta (BBA) - Bioenergetics 1364, 186–206. https://doi.org/10.1016/S0005-2728(98)00027-9

Ohnishi, T., Nakamaru-Ogiso, E., Ohnishi, S.T., 2010. A new hypothesis on the simultaneous direct and indirect proton pump mechanisms in NADH-quinone oxidoreductase (complex I). FEBS Lett 584, 4131–4137. https://doi.org/10.1016/J.FEBSLET.2010.08.039

Ong, S.T., Shan Ho, J.Z., Ho, B., Ding, J.L., 2006. Iron-withholding strategy in innate immunity. Immunobiology 211, 295–314. https://doi.org/10.1016/J.IMBIO.2006.02.004

Opperdoes, F.R., Borst, P., Bakker, S., Leene, W., 1977. Localization of Glycerol-3-Phosphate Oxidase in the Mitochondrion and Particulate NAD+-Linked Glycerol-3-Phosphate Dehydrogenase in the Microbodies of the Bloodstream Form of *Trypanosoma brucei*. Eur J Biochem 76, 29–39. https://doi.org/10.1111/J.1432-1033.1977.TB11567.X

Opperdoes, F.R., de Jonckheere, J.F., Tielens, A.G.M., 2011. *Naegleria gruberi metabolism*. Int J Parasitol 41, 915–924. https://doi.org/10.1016/J.IJPARA.2011.04.004

Orrenius, S., Gogvadze, V., Zhivotovsky, B., 2015. Calcium and mitochondria in the regulation of cell death. Biochem Biophys Res Commun 460, 72–81. https://doi.org/10.1016/J.BBRC.2015.01.137

Palmer, L.D., Skaar, E.P., 2016. Transition Metals and Virulence in Bacteria. Annu Rev Genet 50, 67–91. https://doi.org/10.1146/ANNUREV-GENET-120215-035146

Palumaa, P., 2013. Copper chaperones. The concept of conformational control in the metabolism of copper. FEBS Lett 587, 1902–1910. https://doi.org/10.1016/j.febslet.2013.05.019

Panek, H., O'Brian, M.R., 2002. A whole genome view of prokaryotic haem biosynthesis. Microbiology (Reading) 148, 2273–2282. https://doi.org/10.1099/00221287-148-8-2273

Paul, V.D., Lill, R., 2015. Biogenesis of cytosolic and nuclear iron–sulfur proteins and their role in genome stability. Biochimica et Biophysica Acta (BBA) - Molecular Cell Research 1853, 1528–1539. https://doi.org/10.1016/J.BBAMCR.2014.12.018

Pays, E., Vanhollebeke, B., Vanhamme, L., Paturiaux-Hanocq, F., Nolan, D.P., Pérez-Morga, D., 2006. The trypanolytic factor of human serum. Nature Reviews Microbiology 2006 4:6 4, 477–486. https://doi.org/10.1038/nrmicro1428

Pedersen, P.L., Amzel, L.M., 1993. ATP synthases. Structure, reaction center, mechanism, and regulation of one of nature's most unique machines. Journal of Biological Chemistry 268, 9937–9940. https://doi.org/10.1016/S0021-9258(18)82152-4

Philpott, C.C., 2006. Iron uptake in fungi: A system for every source. Biochimica et Biophysica Acta (BBA) - Molecular Cell Research 1763, 636–645. https://doi.org/10.1016/J.BBAMCR.2006.05.008

Picozzi, K., Fèvre, E.M., Odiit, M., Carrington, M., Eisler, M.C., Maudlin, I., Welburn, S.C., 2005. Sleeping sickness in Uganda: a thin line between two fatal diseases. BMJ : British Medical Journal 331, 1238. https://doi.org/10.1136/BMJ.331.7527.1238

Pizzino, G., Irrera, N., Cucinotta, M., Pallio, G., Mannino, F., Arcoraci, V., Squadrito, F., Altavilla, D., Bitto, A., 2017. Oxidative Stress: Harms and Benefits for Human Health. Oxid Med Cell Longev 2017, 1–13. https://doi.org/10.1155/2017/8416763

Poprac, P., Jomova, K., Simunkova, M., Kollar, V., Rhodes, C.J., Valko, M., 2017. Targeting Free Radicals in Oxidative Stress-Related Human Diseases. Trends Pharmacol Sci 38, 592–607. https://doi.org/10.1016/j.tips.2017.04.005

Porteous, C.M., Logan, A., Evans, C., Ledgerwood, E.C., Menon, D.K., Aigbirhio, F., Smith, R.A.J., Murphy, M.P., 2010. Rapid uptake of lipophilic triphenylphosphonium cations by mitochondria in vivo following intravenous injection: implications for mitochondria-specific therapies and probes. Biochim Biophys Acta 1800, 1009–1017. https://doi.org/10.1016/J.BBAGEN.2010.06.001

Posey, J.E., Gherardini, F.C., 2000. Lack of a role for iron in the Lyme disease pathogen. Science 288, 1651–1653. https://doi.org/10.1126/SCIENCE.288.5471.1651

Poulos, T.L., 2014. Heme enzyme structure and function. Chem Rev 114, 3919–3962. https://doi.org/10.1021/CR400415K/ASSET/IMAGES/LARGE/CR-2013-00415K_0042.JPEG

Priest, J.W., Hajduk, S.L., 1994. Developmental regulation of mitochondrial biogenesis in *Trypanosoma brucei*. Journal of Bioenergetics and Biomembranes 1994 26:2 26, 179–191. https://doi.org/10.1007/BF00763067

Rasmussen, T., Scheide, D., Brors, B., Kintscher, L., Weiss, H., Friedrich, T., 2001. Identification of two tetranuclear FeS clusters on the ferredoxin-type subunit of NADH:ubiquinone oxidoreductase (complex I). Biochemistry 40, 6124–6131. https://doi.org/10.1021/BI0026977/ASSET/IMAGES/LARGE/BI0026977F00007.JPEG

Rasmusson, A.G., Svensson, Å.S., Knoop, V., Grohmann, L., Brennicke, A., 1999. Homologues of yeast and bacterial rotenone-insensitive NADH dehydrogenases in higher eukaryotes: two enzymes are present in potato mitochondria. Plant J 20, 79–87. https://doi.org/10.1046/J.1365-313X.1999.00576.X

Rideout, D.C., Calogeropoulou, T., Jaworski, J.S., Dagnino, R., McCarthy, M.R., 1989. Phosphonium salts exhibiting selective anti-carcinoma activity in vitro. Anticancer Drug Des 4, 265–80.

Rifkin, M.R., 1991. Role of phospholipids in the cytotoxic action of high density lipoprotein on trypanosomes. J Lipid Res 32, 639–647. https://doi.org/10.1016/S0022-2275(20)42051-6

Rifkin, M.R., 1978. Identification of the trypanocidal factor in normal human serum: high density lipoprotein. Proc Natl Acad Sci U S A 75, 3450–3454. https://doi.org/10.1073/PNAS.75.7.3450

Riou, G., Delain, E., 1969. Electron microscopy of the circular kinetoplastic DNA from *Trypanosoma cruzi*: occurrence of catenated forms. Proceedings of the National Academy of Sciences 62, 210–217. https://doi.org/10.1073/PNAS.62.1.210

Riou, G., Paoletti, C., 1967. Preparation and properties of nuclear and satellite deoxyribonucleic acid of *Trypanosoma cruzi*. J Mol Biol 28, 377–382. https://doi.org/10.1016/S0022-2836(67)80017-2

Rizzuto, R., Bernardi, P., Pozzan, T., 2000. Mitochondria as all-round players of the calcium game. J Physiol 529 Pt 1, 37–47. https://doi.org/10.1111/J.1469-7793.2000.00037.X

Roditi, I., Schumann, G., Naguleswaran, A., 2016. Environmental sensing by African trypanosomes. Curr Opin Microbiol 32, 26–30. https://doi.org/10.1016/J.MIB.2016.04.011

Rodriguez-Cuenca, S., Cochemé, H.M., Logan, A., Abakumova, I., Prime, T.A., Rose, C., Vidal-Puig, A., Smith, A.C., Rubinsztein, D.C., Fearnley, I.M., Jones, B.A., Pope, S., Heales, S.J.R., Lam, B.Y.H., Neogi, S.G., McFarlane, I., James, A.M., Smith, R.A.J., Murphy, M.P., 2010a. Consequences of long-term oral administration of the mitochondria-targeted antioxidant MitoQ to wild-type mice. Free Radic Biol Med 48, 161–172. https://doi.org/10.1016/J.FREERADBIOMED.2009.10.039

Rodriguez-Cuenca, S., Cochemé, H.M., Logan, A., Abakumova, I., Prime, T.A., Rose, C., Vidal-Puig, A., Smith, A.C., Rubinsztein, D.C., Fearnley, I.M., Jones, B.A., Pope, S., Heales, S.J.R., Lam, B.Y.H., Neogi, S.G., McFarlane, I., James, A.M., Smith, R.A.J., Murphy, M.P., 2010b. Consequences of long-term oral administration of the mitochondria-targeted antioxidant MitoQ to wild-type mice. Free Radic Biol Med 48, 161–172. https://doi.org/10.1016/J.FREERADBIOMED.2009.10.039

Roger, A.J., Muñoz-Gómez, S.A., Kamikawa, R., 2017. The Origin and Diversification of Mitochondria. Current Biology 27, R1177–R1192. https://doi.org/10.1016/J.CUB.2017.09.015

Rogov, A.G., Sukhanova, E.I., Uralskaya, L.A., Aliverdieva, D.A., Zvyagilskaya, R.A., 2014. Alternative oxidase: distribution, induction, properties, structure, regulation, and functions. Biochemistry (Mosc) 79, 1615–1634. https://doi.org/10.1134/S0006297914130112

Rogov, A.G., Zvyagilskaya, R.A., 2015. Physiological role of alternative oxidase (from yeasts to plants). Biochemistry (Moscow) 80, 400–407. https://doi.org/10.1134/S0006297915040021/METRICS

Rohlenova, K., Sachaphibulkij, K., Stursa, J., Bezawork-Geleta, A., Blecha, J., Endaya, B., Werner, L., Cerny, J., Zobalova, R., Goodwin, J., Spacek, T., Alizadeh Pesdar, E., Yan, B., Nguyen, M.N., Vondrusova, M., Sobol, M., Jezek, P., Hozak, P., Truksa, J., Rohlena, J., Dong, L.F., Neuzil, J., 2017. Selective Disruption of Respiratory Supercomplexes as a New Strategy to Suppress Her2high Breast Cancer. Antioxid Redox Signal 26, 84–103. https://doi.org/10.1089/ARS.2016.6677

Rosca, M.G., Hoppel, C.L., 2013. Mitochondrial dysfunction in heart failure. Heart Fail Rev 18, 607–622. https://doi.org/10.1007/S10741-012-9340-0

Ross, M.F., Kelso, G.F., Blaikie, F.H., James, A.M., Cochemé, H.M., Filipovska, A., da Ros, T., Hurd, T.R., Smith, R.A.J., Murphy, M.P., 2005. Lipophilic triphenylphosphonium cations as tools in mitochondrial bioenergetics and free radical biology. Biochemistry (Mosc) 70, 222–230. https://doi.org/10.1007/S10541-005-0104-5

Ross, M.F., Prime, T.A., Abakumova, I., James, A.M., Porteous, C.M., Smith, R.A.J., Murphy, M.P., 2008a. Rapid and extensive uptake and activation of hydrophobic triphenylphosphonium cations within cells. Biochem J 411, 633–645. https://doi.org/10.1042/BJ20080063

Ross, M.F., Prime, T.A., Abakumova, I., James, A.M., Porteous, C.M., Smith, R.A.J., Murphy, M.P., 2008b. Rapid and extensive uptake and activation of hydrophobic triphenylphosphonium cations within cells. Biochem J 411, 633–645. https://doi.org/10.1042/BJ20080063

Rotureau, B., van den Abbeele, J., 2013. Through the dark continent: African trypanosome development in the tsetse fly. Front Cell Infect Microbiol 3, 1–7. https://doi.org/10.3389/FCIMB.2013.00053

Roy, S.L., Atkins, J.T., Gennuso, R., Kofos, D., Sriram, R.R., Dorlo, T.P.C., Hayes, T., Qvarnstrom, Y., Kucerova, Z., Guglielmo, B.J., Visvesvara, G.S., 2015. Assessment of blood–brain barrier penetration of miltefosine used to treat a fatal case of granulomatous amebic encephalitis possibly caused by an unusual Balamuthia mandrillaris strain. Parasitol Res 114, 4431–4439. https://doi.org/10.1007/s00436-015-4684-8

Rugolo, M., Lenaz, G., 1987. Monitoring of the mitochondrial and plasma membrane potentials in human fibroblasts by tetraphenylphosphonium ion distribution. J Bioenerg Biomembr 19, 705–718. https://doi.org/10.1007/BF00762304

Ruiz, L.M., Jensen, E.L., Bustos, R.I., Argüelloa, G., Gutierrez-Garcia, R., González, M., Hernández, C., Paredes, R., Simon, F., Riedel, C., Ferrick, D., Elorza, A.A., 2014. Adaptive responses of mitochondria to mild copper deprivation involve changes in morphology, OXPHOS remodeling and bioenergetics. J Cell Physiol 229, 607–619. https://doi.org/10.1002/JCP.24484

Sagan, L., 1967. On the origin of mitosing cells. J Theor Biol 14. https://doi.org/10.1016/0022-5193(67)90079-3

Schade, A.L., Caroline, L., 1946. An iron-binding component in human blood plasma. Science (1979) 104, 340–341. https://doi.org/10.1126/SCIENCE.104.2702.340/ASSET/3B30E2D5-8EA3-459B-9312-6CA673D63AFB/ASSETS/SCIENCE.104.2702.340.FP.PNG

Schade, A.L., Caroline, L., 1944. Raw hen egg white and the role of iron in growth inhibition of Shigella dysenteria, Staphylococcus aureus, Escherichia coli and Saccharomyces cerevisiae. Science 100, 14–15. https://doi.org/10.1126/SCIENCE.100.2584.14

Schalk, I.J., 2008. Metal trafficking via siderophores in Gram-negative bacteria: specificities and characteristics of the pyoverdine pathway. J Inorg Biochem 102, 1159–1169. https://doi.org/10.1016/J.JINORGBIO.2007.11.017

Schnaufer, A., Clark-Walker, G.D., Steinberg, A.G., Stuart, K., 2005. The F1-ATP synthase complex in bloodstream stage trypanosomes has an unusual and essential function. EMBO J 24, 4029–4040. https://doi.org/10.1038/SJ.EMBOJ.7600862

Schumacker, P.T., 2006. Reactive oxygen species in cancer cells: Live by the sword, die by the sword. Cancer Cell 10, 175–176. https://doi.org/10.1016/J.CCR.2006.08.015

Sehgal, R., Goyal, K., Sehgal, A., 2012. Trichomoniasis and lactoferrin: future prospects. Infect Dis Obstet Gynecol 2012, 1–8. https://doi.org/10.1155/2012/536037

Shackelford, D.B., Abt, E., Gerken, L., Vasquez, D.S., Seki, A., Leblanc, M., Wei, L., Fishbein, M.C., Czernin, J., Mischel, P.S., Shaw, R.J., 2013. LKB1 Inactivation Dictates Therapeutic Response of Non-Small Cell Lung Cancer to the Metabolism Drug Phenformin. Cancer Cell 23, 143–158. https://doi.org/10.1016/J.CCR.2012.12.008

Shaw, S., Knüsel, S., Abbühl, D., Naguleswaran, A., Etzensperger, R., Benninger, M., Roditi, I., 2022. Cyclic AMP signalling and glucose metabolism mediate pH taxis by African trypanosomes. Nat Commun 13, 1–13. https://doi.org/10.1038/S41467-022-28293-W

Shchepina, L.A., Pletjushkina, O.Y., Avetisyan, A. v., Bakeeva, L.E., Fetisova, E.K., Izyumov, D.S., Saprunova, V.B., Vyssokikh, M.Y., Chernyak, B. v., Skulachev, V.P., 2002. Oligomycin, inhibitor of the F0 part of H+-ATP-synthase, suppresses the TNF-induced apoptosis. Oncogene 2002 21:53 21, 8149–8157. https://doi.org/10.1038/sj.onc.1206053

Shoshan-Barmatz, V., de Pinto, V., Zweckstetter, M., Raviv, Z., Keinan, N., Arbel, N., 2010. VDAC, a multi-functional mitochondrial protein regulating cell life and death. Mol Aspects Med 31, 227–285. https://doi.org/10.1016/J.MAM.2010.03.002

Siddiqui, R., Ali, I.K.M., Cope, J.R., Khan, N.A., 2016. Biology and pathogenesis of *Naegleria fowleri*. Acta Trop 164, 375–394. https://doi.org/10.1016/J.ACTATROPICA.2016.09.009

Simons, B.H., Millenaar, F.F., Mulder, L., van Loon, L.C., Lambers, H., 1999. Enhanced Expression and Activation of the Alternative Oxidase during Infection of Arabidopsis with *Pseudomonas syringae* pv tomato. Plant Physiol 120, 529–538. https://doi.org/10.1104/PP.120.2.529

Slater, E.C., 1983. The Q cycle, an ubiquitous mechanism of electron transfer. Trends Biochem Sci 8, 239–242. https://doi.org/10.1016/0968-0004(83)90348-1

Smith, A.D., Logeman, B.L., Thiele, D.J., 2017. Copper Acquisition and Utilization in Fungi. Annu Rev Microbiol 71, 597. https://doi.org/10.1146/ANNUREV-MICRO-030117-020444

Smith, R.A.J., Hartley, R.C., Cochemé, H.M., Murphy, M.P., 2012. Mitochondrial pharmacology. Trends Pharmacol Sci 33, 341–352. https://doi.org/10.1016/J.TIPS.2012.03.010

Smith, R.A.J., Hartley, R.C., Murphy, M.P., 2011. Mitochondria-targeted small molecule therapeutics and probes. Antioxid Redox Signal 15, 3021–3038. https://doi.org/10.1089/ARS.2011.3969

Smith, R.A.J., Porteous, C.M., Gane, A.M., Murphy, M.P., 2003. Delivery of bioactive molecules to mitochondria in vivo. Proc Natl Acad Sci U S A 100, 5407. https://doi.org/10.1073/PNAS.0931245100

Smutná, T., Dohnálková, A., Sutak, R., Narayanasamy, R.K., Tachezy, J., Hrdý, I., 2022. A cytosolic ferredoxin-independent hydrogenase possibly mediates hydrogen uptake in *Trichomonas vaginalis*. Current Biology 32, 124–135. https://doi.org/10.1016/j.cub.2021.10.050

Snow, B.J., Rolfe, F.L., Lockhart, M.M., Frampton, C.M., O'Sullivan, J.D., Fung, V., Smith, R.A.J., Murphy, M.P., Taylor, K.M., 2010. A double-blind, placebo-controlled study to assess the mitochondria-targeted antioxidant MitoQ as a disease-modifying therapy in Parkinson's disease. Mov Disord 25, 1670–1674. https://doi.org/10.1002/MDS.23148

Stannard, J.N., Horecker, B.L., 1948. The in vitro inhibition of cytochrome oxidase by azide and cyanide. J Biol Chem 172, 599–608.

Stearman, R., Yuan, D.S., Yamaguchi-Iwai, Y., Klausner, R.D., Dancis, A., 1996. A Permease-Oxidase Complex Involved in High-Affinity Iron Uptake in Yeast. Science (1979) 271, 1552–1557. https://doi.org/10.1126/SCIENCE.271.5255.1552

Stehling, O., Mascarenhas, J., Vashisht, A.A., Sheftel, A.D., Niggemeyer, B., Rösser, R., Pierik, A.J., Wohlschlegel, J.A., Lill, R., 2013. Human CIA2A-FAM96A and CIA2B-FAM96B integrate iron homeostasis and maturation of different subsets of cytosolic-nuclear iron-sulfur proteins. Cell Metab 18, 187–198. https://doi.org/10.1016/j.cmet.2013.06.015

St-Pierre, J., Brand, M.D., Boutilier, R.G., 2000. Mitochondria as ATP consumers: Cellular treason in anoxia. Proc Natl Acad Sci U S A 97, 8670–8674. https://doi.org/10.1073/PNAS.140093597

Surve, S., Heestand, M., Panicucci, B., Schnaufer, A., Parsons, M., 2012. Enigmatic presence of mitochondrial complex I in *Trypanosoma brucei* bloodstream forms. Eukaryot Cell 11, 183–193. https://doi.org/10.1128/EC.05282-11/SUPPL_FILE/SUPPMETHODS_TABLES1-S2_FIGS1-S8.PDF

Sutak, R., Lesuisse, E., Tachezy, J., Richardson, D.R., 2008. Crusade for iron: iron uptake in unicellular eukaryotes and its significance for virulence. Trends Microbiol 16, 261–268. https://doi.org/10.1016/J.TIM.2008.03.005

Szewczyk, A., Wojtczak, L., 2002. Mitochondria as a pharmacological target. Pharmacol Rev 54, 101–127. https://doi.org/10.1124/PR.54.1.101

Takahashi, Y., Tokumoto, U., 2002. A third bacterial system for the assembly of iron-sulfur clusters with homologs in Archaea and plastids. Journal of Biological Chemistry 277, 28380–28383. https://doi.org/10.1074/jbc.C200365200

Talley, J.T., Mohiuddin, S.S., 2022. Biochemistry, Fatty Acid Oxidation, StatPearls. StatPearls Publishing.

Tan, G., Cheng, Z., Pang, Y., Landry, A.P., Li, J., Lu, J., Ding, H., 2014. Copper binding in IscA inhibits iron-sulphur cluster assembly in *Escherichia coli*. Mol Microbiol 93, 629–644. https://doi.org/10.1111/mmi.12676

Tovar, J., León-Avila, G., Sánchez, L.B., Sutak, R., Tachezy, J., van der Giezen, M., Hernández, M., Müller, M., Lucocq, J.M., 2003. Mitochondrial remnant organelles of *Giardia* function in iron-sulphur protein maturation. Nature 2003 426:6963 426, 172–176. https://doi.org/10.1038/nature01945

Traaseth, N., Elfering, S., Solien, J., Haynes, V., Giulivi, C., 2004. Role of calcium signaling in the activation of mitochondrial nitric oxide synthase and citric acid cycle. Biochimica et Biophysica Acta (BBA) - Bioenergetics 1658, 64–71. https://doi.org/10.1016/J.BBABIO.2004.04.015

Troxell, B., Xu, H., Yang, X.F., 2012. Borrelia burgdorferi, a Pathogen That Lacks Iron, Encodes Manganese-dependent Superoxide Dismutase Essential for Resistance to Streptonigrin. J Biol Chem 287, 19284–19293. https://doi.org/10.1074/JBC.M112.344903

Tsaousis, A.D., Nývltová, E., Šuták, R., Hrdý, I., Tachezy, J., 2014. A Nonmitochondrial Hydrogen Production in Naegleria gruberi. Genome Biol Evol 6, 792–799. https://doi.org/10.1093/GBE/EVU065

Uyemura, S., Luo, S., Vieira, M., Moreno, R., Docampo, R., 2004. Oxidative phosphorylation and rotenone-insensitive malate- and NADH-quinone oxidoreductases in *Plasmodium yoelii yoelii* mitochondria in situ. J Biol Chem 279, 385–393. https://doi.org/10.1074/JBC.M307264200

Vanlerberghe, G.C., 2013. Alternative oxidase: a mitochondrial respiratory pathway to maintain metabolic and signaling homeostasis during abiotic and biotic stress in plants. Int J Mol Sci 14, 6805–47. https://doi.org/10.3390/ijms14046805

Vásquez-Trincado, C., García-Carvajal, I., Pennanen, C., Parra, V., Hill, J.A., Rothermel, B.A., Lavandero, S., 2016. Mitochondrial dynamics, mitophagy and cardiovascular disease. J Physiol 594, 509–525. https://doi.org/10.1113/JP271301

Verma, K., Saito-Nakano, Y., Nozaki, T., Datta, S., 2015. Insights into endosomal maturation of human holo-transferrin in the enteric parasite *Entamoeba histolytica*: essential roles of Rab7A and Rab5 in biogenesis of giant early endocytic vacuoles. Cell Microbiol 17, 1779–1796. https://doi.org/10.1111/CMI.12470

Verner, Z., Škodová, I., Poláková, S., Ďurišová-Benkovičová, V., Horváth, A., Lukeš, J., 2013. Alternative NADH dehydrogenase (NDH2): intermembrane-space-facing counterpart of mitochondrial complex I in the procyclic *Trypanosoma brucei*. Parasitology 140, 328–337. https://doi.org/10.1017/S003118201200162X

Vickerman, K., 1965. Polymorphism and Mitochondrial Activity In Sleeping Sickness Trypanosomes. Nature 1965 208:5012 208, 762–766. https://doi.org/10.1038/208762a0

Vickerman, K., 1962. The mechanism of cyclical development in trypanosomes of the *Trypanosoma brucei* sub-group: An hypothesis based on ultrastructural observations. Trans R Soc Trop Med Hyg 56, 487–495. https://doi.org/10.1016/0035-9203(62)90072-X

Vishwakarma, A., Tetali, S.D., Selinski, J., Scheibe, R., Padmasree, K., 2015. Importance of the alternative oxidase (AOX) pathway in regulating cellular redox and ROS homeostasis to optimize photosynthesis during restriction of the cytochrome oxidase pathway in *Arabidopsis thaliana*. Ann Bot 116, 555–569. https://doi.org/10.1093/AOB/MCV122

Visvesvara, G.S., Moura, H., Schuster, F.L., 2007. Pathogenic and opportunistic free-living amoebae: *Acanthamoeba spp*., *Balamuthia mandrillaris*, *Naegleria fowleri*, and *Sappinia diploidea*. FEMS Immunol Med Microbiol. https://doi.org/10.1111/j.1574-695X.2007.00232.x

Vogelsinger, H., Weiler, S., Djanani, A., Kountchev, J., Bellmann-Weiler, R., Wiedermann, C.J., Bellmann, R., 2006. Amphotericin B tissue distribution in autopsy material after treatment with liposomal amphotericin B and amphotericin B colloidal dispersion. Journal of Antimicrobial Chemotherapy 57, 1153–1160. https://doi.org/10.1093/jac/dkl141

Walker, J.E., 1992. The NADH:ubiquinone oxidoreductase (complex I) of respiratory chains. Q Rev Biophys 25, 253–324. https://doi.org/10.1017/S003358350000425X

Wang, J., Li, J., Xiao, Y., Fu, B., Qin, Z., 2020. TPP-based mitocans: a potent strategy for anticancer drug design. RSC Med Chem 11, 858–875. https://doi.org/10.1039/C9MD00572B

Warburg, O., 1956. On the origin of cancer cells. Science (1979) 123, 309–314. https://doi.org/10.1126/SCIENCE.123.3191.309/ASSET/A8D38B53-799F-4009-AAD3-E77CEF33D301/ASSETS/SCIENCE.123.3191.309.FP.PNG

Warburg, O., Wind, F., Negelein, E., 1927. The metabolism of tumors in the body. J Gen Physiol 8, 519–530. https://doi.org/10.1085/JGP.8.6.519

Weik, R.R., John, D.T., 1979. Cell and mitochondria respiration of *Naegleria fowleri*. Journal of Parasitology 65, 700–708. https://doi.org/10.2307/3280348

Weiss, H., von Jagow, G., Klingenberg, M., Bücher, T., 1970. Characterization of *Neurospora crassa* mitochondria prepared with a grind-mill. Eur J Biochem 14, 75–82. https://doi.org/10.1111/J.1432-1033.1970.TB00263.X

Wenner, C.E., Spirtes, M.A., Weinhouse, S., 1952. Metabolism of Neoplastic Tissue : II. A Survey of Enzymes of the Citric Acid Cycle in Transplanted Tumors. Cancer Res 12, 44–49.

Wikström, M., 1984. Two protons are pumped from the mitochondrial matrix per electron transferred between NADH and ubiquinone. FEBS Lett 169, 300–304. https://doi.org/10.1016/0014-5793(84)80338-5

Willcox, J.K., Ash, S.L., Catignani, G.L., 2004. Antioxidants and prevention of chronic disease. Crit Rev Food Sci Nutr 44, 275–295. https://doi.org/10.1080/10408690490468489

Williams, R.J.P., 2012. Iron in evolution. FEBS Lett 586, 479–484. https://doi.org/10.1016/J.FEBSLET.2011.05.068

Wisnovsky, S., Lei, E.K., Jean, S.R., Kelley, S.O., 2016. Mitochondrial Chemical Biology: New Probes Elucidate the Secrets of the Powerhouse of the Cell. Cell Chem Biol 23, 917–927. https://doi.org/10.1016/j.chembiol.2016.06.012

Yagi, T., 1991. Bacterial NADH-quinone oxidoreductases. Journal of Bioenergetics and Biomembranes 1991 23:2 23, 211–225. https://doi.org/10.1007/BF00762218

Young, I.S., Woodside, J. v., 2001. Antioxidants in health and disease. J Clin Pathol 54, 176–186. https://doi.org/10.1136/JCP.54.3.176

Zelko, I.N., Mariani, T.J., Folz, R.J., 2002. Superoxide dismutase multigene family: A comparison of the CuZn-SOD (SOD1), Mn-SOD (SOD2), and EC-SOD (SOD3) gene structures, evolution, and expression. Free Radic Biol Med 33, 337–349. https://doi.org/10.1016/S0891-5849(02)00905-X

Ženíšková, K., Grechnikova, M., Sutak, R., 2022. Copper Metabolism in Naegleria gruberi and Its Deadly Relative Naegleria fowleri. Front Cell Dev Biol 10, 1–17. https://doi.org/10.3389/FCELL.2022.853463

Zhao, R.Z., Jiang, S., Zhang, L., Yu, Z. bin, 2019. Mitochondrial electron transport chain, ROS generation and uncoupling (Review). Int J Mol Med 44, 3–15. https://doi.org/10.3892/IJMM.2019.4188/HTML

Zhivotovsky, B., Orrenius, S., 2011. Calcium and cell death mechanisms: a perspective from the cell death community. Cell Calcium 50, 211–21. https://doi.org/10.1016/j.ceca.2011.03.003

Zielonka, J., Joseph, J., Sikora, A., Hardy, M., Ouari, O., Vasquez-Vivar, J., Cheng, G., Lopez, M., Kalyanaraman, B., 2017. Mitochondria-Targeted Triphenylphosphonium-Based Compounds:

Syntheses, Mechanisms of Action, and Therapeutic and Diagnostic Applications. Chem Rev 117, 10043–10120. https://doi.org/10.1021/ACS.CHEMREV.7B00042

Zíková, A., 2022. Mitochondrial adaptations throughout the *Trypanosoma brucei* life cycle. J Eukaryot Microbiol. https://doi.org/10.1111/JEU.12911

Zíková, A., Verner, Z., Nenarokova, A., Michels, P.A.M., Lukeš, J., 2017. A paradigm shift: The mitoproteomes of procyclic and bloodstream *Trypanosoma brucei* are comparably complex. PLoS Pathog 13. https://doi.org/10.1371/JOURNAL.PPAT.1006679

Zoltani, C.K., 2015. Cardiovascular System as a Target of Chemical Warfare Agents. Handbook of Toxicology of Chemical Warfare Agents: Second Edition 519–533. https://doi.org/10.1016/B978-0-12-800159-2.00037-3

PLOS NEGLECTED TROPICAL DISEASES

RESEARCH ARTICLE

Adaptive iron utilization compensates for the lack of an inducible uptake system in *Naegleria fowleri* and represents a potential target for therapeutic intervention

Dominik Arbon[1], Kateřina Ženíšková[1], Jan Mach[1], Maria Grechnikova[1], Ronald Malych[1], Pavel Talacko[2], Robert Sutak[1]*

1 Department of Parasitology, Faculty of Science, BIOCEV, Charles University, Vestec, Czech Republic, **2** BIOCEV proteomics core facility, Faculty of Science, BIOCEV, Charles University, Vestec, Czech Republic

* robert.sutak@natur.cuni.cz

Citation: Arbon D, Ženíšková K, Mach J, Grechnikova M, Malych R, Talacko P, et al. (2020) Adaptive iron utilization compensates for the lack of an inducible uptake system in *Naegleria fowleri* and represents a potential target for therapeutic intervention. PLoS Negl Trop Dis 14(6): e0007759. https://doi.org/10.1371/journal.pntd.0007759

Editor: Steven M. Singer, Georgetown University, UNITED STATES

Received: September 4, 2019

Accepted: April 20, 2020

Published: June 18, 2020

Data Availability Statement: All relevant data are within the manuscript and its Supporting Information files.

Funding: This work was supported by "The equipment for metabolomic and cell analyses" (CZ.1.05/2.1.00/19.0400, Research and Development for Innovations Operational Programme); Czech-BioImaging large RI projects (LM2015062 and CZ.02.1.01/0.0/0.0/16_013/0001775) and LQ1604 NPU II funded by Ministry

Abstract

Naegleria fowleri is a single-cell organism living in warm freshwater that can become a deadly human pathogen known as a brain-eating amoeba. The condition caused by *N. fowleri*, primary amoebic meningoencephalitis, is usually a fatal infection of the brain with rapid and severe onset. Iron is a common element on earth and a crucial cofactor for all living organisms. However, its bioavailable form can be scarce in certain niches, where it becomes a factor that limits growth. To obtain iron, many pathogens use different machineries to exploit an iron-withholding strategy that has evolved in mammals and is important to host-parasite interactions. The present study demonstrates the importance of iron in the biology of *N. fowleri* and explores the plausibility of exploiting iron as a potential target for therapeutic intervention. We used different biochemical and analytical methods to explore the effect of decreased iron availability on the cellular processes of the amoeba. We show that, under iron starvation, nonessential, iron-dependent, mostly cytosolic pathways in *N. fowleri* are downregulated, while the metal is utilized in the mitochondria to maintain vital respiratory processes. Surprisingly, *N. fowleri* fails to respond to acute shortages of iron by inducing the reductive iron uptake system that seems to be the main iron-obtaining strategy of the parasite. Our findings suggest that iron restriction may be used to slow the progression of infection, which may make the difference between life and death for patients.

Author summary

Naegleria fowleri is a unicellular amoeba living in warm freshwater that is able to infect humans and cause a serious and mostly fatal disease with rapid progression. When water with the amoeba enters the nose, *Naegleria* penetrates the mucosa and invades the human brain, where it destroys cells and causes massive inflammation. It is a rare infection with unspecific symptoms, which slows the critical process of identifying the cause of the disease. Iron is a necessary element for all living organisms used in many biological

of Education, Youth and Sports of the Czech Republic; Czech Science Foundation (18-07822S; 20-28072S); MiCoBion project funded from EU Horizon 2020 (No 810224) and CePaViP provided by The European Regional Development Fund and Ministry of Education, Youth and Sports of the Czech Republic (CZ.02.1.01/0.0/0.0/16_019/0000759). The funders had no role in study design, data collection and analysis, decision to publish, or preparation of the manuscript.

Competing interests: The authors have declared that no competing interests exist.

pathways; therefore, iron acquisition and iron metabolism have the potential to be exploited against this parasite to clear or slow the infection. It was discovered that *N. fowleri* is unable to efficiently regulate iron uptake in an environment with a low iron concentration and merely changes its energy metabolism to handle the lack of this element. Because of this limited response, *N. fowleri* is more sensitive to low iron conditions than are human cells, and treatment by iron chelators has the potential to kill the pathogen or slow the infection in the host.

Introduction

There are several free-living protists that, under certain conditions, are able to parasitize suitable hosts. The genus *Naegleria* consists of several species, the most studied of which are *Naegleria gruberi* and *Naegleria fowleri*, the latter being widely known as the "brain-eating amoeba". Its rather vivid nickname is attributed to the condition known as primary amoebic meningoencephalitis (PAM). The amoeba is found in warm freshwaters across most continents and can transition between three distinguishable forms: a durable cyst, trophozoite amoeba and mobile flagellate [1]. Its presence in water is a health risk for people participating in recreational activities involving bodies of water [2]. The disease is acquired when *N. fowleri* trophozoites forcefully enter through the nasal cavity, invade the olfactory neuroepithelium and follow the olfactory nerve to the brain, which is their final destination [3]. The disease has a rapid onset, and the nonspecific symptoms resemble those of more common bacterial or viral meningoencephalitis–headache, fever, vomiting–with rapid progress, causing seizures, coma, and death [4,5]. Since PAM occurs commonly in healthy individuals, *N. fowleri* is regarded not as an opportunistic parasite but as a pathogen [3]. The fatality rate for PAM is reported to be above 97% [6]. Treating PAM is difficult because the symptoms are typical of other maladies and have rapid onset and because no specific or efficient medication is available for ameliorating the disease. For successful treatment, it is crucial that a correct diagnosis is made quickly and that therapy is immediately delivered. The currently accepted treatment includes administering several medications simultaneously, such as amphotericin B, fluconazole, rifampin, azithromycin and/or miltefosine, in combination with methods that decrease brain swelling [4,7]. Thus, the need for an efficient cure or at least novel compounds that will slow the progression of the infection persists. Among other free-living amoebae, that can cause life-threatening diseases are species of *Acanthamoeba*, *Balamuthia* and *Sappinia*. These amoebae cause rare granulomatous amoebic encephalitis, a deadly disease with symptoms similar to PAM but that progress more slowly and with additional manifestations [8,9]. Nevertheless, the issues with battling these diseases, such as difficulty making a diagnosis, are the same.

There is very limited knowledge about the biochemistry and physiology of *N. fowleri*, and practically nothing is known about its metabolism of iron, even though this metal may represent the parasite's Achilles heel. Iron is an essential constituent of many biochemical processes, including redox reactions, the detoxification of oxygen, and cell respiration, and is a cofactor of various enzymes [10]. The ubiquitous role of iron is mainly due to its ability to transition between different oxidation states, enabling to participate in redox reactions, often in the form of iron-sulfur clusters [11]. Iron is essential for virtually all known forms of life, and its availability is shown to be the factor that limits organism growth in certain locations [12]. Its acquisition becomes especially challenging for pathogens that inhabit another living organism, as demonstrated by *Plasmodium*, in which iron-deficient human and mouse models manifest unfavorable conditions for parasite development; therefore, iron is a limiting factor for parasite

propagation [13,14]. As a defense mechanism, mammals minimize the presence of free iron in their body using several proteins, such as lactoferrin, ferritin or transferrin, which bind the metal, decreasing its bioavailability [15]. Parasitic organisms are known to have adopted various means of acquiring iron from their environments, ranging from engaging in opportunistic xenosiderophore uptake to expressing specific receptors for mammalian iron-containing proteins [16]. This two-sided competition between pathogens and their hosts indicates the importance of iron metabolism in disease and underlines the importance of further research on this topic in the search for new methods of therapeutic intervention.

In this study, we demonstrate how *N. fowleri* acquires iron from its environment and how it adapts to iron-deficient conditions and we propose that the amoeba iron metabolism can be exploited to the advantage of PAM patients. We tested several potential iron uptake mechanisms and observed that the iron uptake system was not induced under iron starvation conditions and that the parasite used no alternative metabolic pathway to adjust for the resulting iron deficiency. Proteomic and metabolomic investigations showed that *N. fowleri* responded to low iron levels by maintaining iron-containing proteins in mitochondria, while the activity of nonvital, mostly cytosolic, iron-requiring pathways declined. These findings revealed a possible exploitable weakness in the survival strategy of the amoeba within the host. Although the host brain is relatively rich in iron content [17], not all of the iron is readily available for the parasite to use, as we have shown that it is not able to utilize iron bound to transferrin, the main source of iron in the human brain [18]. Thus, by using artificial chelators to decrease the availability of iron in this organ, we show a possible complementary antiparasite strategy, which is already utilized for different purposes, against this deadly pathogen [19].

Results

N. fowleri uses an uninducible reductive mechanism to acquire iron, while transferrin is not utilized

Iron is generally available in the environment in two distinct oxidation states. Due to the different solubilities of the two forms, many organisms use ferric reductase to reduce ferric iron to ferrous iron, which is more soluble and therefore easier to assimilate. To explore the mechanism by which *N. fowleri* acquires iron from its surroundings, cell cultures were supplemented with different sources of iron: ^{55}Fe-transferrin, ^{55}Fe(III)-citrate and ^{55}Fe(II)-ascorbate. For all the experiments conducted in this study, unless stated otherwise, iron deprivation was achieved using 25 μM of the common extracellular chelator bathophenanthroline disulfonic acid (BPS) to create a condition in which cell growth was significantly affected but microscopy showed no encystation or flagellated forms, and the cells did not lose their ability to multiply or attach to the surface. This condition was an important prerequisite, particularly for the proteomic and transcriptomic analysis, where very complex changes are accompanied by unfavorable cell processes that could bias the data. To achieve iron-rich conditions in this study, the cultivation medium was supplemented with 25 μM ferric nitrilotriacetate (Fe-NTA). The results presented in Fig 1A show that ferrous iron is taken up and incorporated into intracellular protein complexes more rapidly than was its trivalent counterpart. Densitometry of the radioactive signal in dried native electrophoresis gels was used to calculate the difference in iron utilization between the two forms: The utilization of ferric iron in comparison to ferrous iron was decreased in iron-rich cells to 65% (±8%; p-value <0.05) and in iron-deficient cells to 61% (±3%; p-value <0.01), suggesting the involvement of ferric reductase in the effective assimilation. Surprisingly, there was no significant difference in iron uptake between cells preincubated in the iron-rich and iron-deficient conditions, showing that the organism failed to stimulate its iron uptake machinery. The insignificant uptake of transferrin, shown in S1(B)

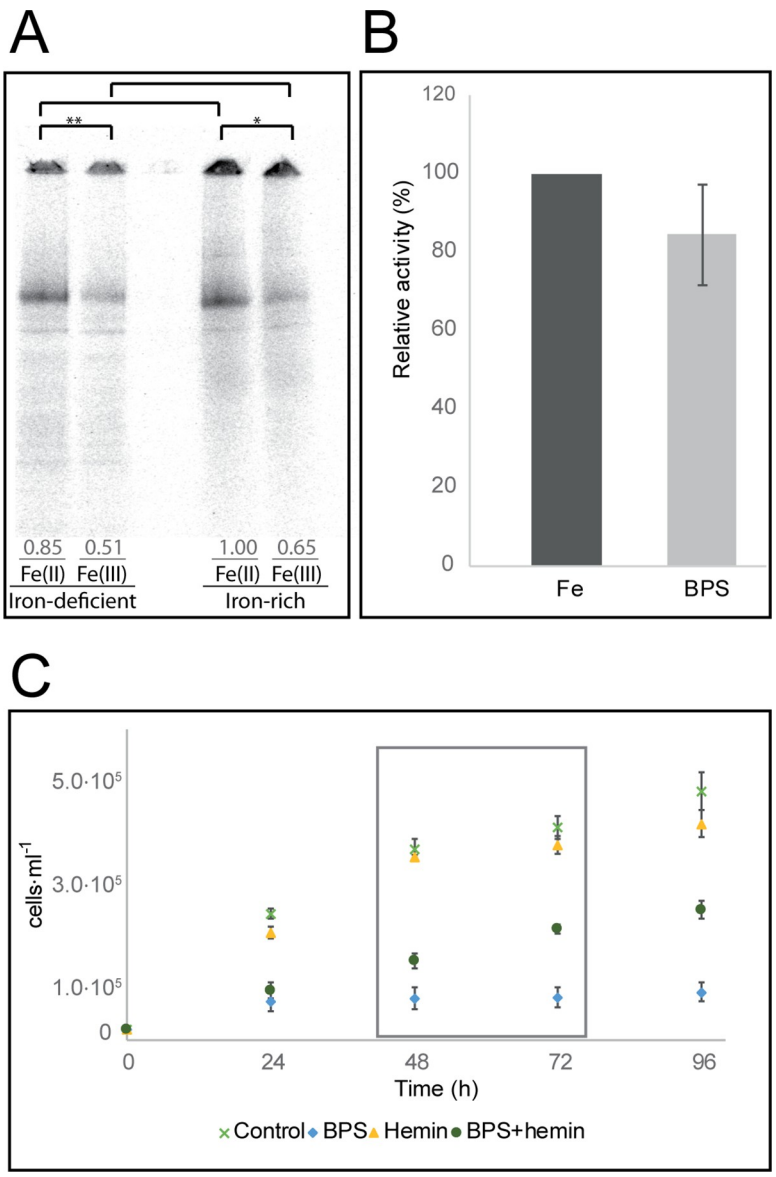

Fig 1. Iron uptake in *N. fowleri*. (A) Ferrous and ferric iron uptake by *N. fowleri* precultivated under iron-rich and iron-deficient conditions. Autoradiography of blue native electrophoresis gels of whole cell extracts from *N. fowleri* previously cultivated for 72 hours under iron-deficient conditions (25 μM BPS) or iron-rich conditions (25 μM Fe-NTA) and further incubated with ^{55}Fe(II) (ferrous ascorbate) or ^{55}Fe(III) (ferric citrate). Equal protein concentrations were loaded, and the loading control is shown in S1(A) Fig. The gel is representative of three independent replicates. Numbers indicate average relative densitometry values for the appropriate lines. Significant differences between band densitometry values are denoted by asterisk (*, $p<0.05$; **, $p<0.01$). (B) Ferric reductase activity under iron-rich and iron-deficient conditions. Relative values of *N. fowleri* ferric reductase activities in the iron-rich (Fe) and iron-deficient (BPS). The difference between the two conditions was not significant, p-value >0.05. Data are presented as the relative percentage ± SD from three independent replicates. (C) Growth restoration of *N. fowleri* in culture by hemin under iron-deficient conditions. Cells in regular growth medium (control) and with 50 μM hemin (hemin) exhibited similar levels of propagation, while the cells under iron-deficient conditions, achieved with 50 μM chelator bathophenanthroline disulfonic acid (BPS), showed stagnated growth in the first 24 hours. The addition of 50 μM hemin to the iron-deficient medium (BPS+hemin) partially restored culture growth. The boxed area indicates the time from which growth restoration was calculated. Data are presented as the means ± SD from four independent replicates.

https://doi.org/10.1371/journal.pntd.0007759.g001

Fig, means that this protein is not a viable source of iron for *N. fowleri*, corresponding to the fact that it is not found in the usual water habitat of this organism.

To confirm that *N. fowleri* uses a reductive iron uptake mechanism, the cell cultures were treated with a ferric iron radionuclide in the presence and absence of the ferrous iron chelator BPS. The results shown in S1(C) Fig demonstrate that, while *N. fowleri* readily incorporates ferric iron into its protein complexes, BPS chelates the initially reduced ferrous iron and prevents it from being further utilized, confirming that ferric iron uptake requires a reduction step.

We have shown that neither ferrous nor ferric iron uptake is induced by iron starvation (Fig 1A). Considering the involvement of the reduction step needed for *N. fowleri* iron acquisition, the activity of a ferric reductase was assessed in cells preincubated under iron-rich and iron-deficient conditions. As shown in Fig 1B, measurements of ferric reductase activity revealed that the level of ferric iron converted to ferrous iron was not significantly changed in the iron-deprived cells (p-value >0.05). This finding confirms that *N. fowleri* cannot efficiently adjust the rate of iron acquisition from its surroundings to overcome its dependence on iron availability.

Heme-containing proteins are potential source of iron or heme for several parasitic protists [20,21]. Although we did not identify a homolog of heme oxygenase in the *N. fowleri* genome, which is necessary for the breakdown of heme and the release of iron, we tested the effect of the presence of hemin in the cultivation medium on the growth of the amoebae. As shown in Fig 1C, cells cultivated in regular growth medium had a propagation pattern similar to that of the cells grown in medium supplemented with 50 μM hemin; therefore, at the given concentration, hemin was not toxic to *N. fowleri*, nor did it significantly support its growth under standard cultivation conditions. The profound iron-deficient conditions achieved with 50 μM BPS arrested culture growth to 31% (±12%) during the first 24 hours, and the propagation at later time points remained below this value. The addition of 50 μM hemin partially restored culture growth to 42% (±10%; p-value <0.01) after 48 hours, and by 72 hours, the growth reached 52% (±7%; p-value <0.01). Therefore, it appears that the hemin compound is used as a partial source of iron for the pathogen, although it cannot fully support its growth when other sources of iron are limited.

Proteomic analysis findings illuminate the iron-starvation response of *N. fowleri*, while the transcriptomic analysis does not reflect the proteomic changes

Since iron has an irrefutable role as a cofactor for various enzymes and its metabolism is dependent on a great number of proteins, we aimed to examine the overall effect of iron availability on the *N. fowleri* proteome. Therefore, we compared the whole-cell proteomes of cells grown under iron-rich and iron-deficient conditions, and we have additionally analyzed membrane-enriched fractions of cells to obtain a higher coverage of the membrane proteins. The aim was to reveal the metabolic remodeling accompanying iron starvation and to identify proteins responsible for iron homeostasis, such as membrane transporters, signaling and storage proteins or proteins involved in iron metabolism, for example, the formation of iron-sulfur clusters.

S1 Table lists the proteins that were significantly upregulated or downregulated under iron-deficient conditions based on the analysis of the *N. fowleri* whole-cell proteome, and S2 Table contains the regulated proteins in the membrane-enriched fraction. No major changes in encystation or flagellation markers or apoptotic pathway proteins between the two conditions were detected in the proteomic analysis. The proteins most relevant for this study are

Table 1. Effect of iron deprivation on the abundance of selected *N. fowleri* proteins.

Gene ID	Protein	Whole cell (membrane fraction) proteomics fold-change in iron deficiency	*p*-value
NF0117840	Protoglobin	ND in iron-deficient	NA
NF0127030	Hemerythrin	-7045.1	<0.05
NF0119700	Hemerythrin	-11.4	NA
NF0106930	Phenylalanine hydroxylase	-5.7	<0.05
NF0008540	Hydrogenase	-3.7	<0.05
NF0081220	HydE	-2.8	<0.05
NF0081230	HydG	-2.4	<0.05
NF0036800	Iron-containing cholesterol desaturase daf-36-like	-2.0 (-3.4)	NA (<0.05)
NF0001470	Tyrosine aminotransferase	-2.0	<0.05
NF0073220	Homogentisate 1,2-dioxygenase	-1.8	<0.05
NF0084900	4-Hydroxyphenylpyruvate dioxygenase	-1.5	<0.05
NF0121200	Catalase	-1.3	<0.05
NF0044680	Iron III Superoxide Dismutase	1.1	0.47
NF0004720	Alternative oxidase	1.5	<0.05
NF0014630	Mitochondrial carnitine/acylcarnitine transferase *	ND (1.5)	NA (0.39)
NF0015750	Manganese superoxide dismutase	1.6	<0.05
NF0079420	Mitoferrin *	1.8 (1.7)	<0.05 (0.08)
NF0020800	Fe superoxide dismutase	1.8	<0.05
NF0048730	Glutathione peroxidase	2.0	<0.05
NF0071710	Deferrochelatase	2.3	<0.05
NF0060430	IscU *	3.0	<0.05
NF0001440	Cysteine desulfurase	3.7	<0.05
NF0030360	Cu-Zn superoxide dismutase	5.8	<0.05
NF0001420	Mitochondrial phosphate carrier protein *	8.0 (8.4)	NA (<0.05)

Proteins were manually annotated using HHPRED or by sequence alignment with homologous proteins from other organisms (denoted with a star). The fold change based on proteomic analysis of whole cells and membrane fractions (for selected proteins; in brackets) is given for cells cultivated under iron-deficient conditions. Significantly regulated proteins (with a fold change above 2.3 and *p*-value not higher than 0.05) are highlighted in green. ND, not detected; NA, not applicable.

https://doi.org/10.1371/journal.pntd.0007759.t001

summarized in Table 1. The list of downregulated proteins based on whole-cell proteomics under iron-deficient conditions contained 20% of predicted iron-containing proteins, most of which were nonheme enzymes such as desaturases and oxygenases, or hydrogenase (NF0008540) and its maturases HydE (NF0081220) and HydG (NF0081230). Importantly, most of the downregulated iron-containing proteins were typically located outside mitochondria. The dramatic downregulation of the hemerythrin homolog (NF0127030) was confirmed by Western blotting using an antibody generated in-house against *N. gruberi* hemerythrin (Fig 2A).

In the phenylalanine catabolism pathway, all three iron-dependent enzymes, phenylalanine hydroxylase (NF0106930), p-hydroxyphenylpyruvate dioxygenase (NF0084900) and homogentisate 1,2-dioxygenase (NF0073220), were downregulated in iron-deprived cells, even though the decrease in the expression of the last two enzymes was below our set threshold.

The proteins upregulated under iron-deficient conditions included two essential mitochondrial components of iron-sulfur cluster assembly machinery, namely, cysteine desulfurase (NF0001440) and iron-sulfur cluster assembly enzyme IscU (NF0060430); two mitochondrial transporters, phosphate carrier (NF0001420) and iron-transporting mitoferrin (NF0079420); and a potential homologue of deferrochelatase (NF0071710). The increase in the expression of mitoferrin was below our set threshold, but the results from the comparative analysis of the

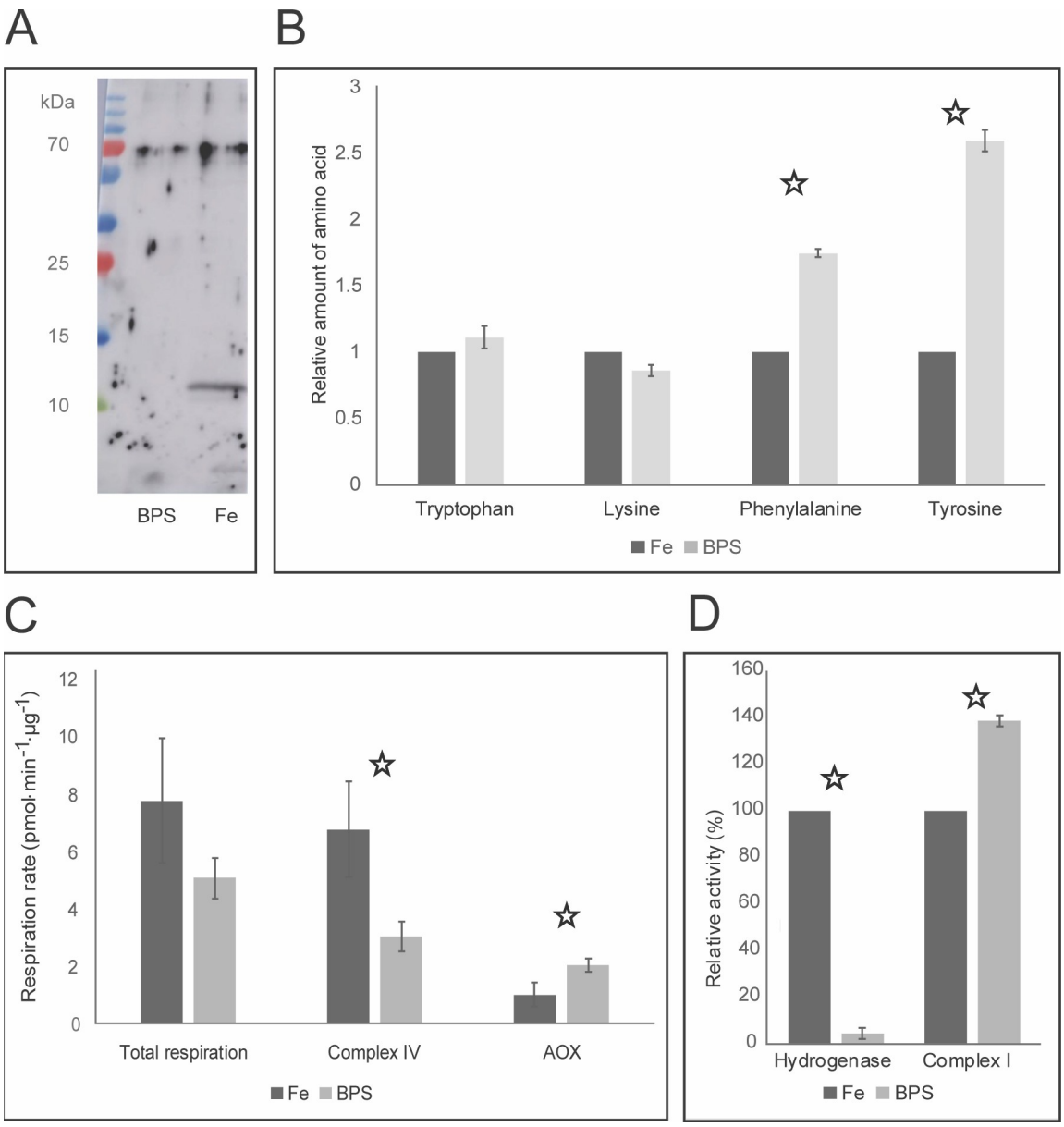

Fig 2. Effect of iron deficiency on *N. fowleri*. (A) Downregulation of *N. fowleri* hemerythrin under iron-deficient conditions. Results from the Western blot analysis of cells cultivated under iron-rich (Fe) and iron-deficient (BPS) conditions using an antibody against *Naegleria gruberi* hemerythrin. Equal protein concentrations were loaded, and the loading control is shown in S1(D) Fig. The gel represents one of three independent replicates. (B) Cellular content of selected amino acids in *N. fowleri* cells cultivated under iron-rich and iron-deficient conditions. Relative amounts of phenylalanine and tyrosine were significantly increased under the iron-deficient condition, while those of tryptophan and lysine remained unchanged. t-test p-values <0.01 are marked with a star. The total protein concentration was equal in all the samples, and the values shown are relative to those under the iron-rich conditions for each amino acid. Fe, cells cultivated under iron-rich conditions; BPS, cells cultivated under iron-deficient conditions. Data are presented as the means ± SD from three independent replicates. (C) Respiration of *N. fowleri* grown under iron-rich and iron-deficient conditions. Using selective inhibitors of complex IV (potassium cyanide) and of alternative oxidase (salicyl-hydroxamic acid), the contribution of alternative oxidase and complex IV activity was assessed with respect to total respiration levels. AOX, alternative oxidase; Fe, cells cultivated under iron-rich conditions; and BPS, cells cultivated under iron-deficient conditions. The t-test p-values <0.01 are marked with a star. Data are presented as the means ± SD from five independent replicates. (D) Activity of hydrogenase and NADH: ubiquinone dehydrogenase (complex I) under iron-rich and iron-deficient conditions. While hydrogenase was significantly downregulated, complex I was significantly upregulated as a result of the iron-deficient conditions. Relative values are shown. Fe, cells cultivated under iron-rich conditions; and BPS, cells cultivated under iron-deficient conditions. The t-test p-values <0.01 are marked with a star. Data are presented as the means ± SD from four independent replicates.

https://doi.org/10.1371/journal.pntd.0007759.g002

membrane-enriched fraction of *N. fowleri* grown under different iron conditions (S2 Table and Table 1) confirmed the upregulation of this transporter as it did for the mitochondrial phosphate carrier. Additionally, in the membrane-enriched proteomic analysis, a carnitine/acylcarnitine transferase (NF0014630) was identified and found to be slightly, although not significantly, upregulated.

Iron metabolism is interconnected with the production and detoxification of reactive oxygen species. Among the antioxidant defense proteins, one family of superoxide dismutases contains iron as a cofactor. Our proteomic analysis showed that while iron-dependent SODs (NF0020800 and NF0044680) were not significantly changed, Cu-Zn-dependent SOD (NF0030360) was upregulated under iron-deficient conditions, suggesting a compensatory mechanism for the mismetallated iron-dependent enzyme. Other radical oxygen species detoxification enzymes, such as catalase (NF0121200), manganese SOD (NF0015750), or glutathione peroxidase (NF0048730), were not significantly regulated under iron-deficient conditions.

To uncover a broader spectrum of the affected proteins that we were unable to detect in the proteomic analysis, we performed a transcriptomic analysis of *N. fowleri* grown under the same conditions of iron availability as used in the proteomic analysis (S3 Table). To our surprise, the data did not correspond to the proteomics results. Overall, the number of genes that were significantly changed in the transcriptomic analysis results was 287 (182 upregulated and 105 downregulated genes), which is more than those regulated in whole cell proteomic analysis; however, the only genes regulated in the same way as the proteins observed in the proteomic analysis were hemerythrins, protoglobin (NF0117840) and the iron-containing cholesterol desaturase daf-36-like (NF0036800). The response of *N. fowleri* to iron starvation is thus most likely posttranslational. The large proportion of nonheme iron-containing enzymes among the downregulated proteins indicates that the degradation of mismetallated/misfolded/nonfunctional proteins plays an important role in iron-induced proteome changes. To confirm the physiological relevance of the changes observed at the proteome level, we further investigated selected biochemical pathways that were indicated by the proteomic results.

N. fowleri responds to iron deficiency by metabolic rearrangement that favors mitochondria

Considering the iron-dependent changes in the abundance of proteins participating in the phenylalanine degradation pathway, the next aim of this study was to analyze this effect by directly detecting metabolites, namely quantifying the cellular levels of corresponding amino acids by metabolomics. Cells grown under iron-rich and iron-deficient conditions were lysed, the protein concentrations were equalized, and the resulting material was analyzed for amino acid content by liquid chromatography coupled with mass spectrometry. Since the phenylalanine degradation pathway was predicted to be downregulated by the proteomic analysis results, we assessed the intracellular amounts of phenylalanine and tyrosine, amino acids likely affected by a decrease in iron-dependent enzymes. As expected, under iron-deficient conditions, the amount of phenylalanine was significantly increased, by 75% (±3%; p-value <0.01), and tyrosine was increased by 160% (±8%; p-value <0.01) (data are shown in Fig 2B). As controls, relative amounts of tryptophan and lysine, the levels of which were not expected to change according to iron levels, were determined in the same samples.

N. fowleri cells possess lactate dehydrogenase and are therefore potentially able to produce lactate from pyruvate while replenishing the level of NAD^+ cofactor, thereby utilizing cytosolic pathways for energy metabolism. To analyze the effect of iron starvation on this metabolic pathway, lactate production was analyzed by gas chromatography coupled with mass

spectrometry detection. The level of intracellular lactate in the iron-deficient cells was decreased by 32% (±13%; p-value <0.05), showing that this metabolic pathway was not used in a compensatory strategy during iron deficiency.

Alternative oxidase (AOX), present in *N. fowleri*, is a part of the mitochondrial respiratory chain. It accepts electrons from ubiquinol to reduce the final electron acceptor, oxygen. Therefore, the function of AOX is similar to that of complex IV; however, the branching electron flow towards AOX bypasses some of the proton pumping complexes, decreasing the effect of the respiration chain. Using selective inhibitors of respiration complex IV and AOX enables the study of their participation in respiration. Here, the effect of decreased iron availability on the respiratory chain was determined. The results are shown in Fig 2C and demonstrate that the total respiration of the cells grown under iron-deficient conditions was decreased by 35%, although this change was not statistically significant (p-value >0.01), and that this decrease was based on the diminished activity of complex IV (55% decrease; p-value <0.01). In contrast, in the iron-deficient cells, the activity of AOX increased by 104% (p-value <0.01). This finding shows that AOX, despite being an iron-containing enzyme, is able to rescue respiration when iron deficiency causes a decrease in complex IV activity.

To further support the hypothesis that iron-starved *N. fowleri* maintains essential mitochondrial iron-dependent proteins at the expense of nonessential cytosolic proteins, we assessed iron-induced changes in the activity levels of mitochondrial NADH:ubiquinone dehydrogenase (complex I) and hydrogenase, which was shown to be cytosolic in *Naegleria* [22]. As shown in Fig 2D, the activity of hydrogenase was dramatically decreased, by 95%, under iron-deficient conditions (p-value <0.01), indicating that it is a dispensable component of the pathway when iron is scarce. In contrast, the activity level of mitochondrial complex I was increased by 39% under iron-deficient conditions (p-value <0.01), thus it was maintained as part of a vital pathway. Hence, the increased activity levels of the mitochondrial iron-containing enzymes AOX and complex I were able to rescue total mitochondrial respiration despite the decrease in the activity of complex IV. This finding demonstrates that the mitochondrial respiration chain is essential and maintained under iron-deficient conditions even if it is strongly iron demanding.

Iron chelators significantly hinder *N. fowleri* growth

Iron plays a vital role in many biochemical processes; therefore, it is rational to expect that decreasing the bioavailability of iron in the surrounding environment would hinder cell growth. To determine the effect of iron on the propagation of *N. fowleri* in culture, three different iron chelators were added to the growth medium: bathophenanthroline disulfonic acid (BPS), 2,2′-dipyridyl (DIP) and deferoxamine (DFO). The compounds inhibited the growth of the cultures to different extents compared to the growth under iron-rich conditions (Table 2 and S2(A) Fig). The most potent effect in hindering culture growth was observed with the siderophore DFO. Both BPS and DIP had notably higher IC_{50} values.

Trophozoites of the amoebae feed on bacteria in their natural environment, making the bacteria potential sources of iron. Moreover, we presume that phagocytosis of human cells can represent one of *N. fowleri* virulence factors [23]. To investigate overall cell viability and to test whether *N. fowleri* cells induce phagocytosis as a potential way to acquire iron, the ability of iron-deficient cells to phagocytose bacteria was investigated. Quantification of phagocytosis was determined by flow cytometry using *Escherichia coli* that present increased fluorescence within acidic endocytic compartments. The values were calculated as percentages of amoebae in the total population with phagocytosed bacteria. Under iron-rich conditions, the percentage of phagocytosing amoebae was 70% (±6%), while under iron-deficient conditions, it was 53%

Table 2. Iron chelator IC_{50} values for *N. fowleri* cultures after 48 hours.

Compound	IC_{50} (μM)
DIP	30.39 (±3.49)
BPS	17.01 (±2.42)
DFO	6.32 (±0.85)

DIP, 2,2′-dipyridyl; BPS, bathophenanthroline disulfonic acid; and DFO, deferoxamine. The data used for the IC_{50} extrapolation are depicted in S2(B) Fig.

https://doi.org/10.1371/journal.pntd.0007759.t002

(±4%). This significant decrease (p-value <0.01) shows that iron availability plays a role in this process. A representative dot plot from the flow cytometry data is shown in S3 Fig, including the controls of *N. fowleri* cells with no bacteria and a bacterial culture. A typical cell phagocytizing fluorescent bacteria is shown in the S1 video.

To show the extent to which iron-deficient *N. fowleri* is able to restore its own growth by phagocytosing bacteria, we presented attenuated *Enterobacter aerogenes* to amoebae cultivated under different iron conditions. As shown in S4 Fig, while the iron-deficient cells proliferated significantly more slowly than the iron-rich cells did, the addition of bacteria did not increase the proliferation of the cells cultivated under iron-deficient or iron-rich conditions. In contrast, the addition of iron to previously iron-deficient cultures fully reestabilished the original cell proliferation rate. In summary, iron is a vital element for *N. fowleri* cell propagation and chelators have a cytostatic effect on amoebae. Phagocytosis of bacteria is not a sufficient strategy of iron acquisition and is even suppressed during iron deficiency.

Discussion

To maintain an optimal level of cellular iron in a hostile environment, such as host tissues, pathogens possess selective and effective mechanisms for iron uptake. These strategies of obtaining iron include the utilization of various sources from the host, including transferrin, lactoferrin or heme, and some parasites even exploit bacterial siderophores as sources of iron [16]. Transferrin, an abundant human blood protein that transports iron to various tissues, including the brain [18], serves as a viable source of iron for different parasites [16]. It was demonstrated that *N. fowleri* possesses proteases able to degrade human holotransferrin, although the study did not identify the intracellular fate of the iron [24]. Our study shows that *N. fowleri* does not appear to have the means of efficiently utilizing iron from this host protein (S1B Fig), perhaps because it is a facultative pathogen with no advantage of such an iron uptake mechanism in its natural environment. We further demonstrated the preference of *N. fowleri* for ferrous iron compared to ferric iron (Fig 1A), the inhibitory effect of ferrous iron chelator on ferric iron uptake (S1C Fig) and the presence of extracellular ferric reductase activity (Fig 1B). Based on these observations, we argue that the main strategy of iron acquisition by this parasite could be the reductive two-step iron uptake mechanism, as described for *Saccharomyces cerevisiae* [16].

S. cerevisiae possesses the ability to upregulate the expression of ferric reductase, which is responsible for the first step of the reductive iron uptake mechanism, up to 55 times under iron-deficient conditions [25], therefore increasing the rate of iron uptake. Our study shows that in *N. fowleri*, the activity of ferric reductase is not induced by iron starvation nor is the ferric and ferrous iron uptake and further incorporation of iron into cellular proteins (Fig 1A and 1B). The lack of an inducible iron uptake system has also been described in the parasite *Tritrichomonas foetus* [26]. However, contrary to *N. fowleri*, the obligatory parasite *T. foetus* appears to be able to utilize a wide range of iron sources, including host transferrin or bacterial

siderophores. Another potential source of iron for *N. fowleri* can be heme from heme-containing proteins. The ability to utilize exogenous metal-containing porphyrins may be advantageous for protists feeding on bacteria. Moreover, *Naegleria* species phagocyte erythrocytes [27,28], and their ability to degrade hemoglobin using proteases was also described [24]. However, it appears that heme oxygenase is not present in the genome of *N. fowleri*; therefore, it is unlikely to be able to employ this enzyme to obtain iron from hemoglobin, as is the case of *T. foetus* [26]. A potential homologue of bacterial deferrochelatase, a protein able to directly acquire iron from heme [29], was identified as significantly upregulated under iron-deficient conditions by proteomic analysis (Table 1); however, further investigation is required to clarify the function of this protein. Nevertheless, hemin was shown to partially restore *N. fowleri* growth in very strong iron-deficient conditions (Fig 1C). Since *N. fowleri* requires exogenous porphyrins for growth [30], the fact that the addition of hemin partly suppresses the conditions of iron starvation can be attributed to a metabolic rearrangement towards heme-dependent pathways. Although phagocytosis could be an alternative strategy for obtaining iron in natural and host environments, according to our data, it does not appear to be utilized under iron-deficient conditions. We showed that the actual rate of phagocytosis was decreased in this case and that the extent of iron-deficient culture propagation could be restored by the addition of iron but not by attenuated bacteria (S4 Fig). Considering these findings, it is important to note that the relationship between decreased phagocytosis and decreased hemerythrin expression was previously described [31]. While *N. fowleri* is unable to utilize iron from transferrin, it is possible that phagocytosis is one of the strategies for obtaining iron from the host and thus may represent a virulence factor that can be diminished by iron starvation. This presents an opportunity to use chelation-based therapy to decrease the ability of the pathogen to gain access to the available iron from host tissues and thereby further increases the iron deficiency of the parasite.

Proteomic analysis proved to be a valuable resource in determining the cellular changes in *N. fowleri* induced by iron starvation and provided a foundation for further discoveries that are shown in this study (Table 1). The most fundamental finding of comparative proteomic analysis is that mainly cytosolic iron-containing proteins were downregulated when iron was limited. These proteins are likely components of nonessential pathways, such as the phenylalanine degradation, hydrogenase maturation and hydrogen production pathways. The accumulation of phenylalanine was observed in *S. cerevisiae*, where iron-deficient cells contained about 50% more of the amino acid than iron-rich cells [32]. On the other hand, mitochondrial iron-dependent proteins were generally unchanged, while some components of the iron-sulfur cluster synthesis machinery were upregulated under iron-deficient conditions, emphasizing the essential role of iron-dependent respiration process. This mitochondrial sequestration of iron to ensure respiration was confirmed by increased complex I activity with a concomitant decrease in the activity level of hydrogenase (Fig 2D) as well as a reduction in the iron-dependent catabolism of amino acids (Fig 2B). Consistent with this observation, the mitochondrial iron transporter was upregulated under iron-deficient conditions. Moreover, the carnitine/acylcarnitine carrier was identified in the membrane-enriched proteomic analysis, and its expression was slightly increased in iron-starved cells. This mitochondrial membrane-bound protein is involved in lipid metabolism, which was recently shown to be vital for *N. gruberi* [33]. Another mitochondrial transport protein, a phosphate carrier, was strongly upregulated under iron-deficient conditions, likely to compensate for impaired respiration and decreased ATP production in the mitochondria of iron-deficient cells.

N. fowleri, as well as *N. gruberi*, possesses an AOX in the mitochondria, and our study indicates one of the possible advantages of this respiratory chain element for these organisms. Under iron-deficient conditions, the activity of AOX was significantly increased (Fig 2C), even

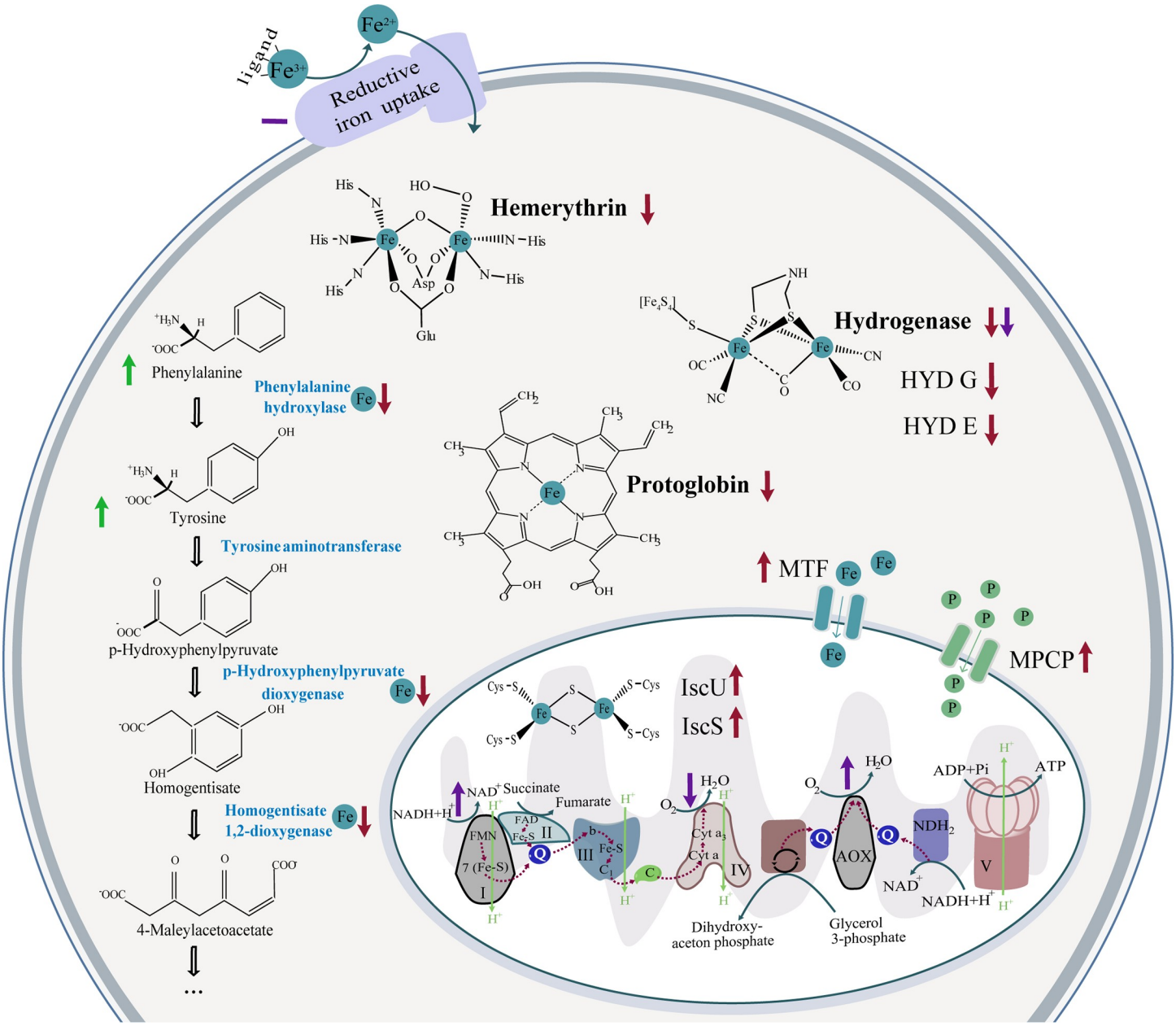

Fig 3. Illustration of the main effects of iron-deficient conditions on the selected cellular processes of *N. fowleri*. The results of proteomic analysis for selected proteins are depicted in red, the results from measured metabolite levels are in green and the assessed enzyme activities are in purple. Upwards pointing arrows stand for increased in the iron-deficient condition, downwards pointing arrows represent decreased in the iron-deficient conditions and dashes mean no significant change in the different iron conditions. Respiration chain complexes are represented by appropriate numbers, Fe represents iron-containing/involving protein/process. C, cytochrome C; MTF, mitoferrin; MPCP, mitochondrial phosphate carrier protein; P, phosphate; Q, ubiquinol/ubiquinone.

https://doi.org/10.1371/journal.pntd.0007759.g003

though it requires iron, suggesting that this unusual branch of the respiratory chain may take over a portion of the activity in the iron-demanding conventional pathway of respiratory complexes III, IV and cytochrome c, an observation noted in the nonpathogenic amoeba *N. gruberi* previously [34]. This could represent a favorable compensation pathway, even though the overall generation of the proton gradient and therefore ATP synthesis is hindered. In addition, we observed an increase in the activity of complex I (Fig 2D), supporting the claim that the respiration is shifted towards the less-efficient but also less iron-dependent AOX pathway.

Considering the reduced efficiency of respiration by iron-starved cells and the presence of lactate dehydrogenase in the genome of *N. fowleri*, it would be reasonable to expect the employment of the lactate dehydrogenase pathway in the regeneration of the cofactor NAD^+. Such an effect was observed in *Trichomonas vaginalis*, where the cells modulate this pathway as a way of compensating for the metronidazole-induced loss of hydrogenosomal metabolism [35]. However, our metabolomic analysis showed the opposite change; the production of lactate was decreased upon iron starvation, suggesting another, most likely nonessential, function of this pathway that is attenuated due to the hindered rate of overall energy metabolism. Another possible compensatory pathway, ethanol production, is improbable because of the absence of pyruvate decarboxylase or bifunctional aldehyde/alcohol dehydrogenase in the *N. fowleri* genome. The function of cytosolic hydrogenase, which was significantly downregulated in the iron-limited conditions together with its maturation factors, is unknown in *Naegleria*.

Consistent with our previous study of iron metabolism in *N. gruberi* [34], hemerythrin was dramatically downregulated under iron-deficient conditions (Fig 2A), while it appears to be an abundant protein under standard conditions, based on the intensities obtained in proteomic analysis from iron-rich cells. The involvement of hemerythrin in the iron metabolism of *Naegleria* is suggestive but unclear. The presence of unbound metals in the cell must be strictly regulated since the imbalance in iron homeostasis can lead to the formation of ROS, mismetallation or other anomalies leading to the incorrect function of proteins. The relationship between hemerythrin and defense against oxidative stress was previously suggested in bacteria [36,37] and so was the role of hemerythrin-related proteins in iron homeostasis [38] or oxygen sensing [39]. One of the basic mechanisms of maintaining the proper intracellular level of metals is the regulation of their acquisition. Since our study shows the lack of such regulation for iron, it is possible that the sequestration of toxic free iron, as well as its storage for use under iron-deficient conditions, is ensured by hemerythrin functioning as a cytosolic iron pool. This hypothesis is supported by the fact that hemerythrin is a nonheme, noniron-sulfur metalloenzyme and is among the most strongly regulated proteins by iron availability, and unlike other proteins, its regulation was detected even at the mRNA level. Another oxygen-binding protein with unclear function, protoglobin, was detected only under iron-sufficient conditions. The role of protoglobin in the metabolism of *N. fowleri* remains to be elucidated.

Due to the irreplaceable role of iron in cellular processes, it is unsurprising that iron chelators have the ability to hinder the proliferation of *N. fowleri* [40]. The different chelators used in this study have distinct properties that influence their impact on cells. DIP is a membrane-permeable compound with affinity to ferrous iron [41] and a ratio of three chelator molecules binding one molecule of metal [42]. BPS is a membrane-impermeable chelator that binds ferrous iron with a ratio of three chelator molecules to one metal ion [43]. Finally, DFO is a membrane-impermeable, ferric iron-binding siderophore [44] with a binding ratio of one iron per molecule [45]. Quite surprisingly, the only tested membrane-permeable iron chelator, DIP, had the highest IC_{50} value (30.39 μM; SD = 3.49). In comparison with BPS, with which it shares an affinity to ferrous iron and the same denticity, DIP was almost half as effective in inhibiting culture growth. BPS and DFO differed not only by the oxidation state of bound iron but also by the ratio of molecules bound to the chelated iron. Their IC_{50} values were 17.01 μM (SD = 2.42) and 6.32 μM (SD = 0.85), respectively, showing an apparent tendency of the approximately three-fold amount of BPS required to have the same effect as DFO, probably because of the binding ratio. Therefore, surprisingly, it appears that from the selected chelators, the membrane-impermeable chelators are more effective against *N. fowleri*. It is important to consider that the growth medium used in this study was adjusted to the amoeba requirements, while in its host, the parasite is expected to meet much harsher conditions. The inhibiting concentrations of chelators shown in this study were of a magnitude that can be

achieved in the human body, such as has been shown for DFO [46], demonstrating that chelation therapy could be considered in the case of PAM. It must be emphasized, that experiments in this study were performed in axenic cultures under optimal growth conditions. Thus, the anticipated *in vivo* antiparasitic effect of suitable chelators may be more pronounced. This laboratory setting undoubtably differs from the natural habitat of the pathogen or the host, where the conditions are harsher, and many interactions take place; therefore, further *in vivo* experiments are required to extend these results towards practical utilization. Our study could not conclusively assess the viability of chelators as suitable therapeutics. However, based on our data, we believe that iron chelation therapy is a promising approach to hinder and attenuate the progress of the disease while not being hazardous to the host, since even long-term intensive exposure of iron chelators can be safely applied to humans [47]. Considering the severity of the disease, we do not assume that chelators may fully cure PAM in patients, but we are aiming to safely hinder the rapid progression of the infection, thus securing more time for correct diagnosis determination and to deploy effective combination therapy.

In conclusion, our study suggests that *N. fowleri* possesses only limited capabilities of adaptation to an iron-deficient environment and is surprisingly not able to utilize transferrin as an alternative source of the metal; neither can it effectively induce the rate of iron acquisition under iron starvation, reflecting the lifestyle of a facultative parasite with limited ability of survival in a host. The main strategy of acquiring iron appears to be reductive iron uptake. Proteomic analysis of the response to iron starvation demonstrated that a large amount of proteins downregulated under the iron-deficient conditions were nonmitochondrial and nonheme enzymes. The exception is the heme-containing protein protoglobin, whose expression is regulated at the transcriptional level, unlike the expression of most other affected proteins. Therefore, it can be hypothesized that the fundamental effect of iron deprivation is the degradation of mismetallated cytosolic proteins with a simultaneous increase in iron delivery to mitochondria and induction of iron-sulfur cluster synthesis machinery to ensure essential cell processes. The overall changes in cellular processes in the iron-deficient conditions discussed in this paper are illustrated in Fig 3. These findings are in agreement with our previous study focused on iron metabolism in the nonpathogenic model organism *N. gruberi* [34], where the mitochondrion was shown to be the center of the iron economy. Together, these results show that iron-deficiency is a highly unfavorable condition for *N. fowleri*, and targeted interference with its uptake could be an effective method of controlling the propagation or viability of this organism in the host.

Materials and methods

Statistical analysis

Unless stated otherwise, two-tailed Student's *t*-test with two-sample equal variance was used to determine the *p*-values. For comparative proteomic analysis, the data was analyzed using the Perseus [48] package Maxquant [49] with two-tailed T-test of equal variance, S0 = 0.5, FDR = 0.01, quantification and normalization procedure MaxLFQ [50] was used.

Unless stated otherwise, all experiments were performed in three or more independent replicates, meaning parallel experiments on independently cultivated cultures.

Organisms

Naegleria fowleri, strain HB-1, kindly provided by Dr. Hana Pecková (Institute of Parasitology, Biology Center CAS) was maintained in 2% Bacto-Casitone (Difco, USA) supplemented with 10% heat-inactivated fetal bovine serum (Thermo Fisher Scientific, USA), penicillin (100 U/ml) and streptomycin (100 μg/ml) in 25 cm^2 aerobic cultivation flasks at 37˚C. When required,

the cells were cultivated for 72 hours with the addition of 25 μM BPS (Sigma-Aldrich, USA), simulating the iron-deficient environment, or with 25 μM Fe-NTA (Sigma-Aldrich, USA) to ensure iron-rich conditions.

Iron uptake

N. fowleri cells grown for 72 hours under iron-rich and iron-deficient conditions were washed with phosphate buffered saline (PBS) (1000 g for 15 min) and transferred to measuring buffer (50 mM glucose; 20 mM HEPES; pH 7.2). Cells were counted using a Guava easyCyte 8HT flow cytometer (Merck, Germany), and 2.5×10^5 cells were equally split onto a 24-well plate. To assess iron uptake, cells were supplemented with 2 μM ^{55}Fe-citrate, 2 μM ^{55}Fe-citrate with 1 mM ascorbate, or 6.3 μM ^{55}Fe-transferrin. Samples were incubated at 37˚C for 1 hour, and then EDTA was added to a final concentration of 1 mM to chelate extracellular iron. Cells were washed three times by measuring buffer, and the protein concentration was assessed using a BCA kit (Sigma-Aldrich, USA). Samples were diluted to equal concentrations and separated using the Novex Native PAGE Bis–Tris Gel system (4–16%; Invitrogen, USA). The gel was vacuum-dried for 2 hours and autoradiographed using a tritium storage phosphor screen. The experiment was performed in three independent replicates. If applicable, densitometry was used to compare signal strength, using Fiji distribution of ImageJ [51].

Ferric reductase activity

To assess the activity of *N. fowleri* ferric reductase under different iron conditions, a ferrozine assay was used to compare the formation of ferrous iron, as described previously [52]. Cells were grown under iron-rich and iron-deficient environments for 72 hours. Samples containing no cells and samples without Fe-EDTA were used as controls. The cells were washed twice and resuspended in glucose buffer (50 mM glucose, 0.5 mM $MgCl_2$, 0.3 mM $CaCl_2$, 5.1 μM KH_2PO_4, 3 μM Na_2HPO_4, pH 7.4). The total amount of proteins was assessed using a BCA kit, and samples were diluted to equal concentrations. All further work was performed with minimum light exposure. Ferrozine was added to a total concentration of 1.3 mM and Fe-EDTA to a concentration of 0.5 mM. Samples were incubated at 37˚C for three hours, pelleted (1000 g for 10 min) and the supernatant was used to determine the formation of the colored Fe(II)-ferrozine complex, accompanied by a change in absorbance at 562 nm using 1 cm cuvettes and a UV-2600 UV-VIS spectrophotometer (Shimadzu, Japan). The experiment was performed in three independent replicates.

Hemin utilization

To assess the ability of *N. fowleri* to utilize hemin, 2×10^4 cells were cultivated in each well of a 24-well plate in fresh growth medium. Cultures were supplemented with 50 μM BPS, 50 μM hemin, or 50 μM hemin and 50 μM BPS. Cells without chelator or hemin were used as a control. The cell concentration was measured every 24 hours for four days using a Guava easyCyte 8HT flow cytometer. The experiment was performed in four independent replicates.

Comparative proteomic analysis

N. fowleri cells were cultivated in 75 cm^2 aerobic cultivation flasks under iron-rich and iron-deficient environments for 72 h. For whole-cell proteomic analysis, cells were washed three times in PBS (1000 g, 15 min, 4˚C) and pelleted. The experiment was performed in three independent replicates.

In addition, a membrane-enriched fraction was prepared. Approximately 1.5×10^7 cells were harvested (1000 g, 15 min, 4˚C), washed in 15 ml of sucrose-MOPS buffer (250 mM sucrose, 20

mM 3-morpholinopropanesulfonic acid, pH 7.4, supplemented with complete EDTA-free protease inhibitors, Roche, Switzerland) and resuspended in 4 ml of sucrose-MOPS buffer. The suspension was sonicated using a Q125 sonicator (Qsonica, USA) (45% amplitude, total time of 4 min using 1 s pulse and 1 s pause). The resulting suspension was centrifuged (5000 g, 5 min) to spin down the unlysed cells. The obtained supernatant was further centrifuged (200 000 g, 20 min). The supernatant was discarded, and the membrane-enriched pellet was washed with distilled water. The experiment was performed in three independent replicates.

Label-free proteomic analysis of the samples was assessed using the method described in *Mach et al. 2018* [34], utilizing liquid chromatography coupled with mass spectrometry. The resulting MS/MS spectra were compared with the *Naegleria fowleri* database, downloaded from amoebaDB [53] on 25/7/2017. The set thresholds to filter proteins were Q-value = 0, unique peptides detected >2, and the protein had to be identified at least twice in one condition from the six runs. For proteins identified only in one of the conditions, intensity of 23 was selected as a lowest value to be included, on basis of previous imputation experience. To distinguish significantly downregulated or upregulated proteins in the iron-deficient conditions in S1 and S2 Tables, the threshold of fold change >2.3 and <-2.3 was chosen, based on previous experience and published results on comparative proteomics in *N. gruberi* and *Ostreococcus tauri* [34,54].

The annotations and identifications of the selected proteins discussed in this study were confirmed using the tool HHPRED [55]. In addition, alignments were constructed using the chosen proteins and their homologues from different organisms: NF0014630 identified as mitochondrial carnitine/acylcarnitine transferase [56], NF0001420 identified as mitochondrial phosphate carrier [57], NF0060430 identified as IscU [58,59] and NF0079420 identified as mitoferrin [60,61]. Alignments with the indicated conserved sequences are shown in S5 Fig and were constructed using Geneious version 11.1.5 software with the muscle alignment tool.

Western blot

To analyze the expression of *N. fowleri* hemerythrin in different iron conditions, cells cultivated in iron-rich and iron-deficient conditions for 72 hours were pelleted, washed by PBS and protein concentration was assessed using BCA kit. Equal amounts were boiled in SDS sample buffer (Merck Millipore, USA) for 5 min and samples were separated using sodium dodecyl sulphate–polyacrylamide gel electrophoresis as first described in [62]. Proteins were transferred to nitrocellulose membrane by western blotting using semi-dry method, for 75 minutes under 1.5 current of mA/cm^2. The proteins were visualized by Ponceau S stain (0.5% Ponceau S, Merck Millipore, USA, 1% acetic acid), confirming a unified loading of the two samples.

The membrane was blocked for one hour, using 5% dried fat-free milk and 0.05% Tween 20 (Sigma-Aldrich, USA) in PBS. Afterwards, the blot was transferred to fresh blocking solution with primary antibody in ratio 500:1 for one hour. The polyclonal antibody was made in-house, against the whole protein (13.5 kDa) in rat with no adjuvants and was previously used in [34]. After washing with fresh blocking solution, secondary anti-rat antibody conjugated with horse-radish peroxidase (Sigma-Aldrich, USA) was added in 1:2000 ratio for one hour. After washing with fresh blocking buffer and PBS, the antibody was visualized using Chemiluminescent Peroxidase Substrate-1 (Sigma-Aldrich, USA) according to manufacturer protocol, on Amersham Imager 600 (GE Life Sciences, USA).

Comparative transcriptomic analysis

To obtain the transcriptome data of *N. fowleri*, five independent replicates of approximately 1×10^6 cells each were grown under iron-rich and iron-deficient conditions for 72 hours. A

High Pure RNA Isolation Kit (Roche, Switzerland) was used to isolate cell RNA, and an Illumina-compatible library was prepared using QuantSeq 3′ mRNA-Seq Library Prep Kit FWD for Illumina (Lexogen, Austria). The RNA concentration was determined using a Quantus fluorometer (Promega, USA), and the quality of RNA was measured on a 2100 Bioanalyzer Instrument (Agilent technologies, USA). Equimolar samples were pooled to 10 pM and sequenced with MiSeq Reagent Kit v3 (Illumina, USA) using 150-cycles on the MiSeq platform. The obtained results were filtered using the p-value of >0.05 followed by analysis on the BlueBee platform with the method DESeq [63].

Amino acid quantification assay

Approximately 3×10^6 cells cultivated under iron-rich and iron-deficient environments were harvested by centrifugation (1000 g, 15 min, 4˚C), washed with PBS supplemented with cOmplete EDTA-free protease inhibitor, and the total concentration of proteins was measured. Cells were transferred to 1 ml of buffer solution (20 mM Tris, 1 mM $MgCl_2$, pH 8, cOmplete EDTA-free protease inhibitor) and sonicated with Sonopuls mini20 (Bandelin, Germany) (90% amplitude, 4˚C, total time 120 s, 1 s pulse and 1 s pause). The resulting suspension was mixed at a ratio of 1:4 with ice-cold acetonitrile and maintained overnight at -20˚C. Samples were centrifuged (16000 g, 20 min, 4˚C) and filtered using Ultrafree Centrifugal Filter Units (Merck Millipore, USA). The experiment was performed in three independent replicates.

Samples were analyzed using liquid chromatography on a Dionex Ultimate 3000 HPLC system with on-line mass spectrometry detection (Thermo Scientific, USA). The separation was achieved using a HILIC column iHILIC-Fusion (150 x 2.1 mm, 1.8 μm particles, 100 Å pore size, HILICON, Sweden). The entire analysis flow rate was 0.3 ml/min, and the column was equilibrated with 100% of solution A (80% acetonitrile in water, 25 mM ammonium formate, pH 4.8) for 3 min. Amino acids were eluted by increasing the gradient of solution B (5% acetonitrile in water, 25 mM ammonium formate, pH 4.8), where 50% of solution B was reached in 7 min. After separation, the column was washed with 80% solution B for 3 min and then equilibrated with 100% solution A for 5 min.

Amino acids were detected by mass spectrometry using the triple quadrupole instrument TSQ Quantiva (Thermo Scientific, USA) in Selected Reaction Monitoring mode. Analytes were ionized using electrospray ionization on an H-ESI ion source and analyzed with positive charge mode with a spray voltage of 3500 V, ion transfer tube temperature of 325˚C, and vaporizer temperature of 350˚C. All transitions, collision energies, and RF voltages were optimized prior to analysis using appropriate amino acid standards. Each analyte was detected using at least two transitions. Cycle time was set to 1.8 s and both Q1 and Q3 resolutions were set to 0.7 s. To analyze the ion chromatograms and calculate peak areas, Skyline daily version 4.2.1.19004 [64] was used.

Lactate production

To assess the difference in the intracellular production of lactate, 3×10^6 cells cultivated under iron-rich or iron-deficient conditions were prepared for analysis in the same way as for quantifying the amino acid content. The experiment was performed in three independent replicates. After incubation with acetonitrile and filtration, the cell sample was dried and resuspended in 100 μl of anhydrous pyridine (Sigma-Aldrich, USA), and 25 μl of a silylation agent (N-tert-butyldimethylsilyl-N-methyl-trifluoroacetamide, Sigma-Aldrich, USA) was added. The sample was incubated at 70˚C for 30 min. After incubation, 300 μl of hexane (Sigma-Aldrich, USA) and 10 μl of an internal standard (102 μg/ml 1-bromononane solution in hexane) were added. Selected compounds were analyzed as tert-butyl silyl derivatives.

Samples were analyzed using two-dimensional gas chromatography coupled with mass detection (GCxGC-MS; Pegasus 4D, Leco Corporation, USA) with ChromaTOF 4.5 software. Mass detection was equipped with an EI ion source and TOF analyzer with unite resolution. A combination of Rxi-5Sil (30 m x 0.25 mm, Restek, Australia) and BPX-50 (0.96 m x 0.1 mm, SGE, Australia) columns were used. The input temperature was set to 300˚C, the injection volume was 1 μl in spitless mode, and constant helium flow of 1 ml/min, modulation time 3 s (hot pulse 1 s) and modulation temperature offset with respect to the secondary oven 15˚C were used. The temperature program applied on the primary oven was 50˚C (hold 1 min), which was increased by the rate of 10˚C/min to a final temperature of 320˚C (hold 3 min). The temperature offset applied on the secondary column was +5˚C.

Cell respiration

Five independent replicates of 3×10^6 *N. fowleri* cells grown for 72 hours under iron-rich and iron-deficient conditions were washed twice and resuspended in 1 ml of glucose buffer, and the protein concentration was assessed using a BCA kit. Total cell respiration was measured as the decrease in oxygen concentration using an Oxygen meter model 782 (Strathkelvin instruments, UK) with Mitocell Mt 200 cuvette of total volume of 700 μl at 37˚C. Measurements were carried out with 5×10^5 cells for 5 min, after which potassium cyanide was added to a final concentration of 4 mM to block complex IV, and after 5 min, salicyl hydroxamic acid was added to a final concentration of 0.2 mM to completely block AOX. Values gained after the addition of potassium cyanide and salicyl hydroxamic acid were subtracted to acquire canonical respiratory chain and AOX activity, respectively.

Hydrogenase and complex I activity levels

Approximately 1×10^6 cells cultivated under iron-rich or iron-deficient conditions were washed and resuspended in 0.2 ml of saccharose-MOPS buffer (250 mM saccharose, 10 mM 3-morpholinopropanesulfonic acid, pH 7.2). To assess the hydrogenase activity, we used a protocol previously described [65]. Briefly, the reaction was initiated by the addition of cells lysed with 0.02% Triton X-100 to 2 ml of measuring buffer (0.1 M Tris; 50 mM KCl buffer, pH 7.4; 1 μM methylviologen and 0.5% β-mercaptoethanol, saturated with hydrogen gas). Activity level was assessed on the basis of the change in 600 nm absorbance using 1-cm quartz cuvettes on a Shimadzu UV-2600 UV-VIS spectrophotometer with UVProbe software (Shimadzu, Japan). To assess the complex I activity level, we used a protocol previously described [66]. Briefly, 1% digitonin-treated cells were added to 2 ml of measuring buffer (0.1 M KPi buffer, pH 7.5, and 0.2 mM NADH), and the reaction was initiated by the addition of 50 μM oxidized coenzyme Q2 (Sigma-Aldrich, USA) suspended in ethanol. Activity level was assessed on the basis of the change in 340 nm absorbance using 1-cm quartz cuvettes on the same spectrophotometer as used to assess hydrogenase activity. As a control, 0.2 mM rotenone was added after the measurement as a specific inhibitor of complex I to confirm that the background activity was negligible. Both experiments were performed in four independent replicates.

Chelators

The growth dependence of *N. fowleri* on iron availability was defined using the iron chelators BPS (Sigma-Aldrich, USA), DIP (Sigma-Aldrich, USA) and DFO (Sigma-Aldrich, USA). 5000 *N. fowleri* cells per ml were cultivated in 24-well plates in a total volume of 1 ml in a humid chamber. Each chelator and control were tested in four independent replicates (final concentrations of 100, 50, 25, 12.5, 6.3, 3.1, 1.6 and 0.8 μM). Cells were cultivated for 48 hours, the plates were placed on ice for 10 min, and the medium was gently pipetted to detach the cells. The number of cells in

each sample was counted using a Guava easyCyte 8HT flow cytometer. The value of half-maximal inhibitory concentration (IC_{50}) was calculated using the online calculator on the AAT Bioquest webpage [67]. Graphs were created using GraphPad Prism 6 (GraphPad software, USA).

Growth curves of the organism under the influence of different iron chelators were constructed by inoculating 5000 cells/ml *N. fowleri* trophozoites into 10 ml of cultivation medium with the appropriate compound (25 μM Fe-NTA; 45 μM DIP; 25 μM BPS or 10 μM DFO) in four independent replicates. Counting the number of the cells in culture at 24, 48 and 72 hours was performed by flow cytometry using a Guava easyCyte 8HT flow cytometer.

N. fowleri bacterial phagocytosis

Approximately 3×10^6 cells cultivated under iron-rich and iron-deficient conditions were washed in cultivation flasks by replacing the growth medium with 10 ml of PBS warmed to 37˚C and resuspending in 7 ml of 37˚C PBS. To assess the ability of the cells to phagocytose, 150 μl of pHrodo Green *E. coli* BioParticles Conjugate for Phagocytosis (Thermo Fisher Scientific, USA) was added, and the cells were incubated for 3 hours at 37˚C. Following incubation, the cells were washed with PBS, detached on ice for 15 min, and the fluorescence caused by the phagocytosed particles was consecutively analyzed using a Guava easyCyte 8HT flow cytometer using a 488 nm laser and a Green-B 525/30 nm detector. A negative control (without the addition of BioParticles) was used to determine an appropriate threshold for *N. fowleri* cells. BioParticles resuspended in PBS were measured in the same way to determine the background noise and gave a negligible signal. The effect of different iron availability on the efficiency of phagocytosis of *N. fowleri* was established as the percentage of cells in culture that had increased fluorescence. The experiment was performed with nine independent replicates.

To visualize the ability of *N. fowleri* to phagocytize, live amoebae incubated with fluorescent *E. coli* were imaged with a Leica TCS SP8 WLL SMD-FLIM microscope (Leica, Germany) equipped with an HC PL APO CS2 63x/1.20 water objective with 509 nm excitation, 526 nm-655 nm excitation was detected with a HyD SMD detector, and a PMT detector was used for brightfield imaging. Images were processed using LAS X 3.5.1.18803 (Leica, Germany).

To test the effect of attenuated strain of bacteria on the propagation of iron-starved *N. fowleri* in culture, we preincubated amoebae under iron-rich and iron-deficient conditions for 72 hours and inoculated approximately 1000 cells into 96-well plates to a total volume of 200 μl under select conditions with or without the equivalent of 1×10^6 *Enterobacter aerogenes* that had been attenuated. Preincubated iron-rich cells were inoculated into iron-rich medium as a control, and simultaneously, preincubated iron-deficient cells were inoculated into either iron-deficient or iron-rich medium. The cells were cultivated in a humid chamber at 37˚C for 48 hours and then counted using a Guava easyCyte 8HT flow cytometer. The experiment was performed with six independent replicates.

Supporting information

S1 Fig. (A) Loading control corresponding to Fig 1A, ferrous and ferric iron uptake by *N. fowleri* precultivated under iron-rich and iron-deficient conditions. Coomassie brilliant blue loading stain showed that equal protein concentrations in the samples were subjected to native electrophoresis gels. The proteins were determined from whole cell extracts of *N. fowleri* previously cultivated for 72 hours under iron-deficient conditions (25 μM BPS) or iron-rich conditions (25 μM Fe-NTA) and further incubated with ^{55}Fe(II) (ferrous ascorbate) and ^{55}Fe (III) (ferric citrate). **(B) Lack of ^{55}Fe-transferrin uptake in *N. fowleri*, cultivated under iron-rich and iron-deficient conditions.** The uptake of transferrin-bound iron was assessed by incubation of *N. fowleri* with ^{55}Fe-transferrin. Tf, pure ^{55}Fe-transferrin; Fe, *N. fowleri*

cultivated under iron-rich conditions for 72 hours, consecutively incubated with ^{55}Fe-transferrin for 1 hour; BPS, *N. fowleri* cultivated under iron-deficient conditions for 72 hours, consecutively incubated with ^{55}Fe-transferrin for 1 hour; Ctr, iron uptake control of *N. fowleri* culture cultivated in iron deficiency incubated with ^{55}Fe(III)-citrate for 1 hour. The utilization of iron was analyzed by blue native electrophoresis as described in the Methods section. Equal protein concentrations were loaded, as shown on the Coomassie brilliant blue loading stain. Gel is a representative from three independent replicates. **(C) Mechanism of ferric iron uptake involves the reductive step.** *N. fowleri* culture was incubated for 1 hour with ^{55}Fe(III)-citrate with and without the addition of 0.2 mM BPS. Incorporation of ^{55}Fe(III)-citrate to cellular proteins was higher in the sample without the presence of BPS, indicating that a reductive iron uptake mechanism takes place. Several distinct signals on the lower part of +BPS probably correspond to residues of BPS complexed with ferrous iron radionuclides. The utilization of iron was analyzed by blue native electrophoresis as described in the Methods section. -BPS, cell sample without addition of BPS chelator; +BPS, cell sample with the addition of BPS chelator. Equal protein concentrations were loaded, as shown on the Coomassie brilliant blue loading stain. Gel is a representative from three independent replicates. **(D) Loading control corresponding to Fig 2A, *N. fowleri* cell lysate for Western blot analysis of hemerythrin expression.** Ponceau S loading stain shows equal protein concentrations of loaded samples of *N. fowleri* cultivated under iron-deficient (BPS) and iron-rich (Fe) conditions.
(TIF)

S2 Fig. (A) A representative growth curve of *N. fowleri* treated with different chelators. The chelators hindered the propagation of the cells in culture. The graphs show the cytostatic effect of chosen concentrations of the iron chelators compared with the effect of iron-rich cultivation conditions. Fe, cells cultivated under iron-rich conditions (25 μM Fe-NTA); DIP, cells cultivated in 45 μM DIP; BPS, cells cultivated in 25 μM BPS; and DFO, cells cultivated in 10 μM DFO. Data are presented as the means ± SD from four independent replicates. **(B) *N. fowleri* growth in different concentrations of chelators after 48 hours.** The shown graphs were used to calculate the IC_{50} values for different chelators. The graph was created using GraphPad Prism 6 (GraphPad software, USA). Data are presented as the means ± SD from four independent replicates.
(TIF)

S3 Fig. *N. fowleri* cell phagocytosis. Representative dot plots of flow cytometry results of *N. fowleri* phagocyting bacteria using a pHrodo green *E. coli* BioParticles conjugate to measure phagocytosis (Thermo Fisher Scientific, USA) in nine independent replicates. *N. fowleri*, control culture with no added bacteria; Bacteria, control for the bacteria cells; *N. fowleri* Fe, *N. fowleri* under iron-rich conditions with added bacteria; *N. fowleri* BPS, *N. fowleri* under iron-deficient conditions with added bacteria.
(TIF)

S4 Fig. Phagocytosis of bacteria is not an iron acquisition strategy of *N. fowleri*. Effect of adding the attenuated bacteria *Enterobacter aerogenes* on the propagation of *N. fowleri* under different iron conditions. After 48 hours, amoebae growth was not changed when bacteria were added under any condition (iron-rich cells, iron-deficient cells or cells preincubated under iron-deficient conditions and subsequently transferred into an iron-rich environment all had p-values >0.05). The propagation of the amoebae in the iron-deficient culture was significantly lower than that in the iron-rich culture (23% with bacteria and 26% without bacteria, p-values <0.01 for both), confirming the effect of iron deficiency on amoeba culture propagation. Furthermore, cultures preincubated under iron-deficient conditions and subsequently

transferred into iron-rich environments had the same propagation as those under the iron-rich culture conditions (p-values >0.05 with and without bacteria). Data are presented as the means ± SD from six independent replicates.
(TIF)

S5 Fig. Alignments of *N. fowleri* proteins with homologues from other organisms. (A) Alignment of *N. fowleri* NF0060430 with the IscU proteins from *Homo sapiens*, *Saccharomyces cerevisiae* and *T. brucei*. Red arrows point to the conserved cysteine required for iron-sulfur cluster assembly, based on a previous study [58]. The red rectangle denotes the conserved LPPVK motif of the IscU proteins [59]. (B) Alignment of *N. fowleri* NF0079420 with the mitoferrin proteins of *Trypanosoma brucei*, *Leishmania mexicana*, *Saccharomyces cerevisiae* and *Homo sapiens*. Red arrows point to the sequence motif Px(D/E)xx(K/R)x(K/R), and yellow circles mark residues in contact with substrate, according to a previous study [60]. Conserved histidine residues responsible for iron transport are marked with blue stars [61]. (C) Alignment of *N. fowleri* NF0001420 with the mitochondrial phosphate carriers of *Saccharomyces cerevisiae*, *Homo sapiens* and *Arabidopsis thaliana*. Red arrows point to residues important for the phosphate transport activity, according to a previous study [57]. (D) Alignment of *N. fowleri* NF0014630 with mitochondrial carnitine/acylcarnitine transferases of *Saccharomyces cerevisiae*, *Arabidopsis thaliana*, *Homo sapiens* and *Caenorhabditis elegans*. The red rectangle denotes the signature motifs Px(D/E)xx(R/K)x(R/K), and the arrows point to conserved residues, according to a previous study [56].
(TIF)

S1 Table. Comparison of whole-cell proteomes of *N. fowleri* in iron-rich and iron-deficient environments. List of whole-cell proteomes of *N. fowleri* compared in iron-rich and iron-deficient conditions sorted into four sheets: raw data, all detected proteins, significantly upregulated proteins and significantly downregulated proteins under iron-deficient conditions. With the exception of raw data, the tables are simplified to show only fold change values. Proteins with > 2.3 (denoting upregulated under iron-deficient conditions) or < -2.3-fold change (denoting downregulated under iron-deficient conditions) are regarded as significantly regulated. Proteins were annotated from amoebaDB [53] on 25/7/2017, and manual annotation was performed for selected proteins, as described in the Methods section. Probable iron-containing proteins of the significantly downregulated and upregulated proteins are highlighted in yellow. Experiment was performed with three independent replicates.
(XLSX)

S2 Table. Comparison of membrane-enriched proteomes of *N. fowleri* in iron-rich and iron-deficient environments. List of membrane-enriched proteomes of *N. fowleri* compared in iron-rich and iron-deficient conditions sorted into four sheets: raw data, all detected proteins, significantly upregulated proteins and significantly downregulated proteins under iron-deficient conditions. With the exception of raw data, the tables are simplified to show only fold change values. Proteins with >2.3 (denoting upregulated under iron-deficient conditions) or < -2.3-fold change (denoting downregulated under iron-deficient conditions) are regarded as significantly regulated. Proteins were annotated from amoebaDB [53] on 25/7/2017, and manual annotation was performed for selected proteins, as described in the Methods section. Experiment was performed with three independent replicates.
(XLSX)

S3 Table. Comparison of transcriptomes of *N. fowleri* in iron-rich and iron-deficient environments. List of genes significantly downregulated and upregulated under iron-deficient conditions. Raw data are included, and manual annotation was performed for selected proteins, as described

in the Methods section. Experiment was performed with five independent replicates.
(XLSX)

S4 Table. Raw data.
(XLSX)

S1 Video. The video shows a demonstration of *N. fowleri* phagocytizing bacteria. In the video, a single *N. fowleri* amoeba phagocytoses several fluorescently modified pHrodo green *E. coli* BioParticles (bright blue). In the lysosomes, they fluoresced due to the decreased pH value. In the background, several non-fluorescing bacteria were observed (dim blue). Images were acquired with a Leica TCS SP8 WLL SMD-FLIM microscope (Leica, Germany) equipped with an HC PL APO CS2 63×/1.20 water objective with 509 nm excitation, 526 nm-655 nm excitation was detected with a HyD SMD detector, and a PMT detector was used for brightfield imaging. Images were processed using LAS X 3.5.1.18803 (Leica, Germany). Video was created and edited using the Fiji distribution package of ImageJ software [51].
(MP4)

Acknowledgments

Special thanks to Ivánek for fruitful biochemical discussions.

Author Contributions

Conceptualization: Robert Sutak.

Data curation: Dominik Arbon, Kateřina Ženíšková.

Funding acquisition: Robert Sutak.

Investigation: Dominik Arbon, Kateřina Ženíšková, Maria Grechnikova, Ronald Malych, Pavel Talacko.

Methodology: Jan Mach, Ronald Malych, Pavel Talacko.

Project administration: Robert Sutak.

Supervision: Jan Mach, Robert Sutak.

Validation: Jan Mach, Robert Sutak.

Visualization: Dominik Arbon, Kateřina Ženíšková.

Writing – original draft: Dominik Arbon.

Writing – review & editing: Jan Mach, Maria Grechnikova, Robert Sutak.

References

1. De Jonckheere JF. What do we know by now about the genus *Naegleria*? Exp Parasitol. 2014 Nov; 145 (S):S2–9.
2. Kelly RB, Francine M-C, Charles PG. Occurrence of *Naegleria fowleri* in Arizona drinking water supply wells. J Am Water Works Assoc. 2009 Nov; 101(11):43–50.
3. Visvesvara GS, Moura H, Schuster FL. Pathogenic and opportunistic free-living amoebae: *Acanthamoeba spp.*, *Balamuthia mandrillaris*, *Naegleria fowleri*, and *Sappinia diploidea*. FEMS Immunol Med Microbiol. 2007 Jun; 50(1):1–26. https://doi.org/10.1111/j.1574-695X.2007.00232.x PMID: 17428307
4. Grace E, Asbill S, Virga K. *Naegleria fowleri*: Pathogenesis, diagnosis, and treatment options. Antimicrob Agents Chemother. 2015 Nov 1; 59(11):6677–81. https://doi.org/10.1128/AAC.01293-15 PMID: 26259797

5. Ma P, Visvesvara GS, Martinez AJ, Theodore FH, Daggett PM, Sawyer TK. *Naegleria* and *acanthamoeba* infections: Review. Clin Infect Dis. 1990 May 1; 12(3):490–513.
6. Centers for Disease Control and Prevention, *Naegleria fowleri* general information. Available at: https://www.cdc.gov/parasites/naegleria/general.html, last modified July 17/7/2018, accessed 15/3/2019 [Internet].
7. Linam WM, Ahmed M, Cope JR, Chu C, Visvesvara GS, Da Silva AJ, et al. Successful treatment of an adolescent with *Naegleria fowleri* primary amebic meningoencephalitis. Pediatrics. 2015 Mar 1; 135(3): e744–8. https://doi.org/10.1542/peds.2014-2292 PMID: 25667249
8. Pana A, Vijayan V, Anilkumar AC. Amebic meningoencephalitis [Internet]. StatPearls. 2019.
9. Cabello-Vílchez AM, Chura-Araujo MA, Anicama Lima WE, Vela C, Asencio AY, García H, et al. Fatal granulomatous amoebic encephalitis due to free-living amoebae in two boys in two different hospitals in Lima, Perú. Neuropathology. 2019 Nov 22;neup.12617.
10. Crichton R. Iron metabolism: From molecular mechanisms to clinical consequences: Fourth edition. Chichester, UK: John Wiley & Sons, Ltd; 2016. 1–556 p.
11. Lill R, Broderick JB, Dean DR. Special issue on iron-sulfur proteins: Structure, function, biogenesis and diseases. Biochim Biophys Acta—Mol Cell Res. 2015 Jun 1; 1853(6):1251–2.
12. Boyd PW, Jickells T, Law CS, Blain S, Boyle EA, Buesseler KO, et al. Mesoscale iron enrichment experiments 1993–2005: Synthesis and future directions. Science (80-). 2007 Feb 2; 315(5812):612–7.
13. Koka S, Föller M, Lamprecht G, Boini KM, Lang C, Huber SM, et al. Iron deficiency influences the course of malaria in *Plasmodium berghei* infected mice. Biochem Biophys Res Commun. 2007 Jun; 357(3):608–14. https://doi.org/10.1016/j.bbrc.2007.03.175 PMID: 17445762
14. Kabyemela ER, Fried M, Kurtis JD, Mutabingwa TK, Duffy PE. Decreased susceptibility to *Plasmodium falciparum* infection in pregnant women with iron deficiency. J Infect Dis. 2008 Jul 15; 198(2):163–6. https://doi.org/10.1086/589512 PMID: 18500927
15. Ganz T. Iron in innate immunity: Starve the invaders. Curr Opin Immunol. 2009; 21(1):63–7. https://doi.org/10.1016/j.coi.2009.01.011 PMID: 19231148
16. Sutak R, Lesuisse E, Tachezy J, Richardson DR. Crusade for iron: Iron uptake in unicellular eukaryotes and its significance for virulence. Trends Microbiol. 2008 Jun 1; 16(6):261–8. https://doi.org/10.1016/j.tim.2008.03.005 PMID: 18467097
17. Singh N, Haldar S, Tripathi AK, Horback K, Wong J, Sharma D, et al. Brain iron homeostasis: From molecular mechanisms to clinical significance and therapeutic opportunities. Antioxidants Redox Signal. 2014 Mar 10; 20(8):1324–63.
18. Leitner DF, Connor JR. Functional roles of transferrin in the brain. Vol. 1820, Biochimica et Biophysica Acta—General Subjects. 2012. p. 393–402.
19. Mobarra N, Shanaki M, Ehteram H, Nasiri H, Sahmani M, Saeidi M, et al. A review on iron chelators in treatment of iron overload syndromes. Vol. 10, International Journal of Hematology-Oncology and Stem Cell Research. Tehran University of Medical Sciences (TUMS); 2016. p. 239–47.
20. Cruz-Castañeda A, López-Casamichana M, Olivares-Trejo JJ. *Entamoeba histolytica* secretes two haem-binding proteins to scavenge haem. Biochem J. 2011 Feb 15; 434(1):105–11. https://doi.org/10.1042/BJ20100897 PMID: 21126234
21. Basu S, Horáková E, Lukeš J. Iron-associated biology of *Trypanosoma brucei*. Vol. 1860, Biochimica et Biophysica Acta—General Subjects. Elsevier; 2016. p. 363–70.
22. Tsaousis AD, Nývltová E, Šuták R, Hrdý I, Tachezy J. A Nonmitochondrial hydrogen production in *Naegleria gruberi*. Genome Biol Evol. 2014 Apr; 6(4):792–9. https://doi.org/10.1093/gbe/evu065 PMID: 24682152
23. Marciano-Cabral FM, Patterson M, John DT, Bradley SG. Cytopathogenicity of *Naegleria fowleri* and *Naegleria gruberi* for established mammalian cell cultures. J Parasitol. 1982 Dec; 68(6):1110–6. PMID: 6816913
24. Martínez-Castillo M, Ramírez-Rico G, Serrano-Luna J, Shibayama M. Iron-binding protein degradation by cysteine proteases of *Naegleria fowleri*. Biomed Res Int. 2015 May 18; 2015:1–8.
25. Dancis A, Roman DG, Anderson GJ, Hinnebusch AG, Klausner RD. Ferric reductase of *Saccharomyces cerevisiae*: Molecular characterization, role in iron uptake, and transcriptional control by iron. Proc Natl Acad Sci U S A. 1992 May 1; 89(9):3869–73. https://doi.org/10.1073/pnas.89.9.3869 PMID: 1570306
26. Sutak R, Chamot C, Tachezy J, Camadro JM, Lesuisse E. Siderophore and haem iron use by *Tritrichomonas foetus*. Microbiology. 2004 Dec 1; 150(12):3979–87.

27. Alonso P, Zubiaur E. Phagocytic activity of three *Naegleria* strains in the presence of erythrocytes of various types. J Protozool. 1985 Nov; 32(4):661–4. https://doi.org/10.1111/j.1550-7408.1985.tb03097.x PMID: 4067878

28. Scaglia M, Gatti S, Brustia R, Chichino G, Rondanelli EG. Phagocytosis of human erythrocytes by *Naegleria* is not related to species pathogenicity. A phase-contrast cinemicrographic study. Microbiologica. 1991 Jan; 14(1):45–53. PMID: 2067415

29. Létoffé S, Heuck G, Delepelaire P, Lange N, Wandersman C. Bacteria capture iron from heme by keeping tetrapyrrol skeleton intact. Proc Natl Acad Sci U S A. 2009 Jul 14; 106(28):11719–24. https://doi.org/10.1073/pnas.0903842106 PMID: 19564607

30. Bradley SG, Toney DM, Zhang Y, Marciano-Cabral F. Dependence of growth, metabolic expression, and pathogenicity of *Naegleria fowleri* on exogenous porphyrins. J Parasitol. 1996 Oct; 82(5):763–8. PMID: 8885886

31. Jung SY, Kim JH, Song KJ, Lee YJ, Kwon MH, Kim K, et al. Gene silencing of nfa1 affects the *in vitro* cytotoxicity of *Naegleria fowleri* in murine macrophages. Mol Biochem Parasitol. 2009 May 1; 165 (1):87–93. https://doi.org/10.1016/j.molbiopara.2009.01.007 PMID: 19393165

32. Shakoury-Elizeh M, Protchenko O, Berger A, Cox J, Gable K, Dunn TM, et al. Metabolic response to iron deficiency in *Saccharomyces cerevisiae*. J Biol Chem. 2010; 285(19):14823–33. https://doi.org/10.1074/jbc.M109.091710 PMID: 20231268

33. Bexkens ML, Zimorski V, Sarink MJ, Wienk H, Brouwers JF, De Jonckheere JF, et al. Lipids Are the Preferred Substrate of the Protist *Naegleria gruberi*, Relative of a Human Brain Pathogen. Cell Rep. 2018 Oct 16; 25(3):537–543.e3. https://doi.org/10.1016/j.celrep.2018.09.055 PMID: 30332635

34. Mach J, Bíla J, Ženíšková K, Arbon D, Malych R, Glavanakovová M, et al. Iron economy in *Naegleria gruberi* reflects its metabolic flexibility. Int J Parasitol. 2018 May 5; 48(9–10):719–27. https://doi.org/10.1016/j.ijpara.2018.03.005 PMID: 29738737

35. Kulda J, Tachezy J, Čerkasovová A. *In vitro* induced anaerobic resistance to metronidazole In *Trichomonas vaginalis*. J Eukaryot Microbiol. 1993 May; 40(3):262–9. https://doi.org/10.1111/j.1550-7408.1993.tb04915.x PMID: 8508165

36. Li X, Li J, Hu X, Huang L, Xiao J, Chan J, et al. Differential roles of the hemerythrin-like proteins of *Mycobacterium smegmatis* in hydrogen peroxide and erythromycin susceptibility. Sci Rep. 2015 Nov 26; 5:16130. https://doi.org/10.1038/srep16130 PMID: 26607739

37. Ma Z, Strickland KT, Cherne MD, Sehanobish E, Rohde KH, Self WT, et al. The Rv2633c protein of *Mycobacterium tuberculosis* is a non-heme di-iron catalase with a possible role in defenses against oxidative stress. J Biol Chem. 2018; 293(5):1590–5. https://doi.org/10.1074/jbc.RA117.000421 PMID: 29242190

38. Selote D, Samira R, Matthiadis A, Gillikin JW, Long TA. Iron-binding e3 ligase mediates iron response in plants by targeting basic helix-loop-helix transcription factors1[open]. Plant Physiol. 2015 Jan; 167 (1):273–86. https://doi.org/10.1104/pp.114.250837 PMID: 25452667

39. Zeng WB, Chen WB, Yan QP, Lin GF, Qin YX. Hemerythrin is required for *Aeromonas hydraphlia* to survive in the macrophages of *Anguilla japonica*. Genet Mol Res. 2016; 15(2).

40. Newsome AL, Wilhelm WE. Inhibition of *Naegleria fowleri* by microbial iron-chelating agents: Ecological implications. Applied and Environmental Microbiology. 1983;45.

41. Romeo AM, Christen L, Niles EG, Kosman DJ. Intracellular chelation of iron by bipyridyl inhibits DNA virus replication: Ribonucleotide reductase maturation as a probe of intracellular iron pools. J Biol Chem. 2001 Jun 29; 276(26):24301–8. https://doi.org/10.1074/jbc.M010806200 PMID: 11301321

42. Megger N, Welte L, Zamora F, Müller J. Metal-mediated aggregation of DNA comprising 2,2′-bipyridine nucleoside, an asymmetrically substituted chiral bidentate ligand. Dalt Trans. 2011 Feb 8; 40(8):1802–7.

43. Nyayapati S, Afshan G, Lornitzo F, Byrnes RW, Petering DH. Depletion of cellular iron by BPS and ascorbate: Effect on toxicity of adriamycin. Free Radic Biol Med. 1996 Jan 1; 20(3):319–29. https://doi.org/10.1016/0891-5849(96)02054-0 PMID: 8720902

44. Ihnat PM, Vennerstrom JL, Robinson DH. Synthesis and solution properties of deferoxamine amides. J Pharm Sci. 2000 Dec; 89(12):1525–36. https://doi.org/10.1002/1520-6017(200012)89:12<1525::aid-jps3>3.0.co;2-t PMID: 11042600

45. Kontoghiorghe CN, Kontoghiorghes GJ. Efficacy and safety of iron-chelation therapy with deferoxamine, deferiprone, and deferasirox for the treatment of iron-loaded patients with non-transfusion-dependent thalassemia syndromes. Drug Des Devel Ther. 2016; 10:465–81. https://doi.org/10.2147/DDDT.S79458 PMID: 26893541

46. Porter JB. Deferoxamine pharmacokinetics. Semin Hematol. 2001 Jan; 38(1 Suppl 1):63–8. https://doi.org/10.1016/s0037-1963(01)90061-7 PMID: 11206963

47. Crichton RR, Ward RJ, Hider RC. The efficacy of iron chelators for removing iron from specific brain regions and the pituitary—Ironing out the brain. Vol. 12, Pharmaceuticals. MDPI AG; 2019.

48. Tyanova S, Temu T, Sinitcyn P, Carlson A, Hein MY, Geiger T, et al. The Perseus computational platform for comprehensive analysis of (prote)omics data. Nature Methods. Nature Publishing Group; 2016; 13. p. 731–40. https://doi.org/10.1038/nmeth.3901 PMID: 27348712

49. Tyanova S, Temu T, Cox J. The MaxQuant computational platform for mass spectrometry-based shotgun proteomics. Nat Protoc. 2016 Dec 1; 11(12):2301–19. https://doi.org/10.1038/nprot.2016.136 PMID: 27809316

50. Cox J, Hein MY, Luber CA, Paron I, Nagaraj N, Mann M. Accurate proteome-wide label-free quantification by delayed normalization and maximal peptide ratio extraction, termed MaxLFQ. Mol Cell Proteomics. 2014 Sep 1; 13(9):2513–26. https://doi.org/10.1074/mcp.M113.031591 PMID: 24942700

51. Schindelin J, Arganda-Carreras I, Frise E, Kaynig V, Longair M, Pietzsch T, et al. Fiji: An open-source platform for biological-image analysis. Vol. 9, Nature Methods. 2012. p. 676–82. https://doi.org/10.1038/nmeth.2019 PMID: 22743772

52. Stookey LL. Ferrozine-a new spectrophotometric reagent for iron. Anal Chem. 1970 Jun; 42(7):779–81.

53. Aurrecoechea C, Barreto A, Brestelli J, Brunk BP, Caler E V., Fischer S, et al. AmoebaDB and MicrosporidiaDB: Functional genomic resources for *Amoebozoa* and *Microsporidia* species. Nucleic Acids Res. 2011 Jan 1; 39(SUPPL. 1):D612–9.

54. Scheiber IF, Pilátová J, Malych R, Kotabova E, Krijt M, Vyoral D, et al. Copper and iron metabolism in: *Ostreococcus tauri* -the role of phytotransferrin, plastocyanin and a chloroplast copper-transporting ATPase. Metallomics. 2019 Oct 1; 11(10):1657–66. https://doi.org/10.1039/c9mt00078j PMID: 31380866

55. Zimmermann L, Stephens A, Nam SZ, Rau D, Kübler J, Lozajic M, et al. A Completely Reimplemented MPI Bioinformatics Toolkit with a New HHpred Server at its Core. J Mol Biol. 2018 Jul 20; 430(15):2237–43. https://doi.org/10.1016/j.jmb.2017.12.007 PMID: 29258817

56. Indiveri C, Iacobazzi V, Tonazzi A, Giangregorio N, Infantino V, Convertini P, et al. The mitochondrial carnitine/acylcarnitine carrier: Function, structure and physiopathology. Mol Aspects Med. 2011 Aug 1; 32(4–6):223–33. https://doi.org/10.1016/j.mam.2011.10.008 PMID: 22020112

57. Hamel P, Saint-Georges Y, De Pinto B, Lachacinski N, Altamura N, Dujardin G. Redundancy in the function of mitochondrial phosphate transport in *Saccharomyces cerevisiae* and *Arabidopsis thaliana*. Mol Microbiol. 2004 Feb 23; 51(2):307–17. https://doi.org/10.1046/j.1365-2958.2003.03810.x PMID: 14756774

58. Šmíd O, Horáková E, Vilimova V, Hrdý I, Cammack R, Horvath A, et al. Knock-downs of iron-sulfur cluster assembly proteins IscS and IscU down-regulate the active mitochondrion of procyclic *Trypanosoma brucei*. J Biol Chem. 2006 Sep 29; 281(39):28679–86. https://doi.org/10.1074/jbc.M513781200 PMID: 16882667

59. Hoff KG, Cupp-Vickery JR, Vickery LE. Contributions of the LPPVK motif of the iron-sulfur template protein IscU to interactions with the Hsc66-Hsc20 chaperone system. J Biol Chem. 2003 Sep 26; 278(39):37582–9. https://doi.org/10.1074/jbc.M305292200 PMID: 12871959

60. Mittra B, Laranjeira-Silva MF, Perrone Bezerra de Menezes J, Jensen J, Michailowsky V, Andrews NW. A trypanosomatid iron transporter that regulates mitochondrial function is required for *Leishmania amazonensis* virulence. Horn D, editor. PLoS Pathog. 2016 Jan 7; 12(1):e1005340. https://doi.org/10.1371/journal.ppat.1005340 PMID: 26741360

61. Brazzolotto X, Pierrel F, Pelosi L. Three conserved histidine residues contribute to mitochondrial iron transport through mitoferrins. Biochem J. 2014 May 15; 460(1):79–89. https://doi.org/10.1042/BJ20140107 PMID: 24624902

62. Laemmli UK. Cleavage of structural proteins during the assembly of the head of bacteriophage T4. Nature. 1970 Aug; 227(5259):680–5. https://doi.org/10.1038/227680a0 PMID: 5432063

63. Anders S, Huber W. Differential expression analysis for sequence count data. Genome Biol. 2010 Oct 27; 11(10):R106. https://doi.org/10.1186/gb-2010-11-10-r106 PMID: 20979621

64. MacLean B, Tomazela DM, Shulman N, Chambers M, Finney GL, Frewen B, et al. Skyline: An open source document editor for creating and analyzing targeted proteomics experiments. Bioinformatics. 2010 Apr 1; 26(7):966–8. https://doi.org/10.1093/bioinformatics/btq054 PMID: 20147306

65. Rasoloson D, Vaňáčová Š, Tomková E, Rázga J, Hrdý I, Tachezy J, et al. Mechanisms of in vitro development of resistance to metronidazole in *Trichomonas vaginalis*. Microbiology. 2002; 148(8):2467–77.

66. Verner Z, Čermáková P, Škodová I, Kriegová E, Horváth A, Lukeš J. Complex I (NADH:ubiquinone oxidoreductase) is active in but non-essential for procyclic *Trypanosoma brucei*. Mol Biochem Parasitol. 2011 Feb; 175(2):196–200. https://doi.org/10.1016/j.molbiopara.2010.11.003 PMID: 21074578

67. IC50 Calculator, available at: https://www.aatbio.com/tools/ic50-calculator, accessed 07/03/2019 [Internet].

frontiers | Frontiers in Cell and Developmental Biology

ORIGINAL RESEARCH
published: 11 April 2022
doi: 10.3389/fcell.2022.853463

Copper Metabolism in *Naegleria gruberi* and Its Deadly Relative *Naegleria fowleri*

*Kateřina Ženíšková, Maria Grechnikova and Robert Sutak**

Department of Parasitology, Faculty of Science, Charles University, BIOCEV, Vestec, Prague, Czechia

Although copper is an essential nutrient crucial for many biological processes, an excessive concentration can be toxic and lead to cell death. The metabolism of this two-faced metal must be strictly regulated at the cell level. In this study, we investigated copper homeostasis in two related unicellular organisms: nonpathogenic *Naegleria gruberi* and the "brain-eating amoeba" *Naegleria fowleri*. We identified and confirmed the function of their specific copper transporters securing the main pathway of copper acquisition. Adjusting to different environments with varying copper levels during the life cycle of these organisms requires various metabolic adaptations. Using comparative proteomic analyses, measuring oxygen consumption, and enzymatic determination of NADH dehydrogenase, we showed that both amoebas respond to copper deprivation by upregulating the components of the branched electron transport chain: the alternative oxidase and alternative NADH dehydrogenase. Interestingly, analysis of iron acquisition indicated that this system is copper-dependent in *N. gruberi* but not in its pathogenic relative. Importantly, we identified a potential key protein of copper metabolism of *N. gruberi*, the homolog of human DJ-1 protein, which is known to be linked to Parkinson's disease. Altogether, our study reveals the mechanisms underlying copper metabolism in the model amoeba *N. gruberi* and the fatal pathogen *N. fowleri* and highlights the differences between the two amoebas.

Keywords: copper, alternative oxidase, alternative NADH dehydrogenase, *Naegleria gruberi*, *Naegleria fowleri*, DJ-1, CTR copper transporters, electron transport chain

OPEN ACCESS

Edited by:
Kourosh Honarmand Ebrahimi, King's College London, United Kingdom

Reviewed by:
Anastasios D. Tsaousis, University of Kent, United Kingdom
Svetlana Lutsenko, Johns Hopkins Medicine, United States

****Correspondence:***
Robert Sutak
sutak@natur.cuni.cz

Specialty section:
This article was submitted to Cellular Biochemistry, a section of the journal Frontiers in Cell and Developmental Biology

Received: *12 January 2022*
Accepted: *18 March 2022*
Published: *11 April 2022*

Citation:
Ženíšková K, Grechnikova M and Sutak R (2022) Copper Metabolism in Naegleria gruberi and Its Deadly Relative Naegleria fowleri. Front. Cell Dev. Biol. 10:853463. doi: 10.3389/fcell.2022.853463

INTRODUCTION

Transition metals are required in many crucial biological processes of all living organisms. The most abundant redox-active metal in cells is iron, which is followed by other metals such as copper, manganese, cobalt, molybdenum, and nickel (Andreini et al., 2008). Both iron and copper are crucial for the survival of organisms; however, excess concentrations of these metals can be toxic: iron can catalyze the generation of free radicals through the Fenton reaction, causing cellular damage, while copper probably binds to proteins and replaces iron from iron-sulfur cluster-containing proteins, impairing their function and causing iron-induced toxicity (Macomber and Imlay, 2009; Festa and Thiele, 2012; García-Santamarina and Thiele, 2015). On the other hand, copper is a cofactor of at least 30 cuproenzymes with a wide variety of roles, such as electron transport in respiration (cytochrome c oxidase CCOX) or free radical detoxification (superoxide dismutase SOD) (Solomon et al., 2014), and its necessity for biological systems arises from its ability to cycle between two redox states, Cu^{1+} and Cu^{2+}, all of which contribute to

organisms needing to evolve mechanisms to strictly regulate intracellular levels of these potentially harmful metals. Homeostatic mechanisms consist of their uptake, transport, storage, and detoxification pathways. Interestingly, the metabolism of iron and copper are linked, which is best demonstrated by the copper dependence of iron acquisition by the cell, as was shown in yeasts with FET3 multicopper oxidase in the high-affinity iron uptake system (Askwith et al., 1994). The best-described mechanism of copper acquisition involves high-affinity copper transporters named Ctrs. Their function and structure are widely conserved from yeast to humans (Nose et al., 2006; Maryon et al., 2007).

Very little is known about copper transporters in parasitic protists. In *Plasmodium falciparum*, a copper efflux P-ATPase has been identified and partly characterized (Rasoloson et al., 2004), as was a copper-binding protein with sequence features characteristic of copper transporters, including three transmembrane domains: an extracellular copper-binding methionine motif and transmembrane Gx_3G and Mx_3M motifs (Choveaux et al., 2012). Copper transporting ATPases were also identified in trypanosomatid parasites (Isah et al., 2020; Paul et al., 2021). Significantly more research has been performed on copper metabolism in pathogenic yeasts. Ctr homologs responsible for cellular copper uptake were identified in *Candida albicans* (CTR1) (Marvin et al., 2003) and in *Cryptococcus neoformans* (CTR1 and CTR4) (Sun et al., 2014). Importantly, homologs of these proteins are present in the genomes of both amoebas used in our study, *Naegleria gruberi* and *Naegleria fowleri* (Fritz-Laylin et al., 2010; Liechti et al., 2019).

N. gruberi and *N. fowleri* are unicellular organisms living worldwide in freshwater environments (De Jonckheere, 2004; Mull et al., 2013). *N. gruberi* is considered to be the best safe system to study the pathogenic "brain-eating amoeba" *N. fowleri*, which can infect people and cause primary amoebic meningoencephalitis (PAM), a rare but almost always fatal disease (Mungroo et al., 2021). The genomes of these organisms suggest canonical aerobic metabolism, such as the employment of cytochromes and ubiquinone in the respiratory chain, as well as properties of anaerobic metabolism, such as Fe-hydrogenase (Tsaousis et al., 2014), which is typically utilized in metabolic processes of organisms adapted to anaerobic conditions (Fritz-Laylin et al., 2011; Herman et al., 2021). Both amoebas were recently shown to be able to adjust their metabolism to reflect iron availability, downregulating nonessential and predominantly cytosolic iron-dependent pathways and utilizing available iron primarily in mitochondria to maintain essential energy metabolism (Mach et al., 2018; Arbon et al., 2020). In our previous study, we described how *N. fowler*i handles copper toxicity by upregulating a specific copper-exporting ATPase, a key protein of the copper detoxification pathway (Grechnikova et al., 2020). Recent study has found that *Cryptococcus neoformans* is able to sense different Cu environment during infection: high Cu in lungs and low Cu level in brain and is able to adapt its Cu acquisition in these different niches (Sun et al., 2014). Consequently, we focused the current study on the effect of copper deficiency on the metabolism of the brain-eating amoeba as well as its related nonpathogenic model amoeba *N. gruberi*. Herein, we show the role of Ctr homologs identified in both amoebas by functional complementation of mutant yeast lacking high-affinity copper transporters and demonstrate the effect of copper availability on several important components of cell proteomes, iron acquisition, and respiration in both amoebas. We demonstrate that both amoebas can reflect copper-limited conditions by upregulating parts of the respiratory chain to maintain maximal cell respiration. *N. gruberi* adapts to copper-limited conditions by inducing alternative oxidase, similar to the mechanism described in *C. albicans* (Broxton and Culotta, 2016), while *N. fowleri* upregulates alternative NDH-2 dehydrogenase. Moreover, we identified the potential key protein of copper metabolism in *N. gruberi*, the homolog of the DJ-1 protein.

MATERIALS AND METHODS

Identification of *Naegleria* CTRs

Naegleria CTR genes were found by BLAST in the genomes of *N. fowleri* in the AmoebaDB database (Amos et al., 2021) and *N. gruberi* in the JGI PhycoCosm database (Grigoriev et al., 2021) using *Saccharomyces cerevisiae* CTR1 (YPR124 W), CTR2 (YHR175 W), and CTR3 (YHR175 W) gene sequences. Two predicted CTRs of *N. fowleri* (NF0078940, NF0118930) and three predicted CTRs of *N. gruberi* (gene IDs: NAEGRDRAFT_61759, NAEGRDRAFT_61987, and NAEGRDRAFT_62836) were identified.

Functional Complementation Spot Assay of Predicted Ctrs of *N. gruberi* and *N. fowleri*

To synthesize *N. gruberi* and *N. fowleri* cDNA, SuperScript™ III reverse transcriptase (Thermo Fisher Scientific, United States) was used according to the manufacturer's protocol. CTR genes were amplified from cDNA using a Q5 (NEB, United States) and Pfu DNA polymerase mixture (Promega, United States). The resulting products were subcloned into a pUG35 plasmid with a GFP tag (Güldener and Hegemann, http://mips.gsf.de/proj/yeast/info/tools/hegemann/gfp.html) and a pCM189 plasmid (Garí et al., 1997) with a tetracycline-regulatable promotor. The yeast mutant strain ctr1Δ/ctr3Δ (kindly provided by Dennis J. Thiele, Duke University, Durham, North Carolina) was transformed with pCM189 plasmids containing one of the predicted CTRs from *N. fowleri* (NF0078940, NF0118930) or *N. gruberi* (NAEGRDRAFT_61759, NAEGRDRAFT_61987, NAEGRDRAFT_62836). To observe the effect of complementation on phenotype, transformed yeasts were grown overnight in liquid SC-ura medium with 2% glucose (complete synthetic medium without uracil) at 30°C. Cells were diluted to an OD_{600} of 0.2, and 5-µl aliquots of four serial 10-fold dilutions were spotted onto SC-ura plates containing 2% raffinose as a carbon source.

Localization of Ctrs by Fluorescence Microscopy

For protein localization, wild-type (WT) yeast BY4741 cells were transformed with pUG35 containing either the NgCTR or NfCTR gene, and transformants were grown overnight at 30°C in liquid SC-ura medium, washed and resuspended in phosphate-buffered saline (PBS), pipetted onto a microscope slide and mixed with the same volume of 2% agarose. The microscope slide was then covered with a cover slide and sealed. A fluorescent signal was detected using a Leica TCS SP8 WLL SMD confocal microscope (Leica, Germany) with an HC PL APO CS2 63x/1.20 water objective, excited at 488 nm and detected within 498–551 nm by a HyD SMD detector. The PMT detector was used for bright-field imaging. The resulting images were processed by LAS X imaging software (Leica Microsystems, Germany) and ImageJ (Schneider et al., 2012). Yeast transformation was performed according to a previously published protocol (Gietz and Schiestl, 2007).

Amoeba Cultivation

Organisms

a) *N. gruberi* strain NEG-M, which was kindly provided by Lilian Fritz-Laylin (University of Massachusetts Amherst, United States), was grown axenically at 27°C in M7 medium (Fulton, 1974) with the addition of penicillin (100 U/ml) and streptomycin (100 μg/ml) in a 25-cm^2 aerobic cultivation flask.
b) Axenic culture of *N. fowleri* strain HB-1, which was kindly provided by Dr. Hana Peckova (Institute of Parasitology, Biology Center CAS), was maintained at 37°C in 2% Bactocasitone (Difco) medium supplemented with 10% heat-inactivated fetal bovine serum (Thermo Fisher Scientific) with the addition of penicillin (100 U/ml) and streptomycin (100 μg/ml).

Cultivation Conditions

a) For comparative proteomic analysis, oxygen consumption measurements, measurement of the enzyme activity of complex I and NDH-2, and preparation of the samples for SDS–PAGE, copper deprivation was achieved by incubation of cells for 72 h in the presence of 5 μM neocuproine or 25 μM bathocuproinedisulfonic acid disodium salt (BCS), while copper enrichment was achieved by the addition of 25 μM Cu_2SO_4.
b) To examine the effect of copper availability on NgDJ-1 expression by western blot, cells were grown in 25 μM BCS or 1 μM, 25 μM, or 750 μM Cu_2SO_4 for 72 h.
c) The localization of NgDJ-1 was determined by western blotting of crude fractions of *N. gruberi* cultivated without the addition of copper or chelators and by fluorescence microscopy of cells cultivated for 72 h with 100 μM Cu_2SO_4 or 25 μM BCS.
d) To investigate the effect of ROS on NgDJ-1 expression, *N. gruberi* cells were preincubated in 10 μM rotenone or 20 μM PEITEC for 24 h, and cells with no addition of ROS-inducing agents were used as a control.

Crude Fractionation of *N. gruberi* and *N. fowleri* Cells

The grown cells were washed twice in S-M buffer (250 mM Saccharose, 10 mM MOPS, pH 7.2) and disrupted by sonication using SONOPULS ultrasonic homogenizer mini20 (BANDELIN, Germany) with the following settings: amplitude 30%, 1/1 s pulse for 1 min on ice. Disrupted cells were evaluated under a microscope, and sonication was repeated until most of the cells were disrupted. The samples were then centrifuged for 10 min at 1,200 g and 4°C. To obtain the mitochondria-enriched fraction, the supernatant was centrifuged at 14,000 g for 20 min at 4°C. The pellet was used as a mitochondrial-enriched fraction and diluted to the same protein concentration as the supernatant (cytosol-enriched fraction).

The Effect of Different Copper Chelators on the Growth of *N. gruberi* and *N. fowleri*

To investigate the effect of copper deprivation on the growth of *N. gruberi* and *N. fowleri*, the cultures were grown in the presence of copper chelators BCS (concentrations: 25 and 100 μM) and neocuproine (concentrations: 5 and 20 μM). Copper-rich conditions (25 μM Cu_2SO_4) were used as a control. Since BCS binds copper extracellularly and consequently its effect may only be evident after a longer period, we observed the effect of this chelator in long-term growth analysis with a dilution of the cells after 2 days. Each condition was set up in three independent biological replicates with starting culture concentrations of 50 000 cell/ml (*N. gruberi*) and 5,000 cell/ml (*N. fowleri*), and the cell concentration was measured every day by a Cell Counter (Beckman Coulter, United States). The effect of the intracellular copper chelator neocuproine was observed only at one time point: 72 h. Cells were grown in three biological replicates with starting concentrations of 1×10^4 cells/ml (*N. gruberi*) and 4×10^3 cells/ml (*N. fowleri*), and the cell concentration was measured on a Guava easyCyte 8HT flow cytometer (Merck, Germany) after treatment with 2% paraformaldehyde.

ICP–MS Analysis

Cultures of *N. gruberi* and *N. fowleri* were grown in triplicate for each condition, washed three times (1,200 g, 10 min, 4°C) in 10 mM HEPES with 140 mM NaCl buffer, pH 7.2, and pelleted by centrifugation. The pellets were dried at 100°C, digested in 65% HNO_3 in Savillex vials overnight at room temperature, incubated for 2 h at 130°C in Savillex vials (Millipore, United States) and diluted to a final volume of 10 ml in deionized water. The copper concentration was determined by inductively coupled plasma–mass spectrometry (ICP–MS) using iCAP Q ICP–MS (Thermo Fisher Scientific).

LC–MS

N. gruberi and *N. fowleri* cells were grown in biological triplicates for each condition. After incubation, cells were pelleted by centrifugation (1,200 g, 10 min, 4°C) and washed three times with phosphate-buffered saline (PBS). Whole-cell label-free

proteomic analysis followed by the same method as that described in (Mach et al., 2018) was performed by applying nanoflow liquid chromatography (LC) coupled with mass spectrometry (MS). Data were evaluated with MaxQuant software (Cox et al., 2014) using the AmoebaDB *N. fowleri* database downloaded in August 2018 or the *N. gruberi* database (downloaded from UniProt August 2018). Selected proteins (lacking annotation) were manually annotated using HHpred (Zimmermann et al., 2018) or NCBI BLAST (Altschul et al., 1990). The resulting data were further processed by Perseus software (Tyanova et al., 2016). Potential contaminants and reverse hits were filtered out. To evaluate significantly changed proteins at the level of the false discovery rate, Student's t test with Benjamini–Hochberg correction was used. Proteins that were significantly changed and those found in only one condition (in at least two of three replicates) were selected. Proteins identified by only one peptide and proteins with Q-value higher than 0 were excluded from the selection.

RT–qPCR

Naegleria cells were grown in copper-rich and copper-deficient conditions, and control untreated cells were grown for 72 h in quadruplicate. Cells were washed twice with PBS and spun (1,200 g, 4°C, 10 min). Total RNA was isolated using the High Pure RNA Isolation Kit (Roche, Switzerland). The KAPA SYBR® FAST One-Step universal kit (Sigma Aldrich, United States) was used for RT–PCR according to the manufacturer's protocol. RT–PCR was performed on a RotorGene 3000 PCR cycler (Corbett Research, Australia) under the following conditions: 42°C for 30 min (reverse transcription), 95°C for 5 min, and 40 cycles of 95°C for 10 s, 55°C for 20 s, and 72°C for 20 s; for melt-curve analysis, the temperature change was set from 55 to 95°C with a 1°C step and 5 s per step. The abundance of transcripts was calculated after normalization to the endogenous reference gene β-actin.

Obtaining the NgDJ-1 Recombinant Protein for Antibody Preparation

The sequence of NgDJ-1 (XP_002680488.1) was obtained from the UniProt database (in August 2019), and bioinformatic analysis was performed by InterProScan in Geneious Prime® 2019 2.3 (www.geneious.com), including protein domain prediction software such as Phobius (Käll et al., 2004), Pfam (Mistry et al., 2021), PANTHER (Thomas et al., 2003), and SignalP 5.0 (Almagro Armenteros et al., 2019) (see **Supplementary Figure S4**). The NgDJ-1 gene was amplified from cDNA without the transmembrane domain at the N-terminal part of the NgDJ-1 gene (primers: forward 5′-CAC CATATGGTCGAGGCTCAGAATATTGATCAC-3′, reverse 5′-CACGGATCCATTTTGCTTATTCAAGAGCTTGT-3′) and subcloned into the vector pET42b (Merck) containing the C-terminal histidine tag. The protein was expressed in *E. coli* BL21 (DE3) (Merck) induced by 0.5 mM isopropyl β-D-1-thiogalactopyranoside (IPTG, Sigma Aldrich) for 4 h at 37°C. Protein was purified under denaturing conditions according to the manufacturer's protocol using Ni-NTA agarose beads (Qiagen, Germany).

NfNDH-2 and NgDJ-1 Antibody Production

NgDJ-1 and NfNDH-2 polyclonal antibodies were produced by David Biotechnology (Germany) in rabbits. NgDJ-1 antibody was prepared using purified HIS-tagged recombinant protein, while NfNDH-2 was prepared by 3 synthesized immunogenic peptides preselected by David Biotechnology (HDRQVSFAKSIHKPNEKKN, HEDYHYFEGKAIAIDTENQR, DPKSKKILVTDHLKVKGFE). To obtain a more specific signal, the produced antibodies NgDJ-1 and NfNDH-2 were purified by the SulfoLink Immobilization Kit for Proteins (Thermo Fisher Scientific) or the AminoLink Plus Immobilization Kit (Thermo Fisher Scientific), respectively. All purification procedures were performed following the manufacturer's manual.

Sample Preparation for SDS–PAGE, Native PAGE, and Western Blot

Cells were grown under specific conditions for 72 h, washed two times with PBS, pelleted at 1,000 g, 10 min, 4°C, and diluted to equal protein concentration determined by BCA Protein Assay Kit (Sigma Aldrich). Denatured samples (100°C for 5 min) were separated by SDS electrophoresis, blotted onto a nitrocellulose membrane (Amersham Protram 0.2 μm PC, GE Healthcare Life Sciences, United States), and incubated with specific polyclonal antibody at the following concentrations: anti-AOX (Agrisera, Sweden) 1:100, anti-NgDJ-1 1 1:50, and anti-NfNDH-2 1:1,000. HRP-conjugated goat anti-rabbit or anti-mouse antibodies (BioRad, United States) were used as secondary antibodies. Antibodies were detected using Immobilon Forte Western HRP substrate (Merck) on an Amersham Imager 600 (GE Health care Life Sciences, United States).

Crude fractions of *N. gruberi* (Chapter 2.5) used for localization of NgDJ-1 by western blot were prepared the same as SDS samples described above, but crude fractions of *N. fowleri* (Chapter 2.5) used for localization of NfNDH-2 were treated with 1% digitonin (Sigma Aldrich), incubated for 5 min on ice and resuspended in ×5 native sample buffer. The samples were then loaded on a native gel (containing 0.1% Triton TX-100, Sigma Aldrich) and separated by PAGE under native conditions.

Immunofluorescence Microscopy

N. gruberi cells were stained with 100 nM MitoTracker Red CMXRos (Thermo Fisher Scientific) for 30 min in M7 medium in the dark at 27°C. After incubation, the medium was exchanged, and the cells were fixed with 1% formaldehyde for another 30 min. The treated cells were then carefully centrifuged (800 g, 5 min, 24°C), resuspended in PEM (100 mM piperazine-N,N′-bis(2-ethane sulfonic acid), 1 mM ethylene glycol-bis(β-aminoethyl ether)-N,N,N′,N′-tetraacetic acid, and 0.2 mM $MgSO_4$) and transferred onto cover slides. The cell slides were then incubated for 1 h in PEMBALG blocking solution (1% BSA, 0.1% NaN_3, 100 mM L-lysin, 0.5% cold water fish skin gelatin in PEM). The NgDJ-1 protein was visualized by an anti-rat antibody coupled to Alexa Fluor 488 (Thermo Fisher Scientific) (dilution 1:1,000) bound to a custom-made rat polyclonal antibody (dilution 1:100). Slides with stained cells were mounted by Vectashield with DAPI (Vector Laboratories,

United States). The signal was detected by a TCS SP8 WLL SMD confocal microscope (Leica) equipped with an HC PL APO CS2 63x/1.20 oil objective, excited by 509 nm and detected within 526–655 nm by a HyD SMD detector. The PMT detector was used for bright-field imaging and processed as described in Chapter 2.3.

N. fowleri microscopy slides for visualization of NfNDH-2 were prepared as described above except that *N. fowleri* cells were immobilized on slides covered with poly-L-lysine and all the staining, including 10 nM MitoTracker Red CMXRos and primary and secondary antibodies, were completed on slides rather than in a cultivation flask.

Measurements of Oxygen Consumption

N. fowleri and *N. gruberi* cells were grown for 72 h in biological triplicates or tetraplicates, respectively, under copper-depleted and copper-rich conditions, pelleted (1,200 g, 10 min, 4°C), washed twice, and resuspended to the same cell concentration in glucose buffer (50 mM glucose, 0.5 mM $MgCl_2$, 0.3 mM $CaCl_2$, 5.1 μM KH_2PO_4, 3 μM Na_2HPO_4, pH 7.4). The cell concentration was measured on a Guava easyCyte 8HT flow cytometer (Merck). Cell respiration in each sample was measured by detecting oxygen decreases using the Clark-type electrode system Oxygen meter Model 782 (Strathkelvin) in a Mitocell Mt 200 cuvette in a total volume of 700 μl. The whole system was calibrated for 27°C for *N. gruberi* and 37°C for *N. fowleri*. Specific inhibitors of alternative oxidase, salicyl hydroxamic acid (SHAM) at concentrations of 0.5 mM (*N. gruberi*) or 0.2 mM (*N. fowleri*), and an inhibitor of complex IV, KCN, at concentrations of 2.4 mM (*N. gruberi*) or 2.05 mM (*N. fowleri*) were used. The protein concentration of the sample was determined using a BCA kit (Sigma Aldrich).

Complex I and NDH-2 Enzyme Activity of *Naegleria fowleri*

Total NADH dehydrogenase activity was measured by the following protocol. Three biological replicates of *N. fowleri* were cultivated for 72 h in copper-rich or copper-deficient conditions. The cells were spun down, washed with S-M buffer (250 mM saccharose, 10 mM MOPS, pH 7.2), and diluted to the same cell concentration. Next, the cells were treated with 1% digitonin (Sigma Aldrich) for 5 min on ice and added to a reaction mixture containing 100 μM KPi buffer at pH 7.5 and 300 μM NADH. The reaction was started by the addition of 50 μM nonnatural coenzyme Q2 (in 99.9% ethanol, Sigma Aldrich), an analog of Q10. The activity was measured for 5 min at 340 nM wavelength on a Shimadzu UV-2600 UV–VIS spectrophotometer (Shimadzu, Japan) with UV Probe software (Shimadzu).

The activity of alternative NADH dehydrogenase (NDH-2) was estimated as the remaining activity measured in digitonine-treated culture preincubated for 5 min with the inhibitor of Complex I, 75 μM rotenone. The activity of complex I was calculated as the remaining activity after NDH-2 activity subtraction from overall NADH dehydrogenase activity. The protein concentration was determined by a BCA kit (Sigma Aldrich).

Iron Uptake

N. fowleri and *N. gruberi* cells were grown in copper-rich and copper-deficient conditions for 72 h, pelleted (1,200 g, 10 min, 4°C), washed twice, resuspended in glucose-HEPES medium (50 mM glucose, 20 mM HEPES, pH 7.2) and diluted to the same cell concentration of 1×10^6 cells per sample. The cell concentration was estimated by a Guava easyCyte 8HT flow cytometer (Merck). Samples were incubated for 1 h with 1 μM ^{55}Fe-citrate or with 1 μM ^{55}Fe-citrate with the addition of 1 m mM ascorbate to reduce iron to the ferrous form. Uptake was stopped by the addition of 1 mM EDTA, and the cells were then washed three times with glucose-HEPES buffer, diluted to the same protein concentration [using a BCA kit (Sigma Aldrich)] and separated using the Novex Native PAGE Bis-Tris Gel system (4–16%, Invitrogen, United States). The gel was dried for 2 h in a vacuum and autoradiographed by Typhoon FLA 7000 (GE Life Sciences, United States) using a tritium storage phosphor screen (GE Life Sciences).

RESULTS

Identification of Copper Uptake Proteins (Ctrs) of *N. gruberi* and *N. fowleri*

In the genomes of both amoebas, we identified several homologs of copper transporters based on a BLAST search using *S. cerevisiae* CTR1, CTR2, and CTR3. To confirm the copper uptake function of these candidate transporters, we performed a functional complementation assay using copper transporter 1 and copper transporter 3 double knockout yeast strain (ctr1Δ/ctr3Δ). One of the selected Ctrs from each amoeba (NgCTR1, NAEGRDRAFT_61759, and NfCTR1, NF0078940) restored copper transporter function in the yeast mutant and showed typical localization to the yeast plasma membrane (**Figure 1A** and **Figure 1B**). The localization of the other homologs is shown in **Supplementary Figure S1**. To determine whether *N. fowleri* and *N. gruberi* regulate the copper acquisition pathway depending on the availability of the metal at the transcriptional level, as shown in *S. cerevisiae* (Winge et al., 1998), we analyzed the abundance of CTR transcripts by RT–PCR in cells grown under low copper and copper-rich conditions. Our data showed no significant copper-induced changes in the RNA levels of the selected CTR genes (NF0078940, NF0118930, NAEGRDRAFT_61759, NAEGRDRAFT_61987, NAEGRDRAFT_62836) (**Supplementary Figure S2**). This result is not unexpected considering our previous study, where we found that iron starvation-induced changes in *N. fowleri* were mostly posttranslational (Arbon et al., 2020).

Comparative Proteomic Analysis Revealed That ETC Components and NgDJ-1 Are the Most Affected by Copper Deprivation

Since *Naegleria* is not prone to genetic manipulations, we chose whole-cell label-free comparative proteomics to gain complex insight into the metabolic adaptation to copper limitations. To

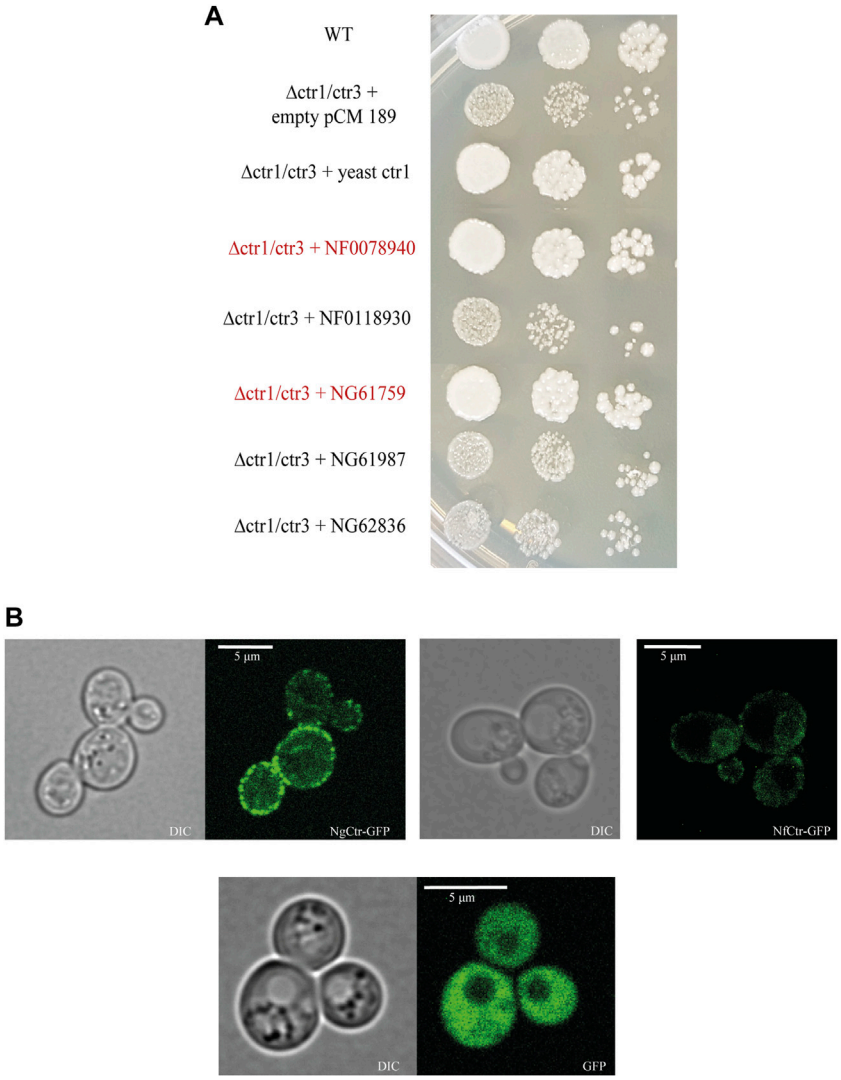

FIGURE 1 | Identification of copper uptake proteins (Ctrs) of *Naegleria gruberi* and *Naegleria fowleri*. **(A)** Functional complementation spot assay of NgCTRs and NfCTRs in Δctr1/ctr3 mutant yeast cells lacking genes for high-affinity copper transporters. Wild-type BY4741 cells transformed with the empty tetracycline-regulated expression vector pCM189 and Δctr1/ctr3 mutant cells transformed with the same plasmid carrying yeast CTR1, NfCTRs (NF0078940, NF0118930) or NgCTRs (NG61759, NG61987, NG62836) were spotted onto synthetic complete medium without uracil with 2% raffinose as the carbon source and grown for 72 h at 30°C. Mutant yeast cells with plasmids containing CTR genes from *N. fowleri* (NF0078940) and *N. gruberi* (NG61759), which functionally complement the missing yeast copper transporters CTR1 and CTR3, are marked in red. **(B)** Localization of NfCtr (NF0078940) and NgCtr (NG61759) by fluorescence microscopy. Wild-type yeast BY4147 expressing copper transporters linked with GFP from *N. gruberi* NgCTR1-GFP (NG61759 + pUG35), *N. fowleri* NfCTR1-GFP (NF0078940 + pUG35), and GFP (empty pUG35 vector).

elucidate the effect of copper deprivation on the viability of *N. gruberi* and *N. fowleri* cells, we cultivated both amoebas for 72 h in the presence of the copper chelators bathocuproinedisulphonic acid (BCS) and neocuproine (Neo). Both chelators are selective for Cu^{+}, and in contrast to the extracellular copper chelator BCS, neocuproine can chelate copper intracellularly.

To determine the amount of copper within the cells grown in the presence of BCS, we analyzed those samples using ICP–MS. **Figure 2A** shows that this extracellular copper chelator causes a significant decrease in copper accumulation compared to control (cells cultivated in presence of 25 μM Cu_2SO_4) after 72 h, while the effect is not further increased using a 10-fold higher concentration. The effect of BCS on copper accumulation was more pronounced in *N. fowleri*, which has a higher overall intracellular amount of copper under control conditions; however, the growth of *N. fowleri*, unlike *N. gruberi*, was not affected by this chelator (**Supplementary Figure S3**). This indicates that *N. fowleri* possesses more efficient copper homeostasis mechanisms than its nonpathogenic relative, and the use of an intracellular chelator is required to observe the physiological response to copper starvation. Based on these results, we decided to perform two proteomic analyses using

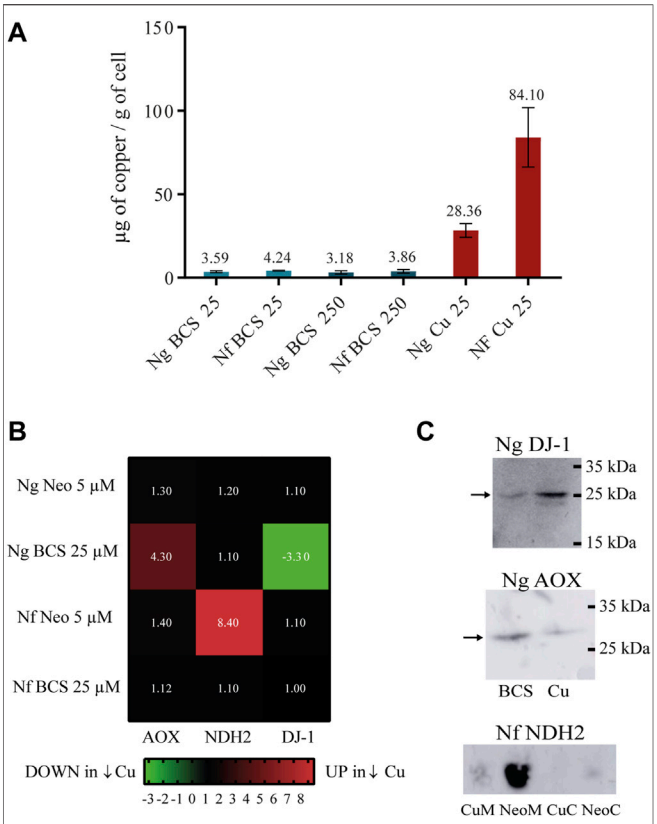

FIGURE 2 | Effect of copper availability on *Naegleria gruberi* and *Naegleria fowleri*. **(A)** Copper contents in *N. gruberi* and *N. fowleri* supplemented with 25 µM Cu_2SO_4, 25 µM BCS, or 250 µM BCS for 72 h. The values represent the mean of copper content of three individual replicates. **(B)** The fold changes of the most relevant proteins in this article are demonstrated on the heatmap; upregulation under copper-limited conditions is indicated by red color and downregulation by green color. The heatmap demonstrates that the chelators have different effects on both amoebas. **(C)** western blot analysis confirming the proteomic results using the specific antibodies antiNgDJ-1, antiNfNDH2, and antiAOX on cell lysates of *N. gruberi* incubated with 25 µM BCS (BCS) or 25 µM Cu_2SO_4 (Cu) and separated by SDS–PAGE and on cytosolic (C) and mitochondrial (M) fractions of *N. fowleri* cells incubated with 25 µM Cu_2SO_4 (Cu) or 5 µM neocuproine (Neo) separated by clear native PAGE.

the cells grown with the addition of 25 µM BCS and the cells grown in 5 µM neocuproine to achieve copper deprivation for both amoebas. To ensure sufficient copper status, the cells cultivated in presence of 25 µM Cu_2SO_4 were used as a control sample for both proteomic analyses. This concentration was used based on our previous work where we elucidated the IC50 of copper being 1 mM for *N. gruberi* and as high as 1.6 mM for *N. fowleri* (Grechnikova et al., 2020).

The list of all proteins that were significantly changed under copper deprivation is presented in **Supplementary Table S1**. In the analysis of the resulting proteomic data, we focused on proteins that are likely to bind copper or are related to copper metabolism, potentially compensating for the lack of copper or being involved in the oxidative stress response or energy metabolism. The selected proteins meeting these criteria are listed in **Table 1**. A heatmap presenting the most relevant proteins identified in this study demonstrates that selected chelators cause different effects on amoebas (**Figure 2B**).

The mitochondrial electron transport chain of *Naegleria gruberi* and *Naegleria fowleri* consists of complexes I, II, and III, two terminal oxidases: alternative oxidase (AOX) and cytochrome c oxidase (complex IV), and an alternative NADH ubiquinone oxidoreductase. Our proteomic analysis revealed that both amoebas responded to copper starvation by upregulating alternative enzymes involved in the electron transport chain. AOX (XP_002681229.1) from *N. gruberi* showed a 4.3-fold upregulation under copper-limited conditions. In contrast to *N. gruberi, N. fowleri* reacted to copper starvation through 8.4-fold upregulation of the protein NF0090420 (partial sequence) identified as nonproton pumping alternative NADH dehydrogenase (NDH-2). The complete sequence of this protein was obtained from genome of *N. fowleri* strain ATCC 30894 (AmoebaDB - FDP41_010952) (**Supplementary Figure S4**).

Additionally, the proteins involved in reactive oxygen species (ROS) detoxification pathways were significantly downregulated in copper-limited *N. gruberi* (thioredoxin reductase and two homologs of glutathione-S-transferase). Furthermore, in both amoebas, we observed significant upregulation in the expression of hemerythrin under copper limitation, a protein that probably plays a role in the defense against oxidative stress in bacteria (Li X. et al., 2015; Ma et al., 2018). Together, these results indicate that copper deprivation in naeglerias may lead to the generation of ROS.

Interestingly, one of the most downregulated proteins (fold change 3.3) of *N. gruberi* in copper-limited conditions was protein XP_002680488.1, which is a homolog of DJ-1 family proteins (**Supplementary Figure S4**). These proteins are thought to perform many functions (Bandyopadhyay and Cookson, 2004; Wei et al., 2007). Some studies on the human homolog of DJ-1 claim its ability to bind copper and serve as a copper chaperone for Cu, Zn superoxide dismutase (Girotto et al., 2014).

The copper-induced changes in protein abundance were also confirmed using western blot analysis with specific antibodies (**Figure 2C**). The localization of NfNDH-2 by fluorescence microscopy to demonstrate the antibody specificity is shown in **Supplementary Figure S5**.

RT qPCR Analysis Revealed That Changes Caused by Copper Deprivation Are Posttranslational

Selected genes encoding copper-regulated proteins (NfNDH-2, NfHemerythrin) were also analyzed by RT qPCR using copper-starved and control cells. Transcript abundance was normalized to the endogenous reference gene β-actin. Analogous to CTRs, no changes in the transcriptional level of these selected genes were observed, suggesting that the proteomic response of both amoebas to copper starvation occurs at the posttranslational level (**Supplementary Figure S2**).

TABLE 1 | Selected *N. gruberi* and *N. fowleri* proteins whose abundance was significantly changed under copper-limited conditions in at least one condition and in one amoeba. Arrows indicate significant upregulation or downregulation, and no arrow sign in proteins with a fold change lower than 1.5 indicates no significant change.

Naegleria gruberi			
Fold Change in BCS	**Fold Change in Neo**	**Accession Number in Database**	**Database Annotation/Manual Annotation**
↑4.3	1.3	XP_002681229.1	AOX
1.1	1.2	XP_002672148.1	NDH-2
↓3.3	1.1	XP_002680488.1	DJ-1
↑2.0	Not Found	XP_002680302.1	Hemerythrin
1.4	↓1.9	XP_002674924.1	Thioredoxin reductase
↓2.2	1.2	XP_002670102.1	Glutathione-S-transferase
↓1.6	1.3	XP_002670607.1	Glutathione-S-transferase III
Naegleria fowleri			
Fold change in BCS	**Fold change in Neo**	**Accession Number in Database**	**Database Annotation/Manual Annotation**
1.1	1.4	NF0004720	AOX
1.1	↑8.4	NF0090420	NDH-2
1	1.1	NF0125230	DJ-1
1.4	↑3.5	NF0127030	Hemerythrin
1.0	1.2	NF0014440	Thioredoxin reductase
1.1	1.3	NF0101120	Glutathione-S-transferase
1.1	Not Found	NF0101840	Glutathione-S-transferase
1.1	1.1	NF0039660	Glutathione-S-transferase

The Activity of NgAOX and NfNADH-2 Reflects Copper Availability

Our proteomic analysis indicated rearrangement of the mitochondrial electron transport chain in both amoebas under copper starvation. To determine the physiological effect of copper availability on respiration, we performed an oxygen consumption assay with amoebas grown in copper-limited conditions. Both organisms possess two terminal oxidases, cytochrome c oxidase (CCOX) and alternative oxidase (AOX), which couple the electron flow from ubiquinol with the reduction of O_2 to H_2O (Cantoni et al., 2020). In contrast with CCOX, AOX does not participate in ATP generation. The activity of NgAOX corresponded to the proteomic results: in copper-limited *N. gruberi,* the activity of AOX was almost twice as high as that in control cells (**Figure 3A**). In *N. fowleri*, copper starvation did not result in the upregulation of alternative oxidase at the protein level, but its activity in neocuproine-treated cells was significantly increased (**Figure 3A**). Interestingly, our results also demonstrate that *N. gruberi* respiration is predominantly mediated by alternative oxidases, whereas *N. fowleri* respires mainly through complex IV (**Figure 3A**).

In addition to the classical rotenone-sensitive NADH dehydrogenase, the electron transport chain of both amoebas additionally contains an alternative rotenone-insensitive NADH dehydrogenase (NDH-2). These enzymes share the same functions, but NDH-2 does not contribute to the generation of the transmembrane proton gradient. The comparative proteomic analysis indicated that *N. fowleri* adapts to copper-deprived conditions by upregulation of NDH-2. The resistance of NDH-2 to rotenone was used to distinguish this enzyme from classical rotenone-sensitive NADH dehydrogenase. When NADH dehydrogenase activity of lysates of control and copper-limited cells were compared, the rotenone-sensitive complex I activity was not affected by copper, while the rotenone-resistant activity was higher in the neocuproine-treated cells than in the control sample. Although we cannot exclude that other enzymes contribute to this activity, considering the proteomic data, we believe that the main enzyme responsible for the measured activity is NfNDH-2 (**Figure 3B**).

Expression of the Mitochondrially Localized Protein NgDJ-1 is Copper-dependent and is Not Induced by ROS Accumulation

One of the most downregulated proteins in copper-deprived *N. gruberi* cells (3.3-fold change downregulation in BCS) is protein XP_002680488.1 (named NgDJ-1 in this article), which shows homology to proteins belonging to the DJ-1/ThiJ/PfpI superfamily (**Supplementary Figure S4**). This superfamily contains functionally and structurally diverse proteins, many of which remain only poorly characterized at the biochemical level (Bandyopadhyay and Cookson, 2004). To confirm the connection between copper availability and NgDJ-1 expression, we performed a western blot analysis of whole-cell lysates of *N. gruberi* grown in copper-deprived conditions as well as in media supplemented with copper at different concentrations (1 μM, 25 μM, and 750 μM). The results demonstrate that the copper-induced expression of DJ-1 observed in our proteomic analysis is even more pronounced when cells are exposed to copper at levels that probably lead to toxicity, indicating a role of this protein in copper metabolism (**Figure 4A**).

The human homolog of DJ-1 has many predicted functions but is mainly annotated as a redox sensor and ROS scavenger (Zhang et al., 2020). Considering this, we analyzed the lysates of

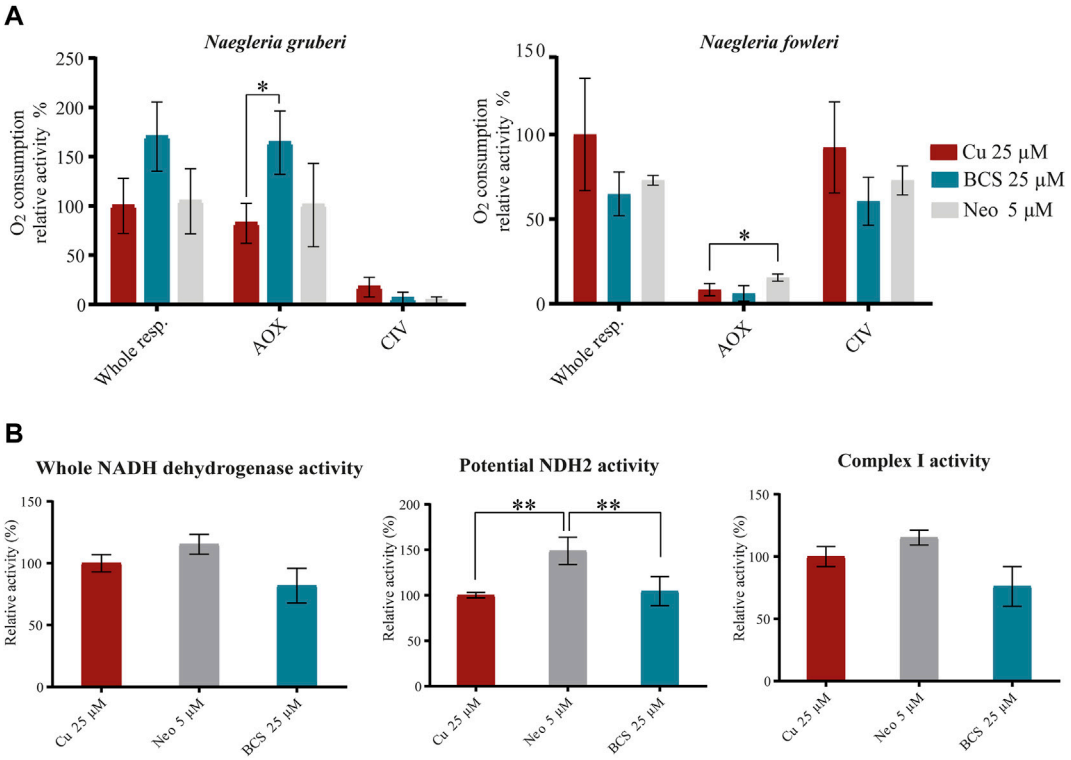

FIGURE 3 | The activity of NgAOX and NfNDH2 reflects the proteomic analysis results. **(A)** Oxygen consumption of NgAOX is increased due to copper deprivation. Oxygen consumption was measured in *N. gruberi* and *N. fowleri* cells incubated for 72 h with 25 M BCS or 5 µM neocuproine, and control cells were supplemented with 25 µM Cu_2SO_4. Specific inhibitors of alternative oxidase (SHAM) and complex IV (KCN) were used to distinguish the activities of these enzymes. For easier interpretation, oxygen consumption activity was calculated as the relative activity, where the whole respiration of control samples (Cu 25 µM) corresponds to 100%. The graphs show the mean of three biological replicates with the standard deviation. To evaluate the statistical confidence, Student's t test was used (* indicates a *p* value ≤0.05). **(B)** The enzyme activity of NfNDH2 is increased under low copper conditions. Spectrophotometric measurement of NADH dehydrogenase activity was measured using nonnatural Q2, the analog of Q10, at 340 nm on *N. fowleri* cells incubated in low or normal copper conditions. The potential NDH2 activity was measured after preincubation of the cells with rotenone. The activity of complex I was calculated by subtracting the potential NDH2 activity from overall NADH dehydrogenase activity. For easier interpretation, the activities are shown as the relative activity (%), and the activities of control cells (Cu 25 µM) correspond to 100%. To evaluate the statistical confidence, Student's t test was used (**indicates a *p* value ≤0.01).

N. gruberi cells exposed for 24 h to two ROS-inducing agents, rotenone and PEITC, by western blot using an NgDJ-1 antibody. Unexpectedly, we observed that treatment with both agents resulted in a decrease in NgDJ-1 expression (**Figure 4B**).

To determine NgDJ-1 cellular localization, we used two different methods: fluorescence microscopy and western blot analysis of crude cell fractions. Both methods revealed mitochondrial localization of NgDJ-1, which is rather unusual for this protein (**Figure 4C**). Predictably, observed molecular weight of DJ-1 on western blots is lower than anticipated (~26 kDa instead of 30 kDa), probably due to cleavage of mitochondrial targeting sequence. More pictures are shown in (**Supplementary Figure S6**).

N. gruberi Iron Uptake is Copper-Regulated

Iron uptake mechanisms in various organisms are frequently interconnected with copper. To determine this connection in both amoebas, we employed blue native electrophoresis analysis allowing visualization of the incorporation of iron radionuclide into cellular protein complexes. In our previous work, we showed that *N. fowleri* prefers to take up the reduced form of iron (Fe^{II}) and that iron acquisition is not induced by iron starvation (Arbon et al., 2020). Here, we show that similarly, the nonpathogenic relative *N. gruberi* preferably acquired a reduced form of iron, indicating a reductive uptake mechanism. Importantly, our results demonstrate that iron uptake is significantly affected by copper availability (**Figure 5A**), suggesting the requirement of copper in some of the iron acquisition system components (e.g., multicopper oxidase). In contrast, iron uptake efficiency in *N. fowleri* remained unaffected by copper deprivation (**Figure 5B**).

DISCUSSION

Copper and host:pathogen Interface

An important host defense process called nutritional immunity occurs at the host-pathogen interface: the host restricts access to essential metals for the pathogen (Hood and Skaar, 2012). Iron sequestration during bacterial infection is well described, and bacterial pathogens have developed a variety of strategies to

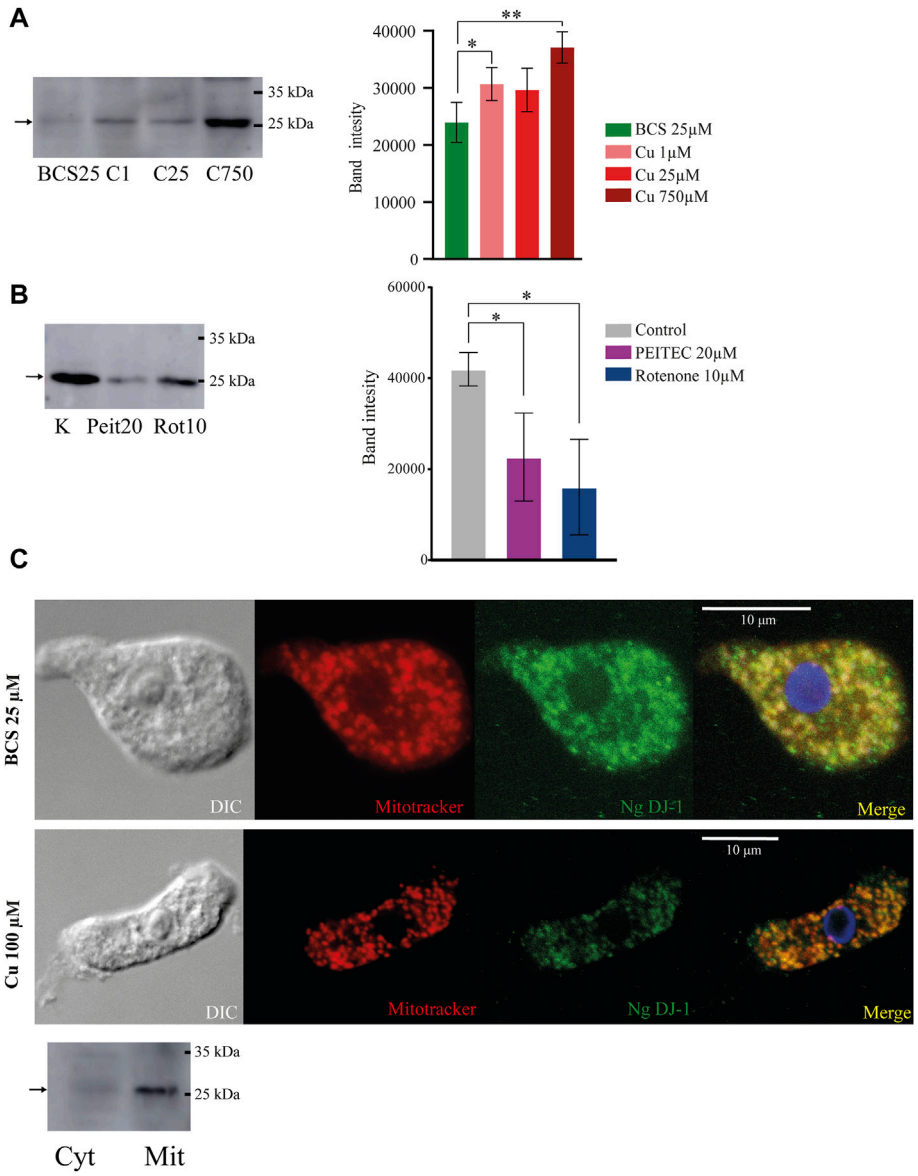

FIGURE 4 | The expression of mitochondrially localized NgDJ-1 is copper-dependent and is not induced by ROS accumulation. **(A)** NgDJ-1 protein expression is copper-dependent. Western blot analysis of whole-cell lysates of cells incubated for 72 h in low or high copper conditions (BCS 25 μM and Cu_2SO_4 1/25/750 μM) using an anti-NgDJ-1 antibody. To compare signal strength in each condition, densitometry of four independent replicates was performed using ImageJ. Changes in signals are demonstrated on the graph showing the mean of the signal with standard deviation error bars (*indicates a *p* value ≤0.05; **indicates a *p* value ≤0.01. **(B)** ROS accumulation does not induce NgDJ-1 expression. Western blot analysis of DJ-1 expression in cells preincubated with the ROS-inducing agents 20 μM PEITC and 10 μM rotenone for 24 h. The control sample (K) was *N. gruberi* without any additions. The graph demonstrates the difference in signal strength in each condition. **(C)** Localization of NgDJ-1 is mitochondrial regardless of copper availability. NgDJ-1 was visualized by immunofluorescence microscopy using a polyclonal antibody (anti-NgDJ-1) on *N. gruberi* cells precultivated with 25 μM BCS and 100 μM Cu_2SO_4 for 72 h. MitoTracker CMXRos (Thermo Fisher) was used for visualization of mitochondria. DIC–differential interference contrast. Mitochondrial localization of NgDJ-1 was also demonstrated by immunoblot detection of cytosolic (Cyt) and mitochondria-enriched (Mit) fractions of *N. gruberi*.

circumvent host-mediated iron limitation (Weinberg, 1975; Posey and Gherardini, 2000; Cassat and Skaar, 2013). In contrast to iron, copper is usually utilized in the opposite manner by host immune cells, which use the toxic properties of this metal to kill pathogens (Festa and Thiele, 2012; Hodgkinson and Petris, 2012; Stafford et al., 2013; Chaturvedi and Henderson, 2014). However, in fungal infections caused by *C. neoformans* and *C. albicans*, the pathogens experience limited copper availability in the host in specific situations. Although host immunity employs the toxic properties of copper in the lungs, which are the main locations of *C. neoformans* infection (Ding et al., 2013), *C. neoformans* tends to disseminate to the brain in immunodeficient hosts, where copper may be restricted. *C. neoformans* adapts to these copper-limited conditions by

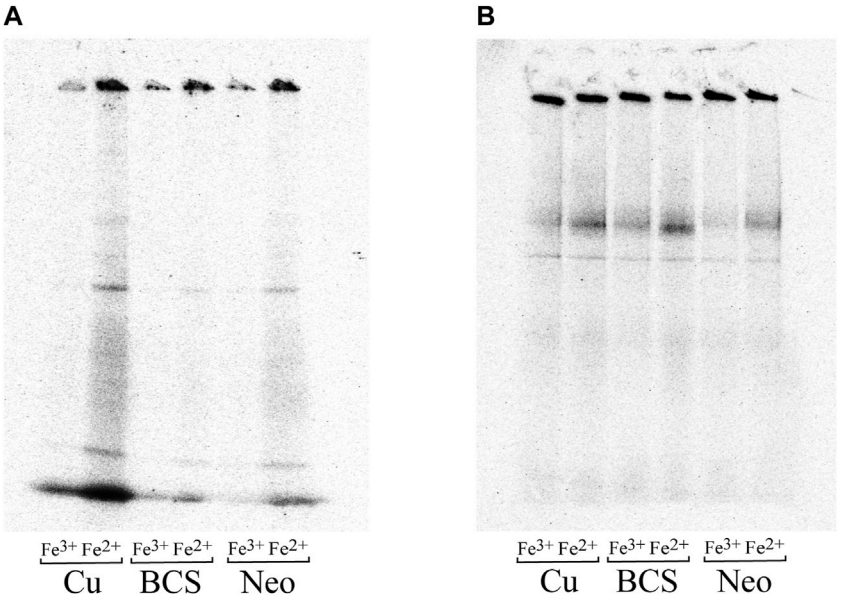

FIGURE 5 | Iron uptake is regulated by copper in *N. gruberi* but not in *N. fowleri*. Ferrous and ferric iron uptake by *N. gruberi* **(A)** and *N. fowleri* **(B)** under copper-rich and copper-deficient conditions. Autoradiography of blue native electrophoresis gels of whole-cell lysates of *N. gruberi* and *N. fowleri* cells incubated with 25 μM BCS (BCS), 5 μM neocuproine (Neo), and 25 μM Cu_2SO_4 (Cu) for 72 h and further incubated with ^{55}Fe(II) (ferrous ascorbate) or ^{55}Fe(III) (ferric citrate) for 1 h.

inducing specific copper uptake transporters (Waterman et al., 2007; Sun et al., 2014). *C. albicans* occupies diverse niches inside the host, but it may disseminate through the bloodstream, and the major location of infection in the murine model is the kidney. In the early stage of kidney infection, copper levels increase briefly, but as the infection progresses, the level of copper drops. *C. albicans* responds to decreasing copper conditions by switching from copper-dependent Cu/Zn SOD to Mn SOD3 and, interestingly, by upregulating alternative oxidase (AOX) to minimize mitochondrial damage and simultaneously maximize COX respiration (Li CX. et al., 2015; Besold et al., 2016; Broxton and Culotta, 2016).

In a recent study, we described how *N. fowleri* handles the toxic properties of copper and identified the key protein of the copper detoxification pathway, a copper-translocating ATPase (Grechnikova et al., 2020). In the present study, we focused on other aspects of copper metabolism and aimed to elucidate the metabolic adaptations of the free-living unicellular organism *N. gruberi* and its pathogenic relative *N. fowleri* to low copper availability.

Copper Acquisition

Our study began with a search for proteins involved in copper acquisition by both amoebas. In eukaryotic cells, the import of copper to the cytoplasm is widely mediated by high-affinity copper transporter (Ctr) localized to the plasma membrane. Ctr is an integral membrane protein conserved from yeast to humans with high specificity for Cu(I) (Zhou and Gitschier, 1997; Kozlowski et al., 2009). In *Saccharomyces cerevisiae*, copper is transported into cells by two high-affinity transporters, CTR1 (Dancis et al., 1994b) and CTR3 (Knight et al., 1996), and a low-affinity copper transporter, CTR2, is responsible for the mobilization of vacuolar copper ions (Rees et al., 2004; Liu et al., 2012). All CTRs of *S. cerevisiae* are regulated by intracellular copper status (Jungmann et al., 1993; Winge et al., 1998). We identified genes encoding potential Ctrs in the genomes of both amoebas, including three genes in *N. gruberi*, and two in *N. fowleri*. Since effective genetic manipulation of these organisms has not been established, we decided to verify copper transport function by expression in yeasts and by functional complementation assay using the ctr1Δ/ctr3Δ mutant yeast strain. One of the proposed CTRs from each amoeba was able to restore copper import function and showed typical localization to the plasma membrane. In contrast to *S. cerevisiae*, neither CTR appears to be regulated by copper starvation at the transcriptional level in *Naegleria*, indicating that the amoebas do not respond to copper starvation at the copper acquisition level or that the regulation is posttranslational.

Branched Mitochondrial ETC

Our proteomic approach to understanding the metabolic adaptations to copper limitation yielded particularly interesting findings: some of the proteins comprising the electron-transporting chain (ETC), the key part of the energy metabolism of a cell, are among the most affected by low copper availability in both amoebas. The ETC of both Naeglerias is branched and, in addition to the classical arrangement of complexes (CI-IV), possesses two nonenergy-conserving components: cyanide insensitive alternative oxidase (AOX) and alternative NADH dehydrogenase (NDH-2), both of which are significantly upregulated in copper-deprived conditions. Branched mitochondrial ETC is also known from plants, fungi, and other

protists, some of which are human pathogens (e.g., *C. albicans*, *C. neoformans*, *Acanthamoeba castellanii*). AOX bypasses complex III and complex IV, but its activity is not coupled to proton translocation; hence, it does not contribute to ATP synthesis. Studies focusing on plants show that two respiration pathways with different energy yields provide the ability to maintain the redox, carbon, and/or energy balance in response to changing demands (Sluse and Jarmuszkiewicz, 1998; Ribas-Carbo et al., 2005; Sieger et al., 2005; Smith et al., 2009; Cvetkovska and Vanlerberghe, 2012; Dahal and Vanlerberghe, 2017). In addition to this function, AOX also decreases the rate of mitochondrial ROS formation (Maxwell et al., 1999; Vishwakarma et al., 2015). In fungi, low copper availability was shown to be connected to impaired respiration (cytochrome c oxidase pathway) (Joseph-Horne et al., 2001), which generally leads to ROS accumulation in the mitochondria; thus, positive regulation of alternative oxidase may compensate for this loss and minimize ROS formation, which was recently demonstrated in *Paracoccidioides brasiliensis* (Petito et al., 2020) and in *C. albicans*, where copper starvation led to mitochondrial SOD1 repression and AOX induction enhanced cytochrome c oxidase activity (Broxton and Culotta, 2016). NDH-2 is a rotenone-insensitive nonproton pumping oxidoreductase that catalyzes a reaction similar to that of complex I, but in contrast to complex I, NDH-2 is not involved in the generation of membrane potential. NDH-2 was identified in plants, fungi, and bacteria as well as in some important parasitic protists, such as *Plasmodium falciparum* and *Toxoplasma gondii* (Marres et al., 1991; Yagi, 1991; Kerscher, 2000; Roberts et al., 2004; Lin et al., 2011). These two members belonging to the phylum Apicomplexa lack genes encoding canonical complex I and possess only homologs of NDH-2 instead (Fry and Beesley, 1991; Gardner et al., 2002; Uyemura et al., 2004). Altogether, NDH-2 is widely distributed in several human pathogens but not in humans themselves; thus, inhibitors of this enzyme could have clinical importance. Several studies have shown that NDH-2 provides a mechanism to remove excessive reducing power to balance the redox state of the cell (Luttik et al., 1998; Overkamp et al., 2000; Melo et al., 2004; Rasmusson et al., 2004). As mentioned above, branched mitochondrial ETC is activated in both studied amoebas upon copper limitation. In addition to AOX, whose activity is increased in both amoebas, NDH-2 is the most upregulated protein in copper-starved *N. fowleri*. Although we cannot conclude the direct consequences of NDH-2 induction for copper starvation in *N. fowleri*, we believe that further studying the exact mechanisms underlying the fascinating maintenance of the delicate balance between ATP production, ROS generation, and redox status in these microorganisms would be exciting.

DJ-1

One of the proteins most affected by copper limitation in *N. gruberi* shows homology to proteins belonging to the DJ-1/ThiJ/PfpI superfamily. Members of this superfamily are present in many organisms from bacteria to humans, and the most studied is the human homolog due to its role in several diseases, such as autosomal recessive early-onset Parkinson's disease (Bonifati et al., 2003). DJ-1 is also suggested to be one of the potential tumor markers and is strongly implicated in the pathogenesis of cancer (Nagakubo et al., 1997; Fan et al., 2015; Yu et al., 2017) and ischemia-reperfusion injury (Wang et al., 2017). Hundreds of publications explore the human homolog of DJ-1 and suggest many diverse functions, with roles as molecular chaperones (Cookson, 2003; Meulener et al., 2005), glyoxalases (Lee et al., 2003), proteases (Chen et al., 2010), and transcriptional regulators (Trempe and Fon, 2013), but the one function connecting these studies is the stress sensor reacting to oxidative stress and protecting cells from ROS (Taira et al., 2004; Inden et al., 2006). Some studies show that cells with a high level of DJ-1 are resistant to oxidative stress and neurotoxins, while lower levels of DJ-1 increase cells' vulnerability to oxidative stress (Inden et al., 2011). Therefore, we assessed the abundance of NgDJ-1 in cells treated with the ROS-inducing agents rotenone and PEITC. However, the expected induction of NgDJ-1 by ROS was not observed; in fact, the protein was downregulated in cells with higher ROS levels.

Human DJ-1 is predominantly localized to the cytoplasm, but it has been reported to be translocated to the mitochondria and nucleus under oxidative stress and to protect cells from oxidative stress-induced cell death (Irrcher et al., 2010; Kim et al., 2012). On the other hand, some studies also show that DJ-1 may be localized to mitochondria even in the absence of oxidative stress, where it directly binds to a subunit of complex I and somehow maintains its activity, since knockdown of DJ-1 in cells decreased complex I activity (Hayashi et al., 2009; Mullett and Hinkle, 2011). A recent study also showed its connection to ATP synthase, where DJ-1 is required for the normal stoichiometry of ATP synthase and to facilitate positioning of the β subunit of ATP synthase to fully close the mitochondrial inner membrane leak (Chen et al., 2019). Interestingly, our results show exclusively mitochondrial localization of NgDJ-1 regardless of copper availability. Only a few studies claim a certain link between copper metabolism and the DJ-1 protein. In 2014, Stefania Girroto and others suggested a putative role of DJ-1 as a copper chaperone for superoxide dismutase (Girotto et al., 2014). Two novel copper-binding sites, one Cu(I) binding site per monomer involving the highly conserved Cys-106 and the second Cu(I) binding site shared between two monomers, were identified, and the kinetics and binding affinity of DJ-1 to copper ions were determined (Girotto et al., 2014). Since the conserved Cys-106 analog is also present in the sequence of NgDJ-1 and the levels of the protein are regulated by copper availability in the amoeba, we may speculate about its role in the copper homeostasis of *N. gruberi*. Because NgDJ-1 is localized only to mitochondria, it may act as a storage site for copper that can be later allocated to complex IV when copper availability is limited, which is somewhat analogous to the case of plastocyanin in *Chlamydomonas* (Kropat et al., 2015). We may also consider the role of this protein as a protein with chelating properties to prevent free copper accumulation, which can cause increased ROS production and lead to impaired respiration. Since the levels of NgDJ-1 are affected by both copper limitation and copper excess, NgDJ-1 may play multiple roles in the amoeba.

Iron Uptake in *N. gruberi*

In our recent work, we showed that *N. fowleri* utilizes a reductive system of iron uptake, as described in the model *S. cerevisiae* (Arbon et al., 2020). This mechanism relies on the extracellular

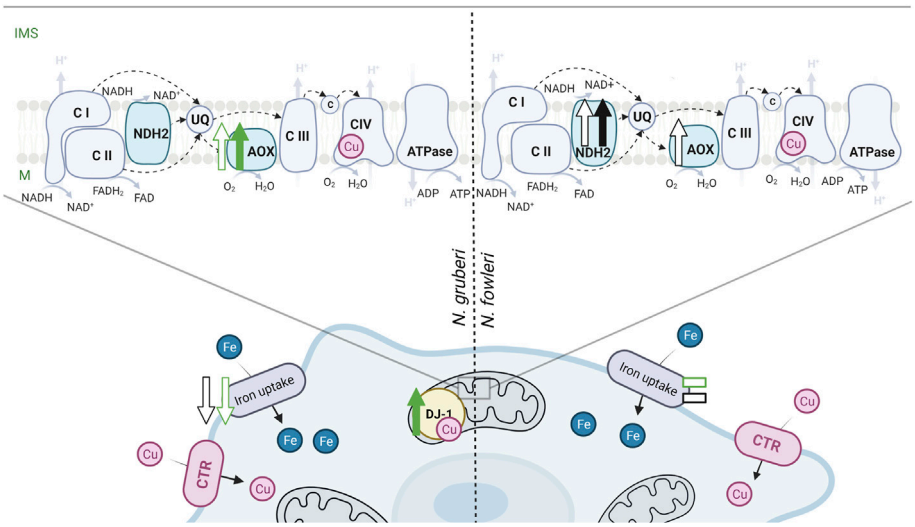

FIGURE 6 | The main effect of copper deprivation on the cellular processes of *N. gruberi* and *N. fowleri*. The green color corresponds to the effect of the copper chelator BCS, and changes caused by neocuproine are depicted in black. Upward pointing arrows represent an increase in copper-deprived conditions, downward pointing arrows denote a decrease in copper-deprived conditions, and dashes indicate no copper-induced changes. Full arrows represent the results from the proteomic analysis, and empty arrows represent the measured activity. Respiration chain complexes are marked by appropriate numbers, UQ–ubichinol/ubichinone, c–cytochrome c. Created with BioRender.com.

reduction of ferric ions from proteins, chelates, or other sources before their import into the cell. In yeast, the high-affinity ferrous-specific iron transport system is composed of multicopper oxidase FET3 and FTR1 permease; thus, copper availability is crucial for maintaining iron homeostasis (Askwith et al., 1994; Kaplan and O'Halloran, 1996; Stearman et al., 1996). Herein, we showed the same preference for the reduced form of iron in *N. gruberi*, but the main and surprising difference is that in contrast to *N. fowleri*, iron uptake efficiency in the nonpathogenic amoeba is decreased in copper-limited conditions, which corresponds to studies on *S. cerevisiae* (Dancis et al., 1994a) and on the model green algae *Chlamydomonas reinhardtii* (Herbik et al., 2002). An interesting question remains whether the pathogenic amoeba employs a copper-independent iron uptake mechanism or prioritizes extremely efficient copper delivery to this system in times of copper deprivation. The second hypothesis is rather unlikely since the *N. fowleri* iron uptake system has been previously shown to not be inducible even by iron starvation (Arbon et al., 2020).

N. gruberi and N. fowleri: So Similar yet so Different. Similarities and Differences

Altogether, our study reveals how *N. gruberi* and *N. fowleri* deal with copper deprivation and highlights the differences between the two amoebas (**Figure 6**). We showed that while both amoebas use Ctr homologs to acquire copper and increase the activity of the branched mitochondrial ETC when copper is limited, their responses to copper limitation differ significantly. Although copper bioavailability limitation in the growth medium results in a more pronounced decrease in the cellular concentration of the metal in *N. fowleri* in comparison to *N. gruberi*, the growth of the pathogen is not affected, and the intracellular copper chelator neocuproine is required to observe a copper-related phenotype. Moreover, even when neocuproine was used to starve the cells for copper, iron uptake efficiency was not affected in *N. fowleri*, unlike *N. gruberi*. To hypothesize whether the particularities in *N. fowleri* copper homeostasis can contribute to its virulence would be an exaggeration, however, one must take into account the fact that copper is an important player in the host-pathogen relationship.

DATA AVAILABILITY STATEMENT

The original contributions presented in the study are included in the article/**Supplementary Material**. The mass spectrometry proteomics data have been deposited to the ProteomeXchange Consortium via the PRIDE (Perez-Riverol et al., 2022) partner repository with the dataset identifier PXD032745, further inquiries can be directed to the corresponding author.

AUTHOR CONTRIBUTIONS

RS, KZ and MG conceived and designed the experiments. KZ, MG performed the experiments. KZ and MG analyzed and interpreted the data. KZ, MG and RS wrote the manuscript. All authors contributed to the article and approved the submitted version.

FUNDING

The project was supported by the Czech Science Foundation (20-28072S), Charles University Grant Agency (343621), CePaViP provided by The European Regional Development Fund and Ministry of Education, Youth and Sports of the Czech Republic (CZ.02.1.01/0.0/0.0/16_019/0000759), the MiCoBion project funded by EU Horizon 2020 (810224), Czech-BioImaging large RI projects (LM2018129 and CZ.02.1.01/0.0/0.0/18_046/0016045, funded by MEYS CR and ERDF), Moore-Simons Project on the Origin of the Eukaryotic Cell (https://doi.org/10.37807/GBMF9738).

ACKNOWLEDGMENTS

Karel Harant and Pavel Talacko from the Laboratory of Mass Spectrometry, Biocev, Charles University, Faculty of Science, where the proteomics and mass spectrometric analyses were performed. Special thanks to Dennis J. Thiele, Ivan Hrdý, Zdeněk Verner and Jan Mach for support and helpful scientific discussions.

SUPPLEMENTARY MATERIAL

The Supplementary Material for this article can be found online at: https://www.frontiersin.org/articles/10.3389/fcell.2022.853463/full#supplementary-material

Supplementary Table 1 | List of whole-cell proteomes of both amoebas under copper-rich and copper-deprived conditions. The list is organized into thirteen sheets containing separately raw data of comparative proteomics results of *N. gruberi* (NG) or *N. fowleri (NF)* cells incubated in 25 μM BCS (BCS) or 5 μM neocuproine (NEO) compared to cells cultured in the presence of 25 μM Cu2SO4 (cu), sheets containing all upregulated (UP) or downregulated (DOWN) proteins under the indicated copper-depleted conditions and the list containing summarized table of significantly changed proteins of both amoebas in both copper-deprived conditions. Upregulated and downregulated proteins were selected and filtered based on the criteria listed in the Methods section.

REFERENCES

Almagro Armenteros, J. J., Tsirigos, K. D., Sønderby, C. K., Petersen, T. N., Winther, O., Brunak, S., et al. (2019). SignalP 5.0 Improves Signal Peptide Predictions Using Deep Neural Networks. *Nat. Biotechnol.* 37, 420–423. doi:10.1038/s41587-019-0036-z

Altschul, S. F., Gish, W., Miller, W., Myers, E. W., and Lipman, D. J. (1990). Basic Local Alignment Search Tool. *J. Mol. Biol.* 215, 403–410. doi:10.1016/s0022-2836(05)80360-2

Amos, B., Aurrecoechea, C., Barba, M., Barreto, A., Basenko, E. Y., Ba˙ Zant, W., et al. (2021). VEuPathDB: The Eukaryotic Pathogen, Vector and Host Bioinformatics Resource center. *Nucleic Acids Res.* 50, D898–D911. doi:10.1093/nar/gkab929

Andreini, C., Bertini, I., Cavallaro, G., Holliday, G. L., and Thornton, J. M. (2008). Metal Ions in Biological Catalysis: From Enzyme Databases to General Principles. *J. Biol. Inorg. Chem.* 13, 1205–1218. doi:10.1007/s00775-008-0404-5

Arbon, D., Ženíšková, K., Mach, J., Grechnikova, M., Malych, R., Talacko, P., et al. (2020). Adaptive Iron Utilization Compensates for the Lack of an Inducible Uptake System in *Naegleria Fowleri* and Represents a Potential Target for Therapeutic Intervention. *Plos Negl. Trop. Dis.* 14, e0007759. doi:10.1371/journal.pntd.0007759

Askwith, C., Eide, D., Van Ho, A., Bernard, P. S., Li, L., Davis-Kaplan, S., et al. (1994). The FET3 Gene of *S. Cerevisiae* Encodes a Multicopper Oxidase Required for Ferrous Iron Uptake. *Cell* 76, 403–410. doi:10.1016/0092-8674(94)90346-8

Bandyopadhyay, S., and Cookson, M. R. (2004). Evolutionary and Functional Relationships within the DJ-1 Superfamily. *BMC Evol. Biol.* 4, 6. doi:10.1186/1471-2148-4-6

Besold, A. N., Culbertson, E. M., and Culotta, V. C. (2016). The Yin and Yang of Copper during Infection. *J. Biol. Inorg. Chem.* 21, 137–144. doi:10.1007/s00775-016-1335-1

Bonifati, V., Rizzu, P., van Baren, M. J., Schaap, O., Breedveld, G. J., Krieger, E., et al. (2003). Mutations in the DJ-1 Gene Associated with Autosomal Recessive Early-Onset Parkinsonism. *Science* 299, 256–259. doi:10.1126/science.1077209

Broxton, C. N., and Culotta, V. C. (2016). An Adaptation to Low Copper in *Candida Albicans* Involving SOD Enzymes and the Alternative Oxidase. *PLoS One* 11, e0168400. doi:10.1371/journal.pone.0168400

Cantoni, D., Osborne, A., Taib, N., Thompson, G., Kazana, E., Edrich, E., et al. (2020). Localization and Functional Characterization of the Alternative Oxidase in *Naegleria*. *bioRxiv*. doi:10.1101/2020.09.26.314807

Cassat, J. E., and Skaar, E. P. (2013). Iron in Infection and Immunity. *Cell Host Microbe* 13, 509–519. doi:10.1016/j.chom.2013.04.010

Chaturvedi, K. S., and Henderson, J. P. (2014). Pathogenic Adaptations to Host-Derived Antibacterial Copper. *Front. Cel. Infect. Microbiol.* 4, 3. doi:10.3389/fcimb.2014.00003

Chen, J., Li, L., and Chin, L.-S. (2010). Parkinson Disease Protein DJ-1 Converts from a Zymogen to a Protease by Carboxyl-Terminal Cleavage. *Hum. Mol. Genet.* 19, 2395–2408. doi:10.1093/hmg/ddq113

Chen, R., Park, H. A., Mnatsakanyan, N., Niu, Y., Licznerski, P., Wu, J., et al. (2019). Parkinson's Disease Protein DJ-1 Regulates ATP Synthase Protein Components to Increase Neuronal Process Outgrowth. *Cell Death Dis* 10 (6), 469. doi:10.1038/s41419-019-1679-x

Choveaux, D. L., Przyborski, J. M., and Goldring, J. P. (2012). A *Plasmodium Falciparum* Copper-Binding Membrane Protein with Copper Transport Motifs. *Malar. J.* 11, 397. doi:10.1186/1475-2875-11-397

Cookson, M. R. (2003). Pathways to Parkinsonism. *Neuron* 37, 7–10. doi:10.1016/s0896-6273(02)01166-2

Cox, J., Hein, M. Y., Luber, C. A., Paron, I., Nagaraj, N., and Mann, M. (2014). Accurate Proteome-Wide Label-Free Quantification by Delayed Normalization and Maximal Peptide Ratio Extraction, Termed MaxLFQ. *Mol. Cel. Proteomics* 13, 2513–2526. doi:10.1074/mcp.m113.031591

Cvetkovska, M., and Vanlerberghe, G. C. (2012). Coordination of a Mitochondrial Superoxide Burst during the Hypersensitive Response to Bacterial Pathogen in *Nicotiana Tabacum*. *Plant Cel Environ.* 35, 1121–1136. doi:10.1111/j.1365-3040.2011.02477.x

Dahal, K., and Vanlerberghe, G. C. (2017). Alternative Oxidase Respiration Maintains Both Mitochondrial and Chloroplast Function during Drought. *New Phytol.* 213, 560–571. doi:10.1111/nph.14169

Dancis, A., Haile, D., Yuan, D. S., and Klausner, R. D. (1994b). The *Saccharomyces Cerevisiae* Copper Transport Protein (Ctr1p). Biochemical Characterization, Regulation by Copper, and Physiologic Role in Copper Uptake. *J. Biol. Chem.* 269, 25660–25667. doi:10.1016/s0021-9258(18)47300-0

Dancis, A., Yuan, D. S., Haile, D., Askwith, C., Eide, D., Moehle, C., et al. (1994a). Molecular Characterization of a Copper Transport Protein in *S. Cerevisiae*: An Unexpected Role for Copper in Iron Transport. *Cell* 76, 393–402. doi:10.1016/0092-8674(94)90345-x

De Jonckheere, J. F. (2004). Molecular Definition and the Ubiquity of Species in the Genus. *Protist* 155, 89–103. doi:10.1078/1434461000167

Ding, C., Festa, R. A., Chen, Y.-L., Espart, A., Palacios, Ò., Espín, J., et al. (2013). *Cryptococcus Neoformans* Copper Detoxification Machinery Is Critical for Fungal Virulence. *Cell Host Microbe* 13, 265–276. doi:10.1016/j.chom.2013.02.002

Fan, J., Yu, H., Lv, Y., and Yin, L. (2015). Diagnostic and Prognostic Value of Serum Thioredoxin and DJ-1 in Non-Small Cell Lung Carcinoma Patients. *Tumor Biol.* 37 (2), 1949–1958. doi:10.1007/s13277-015-3994-x

Festa, R. A., and Thiele, D. J. (2012). Copper at the Front Line of the Host-Pathogen Battle. *Plos Pathog.* 8, e1002887. doi:10.1371/journal.ppat.1002887

Fritz-Laylin, L. K., Ginger, M. L., Walsh, C., Dawson, S. C., and Fulton, C. (2011). The *Naegleria* Genome: A Free-Living Microbial Eukaryote Lends Unique Insights into Core Eukaryotic Cell Biology. *Res. Microbiol.* 162, 607–618. doi:10.1016/j.resmic.2011.03.003

Fritz-Laylin, L. K., Prochnik, S. E., Ginger, M. L., Dacks, J. B., Carpenter, M. L., Field, M. C., et al. (2010). The Genome of *Naegleria Gruberi* Illuminates Early Eukaryotic Versatility. *Cell* 140, 631–642. doi:10.1016/j.cell.2010.01.032

Fry, M., and Beesley, J. E. (1991). Mitochondria of Mammalian *Plasmodium Spp*. *Parasitology* 102 (Pt 1), 17–26. doi:10.1017/s0031182000060297

Fulton, C. (1974). Axenic Cultivation of *Naegleria Gruberi*: Requirement for Methionine. *Exp. Cel Res.* 88, 365–370. doi:10.1016/0014-4827(74)90253-5

García-Santamarina, S., and Thiele, D. J. (2015). Copper at the Fungal Pathogen-Host Axis. *J. Biol. Chem.* 290, 18945–18953. doi:10.1074/jbc.R115.649129

Gardner, M. J., Hall, N., Fung, E., White, O., Berriman, M., Hyman, R. W., et al. (2002). Genome Sequence of the Human Malaria Parasite *Plasmodium Falciparum*. *Nature* 419, 498–511. doi:10.1038/nature01097

Garí, E., Piedrafita, L., Aldea, M., and Herrero, E. (1997). A Set of Vectors with a Tetracycline-Regulatable Promoter System for Modulated Gene Expression in *Saccharomyces Cerevisiae*. *Yeast* 13, 837–848. doi:10.1002/(SICI)1097-0061(199707)13:9<837::AID-YEA145>3.0.CO;2-T

Gietz, R. D., and Schiestl, R. H. (2007). Large-Scale High-Efficiency Yeast Transformation Using the LiAc/SS Carrier DNA/PEG Method. *Nat. Protoc.* 2, 38–41. doi:10.1038/nprot.2007.15

Girotto, S., Cendron, L., Bisaglia, M., Tessari, I., Mammi, S., Zanotti, G., et al. (2014). DJ-1 Is a Copper Chaperone Acting on SOD1 Activation. *J. Biol. Chem.* 289, 10887–10899. doi:10.1074/jbc.m113.535112

Grechnikova, M., Ženíšková, K., Malych, R., Mach, J., and Sutak, R. (2020). Copper Detoxification Machinery of the Brain-Eating Amoeba *Naegleria Fowleri* Involves Copper-Translocating ATPase and the Antioxidant System. *Int. J. Parasitol. Drugs Drug Resist.* 14, 126–135. doi:10.1016/j.ijpddr.2020.10.001

Grigoriev, I. V., Hayes, R. D., Calhoun, S., Kamel, B., Wang, A., Ahrendt, S., et al. (2021). PhycoCosm, a Comparative Algal Genomics Resource. *Nucleic Acids Res.* 49, D1004–D1011. doi:10.1093/nar/gkaa898

Hayashi, T., Ishimori, C., Takahashi-Niki, K., Taira, T., Kim, Y.-C., Maita, H., et al. (2009). DJ-1 Binds to Mitochondrial Complex I and Maintains its Activity. *Biochem. Biophysical Res. Commun.* 390, 667–672. doi:10.1016/j.bbrc.2009.10.025

Herbik, A., Bölling, C., and Buckhout, T. J. (2002). The Involvement of a Multicopper Oxidase in Iron Uptake by the Green Algae *Chlamydomonas Reinhardtii*. *Plant Physiol.* 130, 2039–2048. doi:10.1104/pp.013060

Herman, E. K., Greninger, A., van der Giezen, M., Ginger, M. L., Ramirez-Macias, I., Miller, H. C., et al. (2021). Genomics and Transcriptomics Yields a System-Level View of the Biology of the Pathogen *Naegleria Fowleri*. *BMC Biol.* 19 (1), 142. doi:10.1186/s12915-021-01078-1

Hodgkinson, V., and Petris, M. J. (2012). Copper Homeostasis at the Host-Pathogen Interface. *J. Biol. Chem.* 287, 13549–13555. doi:10.1074/jbc.r111.316406

Hood, M. I., and Skaar, E. P. (2012). Nutritional Immunity: Transition Metals at the Pathogen-Host Interface. *Nat. Rev. Microbiol.* 10, 525–537. doi:10.1038/nrmicro2836

Inden, M., Kitamura, Y., Takahashi, K., Takata, K., Ito, N., Niwa, R., et al. (2011). Protection against Dopaminergic Neurodegeneration in Parkinson's Disease-Model Animals by a Modulator of the Oxidized Form of DJ-1, a Wild-type of Familial Parkinson's Disease-Linked PARK7. *J. Pharmacol. Sci.* 117, 189–203. doi:10.1254/jphs.11151fp

Inden, M., Taira, T., Kitamura, Y., Yanagida, T., Tsuchiya, D., Takata, K., et al. (2006). PARK7 DJ-1 Protects against Degeneration of Nigral Dopaminergic Neurons in Parkinson's Disease Rat Model. *Neurobiol. Dis.* 24, 144–158. doi:10.1016/j.nbd.2006.06.004

Irrcher, I., Aleyasin, H., Seifert, E. L., Hewitt, S. J., Chhabra, S., Phillips, M., et al. (2010). Loss of the Parkinson's Disease-Linked Gene DJ-1 Perturbs Mitochondrial Dynamics. *Hum. Mol. Genet.* 19, 3734–3746. doi:10.1093/hmg/ddq288

Isah, M. B., Goldring, J. P. D., and Coetzer, T. H. T. (2020). Expression and Copper Binding Properties of the N-Terminal Domain of Copper P-type ATPases of African Trypanosomes. *Mol. Biochem. Parasitol.* 235, 111245. doi:10.1016/j.molbiopara.2019.111245

Joseph-Horne, T., Hollomon, D. W., and Wood, P. M. (2001). Fungal Respiration: A Fusion of Standard and Alternative Components. *Biochim. Biophys. Acta - Bioenerg.* 1504, 179–195. doi:10.1016/s0005-2728(00)00251-6

Jungmann, J., Reins, H. A., Lee, J., Romeo, A., Hassett, R., Kosman, D., et al. (1993). MAC1, a Nuclear Regulatory Protein Related to Cu-Dependent Transcription Factors Is Involved in Cu/Fe Utilization and Stress Resistance in Yeast. *EMBO J.* 12, 5051–5056. doi:10.1002/j.1460-2075.1993.tb06198.x

Käll, L., Krogh, A., and Sonnhammer, E. L. L. (2004). A Combined Transmembrane Topology and Signal Peptide Prediction Method. *J. Mol. Biol.* 338, 1027–1036. doi:10.1016/j.jmb.2004.03.016

Kaplan, J., and O'Halloran, T. V. (1996). Iron Metabolism in Eukaryotes-Mars and Venus at it Again. *Science* 271, 1510–1512. doi:10.1126/science.271.5255.1510

Kerscher, S. J. (2000). Diversity and Origin of Alternative NADH:ubiquinone Oxidoreductases. *Biochim. Biophys. Acta - Bioenerg.* 1459, 274–283. doi:10.1016/s0005-2728(00)00162-6

Kim, S.-J., Park, Y.-J., Hwang, I.-Y., Youdim, M. B. H., Park, K.-S., and Oh, Y. J. (2012). Nuclear Translocation of DJ-1 during Oxidative Stress-Induced Neuronal Cell Death. *Free Radic. Biol. Med.* 53, 936–950. doi:10.1016/j.freeradbiomed.2012.05.035

Knight, S. A., Labbé, S., Kwon, L. F., Kosman, D. J., and Thiele, D. J. (1996). A Widespread Transposable Element Masks Expression of a Yeast Copper Transport Gene. *Genes Dev.* 10, 1917–1929. doi:10.1101/gad.10.15.1917

Kozlowski, H., Janicka-Klos, A., Brasun, J., Gaggelli, E., Valensin, D., and Valensin, G. (2009). Copper, Iron, and Zinc Ions Homeostasis and Their Role in Neurodegenerative Disorders (Metal Uptake, Transport, Distribution and Regulation). *Coord. Chem. Rev.* 253, 2665–2685. doi:10.1016/j.ccr.2009.05.011

Kropat, J., Gallaher, S. D., Urzica, E. I., Nakamoto, S. S., Strenkert, D., Tottey, S., et al. (2015). Copper Economy in *Chlamydomonas*: Prioritized Allocation and Reallocation of Copper to Respiration vs. Photosynthesis. *Proc. Natl. Acad. Sci. U.S.A.* 112, 2644–2651. doi:10.1073/pnas.1422492112

Lee, S.-J., Kim, S. J., Kim, I.-K., Ko, J., Jeong, C.-S., Kim, G.-H., et al. (2003). Crystal Structures of Human DJ-1 and *Escherichia coli* Hsp31, Which Share an Evolutionarily Conserved Domain. *J. Biol. Chem.* 278, 44552–44559. doi:10.1074/jbc.m304517200

Li, C. X., Gleason, J. E., Zhang, S. X., Bruno, V. M., Cormack, B. P., and Culotta, V. C. (2015a). *Candida Albicans* Adapts to Host Copper during Infection by Swapping Metal Cofactors for Superoxide Dismutase. *Proc. Natl. Acad. Sci. U. S. A.* 112, E5336–E5342. doi:10.1073/pnas.1513447112

Li, X., Li, J., Hu, X., Huang, L., Xiao, J., Chan, J., et al. (2015b). Differential Roles of the Hemerythrin-Like Proteins of *Mycobacterium Smegmatis* in Hydrogen Peroxide and Erythromycin Susceptibility. *Sci. Rep.* 5, 16130. doi:10.1038/srep16130

Liechti, N., Schürch, N., Bruggmann, R., and Wittwer, M. (2019). Nanopore Sequencing Improves the Draft Genome of the Human Pathogenic Amoeba *Naegleria Fowleri*. *Sci. Rep.* 9, 16040. doi:10.1038/s41598-019-52572-0

Lin, S. S., Gross, U., and Bohne, W. (2011). Two Internal Type II NADH Dehydrogenases of *Toxoplasma Gondii* Are Both Required for Optimal Tachyzoite Growth. *Mol. Microbiol.* 82, 209–221. doi:10.1111/j.1365-2958.2011.07807.x

Liu, L., Qi, J., Yang, Z., Peng, L., and Li, C. (2012). Low-Affinity Copper Transporter CTR2 Is Regulated by Copper-Sensing Transcription Factor Mac1p in *Saccharomyces Cerevisiae*. *Biochem. Biophys. Res. Commun.* 420, 600–604. doi:10.1016/j.bbrc.2012.03.040

Luttik, M. A. H., Overkamp, K. M., Kötter, P., de Vries, S., van Dijken, J. P., and Pronk, J. T. (1998). The *Saccharomyces Cerevisiae* NDE1 and NDE2 Genes Encode Separate Mitochondrial NADH Dehydrogenases Catalyzing the Oxidation of Cytosolic NADH. *J. Biol. Chem.* 273, 24529–24534. doi:10.1074/jbc.273.38.24529

Ma, Z., Strickland, K. T., Cherne, M. D., Sehanobish, E., Rohde, K. H., Self, W. T., et al. (2018). The Rv2633c Protein of *Mycobacterium Tuberculosis* Is a Non-heme Di-iron Catalase with a Possible Role in Defenses against Oxidative Stress. *J. Biol. Chem.* 293, 1590–1595. doi:10.1074/jbc.ra117.000421

Mach, J., Bíla, J., Ženíšková, K., Arbon, D., Malych, R., Glavanakovová, M., et al. (2018). Iron Economy in *Naegleria Gruberi* Reflects its Metabolic Flexibility. *Int. J. Parasitol.* 48 (9-10), 719–727. doi:10.1016/j.ijpara.2018.03.005

Macomber, L., and Imlay, J. A. (2009). The Iron-Sulfur Clusters of Dehydratases Are Primary Intracellular Targets of Copper Toxicity. *Proc. Natl. Acad. Sci. U.S.A.* 106, 8344–8349. doi:10.1073/pnas.0812808106

Marres, C. A. M., Vries, S., and Grivell, L. A. (1991). Isolation and Inactivation of the Nuclear Gene Encoding the Rotenone-Insensitive Internal NADH: Ubiquinone Oxidoreductase of Mitochondria from *Saccharomyces Cerevisiae*. *Eur. J. Biochem.* 195, 857–862. doi:10.1111/j.1432-1033.1991.tb15775.x

Marvin, M. E., Williams, P. H., and Cashmore, A. M. (2003). Tha *Candida Albicans* CTR1 Gene Encodes a Functional Copper Transporter. *Microbiology* 149, 1461–1474. doi:10.1099/mic.0.26172-0

Maryon, E. B., Molloy, S. A., Zimnicka, A. M., and Kaplan, J. H. (2007). Copper Entry into Human Cells: Progress and Unanswered Questions. *Biometals* 20, 355–364. doi:10.1007/s10534-006-9066-3

Maxwell, D. P., Wang, Y., and McIntosh, L. (1999). The Alternative Oxidase Lowers Mitochondrial Reactive Oxygen Production in Plant Cells. *Proc. Natl. Acad. Sci. U.S.A.* 96, 8271–8276. doi:10.1073/pnas.96.14.8271

Melo, A. M. P., Bandeiras, T. M., and Teixeira, M. (2004). New Insights into Type II NAD(P)H:quinone Oxidoreductases. *Microbiol. Mol. Biol. Rev.* 68, 603–616. doi:10.1128/mmbr.68.4.603-616.2004

Meulener, M. C., Graves, C. L., Sampathu, D. M., Armstrong-Gold, C. E., Bonini, N. M., and Giasson, B. I. (2005). DJ-1 Is Present in a Large Molecular Complex in Human Brain Tissue and Interacts with α-synuclein. *J. Neurochem.* 93, 1524–1532. doi:10.1111/j.1471-4159.2005.03145.x

Mistry, J., Chuguransky, S., Williams, L., Qureshi, M., Salazar, G. A., Sonnhammer, E. L. L., et al. (2021). Pfam: The Protein Families Database in 2021. *Nucleic Acids Res.* 49, D412–D419. doi:10.1093/nar/gkaa913

Mull, B. J., Narayanan, J., and Hill, V. R. (2013). Improved Method for the Detection and Quantification of *Naegleria Fowleri* in Water and Sediment Using Immunomagnetic Separation and Real-Time PCR. *J. Parasitol. Res.* 2013, 608367. doi:10.1155/2013/608367

Mullett, S. J., and Hinkle, D. A. (2011). DJ-1 Deficiency in Astrocytes Selectively Enhances Mitochondrial Complex I Inhibitor-Induced Neurotoxicity. *J. Neurochem.* 117, 375–387. doi:10.1111/j.1471-4159.2011.07175.x

Mungroo, M. R., Khan, N. A., Maciver, S., and Siddiqui, R. (2021). Opportunistic Free-Living Amoebal Pathogens. *Pathog. Glob. Health* 49, 1–15. doi:10.1080/21548331.2020.1828888

Nagakubo, D., Taira, T., Kitaura, H., Ikeda, M., Tamai, K., Iguchi-Ariga, S. M. M., et al. (1997). DJ-1, a Novel Oncogene Which Transforms Mouse NIH3T3 Cells in Cooperation Withras. *Biochem. Biophys. Res. Commun.* 231, 509–513. doi:10.1006/bbrc.1997.6132

Nose, Y., Rees, E. M., and Thiele, D. J. (2006). Structure of the Ctr1 Copper trans'PORE'ter Reveals Novel Architecture. *Trends Biochem. Sci.* 31, 604–607. doi:10.1016/j.tibs.2006.09.003

Overkamp, K. M., Bakker, B. M., Kötter, P., van Tuijl, A., de Vries, S., van Dijken, J. P., et al. (2000). *In Vivo* analysis of the Mechanisms for Oxidation of Cytosolic NADH by *Saccharomyces Cerevisiae* Mitochondria. *J. Bacteriol.* 182, 2823–2830. doi:10.1128/jb.182.10.2823-2830.2000

Paul, R., Banerjee, S., Sen, S., Dubey, P., Maji, S., Bachhawat, A. K., et al. (2021). The Novel Leishmanial Copper P-type ATPase Plays a Vital Role in Intracellular Parasite Survival. *J. Biol. Chem.* 298 (2), 101539. doi:10.1016/j.jbc.2021.101539

Perez-Riverol, Y., Bai, J., Bandla, C., García-Seisdedos, D., Hewapathirana, S., Kamatchinathan, S., et al. (2022). The PRIDE Database Resources in 2022: a Hub for Mass Spectrometry-Based Proteomics Evidences. *Nucleic Acids Res.* 50, D543.

Petito, G., de Curcio, J. S., Pereira, M., Bailão, A. M., Paccez, J. D., Tristão, G. B., et al. (2020). Metabolic Adaptation of *Paracoccidioides Brasiliensis* in Response to *In Vitro* Copper Deprivation. *Front. Microbiol.* 11, 1834. doi:10.3389/fmicb.2020.01834

Posey, J. E., and Gherardini, F. C. (2000). Lack of a Role for Iron in the Lyme Disease Pathogen. *Science* 288, 1651–1653. doi:10.1126/science.288.5471.1651

Rasmusson, A. G., Soole, K. L., and Elthon, T. E. (2004). Alternative NAD(P)H Dehydrogenases of Plant Mitochondria. *Annu. Rev. Plant Biol.* 55, 23–39. doi:10.1146/annurev.arplant.55.031903.141720

Rasoloson, D., Shi, L., Chong, C. R., Kafsack, B. F., and Sullivan, D. J. (2004). Copper Pathways in *Plasmodium Falciparum* Infected Erythrocytes Indicate an Efflux Role for the Copper P-ATPase. *Biochem. J.* 381, 803–811. doi:10.1042/bj20040335

Rees, E. M., Lee, J., and Thiele, D. J. (2004). Mobilization of Intracellular Copper Stores by the Ctr2 Vacuolar Copper Transporter. *J. Biol. Chem.* 279, 54221–54229. doi:10.1074/jbc.m411669200

Ribas-Carbo, M., Taylor, N. L., Giles, L., Busquets, S., Finnegan, P. M., Day, D. A., et al. (2005). Effects of Water Stress on Respiration in Soybean Leaves. *Plant Physiol.* 139, 466–473. doi:10.1104/pp.105.065565

Roberts, C. W., Roberts, F., Henriquez, F. L., Akiyoshi, D., Samuel, B. U., Richards, T. A., et al. (2004). Evidence for Mitochondrial-Derived Alternative Oxidase in the Apicomplexan Parasite *Cryptosporidium Parvum*: A Potential Anti-Microbial Agent Target. *Int. J. Parasitol.* 34, 297–308. doi:10.1016/j.ijpara.2003.11.002

Schneider, C. A., Rasband, W. S., and Eliceiri, K. W. (2012). NIH Image to ImageJ: 25 Years of Image Analysis. *Nat. Methods* 9 (7), 671–675. doi:10.1038/nmeth.2089

Sieger, S. M., Kristensen, B. K., Robson, C. A., Amirsadeghi, S., Eng, E. W. Y., Abdel-Mesih, A., et al. (2005). The Role of Alternative Oxidase in Modulating Carbon Use Efficiency and Growth during Macronutrient Stress in Tobacco Cells. *J. Exp. Bot.* 56, 1499–1515. doi:10.1093/jxb/eri146

Sluse, F. E., and Jarmuszkiewicz, W. (1998). Alternative Oxidase in the Branched Mitochondrial Respiratory Network: an Overview on Structure, Function, Regulation, and Role. *Braz. J. Med. Biol. Res.* 31, 733–747. doi:10.1590/s0100-879x1998000600003

Smith, C. A., Melino, V. J., Sweetman, C., and Soole, K. L. (2009). Manipulation of Alternative Oxidase Can Influence Salt Tolerance in *Arabidopsis Thaliana*. *Physiol. Plant* 137, 459–472. doi:10.1111/j.1399-3054.2009.01305.x

Solomon, E. I., Heppner, D. E., Johnston, E. M., Ginsbach, J. W., Cirera, J., Qayyum, M., et al. (2014). Copper Active Sites in Biology. *Chem. Rev.* 114, 3659–3853. doi:10.1021/cr400327t

Stafford, S. L., Bokil, N. J., Achard, M. E., Kapetanovic, R., Schembri, M. A., Mcewan, A. G., et al. (2013). Metal Ions in Macrophage Antimicrobial Pathways: Emerging Roles for Zinc and Copper. *Biosci. Rep.* 33, 541–554. doi:10.1042/BSR20130014

Stearman, R., Yuan, D. S., Yamaguchi-Iwai, Y., Klausner, R. D., and Dancis, A. (1996). A Permease-Oxidase Complex Involved in High-Affinity Iron Uptake in Yeast. *Science* 271, 1552–1557. doi:10.1126/science.271.5255.1552

Sun, T. S., Ju, X., Gao, H. L., Wang, T., Thiele, D. J., Li, J. Y., et al. (2014). Reciprocal Functions of *Cryptococcus Neoformans* Copper Homeostasis Machinery during Pulmonary Infection and Meningoencephalitis. *Nat. Commun.* 5, 5550. doi:10.1038/ncomms6550

Taira, T., Saito, Y., Niki, T., Iguchi-Ariga, S. M. M., Takahashi, K., and Ariga, H. (2004). DJ-1 Has a Role in Antioxidative Stress to Prevent Cell Death. *EMBO Rep.* 5, 213–218. doi:10.1038/sj.embor.7400074

Thomas, P. D., Campbell, M. J., Kejariwal, A., Mi, H., Karlak, B., Daverman, R., et al. (2003). PANTHER: A Library of Protein Families and Subfamilies Indexed by Function. *Genome Res.* 13, 2129–2141. doi:10.1101/gr.772403

Trempe, J.-F., and Fon, E. A. (2013). Structure and Function of Parkin, PINK1, and DJ-1, the Three Musketeers of Neuroprotection. *Front. Neurol.* 4, 38. doi:10.3389/fneur.2013.00038

Tsaousis, A. D., Nývltová, E., Šuták, R., Hrdý, I., and Tachezy, J. (2014). A Nonmitochondrial Hydrogen Production in *Naegleria Gruberi*. *Genome Biol. Evol.* 6, 792–799. doi:10.1093/gbe/evu065

Tyanova, S., Temu, T., Sinitcyn, P., Carlson, A., Hein, M. Y., Geiger, T., et al. (2016). The Perseus Computational Platform for Comprehensive Analysis of (Prote)omics Data. *Nat. Methods* 13, 731–740. doi:10.1038/nmeth.3901

Uyemura, S. A., Luo, S., Vieira, M., Moreno, S. N. J., and Docampo, R. (2004). Oxidative Phosphorylation and Rotenone-Insensitive Malate- and NADH-Quinone Oxidoreductases in *Plasmodium Yoelii* Yoelii Mitochondria *In Situ*. *J. Biol. Chem.* 279, 385–393. doi:10.1074/jbc.m307264200

Vishwakarma, A., Tetali, S. D., Selinski, J., Scheibe, R., and Padmasree, K. (2015). Importance of the Alternative Oxidase (AOX) Pathway in Regulating Cellular Redox and ROS Homeostasis to Optimize Photosynthesis during Restriction of the Cytochrome Oxidase Pathway in *Arabidopsis Thaliana*. *Ann. Bot.* 116, 555–569. doi:10.1093/aob/mcv122

Wang, H., Li, Y.-Y., Qiu, L.-Y., Yan, Y.-F., Liao, Z.-P., and Chen, H.-P. (2017). Involvement of DJ-1 in Ischemic Preconditioning-Induced Delayed Cardioprotection *In Vivo*. *Mol. Med. Rep.* 15, 995–1001. doi:10.3892/mmr.2016.6091

Waterman, S. R., Hacham, M., Hu, G., Zhu, X., Park, Y.-D., Shin, S., et al. (2007). Role of a CUF1/CTR4 Copper Regulatory axis in the Virulence of *Cryptococcus Neoformans*. *J. Clin. Invest.* 117, 794–802. doi:10.1172/jci30006

Wei, Y., Ringe, D., Wilson, M. A., and Ondrechen, M. J. (2007). Identification of Functional Subclasses in the DJ-1 Superfamily Proteins. *PLOS Comput. Biol.* 3, e15. doi:10.1371/journal.pcbi.0030010

Weinberg, E. D. (1975). Nutritional Immunity. Host's Attempt to Withold Iron from Microbial Invaders. *JAMA J. Am. Med. Assoc.* 231, 39–41. doi:10.1001/jama.231.1.39

Winge, D. R., Jensen, L. T., and Srinivasan, C. (1998). Metal-Ion Regulation of Gene Expression in Yeast. *Curr. Opin. Chem. Biol.* 2, 216–221. doi:10.1016/s1367-5931(98)80063-x

Yagi, T. (1991). Bacterial NADH-Quinone Oxidoreductases. *J. Bioenerg. Biomembr.* 23, 211–225. doi:10.1007/bf00762218

Yu, D., Pan, H., Zhang, R., Li, Y., and Nie, X. (2017). Nucleus DJ-1/Park7 Acts as a Favorable Prognostic Factor and Involves Mucin Secretion in Invasive Breast Carcinoma in Chinese Population. *Int. J. Clin. Exp. Med.* 10 (4), 6558–6567.

Zhang, L., Wang, J., Wang, J., Yang, B., He, Q., and Weng, Q. (2020). Role of DJ-1 in Immune and Inflammatory Diseases. *Front. Immunol.* 11, 994. doi:10.3389/fimmu.2020.00994

Zhou, B., and Gitschier, J. (1997). hCTR1: A Human Gene for Copper Uptake Identified by Complementation in Yeast. *Proc. Natl. Acad. Sci. U. S. A.* 94, 7481–7486. doi:10.1073/pnas.94.14.7481

Zimmermann, L., Stephens, A., Nam, S.-Z., Rau, D., Kübler, J., Lozajic, M., et al. (2018). A Completely Reimplemented MPI Bioinformatics Toolkit with a New HHpred Server at its Core. *J. Mol. Biol.* 430, 2237–2243. doi:10.1016/j.jmb.2017.12.007

Conflict of Interest: The authors declare that the research was conducted in the absence of any commercial or financial relationships that could be construed as a potential conflict of interest.

Publisher's Note: All claims expressed in this article are solely those of the authors and do not necessarily represent those of their affiliated organizations, or those of the publisher, the editors and the reviewers. Any product that may be evaluated in this article, or claim that may be made by its manufacturer, is not guaranteed or endorsed by the publisher.

AMERICAN SOCIETY FOR MICROBIOLOGY | Antimicrobial Agents and Chemotherapy®

EXPERIMENTAL THERAPEUTICS

Repurposing of MitoTam: Novel Anti-Cancer Drug Candidate Exhibits Potent Activity against Major Protozoan and Fungal Pathogens

Dominik Arbon,[a] Kateřina Ženíšková,[a] Karolína Šubrtová,[a] Jan Mach,[a] Jan Štursa,[b] Marta Machado,[d] Farnaz Zahedifard,[a] Tereza Leštinová,[e] Carolina Hierro-Yap,[f] Jiri Neuzil,[b,g,h] Petr Volf,[e] Markus Ganter,[c] Martin Zoltner,[a] Alena Zíková,[f,i] Lukáš Werner,[b] Robert Sutak[a]

[a]Department of Parasitology, Faculty of Science, Charles University, BIOCEV, Vestec, Czech Republic
[b]Institute of Biotechnology, Czech Academy of Sciences, BIOCEV, Vestec, Czech Republic
[c]Centre for Infectious Diseases, Parasitology, Heidelberg University Hospital, Heidelberg, Germany
[d]Graduate Program in Areas of Basic and Applied Biology, Instituto de Ciências Biomédicas Abel Salazar, Universidade do Porto, Portugal
[e]Faculty of Sciences, Charles University, Department of Parasitology, Prague, Czech Republic
[f]Institute of Parasitology, Biology Centre, Czech Academy of Sciences, České Budějovice, Czech Republic
[g]School of Pharmacy and Medical Science, Griffith University, Southport, Queensland, Australia
[h]Department of Physiology, Faculty of Science, Charles University, Prague, Czech Republic
[i]Faculty of Science, University of South Bohemia, České Budějovice, Czech Republic

Dominik Arbon and Kateřina Ženíšková contributed equally to this article. Author order was determined alphabetically.

ABSTRACT Many of the currently available anti-parasitic and anti-fungal frontline drugs have severe limitations, including adverse side effects, complex administration, and increasing occurrence of resistance. The discovery and development of new therapeutic agents is a costly and lengthy process. Therefore, repurposing drugs with already established clinical application offers an attractive, fast-track approach for novel treatment options. In this study, we show that the anti-cancer drug candidate MitoTam, a mitochondria-targeted analog of tamoxifen, efficiently eliminates a wide range of evolutionarily distinct pathogens *in vitro*, including pathogenic fungi, *Plasmodium falciparum*, and several species of trypanosomatid parasites, causative agents of debilitating neglected tropical diseases. MitoTam treatment was also effective *in vivo* and significantly reduced parasitemia of two medically important parasites, *Leishmania mexicana* and *Trypanosoma brucei*, in their respective animal infection models. Functional analysis in the bloodstream form of *T. brucei* showed that MitoTam rapidly altered mitochondrial functions, particularly affecting cellular respiration, lowering ATP levels, and dissipating mitochondrial membrane potential. Our data suggest that the mode of action of MitoTam involves disruption of the inner mitochondrial membrane, leading to rapid organelle depolarization and cell death. Altogether, MitoTam is an excellent candidate drug against several important pathogens, for which there are no efficient therapies and for which drug development is not a priority.

KEYWORDS *Candida*, *Cryptococcus*, drug, *Leishmania*, mitochondria, *Plasmodium*, *Trypanosoma*

The ongoing search for novel treatment options to combat medically relevant parasitic protists (e.g., *Plasmodium*, *Trypanosoma,* and *Leishmania* spp.) is driven by the need for more efficient, less toxic, and/or less expensive medications as well as by the emergence and spread of drug resistance (1–3). Drug discovery and development have been facilitated in recent decades by advances in the fields of genetics, molecular biology, medicinal chemistry and the introduction of high-throughput target-based,

Address correspondence to Robert Sutak, sutak@natur.cuni.cz, Lukáš Werner, Lukas.Werner@ibt.cas.cz, or Alena Zíková, azikova@paru.cas.cz.

The authors declare a conflict of interest. The authors of this manuscript have the following competing interests: J.N., J.Š., and L.W. are co-owners of MitoTax s.r.o. and the MitoTam intellectual property. Other authors declare no conflict of interest. Springtide Ventures s.r.o. and SmartBrain s.r.o. financed the MitoTam-01 clinical trial.

Received 27 May 2022
Accepted 7 June 2022
Published 20 July 2022

phenotypic and virtual screening strategies. Nevertheless, repurposing of drugs originally approved for other indications presents a strategy of particular interest for the implementation of novel treatments for neglected diseases (3). As repurposed drugs are typically at least partly characterized or even approved for clinical use, both the time and cost of the drug development process are dramatically reduced. This is particularly appealing for drugs against neglected diseases with little financial incentive for commercial '*de novo*' drug discovery approaches.

Phosphonium salts are lipophilic cations with the ability to readily pass across phospholipid bilayers, and due to their delocalized positive charge, they accumulate at the interface of the inner mitochondrial membrane (IMM) and matrix according to the mitochondrial membrane potential ($\Delta\Psi_m$). The extent of accumulation of lipophilic cations at the IMM follows the Nernst equation, according to which there is a 10-fold increase in the concentration of lipophilic cations at the IMM-matrix interface for every ~60 mV increase in $\Delta\Psi_m$ (4). Phosphonium vectors have been employed for efficient and selective mitochondrial delivery of various cargos such as therapeutic antioxidants (5, 6), liposomes (7), functional probes (8, 9), antimicrobial, anti-fungal and anti-parasitic drugs (10–16) and anti-cancer treatments (10, 17, 18).

MitoTam, a new tamoxifen derivative conjugated to triphenylphosphonium vector (TPP+), is a promising anti-cancer drug candidate acting by mitochondrial destabilization (19). It was originally developed to selectively accumulate the pharmacophore tamoxifen in the mitochondria proportionally to $\Delta\Psi_m$. The compound is well tolerated in the mouse model and recently underwent a phase 1/1b clinical trial with favorable outcome when it was intravenously administered to human advanced-stage cancer patients (MitoTam-01 trial; EudraCT 2017-004441-25). Its molecule consists of three parts: i) the functional pharmacophore residue, tamoxifen, a drug that has been used for decades to treat early and advanced hormone-dependent breast cancer (20), ii) the TPP^+ for mitochondrial targeting, and iii) the 10-carbon linear alkyl linker tethering tamoxifen to the TPP^+ moiety. The compound efficiently kills breast cancer cells and suppresses tumors progression, including treatment-resistant carcinomas with high Her2 protein levels ($Her2^{high}$), for which the original precursor compound tamoxifen was ineffective. Importantly, MitoTam exhibits low toxicity toward nonmalignant cells (19). Similar to the mitochondria-mediated anti-cancer effects of tamoxifen, MitoTam modulates or alters multiple mitochondrial processes, including the function of the respiratory complex I (CI; NADH:ubiquinone dehydrogenase) (19, 21–23). The superior efficacy of MitoTam compared to tamoxifen is due to its accumulation at the interface of the mitochondrial matrix and IMM that leads to suppression of CI-dependent respiration, disruption of respiratory supercomplexes, rapid dissipation of the $\Delta\Psi_m$, increased production of reactive oxygen species (ROS), and ultimately cell death (19). MitoTam is also effective in the treatment of the syngeneic renal cancer murine model, especially in combination with immunotherapy (23). In addition, MitoTam selectively eliminates senescent cells and is, therefore, a candidate for the treatment of age-related disorders (22, 24).

In this work, we tested the potential activity of MitoTam against a wide range of parasitic protists and pathogenic fungi (Table S1). These models were selected for their medicinal and economic relevance and for their suitability as cellular models for research of mitochondrial function. We chose parasites from the Kinetoplastida group: *Trypanosoma cruzi*, an intracellular parasite responsible for Chagas disease; *Leishmania* spp., the etiological agent of a spectrum of disorders ranging from self-healing cutaneous lesions to potentially fatal visceral diseases; and *Trypanosoma brucei*, a highly tractable model organism causing major economical complications in the developing world due to livestock infections and a causative agent of human African trypanosomiasis (sleeping sickness)—a disease that is currently targeted for elimination due to combination of vector control, active case-finding and development of new medicines (25–28).

We also tested the effect of MitoTam on *Plasmodium falciparum*, a parasite responsible for most malaria-related deaths in humans (29); on the pathogenic fungi *Candida*

TABLE 1 MitoTam inhibits the growth of several pathogenic microorganisms *in vitro*[a]

	MitoTam		Tamoxifen		Control		
Pathogen	EC_{50} [μM]	SD	EC_{50} [μM]	SD	Compound	EC_{50} [μM]	SD
Trypanosoma brucei BSF	0.02	≤0.01	7.20	±1.47	Amphotericin B	1.09	±0.09
Trypanosoma brucei PCF	0.16	±0.03	≥10		Amphotericin B	0.24	±0.06
T. brucei gambiense BSF	0.03	≤0.01	≥10		Pentamidine	≤0.01	≤0.001
Trypanosoma cruzi (epimastigotes)	1.55	±0.04	≥10		Benznidazole	≥10	
Leishmania mexicana (amastigotes)	0.35	±0.05	7.93	±0.59	Amphotericin B	0.33	±0.08
Leishmania major (promastigotes)	0.60	±0.10	≥10		Amphotericin B	0.06	±0.02
Plasmodium falciparum (erythrocytic stage)	0.03	±0.01	6.37	±0.11	Chloroquine	0.01	≤0.01
Candida albicans	0.56	±0.07	≥10		Amphotericin B	0.37	±0.01
Cryptococcus neoformans	0.61	±0.12	7.28	±1.97	Amphotericin B	0.12	±0.05
Naegleria fowleri	≥10		≥10		Amphotericin B	0.08	±0.01
Acanthamoeba castellanii	1.95	±0.23	9.93	±0.58	Amphotericin B	6.17	±0.70
Giardia intestinalis	≥10		≥10		Benznidazole	6.22	±0.66
Trichomonas vaginalis	≥10		≥10		Metronidazole	6.54	±0.45

[a]Mean EC_{50} values for MitoTam, tamoxifen (the functional pharmacophore of MitoTam) and specific antimicrobial drugs used as positive controls for each tested organism derived from dose-response curves (Fig. S1) are given in μM ($n > 3$, ± s.d.).

albicans and *Cryptococcus neoformans*, widespread opportunistic pathogens causing life-threatening diseases in immunocompromised individuals (30, 31); on the amphizoic amebae *Naegleria fowleri* and *Acanthamoeba* spp., whose infections lead to rare diseases with extremely high mortality rate (32, 33); and on *Giardia intestinalis* and *Trichomonas vaginalis*, anaerobic parasites with reduced mitochondria, causative agents for widespread intestinal and urogenital infections (34–36). Here, we show that the anti-cancer drug candidate MitoTam efficiently and selectively inhibits viability of a number of these pathogens *in vitro*. In pilot experiments using mouse models of infection with *T. brucei* and *L. mexicana*, MitoTam reduced parasite burdens and significantly prolonged survival for *T. brucei*-infected animals. Furthermore, we demonstrate in *T. brucei* that the trypanocidal activity of MitoTam relies, at least partly, on rapid disruption of IMM. Together, our data provide strong evidence that MitoTam is an excellent candidate for further development as an anti-infective, especially for targeting several neglected diseases.

RESULTS

Low levels of MitoTam are lethal to a variety of pathogenic eukaryotic microorganisms. The mitochondrion is a promising drug target because of its pivotal role in cellular metabolism, proliferation, and cell death signaling (26, 37, 38). We therefore investigated the effect of MitoTam, a mitochondria-targeted tamoxifen derivative, on a wide range of parasitic protists and yeasts. MitoTam proved to have a significant growth inhibitory effect for the majority of these pathogens (Table 1 and Fig. S1) exhibiting nanomolar potencies against *P. falciparum*, *T. b. brucei* and *Leishmania* spp. Notably, the half-maximal effective concentration (EC_{50}) values are considerably lower than corresponding cytotoxicity values reported for various mammalian cells (ranging from 0.6 to 4.5 μM) (19), indicating high selectivity. All pathogens were also challenged with the parental compound tamoxifen lacking the TPP^+ vector for mitochondrial targeting, with efficacy significantly lower than MitoTam (Table 1). This is consistent with similar comparisons reported for the anti-cancer activity of the two molecules (19). Each dose-response analysis was validated using a known, active compound against individual pathogens tested, providing values consistent with published data (Table 1).

The highest efficacy of MitoTam was detected for the bloodstream form (BSF) of *T. brucei*. This value was approximately 30-fold lower than $Her2^{high}$ cancer cells (0.02 μM *versus* 0.65 μM) (19). Interestingly, MitoTam showed low nanomolar efficacy (0.03 μM) against the erythrocytic stage of *P. falciparum*, which is protected inside the parasitophorous vacuole within the host erythrocyte (39), suggesting that MitoTam is able to cross several membranes before reaching its target. Furthermore, MitoTam was found to inhibit the growth of the *T. brucei* procyclic form (PCF), axenically grown *Leishmania mexicana*

amastigotes and *L. major* promastigotes, and the two pathogenic fungi *Candida albicans* and *Cryptococcus neoformans* at submicromolar EC_{50} values. *T. cruzi* epimastigotes also responded to MitoTam treatment with low-micromolar EC_{50}, as did *Acanthamoeba* sp., while no effect was observed on *Naegleria fowleri* proliferation. Also, *Trichomonas vaginalis* and *Giardia intestinalis*, two anaerobic parasites that possess mitochondrion-related organelles characterized by the absence of membrane-bound electron transport chain and therefore by the lack of mitochondrial respiration (36), were insensitive to MitoTam treatment. Overall, MitoTam effectively killed a range of clinically important, evolutionarily distinct pathogens, including intracellular parasites.

MitoTam efficiently eliminates *L. major* and *L. infantum* intracellular amastigotes. The high efficacy of MitoTam against *L. mexicana* axenic amastigotes (EC_{50} 0.35 $\pm$ 0.05 μM) prompted us to investigate the ability of MitoTam to eliminate the intracellular form of the parasite in a macrophage infection model. Murine macrophage cells (J774A.1) were infected with *L. major* or *L. infantum* promastigotes and exposed to different concentrations of MitoTam (0 to 25μM). After controlled lysis of the infected macrophages, the released parasites were quantified using a resazurin-based viability assay (40). In this intramacrophage assay, treatment with MitoTam eliminated intracellular amastigotes of *L. major* and *L. infantum* with EC_{50} values of 175 $\pm$ 51 nM and 293 $\pm$ 29 nM, respectively (Fig. S2). This result is highly encouraging considering how difficult is to effectively target the intracellular *Leishmania* amastigotes *in vivo* since the parasites reside in a parasitophorous vacuole, a phagolysosome-like structure with low pH and a potential drug target is protected by three membranes (plasma membrane of a macrophage, parasitophorous vacuolar membrane and plasma membrane of an amastigote) (26).

MitoTam treatment alleviates parasitemia leading to prolonged survival of mice infected with *T. brucei* and to reduced frequency and lesion size caused by *L. mexicana* infection. Activity for a compound detected in the intramacrophage assay usually translates into activity in an animal infection model (41, 42), apart from potential issues with pharmacokinetics. Hence, we next tested the ability of MitoTam, which is well tolerated in BALB/c mice (19), a mouse infection model of both *L. mexicana* and *T. brucei*. MitoTam dosing regimen was based on the published data (19, 22).

For the *T. brucei* infection model, survival analysis revealed that MitoTam intravenous (IV) administration at doses of 3 mg/kg body weight (bw) on days 3 and 5 postinfection without further treatment delayed the death of *T. brucei* infected animals, which succumb to the infection by 8 days (Fig. 1A).

In a second experiment, we followed *T. brucei* parasitemia levels in infected animals (Fig. 1B). Automated analysis of blood smears revealed the presence of *T. brucei* parasites in samples from mice untreated and treated on days 2 and 4 postinfection, showing that MitoTam-treated animals exhibited a significantly lower parasite load (Fig. 1B). This explains the longer survival of treated animals compared to the untreated controls (Fig. S3).

The effect of MitoTam administration (3 mg/kg bw, intraperitoneally [IP]) in the *L. mexicana* infection model was assessed by monitoring frequency and size of dermal lesions. As shown in Fig. 1C, lesions occurred less frequently in MitoTam-treated BALB/c mice than in the untreated controls during the 12-week course of the experiment (50% versus 90% of mice at weeks 8 to 12 postinfection). In a separate experiment, MitoTam at two doses reduced the size of lesions caused by *L. mexicana* in the weeks following infection (Fig. 1D).

Collectively, these data demonstrate that MitoTam is highly effective against *T. brucei* and *L. mexicana* parasites *in vivo*. Notably, we did not observe any notable adverse effects of MitoTam on the treated animals.

MitoTam treatment causes alteration of *T. brucei* mitochondrial proteome and leads to upregulation of multidrug efflux pumps in *C. albicans*. The potent anti-parasitic properties *in vitro* and the promising *in vivo* experiments prompted us to explore the MitoTam mode of action. First, we performed comparative whole-cell proteomic analysis of control and MitoTam-treated cells for two parasitic model organisms, *C. albicans* and *T. brucei*. In order to restrict indirect, secondary impact resulting from cell

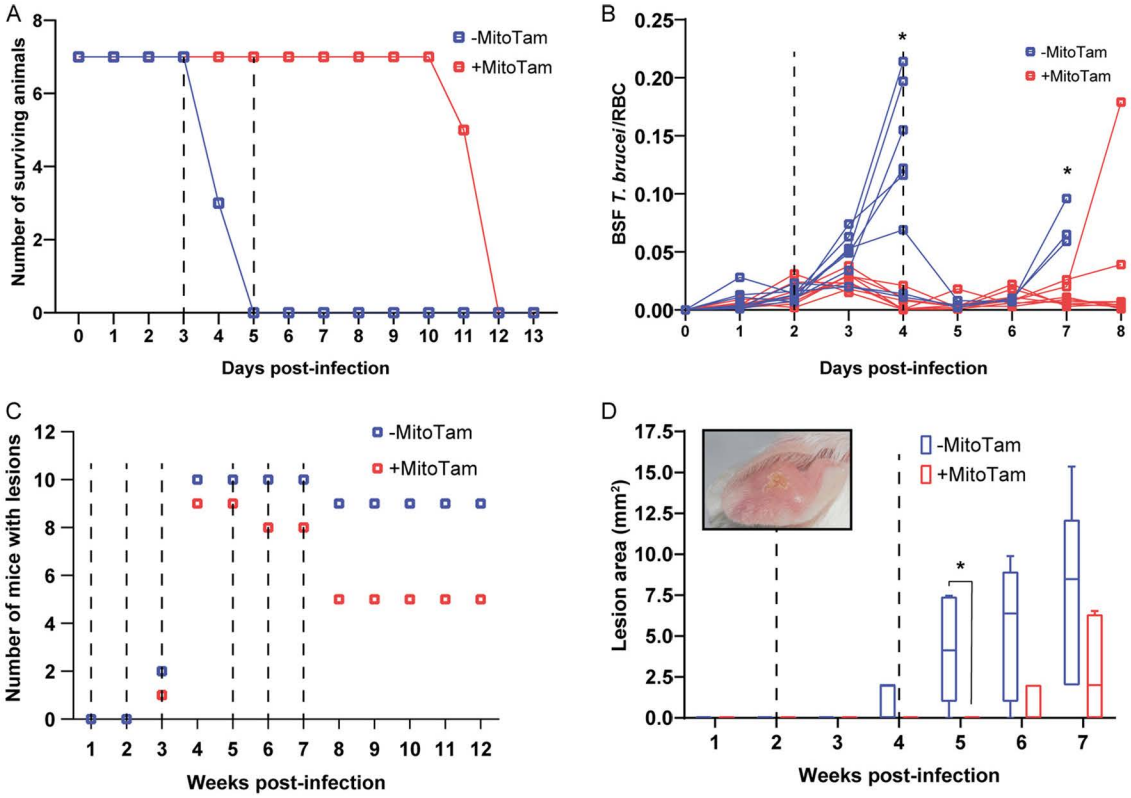

FIG 1 MitoTam is effective against *T. brucei* and *L. mexicana* parasites in mouse infection models. (A) Survival rate of BALB/c mice infected with *T. brucei* was monitored daily for 13 days. Half of the infected mice were injected IV with MitoTam (+MitoTam) on days 3 and 5 (dashed lines) postinfection (3 mg/kg bw). The number of surviving mice from MitoTam treated group (red line) as well as from untreated control group (-MitoTam) (blue line) is plotted against the time (in days). (B) Parasitemia in BALB/c mice infected with *T. brucei* was evaluated microscopically from blood smears. On day 2 and 4 postinfection (dashed lines), eight mice were IV injected with MitoTam (3 mg/kg) (+MitoTam). The ratio of *T. brucei* cells to red blood cells (RBC) was calculated daily and used to quantify the parasitemia levels of each animal from the MitoTam treated group (red line) and the respective untreated control group (-MitoTam) (blue line). Statistically significant differences between the two groups are indicated with an asterisk (*unpaired t test*, *, $P < 0.05$). (C) Formation of dermal lesions in 20 BALB/c mice was followed for 12 weeks after infection with *L. mexicana*. As indicated (dashed lines), half of the infected animals were injected IP with MitoTam (+MitoTam) at 1, 2, 3, 5, 6 and 7 weeks postinfection. The appearance of lesions was monitored (+MitoTam, red) and compared to the number of lesions of animals from the untreated control group (-MitoTam, blue). (D) Size of dermal lesions was recorded in 10 BALB/c mice infected with *L. mexicana*. Five of the infected animals were treated with MitoTam (+MitoTam) at weeks 2 and 4 postinfection as indicated (dashed lines). Throughout the course of the infection, the lesion areas of each animal were measured weekly. The values were averaged for the MitoTam treated group (+MitoTam, in red) and untreated control group (-MitoTam, in blue). Box and whisker graph is shown, statistically significant differences are indicated with an asterisk (paired *t* test, *, $P < 0.05$). A representative lesion image is shown as an inset in the graph.

death, we chose short exposure times: yeast cells were treated with 4.4 μM MitoTam (~7× EC_{50}) for 12 h, while *T. brucei* BSF cells were incubated with 100 nM MitoTam (5× EC_{50}) for 14 h. Proteomic data were processed by label-free quantification in MaxQuant (43) and statistically analyzed in Perseus (44, 45). In *C. albicans*, out of 1,950 detected protein groups, the abundance of only 1.69% of the quantified proteins was significantly altered (Table S2) (Fig. 2A), with two homologs of multidrug efflux pumps being among the most upregulated genes (≥26 times).

In contrast, analysis of the *T. brucei* proteome revealed substantial changes after treatment with MitoTam, with 26.3% of all identified proteins (2,063) significantly altered (Table S3) (Fig. 2B). Data analyses did not reveal any specific single pathway or protein as a direct target of MitoTam. Since MitoTam specifically affects mitochondrial functions in various cells (19, 22, 23), we analyzed enrichment of mitochondrial proteins using a *T. brucei* mitoproteome database (46). While mitochondrial proteins accounted for 14.3% of all detected proteins, we observed an almost 2-fold enrichment (27.6%) in the significantly altered subset of proteins, with 20.8% and 32.1% in the

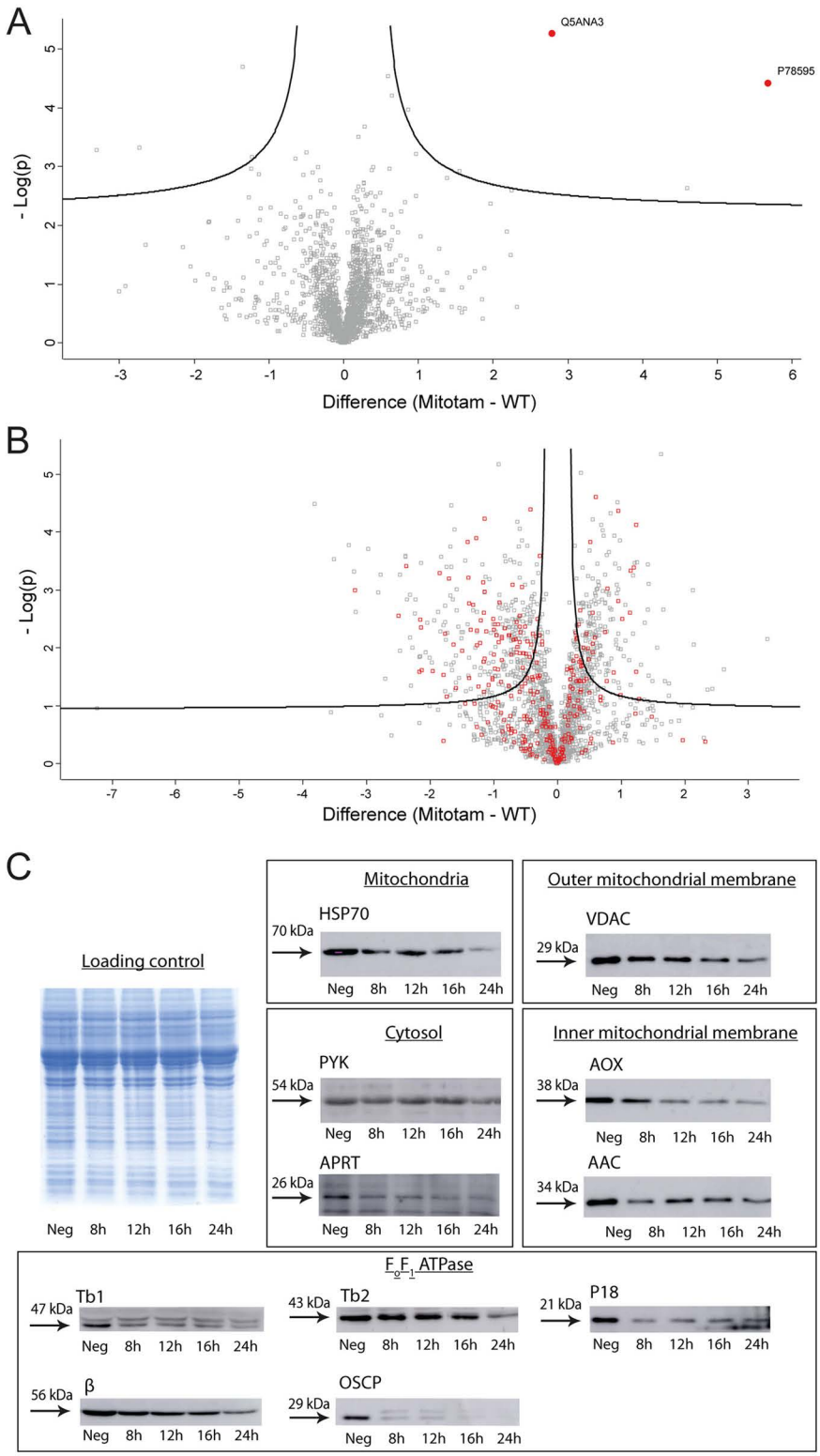

FIG 2 Global proteome changes upon MitoTam exposure. Shown are volcano plots of the *t* test difference from label-free quantification from triplicate experiments, plotted against the respective $-\log_{10}$-transformed *P* values. Untreated control cells were compared to cells treated with MitoTam for *C. albicans* (A) or BSF *T. brucei* (B). (A) Highlighted points are *C. albicans* significantly upregulated efflux pumps (red dots): P78595—multidrug resistance protein CDR2; Q5ANA3—pleiotropic ABC efflux transporter of multiple drugs CDR1. (B) *T. brucei* mitochondrial proteins are in red. (C) Western blot analyses of whole-cell lysates harvested from BSF *T. brucei* cells treated with 100 nM MitoTam for 0 to 24 h as indicated. Equal amounts of total protein were loaded in each lane. A Coomassie stained gel

(Continued on next page)

increased and decreased cohort, respectively. These results indicate that MitoTam treatment induces preferentially a decrease in the levels of various mitochondrial proteins. To validate these results, we analyzed *T. brucei* whole-cell lysates from cultures harvested at 4 different time points of MitoTam exposure (8, 12, 16, and 24 h) by immunoblotting with antibodies against 8 mitochondrial marker proteins and cytosolic pyruvate kinase as a control (Fig. 2C). Consistent with the *T. brucei* proteomics analysis, we detected significant abundance decrease for nine mitochondrial proteins after 8 h of MitoTam treatment.

MitoTam treatment leads to disruption of the mitochondrial inner membrane and rapid loss of $\Delta\Psi_m$ in the bloodstream form of *T. brucei*. MitoTam was reported to directly impact mitochondrial function in renal and breast cancer cells, tumors, and senescent cells (19, 22, 23). In line with this, our proteomic analysis indicated that MitoTam treatment perturbs the mitochondrial proteome in *T. brucei*. *T. brucei* BSF cells lack cytochrome-mediated mitochondrial electron transport chain, respiring exclusively via an alternative pathway consisting of mitochondrial glycerol-3-phosphate dehydrogenase and trypanosome alternative oxidase (AOX), and sustain the $\Delta\Psi_m$ by reversed activity of F_oF_1-ATP synthase (47–49). Importantly, the cancer molecular target of MitoTam, respiratory CI (19) was shown to be dispensable for BSF cells (50), yet our data show that the drug efficiently eliminates these parasites.

To gain deeper insight into the anti-parasitic mode of action of MitoTam, we investigated its effect on mitochondrion in this model protist. When comparing the growth of untreated cells with cells treated with two different concentrations of MitoTam, we found that growth of *T. brucei* cells was significantly inhibited after 24 h (40 nM, 2× EC_{50}) or 12 h (100 nM, 5× EC_{50}) (Fig. 3A). To establish a timeline for further experiments, we performed a live/dead cell assay using the cell-impermeant dye Sytox. This result shows that despite the reduced growth rate, 82.4% and 71% cells were still viable upon 40 nM and 100 nM MitoTam treatment, respectively, after exposure to the drug for 16 h. At 24 h of treatment, the viability was further decreased to 67.3% and 63.6% at 40 and 100 nM MitoTam, respectively (Fig. 3B). This was accompanied by increased level of cellular ROS of cells treated with 100 nM MitoTam for 16 h (Fig. 4A).

To examine whether MitoTam affects mitochondrial activity, we analyzed changes in several cellular attributes associated with mitochondrial function. *T. brucei* BSF cultures were treated for 16 and/or 24 h with 40 nM or 100 nM MitoTam. We found that incubation with 100 nM MitoTam significantly reduced glycerol-3-phosphate-dependent respiration, increased cellular ADP/ATP ratio (by 2.6-fold), and decreased mitochondrial and cytosolic ATP as well as total cellular ATP levels (Fig. 4B to E). Next, we assessed $\Delta\Psi_m$ in live cells using the cell-permeable red fluorescent dye TMRE and using the Safranin O assay in digitonin-permeabilized cells. The results of both assays demonstrate that treatment with 100 nM MitoTam rendered the cell incapable of maintaining $\Delta\Psi_m$ (Fig. 4F and G). Experiments with cultures treated with MitoTam at 40 nM showed a similar but less pronounced overall effect on *T. brucei* mitochondrial activity (Fig. S4).

In agreement with these results, fluorescence microscopy evaluation revealed that treatment with 1 μM MitoTam for 1 h led to an ~8-fold decrease of the signal intensity of MitoTracker Red CMX-ROS, a mitochondrial probe used to stain live cells that relies on $\Delta\Psi_m$ (Fig. 4H).

Furthermore, $\Delta\Psi_m$ was assessed in digitonin-permeabilized wild-type BSF cells by Safranin O dye upon addition of ATP. We found that $\Delta\Psi_m$ was quickly dissipated with 1 μM MitoTam, a phenotype identical to the effect of addition of oligomycin, an inhibitor of ATP synthase (Fig. 4I). Moreover, using mitochondrial superoxide indicator

FIG 2 Legend (Continued)
was used as a control for equal loading. The immunoblots were probed with antibodies against cytosolic pyruvate kinase (PYK) and adenine phosphoribosyltransferase (APRT) and mitochondrial heat shock protein 70 (Hsp70), proteins associated with the outer mitochondrial membrane (VDAC), inner mitochondrial membrane (AOX, AAC), and subunits of the F_oF_1-ATP synthase (β, p18, OSCP, Tb1, Tb2). The relevant masses of the protein molecular weight are indicated.

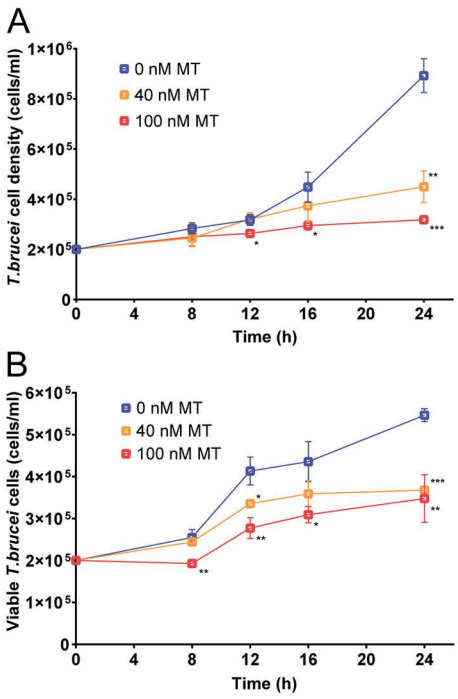

FIG 3 MitoTam affects *T. brucei* viability and alters the mitochondrial function of bloodstream *T. brucei* cells. (A) Growth curve of BSF *T. brucei* cultures was evaluated in unstained cells by flow cytometry. Untreated control BSF cells (0 nM MT, blue) were compared with cells incubated with 40 nM MitoTam (40 nM MT, orange) and 100 nM MitoTam (100 nM MT, red). Statistically significant differences are indicated with an asterisk (paired *t* test, *, $P < 0.05$, **, $P < 0.01$, ***, $P < 0.001$) (mean ± s.d., $n = 3$). (B) Staining with the cell impermeant nucleic acid dye Sytox was used to distinguish viable (Sytox negative) and dead (Sytox positive) BSF *T. brucei* cells. Concentrations of Sytox negative, live cells are plotted. Untreated control cultures (0 nM MT, blue) were compared with cultures incubated in the presence of 40 nM MitoTam (40 nM MT, orange) and 100 nM MitoTam (100 nM MT, red) (paired *t* test, *, $P < 0.05$, **, $P < 0.01$, ***, $P < 0.001$) (mean ± s.d., $n = 3$).

(MitoSOX), we detected a significant decrease of mitochondrial ROS levels upon MitoTam treatment, suggesting that the mode of action of MitoTam in trypanosomes differs from its effect in cancer cells (Fig. 4J).

While the observed changes in the evaluated attributes are consistent with inhibition of F_oF_1-ATP synthase that generates $\Delta\Psi_m$ in BSF *T. brucei* cells (48), we also tested if the rapid drop in $\Delta\Psi_m$ is caused by a physicochemical disruption of the IMM. To this end, we assessed the integrity of isolated mitochondria using the mitochondrial marker threonine dehydrogenase (TDH), whose activity is detectable only if the added substrate threonine can freely pass through 'compromised' mitochondrial membrane. As shown in Fig. 4K, treatment with MitoTam at 7.4 μM decreased mitochondrial membrane integrity by 50%. This relatively high value (369 times higher than EC_{50}) determined in this *in vitro* experiment can be explained by a need to form much larger membrane pores for threonine (molecular weight 119.12 g/mol) to enter mitochondria compared to the formation of much smaller or temporal pores allowing the passage of H^+. In addition, in this experiment, the BSF form mitochondrion is not energized due to the lack of substrates and therefore this could have prevented accumulation of MitoTam from in the organelle.

Furthermore, to corroborate these results we estimated the effect of MitoTam to membrane phase transition temperature. The methodology relies on an estimation of degree of free rotation of membrane fluorescent probes *N,N,N*-trimethyl-4-(6-phenyl-1,3,5,-hexatrien-1-yl), trimenthylammonium *p*-toluenesulfonate (TMA-DPH) and 1,6-diphenyl-1,3,5-hexatriene (DPH) (51, 52). The rigid membrane prevents free rotation of the fluorophore, therefore emitted fluorescence can be vertically and horizontally

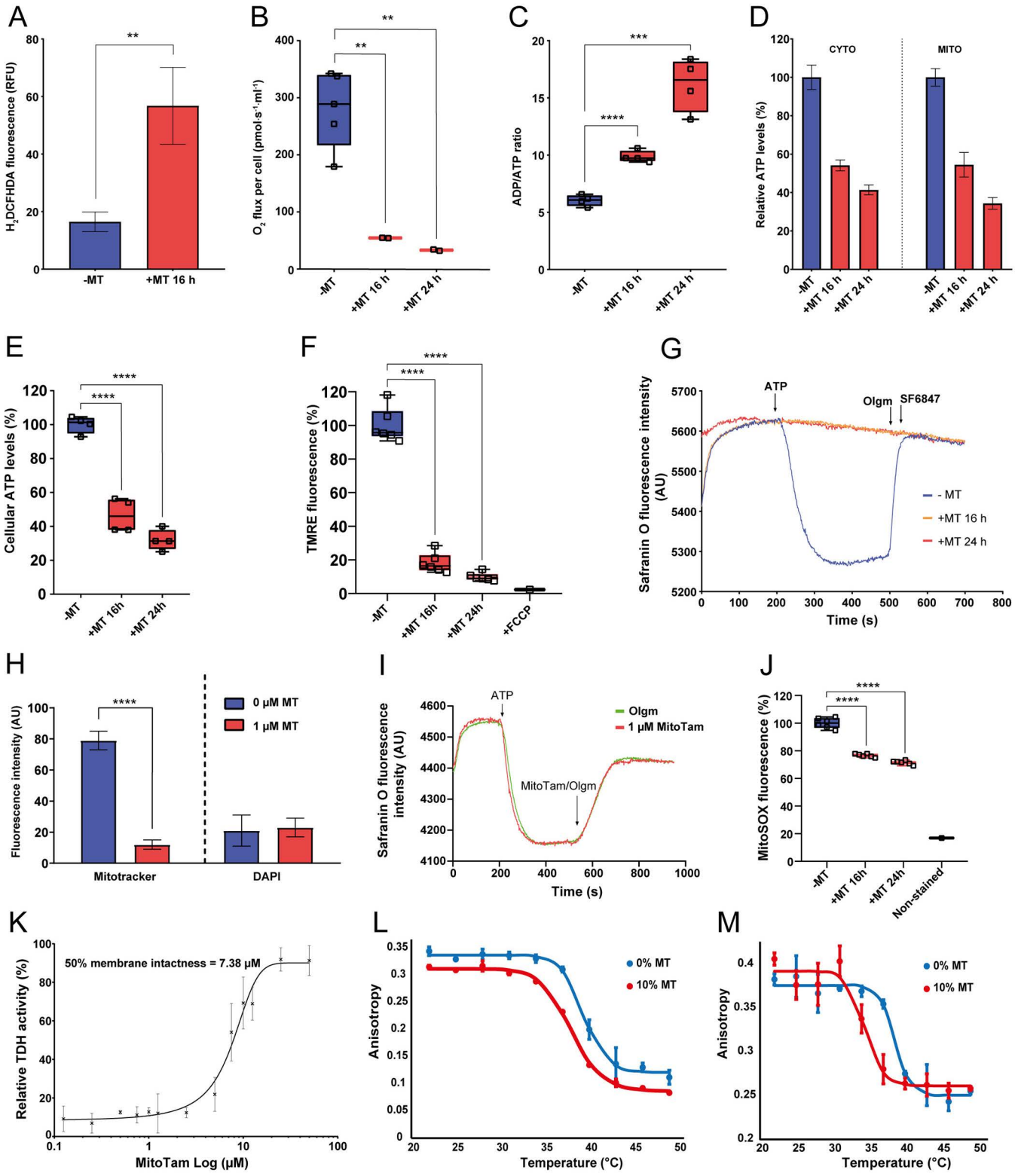

FIG 4 Overall effect of MitoTam on the *T. brucei* cell. (A) Production of intracellular ROS in BSF *T. brucei* was quantified by flow cytometry using DCFH-DA detection reagent in untreated control cells (−MT, blue) and cells treated with 100 nM MitoTam for 16 h (+MT 16 h, red) (mean ± s.d., $n = 3$, **, $P < 0.01$). (B) The O_2 flux per cell using high-resolution respirometry after addition of glycerol-3-phosphate was determined in BSF *T. brucei* untreated control cells (−MT, blue) and BSF cells treated with 100 nM MitoTam for 16 h (+MT 16 h, red) and 24 h (+MT 24 h, red) (box and whisker plot, $n = 3$, **, $P < 0.01$). (C) Relative ADP/ATP ratio analyzed using a bioluminescence assay kit in BSF *T. brucei* untreated control cells (−MT, blue) and BSF cells treated with 100 nM MitoTam for 16 h (+MT 16 h, red) and 24 h (+MT 24 h, red) (box and whisker plot, $n = 3$, ***, $P < 0.001$, ****, $P < 0.0001$). (D) Cytosolic and mitochondrial ATP levels were assessed in transgenic BSF *T. brucei* cell lines expressing firefly luciferase. Untreated control cells (−MT, blue) were compared

(Continued on next page)

polarized. Readout of fluorescence anisotrophy (r) then reflects changes in fluidity of membrane subdomains which allows for construction of a thermotropic profile.

The effect of MitoTam (10 mol%) to artificial membrane prepared from dipalmitoylphosphatidylcholine (DPPC) was measured for both the upper bilayer region (0.2 mol% TMA-DPH) as well as for the hydrophobic region (0.1 mol% DPH) across a range of temperatures (22 – 49°C). Indeed, our analysis of the interaction of 10 mol% MitoTam with DPPC liposomes indicated a significant increase in membrane fluidity (Fig. 4L and M). Interestingly, a bigger phase transition temperature shift occurred at the upper membrane region compared to the hydrophobic region (Δt = 1.6°C versus 4.2°C). Although fluorescence polarization measurements require suprapharmacological concentration of the drug these results suggest that modulation of membrane properties likely occurs at interface IMM/matrix or IMM/intermembrane space, whereas the hydrophobic region is less likely to be affected.

Taken together, our data indicate that MitoTam likely changes physicochemical characteristics and disrupts the integrity of the IMM, which leads to the $\Delta\Psi_m$ collapse and cell death.

DISCUSSION

In cancer cells, MitoTam was shown to inhibit CI-dependent respiration, which leads to a rapid decrease of $\Delta\Psi_m$, increased ROS production, and disruption of respiratory supercomplexes. These effects ultimately trigger cell death. The phenotype is even more pronounced in cancer cells, which exhibit high levels of the Her2 protein in mitochondria and elevated CI-dependent respiration. Consistently, mammalian cells deficient in CI are more resistant to MitoTam (19). In metabolically active senescent cells, MitoTam treatment led to increased levels of ROS, reduced $\Delta\Psi$m, impaired mitochondrial morphology, and metabolic switching to glycolysis for cellular ATP generation (22). Interestingly, the mitochondrial phenotype was alleviated and cell survival prolonged in MitoTam-treated senescent cells overexpressing adenine nucleotide translocase-2 (ANT2), which imports ATP into mitochondria (22). Furthermore, restriction of glycolytic pathways, either by limiting substrate levels or by adding glycolytic inhibitors competing with glucose sensitized control cells to MitoTam (22). In contrast to cancer cells, ROS scavengers failed to rescue MitoTam-treated senescent cells from death. Moreover, treatment with established CI inhibitors (rotenone and piericidin A) alone did not selectively eliminate senescent cells, while they are sensitive to MitoTam treatment (22). Therefore, the senolytic effect of MitoTam appears to involve additional mechanisms to CI inhibition. Taken together, the effect of MitoTam on cancer and

FIG 4 Legend (Continued)
with cells treated with 100 nM MitoTam for 16 h (+MT 16 h, red) and 24 h (+MT 24 h, red). Data were normalized to the values of the untreated control cells and expressed as a percentage (mean ± s.d., n = 4). (E) Total cellular ATP levels in BSF *T. brucei* were determined using a bioluminescence assay kit. Data from cultures treated with MitoTam for 16 h (+MT 16 h, red) and 24 h (+MT 24 h, red) were normalized to the respective values of the untreated control cells (−MT, blue) and expressed in percentage (box and whisker plot, n = 4), ****, $P < 0.0001$). (F) Flow cytometry of TMRE stained cells was used to determine $\Delta\Psi_m$ of BSF *T. brucei*. Data from cultures treated with 100 nM MitoTam for 16 h (16 h +MT, red) and 24 h (+MT 24 h, red) were normalized to the respective values of the untreated control cells (−MT, blue) and expressed in percentage. Uncoupler FCCP was added as a control for $\Delta\Psi_m$ depolarization (box and whisker plot, n = 6, ****, $P < 0.0001$). (G) *In situ* $\Delta\Psi_m$ was measured in digitonin-permeabilized BSF *T. brucei* cells stained with Safranin O dye. Where indicated, the F_oF_1-ATP synthase substrate—ATP, the F_oF_1-ATP synthase inhibitor—oligomycin (Olgm) and the protonophore SF6847 were added. Representative trace from the measurement of untreated control cells (−MT, blue) in comparison with cells treated with 100 nM MitoTam for 16 h (+MT 16 h, orange) and 24 h (+MT 24 h, red) is shown. (H) Automated microscopic analysis of BSF *T. brucei* cells stained with Mitotracker Red CMX-ROS was used to determine $\Delta\Psi_m$ in control untreated cells (0 μM MT) and in cells treated with 1 μM MitoTam for 1 h (1 μM MT). Staining with DAPI was used as an internal control for the analysis. Mean signal intensities of Mitotracker Red CMX-ROS and DAPI are depicted on the y axis (mean ± s.d., ****, $P < 0.0001$). (I) *In situ* $\Delta\Psi_m$ was measured in digitonin-permeabilized BSF *T. brucei* cells stained with Safranin O dye. Where indicated, the F_oF_1-ATP synthase substrate—ATP, the F_oF_1-ATP synthase inhibitor—oligomycin (Olgm, green line) and MitoTam (1 μM, red line) were added. (J) Red mitochondrial superoxide indicator MitoSOX was used to detect intramitochondrial ROS production in untreated BSF *T. brucei* control cells (−MT, blue) and BSF cells treated with 100 nM MitoTam for 16 h (+MT 16 h, red) and 24 h (+MT 24 h, red). Data were normalized to the values of the untreated control cells and expressed as a percentage (mean ± s.d., n = 6, ****, $P < 0.0001$). (K) Integrity of the inner BSF *T. brucei* mitochondrial membrane was assessed in isolated mitochondria incubated with increasing concentration of MitoTam. The mitochondrial enzyme threonine dehydrogenase (TDH) was used as a marker for permeability of the membrane, as the TDH activity is detectable only if a substrate passes freely through compromised mitochondrial membrane (mean ± s.d., n = 3). (L) Phase transition profile of artificial membranes prepared via hydration of lipide film (DPPC + MitoTam [MT] 0 and 10 mol % + 0.1 mol % DPH) with physiological saline and measured over range of temperatures (22 to 49°C). Fluidity change is plotted as a fluorescence anisotropy (r) against temperature. (M) Phase transition profile of artificial membranes prepared via hydration of lipide film (DPPC + MitoTam [MT] 0 and 10 mol % + 0.2 mol % TMA-DPH) with physiological saline and measured over range of temperatures (22 to 49°C). Fluidity change is plotted as a fluorescence anisotropy (r) against temperature.

senescent cells seems to be complex and includes targeting of CI, mitochondrial membrane depolarization, loss of ATP, increased levels of ROS, and possibly interplay between ATP/ADP exchange mechanism and ATP synthase (19, 22).

In this study, we showed that MitoTam inhibits the growth of a variety of parasitic protists and fungi. Different sensitivity to the compound may reflect different metabolic adaptations that the pathogens have developed to thrive in their host organism. High potencies were determined for *T. brucei* BSF and for the erythrocytic stage of *P. falciparum*, the relevant life cycle stages persisting in the mammalian host of both these medically important parasites. Notably, canonical CI is missing in *P. falciparum* (53) and is dispensable in BSF *T. brucei* (50, 54) suggesting that MitoTam has additional molecular targets besides CI. The EC_{50} value of MitoTam was one or 2 orders of magnitude higher (but still in in the micromolar range) for other tested organisms such as *Leishmania*, *Acanthamoeba* sp. and the widespread pathogenic yeasts *C. albicans* and *C. neoformans*. MitoTam was the least active against anaerobic protists *Trichomonas vaginalis* and *Giardia intestinalis*, likely due to the absence of conventional energized mitochondria in these organisms (36). The low activity observed against facultatively parasitic amebae *Naegleria fowleri* requires further research.

Following the encouraging results from *in vitro* testing, we demonstrated that MitoTam significantly decreases parasitemia levels, as well as frequency and size of lesions in animals infected with *T. brucei* and *L. mexicana*, respectively. In agreement with published data (19, 22, 23), repeated injection of MitoTam had no apparent adverse effect on BALB/c mice used in our studies.

To investigate the mode of action of MitoTam in unicellular pathogens, we performed comparative proteomic analysis using two distinct model organisms, *T. brucei* (BSF) and *C. albicans*. Only minor changes were detected in the *C. albicans* proteome upon MitoTam treatment, the most upregulated proteins being two homologues of multidrug efflux pumps, possibly explaining the 28 times higher EC_{50} value compared to BSF *T. brucei* cells. The corresponding analysis in *T. brucei* cells revealed substantial proteome changes upon 12 h MitoTam treatment. While the complexity of the observed alterations failed to pinpoint the exact molecular target(s) of MitoTam, there was a significant impact on the mitochondrion.

To get insight into the complex mode of action that is linked to the function of CI in cancer cells (19), we decided to examine the effect of MitoTam on mitochondrial parameters in BSF *T. brucei*, where the respiratory complex is dispensable (50). Consistent with studies on cancer and senescent cells (19, 22, 23), we found that cells incubated with MitoTam exhibit increased levels of cellular ROS and resulted in rapid dissipation of $\Delta\Psi_m$, which leads to cell death. In contrast, mitochondrial superoxide levels in *T. brucei* cells were decreased upon treatment with MitoTam, indicating that the oxidative burst caused by inhibition of CI-dependent respiration is not responsible for *T. brucei* growth inhibition. Furthermore, *T. brucei* BSF cells incubated with MitoTam exhibited reduced glycerol-3-phosphate-stimulated oxygen consumption, decreased ATP levels, and increased ADP/ATP ratio, suggesting that the biochemical effect of MitoTam could either be due to inhibition of F_oF_1-ATP synthase that generates $\Delta\Psi_m$ in these cells (47, 48) or, simply, due to disruption of the mitochondrial membrane integrity, resulting in $\Delta\Psi_m$ collapse.

Our analysis shows that MitoTam at micromolar concentrations significantly increases the membrane permeability of isolated mitochondria, which could be the cause of the altered mitochondrial phenotype. This effect could be ascribed to a direct interaction of the lipophilic MitoTam molecule with the IMM and alteration in membrane fluidity as demonstrated on artificial liposomal DPPC membrane at suprapharmacological concentration. Disruption or perhaps modulation of the membrane physicochemical properties might indeed rapidly dissipate $\Delta\Psi_m$ in live cells whether it be via unregulated proton leak or via affecting fundamental interactions of IMM and integral proteins, such as F_oF_1-ATP synthase.

Alternatively, the effect of MitoTam on membranes may be due to a disruption of enzymes involved in phospholipid synthesis. Intriguingly, studies on *T. cruzi*, *Leishmania*

spp. and *P. falciparum* indicate that tamoxifen, the functional pharmacophore of MitoTam, has an inhibitory effect on phospholipid metabolic pathways (55–57). Additional experiments are needed to reveal the multifactorial MitoTam mode of action. Nevertheless, our study shows that MitoTam represents a promising candidate to be repurposed as an effective anti-parasitic and anti-fungal compound with high selectivity.

MATERIALS AND METHODS

Pathogen culture. Culture conditions for all organisms used in this study are summarized in Table S4.

Drug sensitivity assays. The cytotoxicity effect of MitoTam was tested in a variety of organisms. Briefly, cells were seeded in 96-well plates at concentrations summarized in Table S4 and grown under standard conditions for 24 to 120 h, as indicated. The drug was serially diluted in a medium using a 2-fold dilution across a plate, resulting in a total volume of 200 μL per well. Each experiment included untreated control cells, as well as a positive control treated with a known growth inhibitory compound for each respective pathogen. The results were statistically analyzed, and dose-response curves plotted using Prism 6.01 (GraphPad Software) and expressed as the half-maximal effective concentration (EC_{50}).

The growth of *C. albicans* and *C. neoformans* cultures was determined from OD_{600} values measured on the I-Mark microplate reader (Bio-Rad). *Plasmodium falciparum* dose-response curves were generated using SYBR green I, as described previously (58). In brief, triplicate 2-fold compound dilution series were set up in 100 μL parasite cultures (~0.2% parasitemia in 2% hematocrit). After two cycles (96 h), parasites were lysed with 20 μL of 6× SYBR green I lysis buffer (0.16% saponin; 20 mM Tris-HCl, 5 mM EDTA, 1.6% Triton X-100, pH 7.4), supplemented with 1:1000 SYBR green I (from 10000× stock, Thermo Fisher). Fluorescence intensity was measured with an Infinite M200 Pro Multimode Microplate Reader (Tecan). *Trypanosoma cruzi* epimastigote cell growth was assessed by CellTiter-Glo 2.0 cell viability assay in a 96-well plate according to the manufacturer's protocol. As indicated, the dose-response curves of *T. brucei* and other pathogens were plotted from cell counts performed on the Guava EasyCyte 8HT flow cytometer (Luminex). The instrument setting and gate selection were adjusted using untreated control for each organism. For *G. intestinalis*, *A. castellanii*, and *N. fowleri*, that tend to adhere to the walls of the cultivation vessel, were placed on ice for 20 min and subsequently paraformaldehyde was added to a final concentration of 2% before counting the cells on the flow cytometer.

***Trypanosoma brucei* growth analysis.** *T. brucei* bloodstream cells were seeded at a concentration of 2×10^5 and 8×10^5 cells/mL of 5 mL HMI-9 medium in aerobic culture flasks. Biological triplicates were analyzed, including untreated control cultures and cultures treated with final concentrations of 40 nM and 100 nM MitoTam, respectively. Cells were grown under standard growth conditions (37°C, 5% CO_2). At each time point (8, 12, 16, 24, and 48 h), 20 μL were sampled, diluted 10× in fresh HMI-9, and the culture concentration was assessed using Guava EasyCyte 8HT flow cytometer (Luminex). The count parameters and gates were set according to previously measured cultures. In parallel, cells were checked under the microscope at each time point to confirm that live, moving cells were present in each culture.

***Trypanosoma brucei* dead cell staining.** *T. brucei* BSF cells were seeded at a concentration of 2×10^5 cells/mL in 5 mL HMI-9 medium in aerobic cultivation flasks. Biological triplicates were set up, including an untreated control group and groups treated with final concentrations of 40 nM and 100 nM MitoTam. The cells were grown under regular growth conditions. At each time point (8, 12, 16, and 24 h), 20 μL were sampled from each flask, 10× diluted in fresh HMI-9 to a final volume of 200 μL and 2 μL of SYTOX Green Dead Cell Stain (Invitrogen) was added. Cells were incubated at standard growth conditions for 30 min, after which live cell counts were analyzed using Guava EasyCyte 8HT flow cytometer (Luminex). The count parameters and gates were set according to previously measured cultures.

Measurement of ROS production in *T. brucei*. Intracellular and intramitochondrial ROS production was monitored using published protocols (59). Intracellular ROS levels were evaluated using three biological replicates of approximately 1×10^6 untreated cells and cells treated with 100 nM MitoTam for 12 h. The samples were collected, incubated with 10 μM 2′,7′-dichlorofluoresceine diacetate (DCFH-DA, Sigma-Aldrich) for 30 min and washed with PBS-G (1× PBS with 6 mM glucose). Using a 488 nm excitation laser and a 530/30 nm detector, 10,000 events were immediately counted on the BD FACSCanto II instrument.

Mitochondrial ROS production was assessed using the MitoSOX indicator (Thermo Fisher Scientific) in untreated cells and cells treated with 40 nM or 100 nM MitoTam. An equal number of cells (1×10^6) for each treatment was collected, washed in PBS-G, resuspended in HMI-9 medium with 5 μM MitoSOX and stained for 30 min at 37°C, 5% CO_2. After staining, cells were spun down, resuspended in PBS, and immediately analyzed by flow cytometry (BD FACS Canto II Instrument, 488 nm excitation laser and 585/15 nm emission). For each sample, 10 000 events were collected. All values were plotted and statistically analyzed using Prism (8.0) (GraphPad Software).

Comparative label-free proteomics. For *T. brucei* bloodstream forms, a final concentration of 100 nM MitoTam was added to approximately 3×10^7 cells in the exponential growth phase and cultures incubated for 14 h. Cell viability was checked microscopically before harvesting and washing three times in PBS (1200g, 10 min, 4°C). An untreated control group was prepared in parallel. Both groups were prepared in three biological replicates. The pellets were subjected to reductive alkylation and tryptic digest using routine procedures. Peptides were then analyzed by liquid chromatography-tandem mass spectrometry on an ultimate3000 nano rapid separation LC system (Dionex) coupled to an Orbitrap Fusion

mass spectrometer (Thermo-Fisher Scientific). Data were analyzed as described in (45, 60) using label-free quantification in MaxQuant (43) searching the TriTrypDB *T. brucei* strain TREU927 protein database version 54 (61).

For *C. albicans*, approximately 1×10^4 cells were inoculated in RPMI medium, as described in (62) and left to grow for 24 h at 35°C without agitation. MitoTam was added to the final concentration of 4.4 μM and cultures incubated for 12 h. Cells were then checked under a microscope, harvested, washed three times with PBS (1 200g, 10 min, 4°C). Pellets were then lyzed using FastPrep 24 5G homogenizer (MP Biomedicals) according to the manufacturer's instructions. Lysates were used for the label-free proteomic analysis and compared with the untreated control group prepared in parallel. Both groups were prepared in three biological replicates. Analysis was performed based on the *C. albicans* protein database downloaded from Uniprot on 12.11.2019 (63). The threshold settings for comparative proteomic analyses and data processing were chosen as described in (45) for both organisms. Briefly, thresholds were set to Q-value = 0, unique peptides detected >2 and the protein had to be identified at least twice in one of the conditions. For proteins found under only one condition, the average $\log_2$ converted intensity of 23 was selected as a minimum threshold. Significantly changed proteins were considered only if the fold change was >2.0.

In the proteomic results of *C. albicans*, localization was predicted based on Uniprot (63). For *T. brucei* proteomic analysis, manual annotation and localization prediction were based on *T. brucei* 927 database or *T. brucei* bloodstream form mitoproteome database obtained from (46). Volcano plots were drawn in Perseus 1.6.15.0 (44). At first, proteins only identified by site, reverse, potential contaminants, and proteins detected in less than two experiments within at least one group were excluded. The imputation was performed using a normal distribution with width 0.3 and downshift of 1.8, separately for each column. The parameters of the volcano plot were set up as following: statistical *t* test for both sides, 250 randomizations, false discovery rate of 0.05 and S_0 of 0.1.

Mitochondrial membrane potential measurements. The mitochondrial membrane potential ($\Delta\Psi$m) of BSF *T. brucei* cells was estimated using the red fluorescent stain MitoTracker Red CMXRos (Invitrogen). MitoTam was added to 5 mL *T. brucei* culture in an exponential growth phase at a final concentration of 1 μM and cells were incubated for 1 h under standard conditions. Subsequently, MitoTracker Red CMXRos was added to a final concentration of 100 nM and samples were incubated for another 10 min. Cultures were spun (1,300 g, 10 min, RT), resuspended in 5 mL of growth medium with 1 μM MitoTam and left for an additional 20 min under standard growth conditions. An untreated control was prepared in parallel. Treated and untreated cells were washed and transferred to 300 μL PBS, spread on microscopy slides, and left to settle. The slides were fixed by immersion in ice-cold methanol for 10 min, once the excess methanol had evaporated, the slides were mounted using Vectashield with DAPI (Vector laboratories), covered with cover slides, and sealed using nail varnish. The slides were imaged on a Leica TCS SP8 WLL SMD-FLIM microscope, using LAS X 3.5.6 imaging software. All images were captured using the exact same microscope setting. Quantification and comparison of signals were performed in NIS-Elements 5.30 (Nikon). Briefly,10 to 20 z-stacks were captured using LAS X automatic settings. A single stack with the highest overall intensity was chosen from the batch, and using the Artificial Intelligence module, areas of signal corresponding to individual cells were mapped and the average intensity was determined from the selected area. Furthermore, cell DNA visualized by DAPI was also quantified in the same manner and compared across all images as a reference value. The signal intensity of MitoTracker Red CMXRos was then compared in treated and untreated control, while the intensity of the DAPI signal was used to confirm the reproducibility of the reading.

Estimation of $\Delta\Psi$m in live cells was performed as described previously (59). Briefly, an equal number of cells (1×10^6) for each treatment was spun (1,400 g, 10 min, RT), the pellets were resuspended in HMI-9 medium with 60 nM TMRE (Thermo Fisher Scientific T669) and stained for 30 min at 37°C, 5% CO_2. After staining, cells were spun down (1,400 g, 10 min, RT) and resuspended in 2 mL of PBS and immediately analyzed by flow cytometry (BD FACS Canto II Instrument). For each sample, 10,000 events were collected. As a control for mitochondrial membrane depolarization, cells were treated with 20 μM protonophore FCCP (carbonyl cyanide 4-[trifluoromethoxy] phenylhydrazone, Sigma). Data were evaluated using BD FACS Diva software (BD Company) and further analyzed using Prism (8.0) (GraphPad Software).

Estimation of the $\Delta\Psi$m was also performed using the fluorescent probe Safranin O (Sigma) according to (59). From each treatment, 2×10^7 cells were collected, spun down (1,400 g, 10 min, RT), and resuspended in ANT buffer (8 mM KCl, 110 mM potassium gluconate, 10 mM NaCl, 10 mM HEPES, 10 mM K_2HPO_4, 0.015 mM EGTA, 0.5 mg/mL fatty acid-free BSA, 10 mM mannitol, 1.5 mM $MgCl_2$) with 5 μM Safranin O. Intact live cells were permeabilized by the addition of 4 μM digitonin (Calbiochem). The fluorescence of all samples was measured at RT and constant stirring and recorded on a Hitachi F-7100 spectrofluorometer (Hitachi High Technologies) at a 5 Hz acquisition rate, using 495 and 585 nm excitation and emission wavelengths, respectively. As indicated, the reaction was started by adding 1 mM ATP (PanReac AppliChem), F_oF_1-ATP synthase substrate, and stopped by the addition of 10 μg/mL oligomycin (Sigma), F_oF_1-ATP synthase inhibitor. The protonophore SF6847 (Enzo Life Sciences) was added at a final concentration of 250 nM as control for maximal depolarization. Fluorescence data were analyzed using Prism (8.0) (GraphPad Software).

High-resolution respirometry. The effect of MitoTam on respiration was analyzed by Oroboros Oxygraph-2K (Oroboros Instruments Corp., Innsbruck, Austria) as described (59). Bloodstream form *T. brucei* cells were incubated with 40 nM or 100 nM MitoTam for 16 h and 24 h, as indicated. For each treated sample and control, 2×10^7 cells were spun down (1,400 g, 10 min, RT) and pellets were washed in Mir05 medium (0.5 mM EGTA, 3 mM $MgCl_2$, 60 mM lactobionic acid, 20 mM taurine, 10 mM KH_2PO_4, 20 mM HEPES, 110 mM sucrose, 1 mg/mL fatty acid-free BSA, pH 7.1). Before the measurement started, the pellets were resuspended in 0.5 mL of Mir05 medium preheated to 37°C and transferred to the respiration chamber. Respiration was monitored at 37°C and with constant stirring. The experiment started with the addition of 10 mM glycerol-3-

phosphate (Sigma), the mitochondrial glycerol-3-phosphate dehydrogenase substrate, and respiration was inhibited by the addition of 250 μM SHAM (Salicylhydroxamic acid), the inhibitor of the trypanosomal alternative oxidase. The acquired data were analyzed using Prism (8.0) (GraphPad Software).

Western blot analysis. *T. brucei* BSF cells were incubated with 100 nM MitoTam and harvested at different time points after addition as indicated (0h, 8h, 12h, 16h and 24h). Cells were spun down (1,400 g, 10 min, RT), pellets were washed in PBS (pH 7.4) and resuspended in 3 $\times$ SDS-Page sample buffer (150 mM Tris pH 6.8, 300 mM 1,4-dithiothreitol, 6% (wt/vol) SDS, 30% (wt/vol) glycerol, 0.02% (wt/vol) bromophenol blue). The whole-cell lysates were denatured at 97°C for 8 min and stored at −80°C. For Western blot analysis, a volume of sample equal to 2.5 $\times$ 10^6 cells per well was loaded onto 12% gel, separated by SDS-Page, blotted onto a nitrocellulose membrane (Amersham Protram 0,2 μm PC GE Healthcare Life Sciences) and probed with a monoclonal (MAb) or polyclonal antibody (pAb). Incubation with primary antibodies was followed by a secondary antibody, either HRP-conjugated goat anti-rabbit or an anti-mouse antibody (1:5,000, Bio-Rad). Antibodies were detected using the enhanced chemiluminescence system (Immobilon Forte Western HRP substrate, Merck) on the Amersham Imager 600 (GE Health Care Life Sciences). The PageRuler^{TM} Plus prestained protein ladder (Thermo Fisher Scientific 26619) was used to determine the size of the detected bands. Primary antibodies were: MAb anti-Hsp70 (1: 2,000), MAb anti-AOX (1:1,000), pAb anti-AAC (1:1,000), anti-VDAC (1:1,000), pAb anti-PYK (pyruvate kinase) (1:1,000), pAb anti-APRT (adenine phosphoribosyl transferase) (1:1,000) and antibodies against F_oF_1-ATP synthase subunits β (1:2,000), p18 (1:1,000), Tb1 (1:1,000), Tb2 (1:1,000), and OSCP (1:1,000) (59, 64–66).

Measurement of the ATP/ADP ratio and total cellular ATP levels. Changes in the ATP/ADP ratio and total cellular ATP were determined in BSF *T. brucei* cells using the d-luciferin-luciferase bioluminescent enzymatic reaction (assay kit Sigma MAK135) according to manufacturer's instructions. Briefly, from each sample 1 $\times$ 10^6 cells were harvested and washed once with PBS supplemented with 6 mM glucose (PBS-G). Pellets were resuspended in PBS-G and the mixture transferred into a microtiter plate (96-well white flat-bottom). The bioluminescence signal was recorded in an Orion II microplate luminometer (Titertek Berthold) and analyzed using Prism (8.0) (GraphPad Software).

***In situ* measurement of ATP levels.** Cytosolic and mitochondrial ATP was measured using BSF *T. brucei* cell lines expressing firefly luciferase with or without N-terminal mitochondrial localization signal (MLS) following published protocols (67). Briefly, MitoTam treated cells, as well as untreated control, were spun (1 $\times$ 10^7 cells) (1,400 g, 10 min, RT) and washed in PBS-G. The pellets were resuspended in HEPES-LUC+Glu buffer (10 mM D-glucose, 20 mM HEPES, 116 mM NaCl, 5.6 mM KCl, 8 mM $MgSO_4$, 1.8 mM $CaCl_2$, pH 7.4) and transferred to a 96-well microtiter plate. ATP-dependent luciferase bioluminescence was recorded on a plate reader (Tecan Infinite M100). The light emission was started with the addition of a D-LUCIFERIN solution (50 μM; Sigma), collected for 5 min, and statistically analyzed using Prism (8.0) (GraphPad Software).

Determination of the mitochondrial membrane integrity. *T. brucei* bloodstream mitochondria were isolated by digitonin fractionation, according to (68). Briefly, approximately 1 $\times$ 10^8 cells were harvested (1400 g, 10 min, RT) and transferred to Hanks' balanced salt solution (Sigma-Aldrich). The protein concentrations of the samples were determined by the BCA assay kit (Sigma-Aldrich, USA). Digitonin (Calbiochem) was added to a protein:mass ratio of 1:0.15, lysate was incubated for 4 min and then spun. The pellet was washed and used as a mitochondria-enriched fraction, while the supernatant was used as a cytosolic fraction. Activities of two marker enzymes were used to assess the purity of fractions and intactness of mitochondrial membranes. The enzyme activities of cytosolic pyruvate kinase (PYK) and mitochondrial threonine dehydrogenase (TDH) were assayed spectrophotometrically at 340 nM by monitoring NADH concentration changes during the reaction. The activity of PYK was measured according to (69) in 0.1 M TEA buffer (ThermoFisher Scientific) (final pH 7.6), 5 mM $MgSO_4$ and 50 mM KCl, with the addition of 2.8 mM phosphoenolpyruvate, 2 mM ADP, 0.3 mM NADH and lactate dehydrogenase. The activity of TDH was measured in 0.2 M Tris-HCl buffer with 0.25 M KCl (final pH 8.6), with the addition of 120 mM threonine and 2.5 mM NAD^+. Different concentrations of MitoTam were added to the reaction and TDH activity was monitored as a marker for disruption of the mitochondrial membranes. Treatment with nonionic detergent Triton X-100 was used to completely disrupt mitochondrial membranes and thus release maximum TDH activity. Data were statistically analyzed and plotted with Prism (8.0) (GraphPad Software).

Membrane fluidity expressed as the regiospecific anisotropy of fluorescence polarization. Artificial membranes were prepared via hydration of lipide film (2.5 mg, 0.0034 mmol DPPC + MitoTam 10 mol.% + 0.1 mol% DPH or 0.2 mol % TMA-DPH) with physiological saline (2 mL). The lipide solution was extruded through polycarbonate membrane with pore size 0.4 μm. An 100 μL aliquot of liposomal solution was diluted with additional 900 μL of physiological saline to give clear solution of subvisible particles ($\approx$ 0.125 mg/mL). Fluorescence anisotropy was measured over range of temperatures (22 – 49°C) in 3°C increments while the slides in the spectrometer FLS1000 were set to 1 to 3 nm. In between the individual temperature measurements was the sample stirred with magnetic stir bar. Each measurement was average of three subsequent scans and the whole data set was collected as triplicate (DPH excitation 360 nm, emission 435 nm; TMA-DPH excitation 365 nm, emission 425 nm). Fluorescence anisotropy (r) is calculated automatically by software provided with the instrument, according to r = (Ivv−IvhG)/(Ivv + 2IvhG), where Ivv and Ivh are the intensities of the vertically and horizontally polarized components of the fluorescent light, respectively, after excitation with vertically polarized light. G = Ihv/Ihh is a grating correction factor for the optical system.

Survival analysis in a mouse model. To evaluate the trypanosomiasis effect of MitoTam on the mortality in mice, a group of 14 BALB/c mice was infected IP with approximately 2 $\times$ 10^5 BSF *T. brucei* cells strain STIB920 and the group of 14 mice was infected with 5 $\times$ 10^5 BSF cells of *T. brucei brucei* 427 strain, both in 100 μL sterile PBS. Mice were monitored every 12 h. Based on previous experience with the progression of the disease, half of the infected mice from each group were IV injected with MitoTam

(3 mg/kg bw) on days 3 and 5 after infection. The survival of the mice was visually monitored for up to 13 days after infection, the day of death was recorded for each animal.

***T. brucei* mouse infection model.** To assess the effect of MitoTam on the morbidity of trypanosomiasis in mice, 16 BALB/c mice were infected with 2×10^5 BSF *T. brucei* cells (strain STIB920) in 100 μL of sterile PBS. On day 2 and 4 postinfection, eight mice were injected with MitoTam at a final concentration of (3 mg/kg bw).

Mice were monitored daily, and blood samples were collected from a tail prick from each animal. Blood drops were smeared on microscopy slides and stained using Wright-Giemsa stain modification, Diff-Quick (Medion Diagnostics) according to the manufacturer's protocol. From each slide three images of random places, where red blood cells were not overlaying, were taken using an inverted widefield microscope Eclipse Ti2 (Nikon) using the CFI Plan Apochromat Lambda 20× objective (Nikon) with NIS-Elements AR 5.20 (Nikon). The images were then processed using the Artificial Intelligence module on NIS-Elements 5.30 (Nikon), manually trained to detect and quantify the number of red blood cells and trypanosomes. The ratio of trypanosomes to red blood cells was calculated and used to plot the data and calculate the statistical difference (Student's *t* test) between the treated and untreated groups in a given days. Data were plotted with Prism (8.0) (GraphPad Software). Animal handling was approved by the Czech Ministry of Agriculture (53659/2019-MZE-18134).

***L. mexicana* mouse subcutaneous leishmaniasis model.** The culture conditions of the *L. mexicana* promastigotes were as indicated in Table S4, their concentration was determined by hemocytometer. Before infection experiments, promastigotes were harvested, washed three times and resuspended in PBS. Twenty BALB/c mice (10 weeks old) were anesthetized IP with a mixture of ketamine (150 mg/kg) and xylazine (15 mg/kg) and infected intradermally in the ear pinnae by injection of 10^7 promastigotes. For a group of 10 animals, MitoTam was administered IP at 1, 2, 3, 5, 6 and 7 weeks after infection at a dose of (3 mg/kg body weight), other 10 animals served as nontreated controls. The presence of lesions was monitored for 12 consecutive weeks.

Rescue assay for *Leishmania* spp. amastigotes. Initially, murine macrophage cells (J774) were seeded in RPMI supplemented with 10% FCS and 50 μg/mL phorbol 12-myristate 13-acetate and left to differentiate for 24 h. Then, after washing the cells once with warm (37°C) serum-free RPMI, stationary phage promastigotes of *L. infantum* or *L. major* were added in a 10:1 ratio (2.5×10^6 cell/mL). After 24 h of incubation, cells were washed five times with serum-free RPMI and exposed to increasing concentration of MitoTam (or amphotericin B, as positive control) in RPMI (2% FCS). After 2 days, macrophages were l ysed with 20 μL of 0.05% SDS in RPMI for 30 s and released *Leishmania* cells were incubated with M199 10% FCS for another 3 days. Finally, the viability of transformed live cells was determined by the resazurin viability assay.

SUPPLEMENTAL MATERIAL

Supplemental material is available online only.

SUPPLEMENTAL FILE 1, PDF file, 1.69 MB.

SUPPLEMENTAL FILE 2, XLSX file, 0.5 MB.

SUPPLEMENTAL FILE 3, XLSX file, 0.5 MB.

SUPPLEMENTAL FILE 4, XLSX file, 0.01 MB.

ACKNOWLEDGMENTS

The project was supported by the Czech Science Foundation (20-28072S) to R.S. and 20-14409S to A.Z., CePaViP provided by The European Regional Development Fund and Ministry of Education, Youth and Sports of the Czech Republic (reg. no. CZ.02.1.01/0.0/0.0/16_019/0000759) to R.S., P.V., M.Z., and A.Z., Grant Agency of Charles University (406722) to D.A., Fundação para a Ciência e Tecnologia (FCT, Portugal)—PD/BD/128002/2016 for providing funds to M.M. and the Deutsche Forschungsgemeinschaft (DFG, German Research Foundation) (240245660 – SFB 1129) and the Baden-Württemberg Foundation (ref: 1.16101.10 and 1.16101.17) to M.G. We thank to Karel Harant and Pavel Talacko from the Laboratory of Mass Spectrometry, Biocev, Charles University, Faculty of Science, where proteomic and mass spectrometric analysis had been done.

We acknowledge Imaging Methods Core Facility at BIOCEV, institution supported by the MEYS CR (Large RI Project LM2018129 Czech-BioImaging) and ERDF (project No. CZ.02.1.01/0.0/0.0/18_046/0016045) for their support with obtaining imaging data presented in this paper.

REFERENCES

1. Lee SM, Kim MS, Hayat F, Shin D. 2019. Recent advances in the discovery of novel antiprotozoal agents. Molecules 24. https://doi.org/10.3390/molecules24213886.
2. Monzote L, Siddiq A. 2011. Drug development to Protozoan Diseases. Open Med Chem J 5:1–3. https://doi.org/10.2174/1874104501105010001.
3. Andrews KT, Fisher G, Skinner-Adams TS. 2014. Drug repurposing and human parasitic protozoan diseases. Int J Parasitol Drugs Drug Resist 4:95–111. https://doi.org/10.1016/j.ijpddr.2014.02.002.
4. Murphy MP, Smith RAJ. 2007. Targeting Antioxidants to Mitochondria by Conjugation to Lipophilic Cations. Annu Rev Pharmacol

Toxicol 47:629–656. https://doi.org/10.1146/annurev.pharmtox.47.120505.105110.
5. Teixeira J, Soares P, Benfeito S, Gaspar A, Garrido J, Murphy MP, et al. 2012. Rational discovery and development of a mitochondria-targeted antioxidant based on cinnamic acid scaffold. Free Radic Res 46. https://doi.org/10.3109/10715762.2012.662593.
6. Kelso GF, Porteous CM, Coulter CV, Hughes G, Porteous WK, Ledgerwood EC, Smith RA, Murphy MP. 2001. Selective targeting of a redox-active ubiquinone to mitochondria within cells: antioxidant and antiapoptotic properties. J Biol Chem 276:4588–4596. https://doi.org/10.1074/jbc.M009093200.
7. Benien P, Benein P, Almuteri MA, Mehanna AS, D'Souza GGM. 2015. Synthesis of triphenylphosphonium phospholipid conjugates for the preparation of mitochondriotropic liposomes. Methods Mol Biol 1265:51–57. https://doi.org/10.1007/978-1-4939-2288-8_4.
8. Du F, Min Y, Zeng F, Yu C, Wu S. 2014. A targeted and FRET-based ratiometric fluorescent nanoprobe for imaging mitochondrial hydrogen peroxide in living cells. Small 10:964–972. https://doi.org/10.1002/smll.201302036.
9. Cairns AG, McQuaker SJ, Murphy MP, Hartley RC. 2015. Targeting mitochondria with small molecules: the preparation of MitoB and MitoP as exomarkers of mitochondrial hydrogen peroxide. Methods Mol Biol 1265:25–50. https://doi.org/10.1007/978-1-4939-2288-8_3.
10. Terekhova NV, Tatarinov DA, Shaihutdinova ZM, Pashirova TN, Lyubina AP, Voloshina AD, Sapunova AS, Zakharova LY, Mironov VF. 2020. Design and synthesis of amphiphilic 2-hydroxybenzylphosphonium salts with antimicrobial and antitumor dual action. Bioorg Med Chem Lett 30:127234. https://doi.org/10.1016/j.bmcl.2020.127234.
11. Kinnamon KE, Steck EA, Rane DS. 1979. A new chemical series active against African Trypanosomes: benzyltriphenylphosphonium salts. J Med Chem 22. https://doi.org/10.1021/jm00190a019.
12. Fueyo González FJ, Ebiloma GU, Izquierdo García C, Bruggeman V, Sánchez Villamañán JM, Donachie A, Balogun EO, Inaoka DK, Shiba T, Harada S, Kita K, de Koning HP, Dardonville C. 2017. Conjugates of 2,4-dihydroxybenzoate and salicylhydroxamate and lipocations display potent antiparasite effects by efficiently targeting the Trypanosoma brucei and Trypanosoma congolense mitochondrion. J Med Chem 60:1509–1522. https://doi.org/10.1021/acs.jmedchem.6b01740.
13. Alkhaldi AAM, Martinek J, Panicucci B, Dardonville C, Zíková A, de Koning HP. 2016. Trypanocidal action of bisphosphonium salts through a mitochondrial target in bloodstream form Trypanosoma brucei. Int J Parasitol Drugs Drug Resist 6:23–34. https://doi.org/10.1016/j.ijpddr.2015.12.002.
14. Long TE, Lu X, Galizzi M, Docampo R, Gut J, Rosenthal PJ. 2012. Phosphonium lipocations as antiparasitic agents. Bioorg Med Chem Lett 22:2976–2979. https://doi.org/10.1016/j.bmcl.2012.02.045.
15. Manzano JI, Cueto-Díaz EJ, Olías-Molero AI, Perea A, Herraiz T, Torrado JJ, Alunda JM, Gamarro F, Dardonville C. 2019. Discovery and pharmacological studies of 4-hydroxyphenyl-derived phosphonium salts active in a mouse model of visceral leishmaniasis. J Med Chem 62:10664–10675. https://doi.org/10.1021/acs.jmedchem.9b00998.
16. Taladriz A, Healy A, Flores Pérez EJ, Herrero García V, Ríos Martínez C, Alkhaldi AAM, Eze AA, Kaiser M, de Koning HP, Chana A, Dardonville C. 2012. Synthesis and structure-activity analysis of new phosphonium salts with potent activity against African trypanosomes. J Med Chem 55:2606–2622. https://doi.org/10.1021/jm2014259.
17. Jara JA, Castro-Castillo V, Saavedra-Olavarría J, Peredo L, Pavanni M, Jaña F, Letelier ME, Parra E, Becker MI, Morello A, Kemmerling U, Maya JD, Ferreira J. 2014. Antiproliferative and uncoupling effects of delocalized, lipophilic, cationic gallic acid derivatives on cancer cell lines. Validation in vivo in singenic mice. J Med Chem 57:2440–2454. https://doi.org/10.1021/jm500174v.
18. Dong L, Gopalan V, Holland O, Neuzil J. 2020. Mitocans revisited: mitochondrial targeting as efficient anti-cancer therapy. Int J Mol Sci 21:7941. https://doi.org/10.3390/ijms21217941.
19. Rohlenova K, Sachaphibulkij K, Stursa J, Bezawork-Geleta A, Blecha J, Endaya B, Werner L, Cerny J, Zobalova R, Goodwin J, Spacek T, Alizadeh Pesdar E, Yan B, Nguyen MN, Vondrusova M, Sobol M, Jezek P, Hozak P, Truksa J, Rohlena J, Dong L-F, Neuzil J. 2017. Selective disruption of respiratory supercomplexes as a new strategy to suppress Her2 high breast cancer. Antioxid Redox Signal 26:84–103. https://doi.org/10.1089/ars.2016.6677.
20. Jordan VC. 2003. Tamoxifen: a most unlikely pioneering medicine. Nat Rev Drug Discov 2:205–213. https://doi.org/10.1038/nrd1031.
21. Unten Y, Murai M, Koshitaka T, Kitao K, Shirai O, Masuya T, Miyoshi H. 2022. Comprehensive understanding of multiple actions of anticancer drug tamoxifen in isolated mitochondria. Biochim Biophys Acta Bioenerg 1863:148520. https://doi.org/10.1016/j.bbabio.2021.148520.
22. Hubackova S, Davidova E, Rohlenova K, Stursa J, Werner L, Andera L, Dong L, Terp MG, Hodny Z, Ditzel HJ, Rohlena J, Neuzil J. 2019. Selective elimination of senescent cells by mitochondrial targeting is regulated by ANT2. Cell Death Differ 26:276–290. https://doi.org/10.1038/s41418-018-0118-3.
23. Hubackova S, Zobalova R, Dubisova M, Smigova J, Dvorakova S, Korinkova K. 2022. Simultaneous targeting of mitochondrial metabolism and immune checkpoints as a new strategy for renal cancer therapy. Clin Transl Med.
24. Vacurova E, Trnovska J, Svoboda P, Skop V, Endaya B, Novosadova V, et al. 2022. Targeting mitochondria as a novel approach to treatment of metabolic diseases. Nat Commun. Forthcomin.
25. Stuart K, Brun R, Croft S, Fairlamb A, Gürtler RE, McKerrow J, Reed S, Tarleton R. 2008. Kinetoplastids: related protozoan pathogens, different diseases. J Clin Invest 118:1301–1310. https://doi.org/10.1172/JCI33945.
26. Field MC, Horn D, Fairlamb AH, Ferguson MAJ, Gray DW, Read KD, De Rycker M, Torrie LS, Wyatt PG, Wyllie S, Gilbert IH. 2017. Anti-trypanosomatid drug discovery: an ongoing challenge and a continuing need. Nat Rev Microbiol 15:217–231. https://doi.org/10.1038/nrmicro.2016.193.
27. Mesu VKBK, Kalonji WM, Bardonneau C, Mordt OV, Blesson S, Simon F, Delhomme S, Bernhard S, Kuziena W, Lubaki J-PF, Vuvu SL, Ngima PN, Mbembo HM, Ilunga M, Bonama AK, Heradi JA, Solomo JLL, Mandula G, Badibabi LK, Dama FR, Lukula PK, Tete DN, Lumbala C, Scherrer B, Strub-Wourgaft N, Tarral A. 2018. Oral fexinidazole for late-stage African Trypanosoma brucei gambiense trypanosomiasis: a pivotal multicentre, randomised, non-inferiority trial. Lancet 391:144–154. https://doi.org/10.1016/S0140-6736(17)32758-7.
28. Dickie EA, Giordani F, Gould MK, Mäser P, Burri C, Mottram JC, Rao SPS, Barrett MP. 2020. New drugs for human African trypanosomiasis: a twenty first century success story. TropicalMed 5:29. https://doi.org/10.3390/tropicalmed5010029.
29. WHO. 2021. Malaria. Available: https://www.who.int/news-room/fact-sheets/detail/malaria#:~:text=Malaria%20is%20a%20life%2Dthreatening,at%20627%20000%20in%202020.
30. Dadar M, Tiwari R, Karthik K, Chakraborty S, Shahali Y, Dhama K. 2018. Candida albicans - Biology, molecular characterization, pathogenicity, and advances in diagnosis and control – An update. Microb Pathog 117:128–138. Academic Press. https://doi.org/10.1016/j.micpath.2018.02.028.
31. Maziarz EK, Perfect JR. 2016. Cryptococcosis. Infect Dis Clin North Am 30:179–206. https://doi.org/10.1016/j.idc.2015.10.006.
32. Grace E, Asbill S, Virga K. 2015. Naegleria fowleri: pathogenesis, diagnosis, and treatment options. Antimicrob Agents Chemother 59:6677–6681. https://doi.org/10.1128/AAC.01293-15.
33. Kot K, Łanocha-Arendarczyk NA, Kosik-Bogacka DI. 2018. Amoebas from the genus Acanthamoeba and their pathogenic properties. Ann Parasitol 64:299–308.
34. Ryan U, Hijjawi N, Feng Y, Xiao L. 2019. Giardia: an under-reported foodborne parasite. Int J Parasitol 49:1–11. https://doi.org/10.1016/j.ijpara.2018.07.003.
35. Van Gerwen OT, Muzny CA. 2019. Recent advances in the understanding and management of of Trichomonas vaginalis infection. F1000Res 8:1666–1610. https://doi.org/10.12688/f1000research.20411.1.
36. Tachezy J. 2008. Hydrogenosomes and Mitosomes: mitochondria of Anaerobic Eukaryotes.
37. Kita K, Nihei C, Tomitsuka E. 2003. Parasite mitochondria as drug target: diversity and dynamic changes during the life cycle. Curr Med Chem 10:2535–2548. https://doi.org/10.2174/0929867033456549.
38. Shingu-Vazquez M, Traven A. 2011. Mitochondria and fungal pathogenesis: drug tolerance, virulence, and potential for antifungal therapy. Eukaryot Cell 10:1376–1383. https://doi.org/10.1128/EC.05184-11.
39. Goldberg DE, Zimmerberg J. 2020. Hardly vacuous: the parasitophorous vacuolar membrane of malaria parasites. Trends Parasitol 36:138–146. https://doi.org/10.1016/j.pt.2019.11.006.
40. De Rycker M, Hallyburton I, Thomas J, Campbell L, Wyllie S, Joshi D, Cameron S, Gilbert IH, Wyatt PG, Frearson JA, Fairlamb AH, Gray DW. 2013. Comparison of a high-throughput high-content intracellular Leishmania donovani assay with an axenic amastigote assay. Antimicrob Agents Chemother 57:2913–2922. https://doi.org/10.1128/AAC.02398-12.
41. Don R, Ioset JR. 2014. Screening strategies to identify new chemical diversity for drug development to treat kinetoplastid infections. Parasitology 141:140–146. https://doi.org/10.1017/S003118201300142X.

42. Wyllie S, Brand S, Thomas M, De Rycker M, Chung C-W, Pena I, Bingham RP, Bueren-Calabuig JA, Cantizani J, Cebrian D, Craggs PD, Ferguson L, Goswami P, Hobrath J, Howe J, Jeacock L, Ko E-J, Korczynska J, MacLean L, Manthri S, Martinez MS, Mata-Cantero L, Moniz S, Nühs A, Osuna-Cabello M, Pinto E, Riley J, Robinson S, Rowland P, Simeons FRC, Shishikura Y, Spinks D, Stojanovski L, Thomas J, Thompson S, Viayna Gaza E, Wall RJ, Zuccotto F, Horn D, Ferguson MAJ, Fairlamb AH, Fiandor JM, Martin J, Gray DW, Miles TJ, Gilbert IH, Read KD, Marco M, Wyatt PG. 2019. Preclinical candidate for the treatment of visceral leishmaniasis that acts through proteasome inhibition. Proc Natl Acad Sci U S A 116:9318–9323. https://doi.org/10.1073/pnas.1820175116.
43. Cox J, Mann M. 2008. MaxQuant enables high peptide identification rates, individualized p.p.b.-range mass accuracies and proteome-wide protein quantification. Nat Biotechnol 26:1367–1372. https://doi.org/10.1038/nbt.1511.
44. Tyanova S, Temu T, Sinitcyn P, Carlson A, Hein MY, Geiger T, Mann M, Cox J. 2016. The Perseus computational platform for comprehensive analysis of (prote)omics data. Nat Methods 13:731–740. https://doi.org/10.1038/nmeth.3901.
45. Arbon D, Ženíšková K, Mach J, Grechnikova M, Malych R, Talacko P, Sutak R. 2020. Adaptive iron utilization compensates for the lack of an inducible uptake system in Naegleria fowleri and represents a potential target for therapeutic intervention. Singer SM, editor. PLoS Negl Trop Dis 14:e0007759. https://doi.org/10.1371/journal.pntd.0007759.
46. Zíková A, Verner Z, Nenarokova A, Michels PAM, Lukeš J. 2017. A paradigm shift: the mitoproteomes of procyclic and bloodstream Trypanosoma brucei are comparably complex. PLoS Pathog 13:e1006679. https://doi.org/10.1371/journal.ppat.1006679.
47. Smith TK, Bringaud F, Nolan DP, Figueiredo LM. 2017. Metabolic reprogramming during the Trypanosoma brucei life cycle. F1000Res 6:683. https://doi.org/10.12688/f1000research.10342.1.
48. Schnaufer A, Clark-Walker GD, Steinberg AG, Stuart K. 2005. The F1-ATP synthase complex in bloodstream stage trypanosomes has an unusual and essential function. EMBO J 24:4029–4040. https://doi.org/10.1038/sj.emboj.7600862.
49. Nolan DP, Voorheis HP. 1992. The mitochondrion in bloodstream forms of Trypanosoma brucei is energized by the electrogenic pumping of protons catalysed by the F1F0-ATPase. Eur J Biochem 209:207–216. https://doi.org/10.1111/j.1432-1033.1992.tb17278.x.
50. Surve S, Heestand M, Panicucci B, Schnaufer A, Parsons M. 2012. Enigmatic presence of mitochondrial complex I in Trypanosoma brucei bloodstream forms. Eukaryot Cell 11:183–193. https://doi.org/10.1128/EC.05282-11.
51. Poojari C, Wilkosz N, Lira RB, Dimova R, Jurkiewicz P, Petka R, Kepczynski M, Róg T. 2019. Behavior of the DPH fluorescence probe in membranes perturbed by drugs. Chem Phys Lipids 223:104784. https://doi.org/10.1016/j.chemphyslip.2019.104784.
52. Grebowski J, Krokosz A, Puchala M. 2013. Membrane fluidity and activity of membrane ATPases in human erythrocytes under the influence of polyhydroxylated fullerene. Biochim Biophys Acta 1828:241–248. https://doi.org/10.1016/j.bbamem.2012.09.008.
53. Gardner MJ, Hall N, Fung E, White O, Berriman M, Hyman RW, Carlton JM, Pain A, Nelson KE, Bowman S, Paulsen IT, James K, Eisen JA, Rutherford K, Salzberg SL, Craig A, Kyes S, Chan M-S, Nene V, Shallom SJ, Suh B, Peterson J, Angiuoli S, Pertea M, Allen J, Selengut J, Haft D, Mather MW, Vaidya AB, Martin DMA, Fairlamb AH, Fraunholz MJ, Roos DS, Ralph SA, McFadden GI, Cummings LM, Subramanian GM, Mungall C, Venter JC, Carucci DJ, Hoffman SL, Newbold C, Davis RW, Fraser CM, Barrell B. 2002. Genome sequence of the human malaria parasite Plasmodium falciparum. Nature 419:498–511. https://doi.org/10.1038/nature01097.
54. Verner Z, Čermáková P, Škodová I, Kriegová E, Horváth A, Lukeš J. 2011. Complex i (NADH:ubiquinone oxidoreductase) is active in but non-essential for procyclic *Trypanosoma brucei*. Mol Biochem Parasitol 175:196–200. https://doi.org/10.1016/j.molbiopara.2010.11.003.
55. Trinconi CT, Miguel DC, Silber AM, Brown C, Mina JGM, Denny PW, Heise N, Uliana SRB. 2018. Tamoxifen inhibits the biosynthesis of inositolphosphorylceramide in Leishmania. Int J Parasitol Drugs Drug Resist 8:475–487. https://doi.org/10.1016/j.ijpddr.2018.10.007.
56. Piñero TA, Landoni M, Duschak VG, Katzin AM, Couto AS. 2018. Effect of tamoxifen on the sphingolipid biosynthetic pathway in the different intraerythrocytic stages of the apicomplexa Plasmodium falciparum. Biochem Biophys Res Commun 497. https://doi.org/10.1016/j.bbrc.2018.02.183.
57. Landoni M, Piñero T, Soprano LL, Garcia-Bournissen F, Fichera L, Esteva MI, Duschak VG, Couto AS. 2019. Tamoxifen acts on Trypanosoma cruzi sphingolipid pathway triggering an apoptotic death process. Biochem Biophys Res Commun 516:934–940. https://doi.org/10.1016/j.bbrc.2019.06.149.
58. Johnson JD, Dennull RA, Gerena L, Lopez-Sanchez M, Roncal NE, Waters NC. 2007. Assessment and continued validation of the malaria SYBR Green I-based fluorescence assay for use in malaria drug screening. Antimicrob Agents Chemother 51:1926–1933. https://doi.org/10.1128/AAC.01607-06.
59. Hierro-Yap C, Šubrtová K, Gahura O, Panicucci B, Dewar C, Chinopoulos C, Schnaufer A, Zíková A. 2021. Bioenergetic consequences of FoF1–ATP synthase/ATPase deficiency in two life cycle stages of Trypanosoma brucei. J Biol Chem 296:100357. https://doi.org/10.1016/j.jbc.2021.100357.
60. Mach J, Bíla J, Ženíšková K, Arbon D, Malych R, Glavanakovová M, Nývltová E, Sutak R. 2018. Iron economy in Naegleria gruberi reflects its metabolic flexibility. Int J Parasitol 48:719–727. https://doi.org/10.1016/j.ijpara.2018.03.005.
61. Aslett M, Aurrecoechea C, Berriman M, Brestelli J, Brunk BP, Carrington M, Depledge DP, Fischer S, Gajria B, Gao X, Gardner MJ, Gingle A, Grant G, Harb OS, Heiges M, Hertz-Fowler C, Houston R, Innamorato F, Iodice J, Kissinger JC, Kraemer E, Li W, Logan FJ, Miller JA, Mitra S, Myler PJ, Nayak V, Pennington C, Phan I, Pinney DF, Ramasamy G, Rogers MB, Roos DS, Ross C, Sivam D, Smith DF, Srinivasamoorthy G, Stoeckert CJ, Subramanian S, Thibodeau R, Tivey A, Treatman C, Velarde G, Wang H. 2010. TriTrypDB: a functional genomic resource for the Trypanosomatidae. Nucleic Acids Res 38:D457–D462. https://doi.org/10.1093/nar/gkp851.
62. NCCLS. 2008. Reference method for broth dilution antifungal susceptibility testing of filamentous fungi; approved standard serving the world's medical science community through voluntary consensus. Nccls.
63. Bateman A, Martin MJ, Orchard S, Magrane M, Agivetova R, Ahmad S, et al. 2021. UniProt: the universal protein knowledgebase in 2021. Nucleic Acids Res 49. https://doi.org/10.1093/nar/gkaa1100.
64. Panigrahi AK, Zíková A, Dalley RA, Acestor N, Ogata Y, Anupama A, Myler PJ, Stuart KD. 2008. Mitochondrial complexes in Trypanosoma brucei: a novel complex and a unique oxidoreductase complex. Mol Cell Proteomics 7:534–545. https://doi.org/10.1074/mcp.M700430-MCP200.
65. Šubrtová K, Panicucci B, Zíková A. 2015. ATPaseTb2, a unique membrane-bound FoF1-ATPase component, is essential in bloodstream and dyskinetoplastic trypanosomes. PLoS Pathog 11:e1004660. https://doi.org/10.1371/journal.ppat.1004660.
66. Doleželová E, Klejch T, Špaček P, Slapničková M, Guddat L, Hocková D, Zíková A. 2021. Acyclic nucleoside phosphonates with adenine nucleobase inhibit Trypanosoma brucei adenine phosphoribosyltransferase in vitro. Sci Rep 11:13317. https://doi.org/10.1038/s41598-021-91747-6.
67. Gnipová A, Šubrtová K, Panicucci B, Horváth A, Lukeš J, Zíková A. 2015. The ADP/ATP carrier and its relationship to oxidative phosphorylation in ancestral protist trypanosoma brucei. Eukaryot Cell 14:297–310. https://doi.org/10.1128/EC.00238-14.
68. Smíd O, Horáková E, Vilímová V, Hrdy I, Cammack R, Horváth A, Lukes J, Tachezy J. 2006. Knock-downs of iron-sulfur cluster assembly proteins IscS and IscU down-regulate the active mitochondrion of procyclic *Trypanosoma brucei*. J Biol Chem 281:28679–28686. https://doi.org/10.1074/jbc.M513781200.
69. Opperdoes FR, Markos A, Steiger RF. 1981. Localization of malate dehydrogenase, adenylate kinase and glycolytic enzymes in glycosomes and the threonine pathway in the mitochondrion of cultured procyclic trypomastigotes of Trypanosoma brucei. Mol Biochem Parasitol 4:291–309. https://doi.org/10.1016/0166-6851(81)90062-1.